INTERNAL SOLITONS GENERATED BY MOVING DISTURBANCES

Thesis by

Jinlin Zhu

In Partial Fulfillment of the Requirements

for the Degree of

Doctor of Philosophy

California Institute of Technology

Pasadena, California

1986

(Submitted May 22, 1986)

ACKNOWLEDGMENTS

My sincere thanks and respect go to my advisor, Professor Theodore Yao-Tsu Wu, for his valuable guidance throughout my graduate study, his introduction and encouragement to this versatile research field of wave, his enthusiasm and insight in scientific development. I have greatly benefited from his experience, guidance and his previous work in this field, which are the bases of some work in this thesis. I gratefully acknowledge the many contributions Dr. Wu has made to my personal and scientific development.

Special thanks are due Dr. George T. Yates for his friendly help in the computer operations and the experiments and many valuable discussions on the research. I appreciate greatly his assistance in the final correction of the manuscript.

I would like to thank Professor Fredric Raichlen for his friendly help in the experiments and his valuable suggestions which have been used in the experiments of this thesis.

I am deeply indebted to Miss Helen F. Burrus, who provided friendship and encouragement all these years, assisted in the correction of the manuscript and typed this thesis.

I would like to thank Mr. Raymond Mak, Mr. John Kao and Dr. Keh-hen Wang for the valuable help in the experiments.

This research has been supported by the National Science Foundation Grant MSM-8118429 and the United States Navy, Office of Naval Research Contracts N00014-82-K-0443 and N00014-85-K-0536. I gratefully acknowledge their support and the tuition fellowships received from Caltech.

ABSTRACT

A new phenomenon of the generation of internal solitons is investigated in this thesis by applying theoretical models and is observed in both numerical and experimental results. By imposing an external disturbance, such as a top surface pressure or a bottom bump, that moves with a constant velocity within a transcritical range after an impulsive start from rest, upon a two-layered or a continuously stratified fluid system, a series of solitons are generated, one after another periodically, each surging ahead of the disturbance in turn. Two theoretical models, belonging to the generalized Boussinesq class, are developed to investigate the generation of weakly nonlinear and weakly dispersive long waves and their evolution in an inviscid, immiscible, and incompressible stratified fluid system under the forcing of the external disturbances. The top surface may be either free or covered by a rigid horizontal plate. For the generalized Boussinesq class for two-layered fluid systems, we have derived the FOUR-equation model for the free top-surface case and the THREE-equation model for the rigid horizontal top-surface case; these are extensions of the one-layer homogeneous fluid system previously considered by Wu (1979). For primarily unidirectional motions a forced KdV equation is obtained which represents each normal mode of a two-layer system or a continuously stratified fluid system. Numerical schemes have been successfully developed to solve these equations. Experiments were performed to investigate this phenomenon using fresh water to form the upper layer and brine

the lower layer. The relationship between the main properties (the amplitude and the period of generation) of the generated solitons and the forcing function configurations is discussed along with comparisons of theoretical, numerical and experimental results. Qualitatively all the results are consistent in exhibiting the salient features of the resulting motion. Quantitatively the numerical results based on the continuously stratified fluid model seem to be more satisfactory than those given by the two-layered fluid model in comparison with the present experiments. The discrepancy between the theory and experiment is supposedly due to the viscous effects, which will be left for future work.

TABLE OF CONTENTS

LIST OF FIGURES

LIST OF FIGURES (cont'd)

LIST OF FIGURES (cont'd)

LIST OF FIGURES (cont'd)

LIST OF FIGURES (cont'd)

LIST OF FIGURES (cont')

LIST OF FIGURES (cont'd)

I. INTRODUCTION

This thesis is mainly concerned with the generation of internal solitons* that move ahead of disturbances moving with a transcritical velocity in a shallow stratified fluid system. Internal waves, including all kinds of wave phenomena inside a stratified fluid system, have been a subject of interest for a long time in geophysics, ocean engineering, applied mathematics and hydrodynamics. The vast oceans on the earth are a complex stratified fluid system widely distributed with pycnoclines, which are horizontally layered regions with a large density variation, commonly located about 50-150 meters below the ocean surface. With the development of oceanography and ocean engineering, more and more publications on internal waves in nature have appeared. Lock (1980), Osborn, Burch & Scarlet (1978) and Osborn & Burch (1980) reported field observations in the deep waters of the Andaman Sea off Thailand. Other investigations have been reported by Perry & Schimke (1970) on internal waves and internal solitary waves in the area of the Northwest Coast of Sumatra, by Ziegenbein (1969, 1970) in the Strait of Gibraltar, Eriksen (1978) in the Bermuda Area, Gargett (1976) and Farmer & Smith (1980) in the Western Coast Area of Canada and by Halpern (1971), Haury (1979) and Chereskin (1983) in the Massachusetts Bay. A significant feature

---

* The term soliton (or solitary wave) used in this work is intended to name the waves which are completely above or completely below the mean-water line. They are generated, one after another, by moving disturbances and each of them carries the essential qualities of a single solitary wave.

of these observations is the discovery of how large the amplitude of these internal waves occurring in nature can be. Internal solitary waves as high as 60m in amplitude have been reported (Osborn et al. (1980)) although the top surface waves that accompany such giant internal waves are invariably very small. It was noticed long ago that ocean-going vessels off the coast of Norway suddenly found themselves unable to maintain their accustomed speed as they moved past the mouth of a fjord. This "dead water" phenomenon is related to the internal waves as explained by the Swedish oceanographer Ekman. At certain speeds, much of the power from the ship's engines is spent, wastefully, on the creation of internal waves (Long (1970)). Internal waves are also responsible for the flexing of drilling risers of offshore drilling rigs in the deep waters of the Andaman Sea (Locke (1980)).

Important experimental studies on internal waves have been conducted by many researchers. Among them are Yih & Guha (1955), Lee & Beardsley (1974), Hurdis & Pao (1975), Baines (1977, 1979), Maxworthy (1979), Hammack (1980), Koop & Butler (1981), Lansing & Maxworthy (1984), Kao (1985) and Gilreath & Brandt (1985).

The phenomenon of generation and evolution of internal waves in a stably stratified fluid has been a subject of considerable recent interest. Internal waves have been investigated theoretically by Keulegan (1953), Long (1956), Peters & Stoker (1960), Benjamin (1966, 1967) and Koop & Butler (1981) for two-layer fluid systems, and Peters & Stoker (1960), Benney (1966), Benjamin (1966, 1967), Wu (1966), Wu & Mei (1967), Ono (1975), Joseph (1977), Kubota, Ko

& Dobbs (1978) and by Liu, Kubota & Ko (1980) for continuously stratified fluid systems.

Most of these research studies are concerned only with "free" wave propagation — there being no external forcings except the conservative gravity field acting as a restoring force. Among a few of the papers that have considered external forcing disturbances such as a surface pressure or the forcing due to bottom unevenness, we can mention Lansing & Maxworthy (1984) who investigated, both theoretically and experimentally, the generation and evolution of internal waves in a two-layer system by towing an obstacle with a sinusoidal motion. They concluded that the generation mechanism of an internal wave train by tidal flows in the ocean is: "As the ebb tide proceeds, a depression, i. e., a lee wave, is formed behind the obstacle..... As the ebb tide slackens, the depression, which has gained a large potential energy, moves upstream against the flow. As the depression propagates away from the obstacle it evolves into a number of solitary waves."

The phenomenon of soliton generation by moving disturbances was first discovered in the homogeneous one-layer case. This runaway soliton phenomenon was first identified and reported by Wu & Wu (1982) from their numerical calculations and later it was confirmed by experiments with both two and three-dimensional disturbances in the homogeneous one-layer case, namely by Lee (1985) for two-dimensional disturbance and Ertekin (1984) for three-dimensional disturbance. Also there have been some theoretical investigations on

this phenomenon (see Huang et al. (1982), Akylas (1984), Cole (1985), Mei (1986) and Wu (1984, 1986)).

Recently, Grimshaw & Smyth (1985) investigated the flow of a stratified fluid over localized topography and obtained a forced KdV equation to model the generation and evolution of internal waves by uneven bottoms. From their forced KdV equation they showed solitons were generated ahead of the disturbance in resonant cases.

The main objective of this thesis is to study the runaway soliton phenomenon in stratified fluid systems theoretically, numerically and experimentally. It is expected to find some new behaviors as well as similar behaviors to those already known for the homogeneous one-layer case. The second objective is to develop some theoretical models for investigating weakly nonlinear and weakly dispersive internal waves in inviscid and incompressible stratified fluid systems, which may be useful for solving other related problems such as internal wave interactions, in addition to the runaway soliton problem.

The first theoretical model developed belongs to the Boussinesq class which allows waves to propagate in all directions through a two-layer fluid system having a free top surface. The second model belongs to the Korteweg-de Vries class, which describes waves propagating in one direction for two-layer fluid systems with a free top surface. The third and fourth models belong to the Boussinesq class and the Korteweg-de Vries class, respectively, both for two-layer fluid systems covered by a rigid horizontal top surface. The fifth model is the forced KdV equation for continuously stratified fluid systems with a free top surface or a rigid horizontal top surface.

Two very general types of external forcing disturbances are considered. A system may have an undular bottom in motion, as is admissible to all the models, and pressure disturbances can be applied on the top surface in the models applicable to systems having a free top surface. Disturbances should be small since our models are not fully nonlinear.

Several numerical schemes for solving the basic equations of each model have been developed and the numerical results will be discussed in Chapter VIII. Experiments were done with fresh water forming the upper layer and brine the lower layer. The external forcing was provided by a bottom bump, which has a circular-arc top surface and flat bottom surface, which can be driven to move along the floor of a water tank with a uniform velocity, started impulsively from rest. From the numerical results of the various theoretical models and the experimental results it is found that when a disturbance moves horizontally at a constant transcritical velocity through a stratified fluid, a sequence of solitons are generated, one after another to surge ahead of the disturbance. For a two-layer fluid system, there are two characteristic velocities, c_s for the slow mode and c_f for the fast mode, which can be determined on the linear theory or on the lowest order results of weakly nonlinear theory. When the density difference of the two layers is small, c_f is nearly equal to the characteristic velocity of the homogeneous one-layer system (as if the density is uniform), whereas c_s is much smaller than c_f; in fact, $\frac{c_s}{c_f} = O((1-\sigma)^{1/2})$, where σ is the density ratio of the upper to the lower layer. In the fast mode, when the velocity of the moving disturbance is near c_f, wave behaviors are

almost the same as those in the homogeneous one-layer case with the amplitude of top surface larger than that of interface. In the slow mode, when the velocity of the moving disturbance is near c_s, which is the case of our main interest, waves along the interface are much greater than those on the top surface, a picture very much like the behavior of internal waves found in the field observations. Because of this similarity, the slow mode is sometimes called the internal wave mode and the fast mode, the top-surface wave mode. The theoretical model for continuously stratified fluid systems is developed with the intention of modeling our experiments more accurately since water and brine are miscible and mass diffusion is inevitable in our experiments. There are infinitely many modes of wave motions in every continuously stratified fluid systems. For the free top surface case, the first mode (with the largest characteristic velocity and with no zero point in its characteristic function within the depth range of the system) is similar to the previous top surface wave mode and the second mode (with the next largest characteristic velocity and only one zero point in its characteristic function in the depth range of the system) is similar to the internal wave mode of a two-layer fluid system just mentioned. In fact, the two-layer stratification is a close approximation of the situation in our experiment, which consists of two regions of very slowly varying density connected by a region of fast density variation. The numerical results of the theoretical models explored and the experimental results all exhibited the phenomenon of internal soliton generation by disturbances moving with CONSTANT velocity in both two-layer systems and continuously

stratified fluid systems whether the top surface is free or covered by a rigid horizontal plate. The relationship between the amplitude and generation period of internal runaway solitons, and the velocity and size of forcing distributions, and the background density profile will be discussed in Chapter VIII.

A summary of the contents of this thesis can be given as follows. In Chapter II, a system of basic equations of the Boussinesq class is derived for two-layer systems with a free top surface following a similar procedure as that developed by Wu (1979), originally for homogeneous one-layer systems. To provide a method of solution based on this generalized Boussinesq model, a numerical scheme consisting of two-step finite differencing is presented in Chapter III. In Chapter IV, the forced KdV model is developed for the cases considered in Chapter II by using the 2-timing perturbation method, followed by providing a numerical scheme specially designed for using this model. Chapter V is concerned with two-layer systems with a rigid horizontal top surface. First, a model of the Boussinesq class is developed following a procedure similar to that used in Chapter II, for which a numerical scheme is derived. Secondly, the forced KdV model is derived for this case by applying the perturbation method after that introduced by Gardner & Morikawa (1960). The theoretical internal wave model for systems with continuous stratification is derived in Chapter VI by applying the mass conservation principle and the momentum equations of the system. The experimental aspects are presented in Chapter VII. All the results, theoretical, numerical and experimental, are discussed in Chapter VIII and in the last chapter.

II. WEAKLY NONLINEAR LONG-WAVE MODEL IN TWO-LAYER SYSTEMS

The equations of motion for weakly nonlinear and weakly dispersive long waves propagating in a two-layered fluid system with external forcing, such as a moving surface pressure distribution or a changing bottom topography, are derived from the layer-mean Bernoulli equations and the mass conservation principle. The resulting equations are (3.1)-(3.4), which present a FOUR-equation model of the generalized Boussinesq class. Some numerical solutions will be presented later.

2.1 Basic Equations

The first class of fluid systems which we consider here consists of two layers of immiscible incompressible fluids under the action of gravity and external forcing disturbances. The density of the upper layer, ρ_1, is less than that of the lower layer, ρ_2, so that the system can maintain a stable equilibrium with respect to small disturbances. When at rest, the upper layer has a uniform depth h_1 and the depth of the lower layer, h_2, may be a function of space and possibly time when the bottom is in motion. (cf. Figure 2.1).

Both fluids are assumed to be inviscid and the flow irrotational so that a velocity potential, ϕ, exists. In addition, the effects of surface tension are neglected.

In the analysis of the generation of weakly nonlinear and weakly dispersive long waves by moving disturbances and the subsequent evolution of these waves, two small parameters are of importance;

one measures the nonlinear effects of relative order

$$\alpha = \frac{a}{h_o} \quad , \tag{2.1}$$

where a is a typical wave amplitude with reference to the total liquid depth h_o and the other parameter gives a measure of the relative order of the dispersive effects

$$\epsilon = \frac{h_o}{\lambda} \quad , \tag{2.2}$$

where λ is a representative wavelength. Both parameters are assumed small. The ratio

$$Ur = \frac{\alpha}{\epsilon^2} = \frac{a\lambda^2}{h_o^3} \quad ,$$

called the Ursell number, gives a measure of the comparative importance of the nonlinear and dispersive effects. For $Ur \ll 1$, the model belongs to the class of linear theory; for $Ur \gg 1$, it belongs to the Airy class in which the nonlinear effects predominate; and for $Ur = 0(1)$, it belongs to the Boussinesq class (Ursell (1953)). In the Boussinesq class, nonlinear effects balance the dispersive effects so that solitary waves and cnoidal waves are possible. In the present investigation, we assume

$$Ur = O(1)$$

i.e. $\alpha = O(\epsilon^2)$.

For the irrotational flow of inviscid fluids occurring in the gravitational field, Bernoulli's equation holds, separately, for both upper and lower layers, namely,

$$\frac{p}{\rho} + \frac{\partial \phi}{\partial t} + \frac{1}{2} \underline{U}^2 + gz = 0 \ , \tag{2.3}$$

where p is the pressure, $\underline{U}$ is the fluid velocity and z the vertical coordinate.

The transport theorem, equation (7) in Wu (1979), is valid for any material layer of a homogeneous fluid — that is, any layer between two material surfaces, say $z_1(x, y, t)$ and $z_2(x, y, t)$ (x, y are the horizontal Cartesian coordinates), each consisting always of the same material (fluid particles) throughout the motion. The theorem states that

$$\left[\frac{df}{dt}\right] = \frac{\partial}{\partial t} [f] + \nabla \cdot [\underline{u} f] \ , \tag{2.4}$$

where $f(x, y, z, t)$ is any flow quantity, $\underline{u} = (u, v)$ is the horizontal projection of the velocity vector, $\nabla = (\frac{\partial}{\partial x}, \frac{\partial}{\partial y})$ is the corresponding two-dimensional vector operator and

$$[F] = \int_{z_1(x, y, t)}^{z_2(x, y, t)} F(x, y, z, t) dz = (z_2 - z_1)\overline{F} \ , \tag{2.5}$$

is the integral of a quantity F across the vertical range of the material layers $z_1 < z < z_2$ at a fixed horizontal position $\underline{r} = (x, y)$ and at a fixed time t, and $\overline{F}$ is the average value of F over the vertical layer. df/dt denotes the material derivative.

If f is taken as $f = 1$ and $f = \underline{u}$ within each of the layers, the transport theorem gives the following equations:

$$\dot{\eta}_1 + \nabla \cdot (\eta_1 \bar{\underline{u}}_1) = 0 \quad , \tag{2.6}$$

$$\dot{\eta}_2 + \nabla \cdot (\eta_2 \bar{\underline{u}}_2) = 0 \quad , \tag{2.7}$$

$$(\eta_1 \bar{\underline{u}}_1)_t + \nabla \cdot (\eta_1 \overline{\underline{u}_1 \underline{u}_1}) = -\frac{1}{\rho_1} \eta_1 \overline{\nabla p_1} \quad ,$$

$$(\eta_2 \bar{\underline{u}}_2)_t + \nabla \cdot (\eta_2 \overline{\underline{u}_2 \underline{u}_2}) = -\frac{1}{\rho_2} \eta_2 \overline{\nabla p_2} \quad ,$$

where subscripts 1 and 2 denote quantities for the upper and the lower layers, respectively, and the partial differentiation with respect to time t is denoted by a subscript t or, alternatively, by an overhead dot sign, such as those in equations (2.6) and (2.7). η_1 and η_2 are the total depths of the individual layers. If ζ_1 and ζ_2 denote the displacements of the top surface and the interface relative to their undisturbed levels (cf. Figure 2.1), we have

$$\eta_1 = h_1 + \zeta_1 - \zeta_2 \quad , \tag{2.8}$$

$$\eta_2 = h_2 + \zeta_2 \quad . \tag{2.9}$$

The conditions of irrotationality and incompressibility result in Laplace's equation

$$\nabla^2 \phi + \frac{\partial^2}{\partial z^2} \phi = 0 \quad , \tag{2.10}$$

which applies everwhere in the upper layer for the potential ϕ_1, and in the lower layer for the potential ϕ_2, and where $\nabla^2 = \frac{\partial^2}{\partial x^2} + \frac{\partial^2}{\partial y^2}$.

2.2 Boundary Conditions

For the two-layer system six boundary conditions are required: two for the top surface, one for the bottom surface and three for the interface between the two layers.

Taking gravity in the negative z direction and the undisturbed position of the top surface at $z = 0$, the kinematic and dynamic boundary conditions are applied at the top surface and give

$$w = (\frac{\partial}{\partial t} + \underline{u}_1 \cdot \nabla)\zeta_1 \qquad \text{at } z = \zeta_1(x, y, t) \qquad (2.11)$$

and

$$p = p_o(x, y, t) \qquad \text{at } z = \zeta_1(x, y, t) \qquad (2.12)$$

where p_o is the external pressure applied at the top surface and w is the component of fluid velocity in the z direction.

The kinematic boundary condition at the bottom is

$$w = -(\frac{\partial}{\partial t} + \underline{u}_2 \cdot \nabla)h_2 \qquad \text{at } z = -h_1 - h_2(x, y, t) \ . \qquad (2.13)$$

The kinematic and dynamic boundary conditions at the interface are

$$w_1 = \frac{\partial \zeta_2}{\partial t} + \underline{u}_1 \cdot \nabla\zeta_2 \qquad \text{at } z = \zeta_2 - h_1 \ , \qquad (2.14)$$

$$w_2 = \frac{\partial \zeta_2}{\partial t} + \underline{u}_2 \cdot \nabla\zeta_2 \qquad \text{at } z = \zeta_2 - h_1 \ , \qquad (2.15)$$

and

$$p_1 = p_2 \qquad \text{at } z = \zeta_2 - h_1 \ . \qquad (2.16)$$

where w_1 is the vertical velocity in the upper layer and w_2 in the lower layer.

2.3 The Dimensionless Form

The same dimensionless variables (with one exception for pressure) as those used in Wu (1979, equation 21) for the single-layer homogeneous system are adopted here for the two-layer system (as well as for the continuously stratified fluid system to be considered later). In the following "*" indicates a dimensionless variable, λ is a characteristic wavelength, and $c = \sqrt{gh_o}$ is a typical wave speed for the homogeneous-fluid-layer case (g is the gravitational acceleration).

The horizontal coordinates are nondimensionalized by λ, z and all depths or surface elevations are nondimensionalized by h_o, the time is scaled by $\frac{\lambda}{c}$ and ϕ by $c\lambda$. Thus

$$(x^*, y^*) = \frac{(x, y)}{\lambda} \qquad (z^*, h^*, \eta^*, \zeta^*) = (z, h, \eta, \zeta)/h_o \ ,$$

$$t^* = \frac{ct}{\lambda} \ , \quad (u^*, v^*, w^*) = (u, v, w)/c, \quad \phi^* = \frac{\phi}{c\lambda} \ . \tag{2.17}$$

Because the density is different for each layer, we take the nondimensionalization of the pressure as

$$p_1^* = \frac{p_1}{\rho_1 g h_o} \qquad \text{for the upper layer,}$$

and

$$p_2^* = \frac{p_2}{\rho_2 g h_o} \qquad \text{for the lower layer.} \tag{2.18}$$

Substituting (2.17) and (2.18) into (2.10) and (2.3) and immediately omitting the superscript *, we obtain the Laplace equation:

$$\frac{\partial^2 \phi}{\partial z^2} = -\epsilon^2 \nabla^2 \phi \ , \tag{2.19}$$

and Bernoulli's equation:

$$p + \dot{\phi} + \frac{1}{2}\underline{U}^2 + z = 0 \ , \tag{2.20}$$

with suffix 1 (for the upper layer) and suffix 2 (for the lower layer) respectively.

Equations (2.6) and (2.7) remain the same as before, namely,

$$\begin{aligned} \dot{\eta}_1 + \nabla\cdot(\eta_1\overline{\underline{u}_1}) &= 0 \ , \\ \dot{\eta}_2 + \nabla\cdot(\eta_2\overline{\underline{u}_2}) &= 0 \ . \end{aligned} \tag{2.21}$$

The boundary conditions now become as follows:

$$p = p_o \qquad \text{at } z = \zeta_1(x, y, t) \quad \text{(top surface)}, \tag{2.22}$$

$$w = \epsilon\frac{d\zeta_1}{dt} \qquad \text{at } z = \zeta_1 \ , \tag{2.23}$$

$$\begin{aligned} w_1 &= \epsilon\left(\frac{\partial\zeta_2}{\partial t} + \underline{u}_1\cdot\nabla\zeta_2\right) \qquad \text{at } z = \zeta_2 - h_1 \ , \\ w_2 &= \epsilon\left(\frac{\partial\zeta_2}{\partial t} + \underline{u}_2\cdot\nabla\zeta_2\right) \qquad \text{at } z = \zeta_2 - h_1 \ , \end{aligned} \tag{2.24}$$

$$p_2 = \sigma p_1 \qquad \text{at } z = \zeta_2 - h_1 \ , \tag{2.25}$$

$$w = -\epsilon\frac{dh_2}{dt} \qquad \text{at } z = -h_1 - h_2 \ \text{(bottom)} \ , \tag{2.26}$$

where σ is the density ratio

$$\sigma = \frac{\rho_1}{\rho_2} \ . \tag{2.27}$$

For the equilibrium of a two-layer system to be stable, we require that

$$0 < \sigma < 1.$$

In addition, the dimensionless velocity components are given by

$$\underline{u} = \nabla\phi \quad , \tag{2.28}$$

$$w = \frac{1}{\epsilon} \frac{\partial\phi}{\partial z} \quad . \tag{2.29}$$

With the small amplitude assumption and the relations between the variables involved, the following order estimates and assumptions appear to be consistent for both the upper and lower layers:

$$\begin{aligned} \zeta &= O(\alpha) \ , \\ \underline{u} &= O(\alpha) \ , \\ w &= O(\alpha\epsilon) \ , \\ h_2 &= H_2 - d \ \text{ with } \ H_2 = \text{const} \ \text{ and } \ d = O(\alpha) \ . \end{aligned} \tag{2.30}$$

Notice the last formula, which implies small variations of the bottom topography in order to maintain the wave amplitude small in the problem formulated.

2.4 The Series Expansion

An expansion of the following form is assumed for each layer:

$$\phi = \alpha \sum_{n=o}^{\infty} \epsilon^{2n} \Phi_{(2n)} (\underline{r}, z, t) \quad . \tag{2.31}$$

Upon substituting (2.31) in (2.19), the $\Phi_{(2n)}$'s are obtained in the form

$$\Phi_{(o)} = \varphi_{(o)} (\underline{r}, t) \quad , \tag{2.32}$$

$$\Phi_{(2)} = \varphi_{(2)} (\underline{r}, t) + z\varphi_{(3)}(\underline{r}, t) - \frac{1}{2} z^2 \nabla^2 \varphi_{(o)} \quad , \tag{2.33}$$

and so on, the linear term of z in $\Phi_{(o)}$ is deleted because $\Phi_{(o)z} = 0$ as a consequence of the bottom boundary condition (2.26), the interface boundary condition (2.24), the assumption $d = O(\alpha)$ and the relation (2.29).

Accordingly, we have for $\underline{u}$ and w the expansions

$$\underline{u} = \nabla\phi = \alpha[\underline{u}_{(o)} + \epsilon^2 \underline{u}_{(1)} + \epsilon^4 \underline{u}_{(2)} + \dots] \quad , \tag{2.34}$$

$$w = \frac{1}{\epsilon} \frac{\partial \phi}{\partial z} = \alpha\epsilon \, [w_{(1)} + \epsilon^2 w_{(2)} + \dots] \quad , \tag{2.35}$$

with the relations

$$\underline{u}_{(o)} = \nabla \varphi_{(o)}(\underline{r}, t) = \alpha^{-1} \nabla \overline{\phi} + O(\epsilon^2) \quad , \tag{2.36}$$

$$u_{(1)} = \nabla \Phi_{(2)} \quad , \tag{2.37}$$

$$w_{(1)} = \frac{\partial \Phi_{(2)}}{\partial z} = \varphi_{(3)} - z \nabla^2 \varphi_{(o)} \, . \tag{2.38}$$

Substituting the above expansion for w into the bottom boundary condition (2.26), $\varphi_{(3)}$ of the lower layer is determined as

$$\varphi_{2(3)} = -\dot{h}_2 \alpha^{-1} - (h_1 + H_2) \nabla^2 \varphi_{2(o)} \quad , \tag{2.39}$$

where the order estimate of $d = O(\alpha)$ has been used and φ_2 is the φ for the lower layer and similar notations are used for other quantities.

To obtain $\varphi_{(3)}$ for the upper layer, the interface boundary conditions must be used. In fact, the difference between the two equations in (2.24) yields

$$w_1 - w_2 = \epsilon (\underline{u}_1 - \underline{u}_2) \cdot \nabla \zeta_2 = O(\alpha^2 \epsilon) \quad \text{at} \quad z = \zeta_2 - h_1 \ . \tag{2.40}$$

which indicates that the interface is a vortex sheet in general, with a velocity jump aligned with the interface. Since $\varphi_{(o)}, \varphi_{(1)}, \varphi_{(3)}$ are independent of z, the following formula for $\varphi_{1(3)}$ can be obtained upon substituting the expansions for w into (2.40):

$$\varphi_{1(3)} = -\dot{h}_2 \alpha^{-1} - h_1 \nabla^2 \varphi_{1(o)} - H_2 \nabla^2 \varphi_{2(o)} \ . \tag{2.41}$$

2.5 The Layer-mean Bernoulli Equations

At the top surface and the interface Bernoulli's equation (2.20) provides the following relations:

$$p_o + \zeta_1 + \hat{\dot{\phi}}_1 + \frac{1}{2} (\hat{\underline{u}} \cdot \hat{\underline{u}} + \hat{w}^2) = 0 \ , \tag{2.42}$$

$$\tilde{p}_1 + \tilde{\dot{\phi}}_1 + \frac{1}{2} (\tilde{\underline{u}} \cdot \tilde{\underline{u}} + \tilde{w}^2)_1 + \zeta_2 - h_1 = 0 \ , \tag{2.43}$$

$$\tilde{p}_2 + \tilde{\dot{\phi}}_2 + \frac{1}{2} (\tilde{\underline{u}} \cdot \tilde{\underline{u}} + \tilde{w}^2)_2 + \zeta_2 - h_1 = 0 \ , \tag{2.44}$$

where a "$\hat{\ }$" above a variable denotes the quantity is evaluated at the top surface and a "$\sim$" denotes evaluation at the interface. From these equations we obtain the following relations:

$$\bar{\dot{\phi}}_1 + \frac{1}{2} (\nabla \bar{\phi}_1)^2 + \zeta_1 + p_o = \bar{\dot{\phi}}_1 + \frac{1}{2} (\nabla \bar{\phi}_1)^2 - \hat{\dot{\phi}}_1 - \frac{1}{2} (\hat{\underline{u}} \cdot \hat{\underline{u}} + \hat{w}^2) \ , \tag{2.45}$$

$$\bar{\dot{\phi}}_1 + \frac{1}{2} (\nabla \bar{\phi}_1)^2 + \zeta_2 + \tilde{p}_1 = \bar{\dot{\phi}}_1 + \frac{1}{2} (\nabla \bar{\phi}_1)^2 - \tilde{\dot{\phi}}_1 - \frac{1}{2} (\tilde{\underline{u}} \cdot \tilde{\underline{u}} + \tilde{w}^2)_1 + h_1 \ , \tag{2.46}$$

$$\dot{\bar{\phi}}_2 + \frac{1}{2}(\nabla\bar{\phi}_2)^2 + \zeta_2 + \tilde{p}_2 = \dot{\bar{\phi}}_2 + \frac{1}{2}(\nabla\bar{\phi}_2)^2 - \dot{\tilde{\phi}}_2 - \frac{1}{2}(\tilde{\underline{u}}\cdot\tilde{\underline{u}} + \tilde{w}^2)_2 + h_1 , \tag{2.47}$$

where $\dot{\bar{\phi}}$ means $\frac{\partial\bar{\phi}}{\partial t}$.

By using the expansion of the potential to cancel the lower order terms on the right hand side of the above equations and by taking the average across the depth and subtracting, the following equations result:

$$\dot{\bar{\phi}}_1 + \frac{1}{2}(\nabla\bar{\phi}_1)^2 + \zeta_1 + p_o = \alpha\epsilon^2(-\frac{h_1}{2}\dot{\varphi}_{1(3)} - \frac{1}{6}h_1^2\nabla^2\dot{\varphi}_{1(o)}) + O(\alpha^2\epsilon^2, \alpha\epsilon^4), \tag{2.48}$$

$$\dot{\bar{\phi}}_1 + \frac{1}{2}(\nabla\bar{\phi}_1)^2 + \zeta_2 + \tilde{p}_1 = h_1 + \alpha\epsilon^2[\frac{h_1}{2}\dot{\varphi}_{1(3)} + \frac{1}{3}h_1^2\nabla^2\dot{\varphi}_{1(o)}] + O(\alpha^2\epsilon^2, \alpha\epsilon^4), \tag{2.49}$$

$$\dot{\bar{\phi}}_2 + \frac{1}{2}(\nabla\bar{\phi}_2)^2 + \zeta_2 + \tilde{p}_2 = h_1 + \alpha\epsilon^2[-\frac{H_2}{2}\dot{\varphi}_{2(3)} - \frac{1}{2}(h_1H_2 + \frac{1}{3}H_2^2)\nabla^2\dot{\varphi}_{2(o)}] + O(\alpha^2\epsilon^2, \alpha\epsilon^4) , \tag{2.50}$$

in which (2.30) and the following relations have been used

$$\bar{z}_1 = -\frac{h_1}{2} + O(\alpha) ,$$

$$\bar{z}_2 = -h_1 - \frac{H_2}{2} + O(\alpha) ,$$

$$\overline{z_1^2} = \frac{1}{3}h_1^2 + O(\alpha) ,$$

$$\overline{z_2^2} = h_1^2 + h_1H_2 + \frac{1}{3}H_2^2 + O(\alpha) ,$$

which are readily derived using the definition (2.5) for $\overline{F}$ and the assumption (2.30). Here the subscript 1 or 2 for $\overline{z}$ and $\overline{z^2}$ signifies the depth average being taken across the upper or the lower layer.

Substituting the expression for $\varphi_{(3)}$ (equations (2.39) and (2.41)) into (2.48), (2.49) and (2.50) and using the relation (2.36), we obtain the following:

$$\dot{\overline{\phi}}_1 + \frac{1}{2}(\nabla\overline{\phi}_1)^2 + \zeta_1 + p_o = \epsilon^2\{\frac{h_1}{2}\frac{\partial}{\partial t}[\dot{h}_2 + h_1\nabla^2\overline{\phi}_1 + H_2\nabla^2\overline{\phi}_2] - \frac{1}{6}h_1^2\frac{\partial}{\partial t}\nabla^2\overline{\phi}_1\} + O(\alpha\epsilon^4, \alpha^2\epsilon^2) \quad , \tag{2.51}$$

$$\dot{\overline{\phi}}_1 + \frac{1}{2}(\nabla\overline{\phi}_1)^2 + \zeta_2 + \widetilde{p}_1 = h_1 + \epsilon^2\{-\frac{h_1}{2}\frac{\partial}{\partial t}[\dot{h}_2 + h_1\nabla^2\overline{\phi}_1 + H_2\nabla^2\overline{\phi}_2] + \frac{1}{3}h_1^2\frac{\partial}{\partial t}\nabla^2\overline{\phi}_1\} + O(\alpha\epsilon^4, \alpha^2\epsilon^2) \quad , \tag{2.52}$$

$$\dot{\overline{\phi}}_2 + \frac{1}{2}(\nabla\overline{\phi}_2)^2 + \zeta_2 + \widetilde{p}_2 = h_1 + \epsilon^2\{\frac{H_2}{2}\frac{\partial}{\partial t}[\dot{h}_2 + (h_1 + H_2)\nabla^2\overline{\phi}_2] - \frac{H_2}{2}(h_1 + \frac{1}{3}H_2)\frac{\partial}{\partial t}\nabla^2\overline{\phi}_2\} + O(\alpha\epsilon^4, \alpha^2\epsilon^2) \quad . \tag{2.53}$$

Finally, by making use of (2.25), $\widetilde{p}_2 = \sigma\widetilde{p}_1$, $\widetilde{p}_1$ and $\widetilde{p}_2$ can be eliminated from (2.53) - σ · (2.52), giving

$$\frac{\partial}{\partial t}(\sigma\overline{\phi}_1 - \overline{\phi}_2) + \frac{1}{2}\sigma(\nabla\overline{\phi}_1)^2 - \frac{1}{2}(\nabla\overline{\phi}_2)^2 + (\sigma - 1)\zeta_2 = \tag{2.54}$$

$$(\sigma - 1)h_1 + \epsilon^2\sigma\{-\frac{h_1}{2}\frac{\partial}{\partial t}[\dot{h}_2 + h_1\nabla^2\overline{\phi}_1 + H_2\nabla^2\overline{\phi}_2] + \frac{1}{3}h_1^2\nabla^2\dot{\overline{\phi}}_1\}$$

$$-\epsilon^2\{\frac{H_2}{2}\frac{\partial}{\partial t}[\dot{h}_2 + (h_1 + H_2)\nabla^2\overline{\phi}_2] - \frac{H_2}{2}(h_1 + \frac{1}{3}H_2)\nabla^2\dot{\overline{\phi}}_2\} + O(\alpha\epsilon^4, \alpha^2\epsilon^2).$$

Thus, the layer-mean Bernoulli equations (2.51) and (2.54) have been obtained, which will be used later for numerical calculations. There are four unknowns here, namely ζ_1, ζ_2, $\overline{\phi}_1$ and $\overline{\phi}_2$. Two additional equations are needed; they are furnished by invoking the principle of conservation of mass for each layer as given below.

Because the velocity potentials are determinate up to an arbitrary function of time, the first term on the right hand side of (2.54), which is a constant, can be absorbed into the potentials. Consequently, this constant term will be omitted in the sequel; this procedure is found to further facilitate application of the open boundary condition used in our numerical computation of the solution.

2.6 Mass Conservation

The conservation of mass in each layer is assured by equation (2.21), which can be written as

$$\dot{\zeta}_1 + \nabla \cdot [(\zeta_1 + h_1 - \zeta_2) \nabla \overline{\phi}_1] = \dot{\zeta}_2 + O(\alpha\epsilon^4, \alpha^2\epsilon^2) \ , \qquad (2.55)$$

$$\dot{\zeta}_2 + \nabla \cdot [(\zeta_2 + h_2) \nabla \overline{\phi}_2] = -\dot{h}_2 + O(\alpha\epsilon^4, \alpha^2\epsilon^2) \ , \qquad (2.56)$$

where the following relations have been used:

$$\overline{\nabla\phi_1} - \nabla\overline{\phi}_1 = O(\alpha\epsilon^4, \alpha^2\epsilon^2)$$

$$\overline{\nabla\phi_2} - \nabla\overline{\phi}_2 = O(\alpha\epsilon^4, \alpha^2\epsilon^2)$$

as can be readily deduced from the expansion expressions for the potentials, the expressions of $\varphi_{(3)}$ and the order estimate for d.

This completes the formulation of the problem. We now have

four equations (2.51), (2.54), (2.55) and (2.56) for four unknowns ζ_1, ζ_2, $\overline{\phi}_1$ and $\overline{\phi}_2$. The system of equations describes the evolution of weakly nonlinear and weakly dispersive long waves and is capable of describing three-dimensional waves. The bottom of the fluid system can be variable and in motion and an unsteady external pressure may act at the top surface.

III. NUMERICAL METHOD

In this chapter, a numerical scheme using finite differencing is developed for solving the set of basic equations presented in the last chapter.

For convenience, the bar over ϕ will be omitted in the sequel and the four equations to be solved are rewritten as follows:

CONTINUITY EQUATIONS:

$$\dot{\zeta}_1 + \nabla \cdot [(\zeta_1 + h_1 - \zeta_2)\nabla\phi_1] = \dot{\zeta}_2 + O(\alpha\epsilon^4, \alpha^2\epsilon^2) \ , \tag{3.1}$$

$$\dot{\zeta}_2 + \nabla \cdot [(\zeta_2 + h_2)\nabla\phi_2] = -\dot{h}_2 + O(\alpha\epsilon^4, \alpha^2\epsilon^2) \ , \tag{3.2}$$

LAYER-MEAN BERNOULLI EQUATIONS:

$$\dot{\phi}_1 + \frac{1}{2}(\nabla\phi_1)^2 + \zeta_1 + p_o = \epsilon^2\{\frac{h_1}{2}\frac{\partial}{\partial t}[\dot{h}_2 + H_2\nabla^2\phi_2] + \frac{1}{3}h_1^2\nabla^2\dot{\phi}_1\} + O(\alpha\epsilon^4, \alpha^2\epsilon^2) \ , \tag{3.3}$$

$$\sigma\dot{\phi}_1 - \dot{\phi}_2 + \frac{1}{2}\sigma(\nabla\phi_1)^2 - \frac{1}{2}(\nabla\phi_2)^2 + (\sigma-1)\zeta_2 = -\frac{1}{2}\epsilon^2(h_1\sigma + H_2)\ddot{h}_2 - \frac{1}{6}\epsilon^2\sigma h_1^2\nabla^2\dot{\phi}_1 + \frac{1}{2}\epsilon^2 H_2(-\frac{2}{3}H_2 - h_1\sigma)\nabla^2\dot{\phi}_2 + O(\alpha\epsilon^4, \alpha^2\epsilon^2) \ , \tag{3.4}$$

where the first constant term on the right hand side of (2.54) has been combined into the potentials.

For further reference, the four equations (3.1)-(3.4) will be called the FOUR-equation model, there being four unknowns: ζ_1, ζ_2, ϕ_1 and ϕ_2.

3.1 Finite Difference Scheme

A finite difference method is developed for solving the four equations (3.1)-(3.4). In advancing ζ and ϕ at every time step, the improved Euler-Cauchy method following a two-step predictor-corrector procedure is applied. This scheme is similar to that employed by Wu & Wu (1982), but is considerably more complicated because there are twice as many unknowns and twice as many equations involved in the present two-layer case as compared with the homogeneous single-layer case. In addition, a direct method of solving the resulting linear algebraic equations, which are formed from the implicit scheme for solving the two layer-mean Bernoulli equations, is used rather than the iteration method used in the earlier study.

The spatial derivatives are approximated by central differences. More specifically, we consider the time interval Δt between time $t = k\Delta t$ and time $t = (k+1)\Delta t$. The quantities to be calculated at time level $k+1$ are first replaced by the provisional values at the provisional level $\overline{k+1}$ given by the predictor scheme. Then they are changed to new values at the next time level $k+1$ given by the corrector, as depicted by the following diagram:

$$(\cdot)^{k} \xrightarrow{\text{predictor}} (\cdot)^{\overline{k+1}} \xrightarrow{\text{corrector}} (\cdot)^{k+1} .$$

where $(\cdot)^{k}$ denotes a quantity at time level k. Thus, the time derivatives are approximated by the difference between the quantities at the time-levels k and $\overline{k+1}$ for the predictor stage and those at time-levels k and $k+1$ for the corrector stage.

All spatial derivatives (without time differentiation), are known from the previous time-step calculation. The time-level k values are taken for the predictor stage and the average of the time-level k and time-level $\overline{k+1}$ values are taken for the corrector stage.

The terms with time and space cross derivatives are approximated by the values at the corresponding time levels, i.e., by the time-level k and time-level $\overline{k+1}$ for the predictor stage and by the time-level k and time-level k+1 for the corrector stage. They are summarized as follows:

	$\frac{\partial(\cdot)}{\partial t}$	$\frac{\partial^n(\cdot)}{\partial x^n}$ (n = 0, 1, 2), $\frac{\partial^3}{(\partial x^2 \partial t)}$ and $\ddot{h}_2$
predictor	$\overline{k+1}$, k	k
corrector	k+1, k	$\frac{1}{2}$ ([k] + [$\overline{k+1}$])

Although this theoretical model (in the homogeneous single-layer case) has been applied to two-dimensional cases by Wu & Wu (1982) and Lee (1985) and to three-dimensional cases by Lepelletier (1981) and Schember (1982), all the calculations in this thesis will be done for the two-dimensional case involving the horizontal coordinate x and the vertical coordinate z.

In summary, the present numerical scheme of approximating the equations (3.1)-(3.4) is listed below in the conventional notation: a subscript i denotes the i-th x position and the superscripts denote the various time levels as defined above. In these equations the error terms of $O(\alpha\epsilon^4, \alpha^2\epsilon^2)$ are neglected.

PREDICTOR STAGE:

(3.2):

$$\overline{\zeta^{k+1}_{2,i}} = \zeta^{k}_{2,i} + h^{k}_{2,i} - h^{k+1}_{2,i} - \frac{\Delta t}{\Delta x^2}\left[\frac{1}{4}(\zeta^{k}_{2,i+1} - \zeta^{k}_{2,i-1} + h^{k}_{2,i+1} - h^{k}_{2,i-1})\right.$$

$$\left.(\phi^{k}_{2,i+1} - \phi^{k}_{2,i-1}) + (\zeta^{k}_{2,i} + h^{k}_{2,i})(\phi^{k}_{2,i-1} + \phi^{k}_{2,i+1} - 2\phi^{k}_{2,i})\right] , \tag{3.5}$$

(3.1):

$$\overline{\zeta^{k+1}_{1,i}} = \zeta^{k}_{1,i} + \overline{\zeta^{k+1}_{2,i}} - \zeta^{k}_{2,i} - \frac{\Delta t}{\Delta x^2}\left[\frac{1}{4}(\zeta^{k}_{1,i+1} - \zeta^{k}_{1,i-1} - \zeta^{k}_{2,i+1} + \zeta^{k}_{2,i-1})\right.$$

$$\left.(\phi^{k}_{1,i+1} - \phi^{k}_{1,i-1}) + (\zeta^{k}_{1,i} - \zeta^{k}_{2,i} + h_1)(\phi^{k}_{1,i-1} + \phi^{k}_{1,i+1} - 2\phi^{k}_{1,i})\right] , \tag{3.6}$$

(3.3):

$$-\frac{1}{3}\epsilon^2 h_1^2 \overline{\phi^{k+1}_{1,i-1}} - \frac{1}{2}\epsilon^2 h_1 H_2 \overline{\phi^{k+1}_{2,i-1}} + (\Delta x^2 + \frac{2}{3}\epsilon^2 h_1^2)\phi^{k+1}_{1,i}$$

$$+ \epsilon^2 h_1 H_2 \overline{\phi^{k+1}_{2,i}} - \frac{1}{3}\epsilon^2 h_1^2 \overline{\phi^{k+1}_{1,i+1}} - \frac{1}{2}\epsilon^2 h_1 H_2 \overline{\phi^{k+1}_{2,i+1}} =$$

$$\Delta x^2 \phi^{k}_{1,i} - \Delta t\left[\frac{1}{8}(\phi^{k}_{1,i+1} - \phi^{k}_{1,i-1})^2 + (\zeta^{k}_{1,i} + p^{k}_{o,i})\Delta x^2\right]$$

$$+ \frac{h_1}{2}\epsilon^2 \Delta t \Delta x^2 \ddot{h}^{k}_{2,i} - \frac{1}{3}\epsilon^2 h_1^2(\phi^{k}_{1,i+1} + \phi^{k}_{1,i-1} - 2\phi^{k}_{1,i})$$

$$- \frac{1}{2}\epsilon^2 h_1 H_2(\phi^{k}_{2,i+1} + \phi^{k}_{2,i-1} - 2\phi^{k}_{2,i}) , \tag{3.7}$$

(3.4):

$$\frac{1}{6}\epsilon^2\sigma h_1^2\,\phi^{\overline{k+1}}_{1,i-1} + \epsilon^2 H_2(\frac{1}{3}H_2 + \frac{1}{2}h_1\sigma)\phi^{\overline{k+1}}_{2,i-1} + (\sigma\Delta x^2 - \frac{1}{3}\epsilon^2\sigma h_1^2)\phi^{\overline{k+1}}_{1,i}$$

$$+ [-\Delta x^2 - \epsilon^2 H_2(\frac{2}{3}H_2 + h_1\sigma)]\phi^{\overline{k+1}}_{2,i} + \frac{1}{6}\epsilon^2\sigma h_1^2\,\phi^{\overline{k+1}}_{1,i+1}$$

$$+ \epsilon^2 H_2(\frac{1}{3}H_2 + \frac{1}{2}h_1\sigma)\phi^{\overline{k+1}}_{2,i+1} = [\sigma\phi^k_{1,i} - \phi^k_{2,i} - (\sigma-1)\zeta^k_{2,i}\Delta t]$$

$$\Delta x^2 - \frac{1}{8}\sigma\Delta t(\phi^k_{1,i+1} - \phi^k_{1,i-1})^2 + \frac{1}{8}\Delta t(\phi^k_{2,i+1} - \phi^k_{2,i-1})^2$$

$$+ \frac{1}{6}\epsilon^2\sigma h_1^2(\phi^k_{1,i+1} + \phi^k_{1,i-1} - 2\phi^k_{1,i}) + \epsilon^2 H_2(\frac{1}{3}H_2 + \frac{1}{2}h_1\sigma)$$

$$(\phi^k_{2,i+1} + \phi^k_{2,i-1} - 2\phi^k_{2,i}) - \frac{1}{2}\epsilon^2(h_1\sigma + h^k_{2,i})\Delta t\Delta x^2\ddot{h}_2 \quad , \tag{3.8}$$

CORRECTOR STAGE:

(3.2):

$$\zeta^{k+1}_{2,i} = \zeta^k_{2,i} + h^k_{2,i} - h^{k+1}_{2,i} - \frac{\Delta t}{2\Delta x^2}[\frac{1}{4}(\zeta^k_{2,i+1} - \zeta^k_{2,i-1} + h^k_{2,i+1} - h^k_{2,i-1})$$

$$(\phi^k_{2,i+1} - \phi^k_{2,i-1}) + (\zeta^k_{2,i} + h^k_{2,i})(\phi^k_{2,i-1} + \phi^k_{2,i+1} - 2\phi^k_{2,i})$$

$$+ \frac{1}{4}(\zeta^{\overline{k+1}}_{2,i+1} - \zeta^{\overline{k+1}}_{2,i-1} + h^{k+1}_{2,i+1} - h^{k+1}_{2,i-1})(\phi^{\overline{k+1}}_{2,i+1} - \phi^{\overline{k+1}}_{2,i-1})$$

$$+ (\zeta^{\overline{k+1}}_{2,i} + h^{k+1}_{2,i})(\phi^{\overline{k+1}}_{2,i-1} + \phi^{\overline{k+1}}_{2,i+1} - 2\phi^{\overline{k+1}}_{2,i})] \quad , \tag{3.9}$$

(3.1):

$$\zeta_{1,i}^{k+1} = \zeta_{1,i}^{k} + \zeta_{2,i}^{k+1} - \zeta_{2,i}^{k} - \frac{\Delta t}{2\Delta x^2}\left[\frac{1}{4}(\zeta_{1,i+1}^{k} - \zeta_{1,i-1}^{k} - \zeta_{2,i+1}^{k} + \zeta_{2,i-1}^{k})\right.$$

$$(\phi_{1,i+1}^{k} - \phi_{1,i-1}^{k}) + (\zeta_{1,i}^{k} - \zeta_{2,i}^{k} + h_1)(\phi_{1,i-1}^{k} + \phi_{1,i+1}^{k} - 2\phi_{1,i}^{k})$$

$$+ \frac{1}{4}(\zeta_{1,i+1}^{\overline{k+1}} - \zeta_{1,i-1}^{\overline{k+1}} - \zeta_{2,i+1}^{\overline{k+1}} + \zeta_{2,i-1}^{\overline{k+1}})(\phi_{1,i+1}^{\overline{k+1}} - \phi_{1,i-1}^{\overline{k+1}})$$

$$\left. + (\zeta_{1,i}^{\overline{k+1}} - \zeta_{2,i}^{\overline{k+1}} + h_1)(\phi_{1,i-1}^{\overline{k+1}} + \phi_{1,i+1}^{\overline{k+1}} - 2\phi_{1,i}^{\overline{k+1}})\right] , \qquad (3.10)$$

(3.3):

$$-\frac{1}{3}\epsilon^2 h_1^2 \phi_{1,i-1}^{k+1} - \frac{1}{2}\epsilon^2 h_1 H_2 \phi_{2,i-1}^{k+1} + (\Delta x^2 + \frac{2}{3}\epsilon^2 h_1^2)\phi_{1,i}^{k+1}$$

$$+ \epsilon^2 h_1 H_2 \phi_{2,i}^{k+1} - \frac{1}{3}\epsilon^2 h_1^2 \phi_{1,i+1}^{k+1} - \frac{1}{2}\epsilon^2 h_1 H_2 \phi_{2,i+1}^{k+1} =$$

$$\Delta x^2 \phi_{1,i}^{k} - \frac{1}{2}\Delta t\left[\frac{1}{8}(\phi_{1,i+1}^{k} - \phi_{1,i-1}^{k})^2 + (\zeta_{1,i}^{k} + p_{o,i}^{k})\Delta x^2\right]$$

$$- \frac{1}{2}\Delta t\left[\frac{1}{8}(\phi_{1,i+1}^{\overline{k+1}} - \phi_{1,i-1}^{\overline{k+1}})^2 + (\zeta_{1,i}^{\overline{k+1}} + p_{o,i}^{k+1})\Delta x^2\right]$$

$$+ \frac{1}{4}\epsilon^2 h_1 \Delta t \Delta x^2 (\ddot{h}_{2,i}^{k} + \ddot{h}_{2,i}^{k+1}) - \frac{1}{3}\epsilon^2 h_1^2 (\phi_{1,i+1}^{k} + \phi_{1,i-1}^{k} - 2\phi_{1,i}^{k})$$

$$- \frac{1}{2}\epsilon^2 h_1 H_2 (\phi_{2,i+1}^{k} + \phi_{2,i-1}^{k} - 2\phi_{2,i}^{k}) , \qquad (3.11)$$

(3.4):

$$\frac{1}{6}\epsilon^2\sigma h_1^2\,\phi_{1,i-1}^{k+1} + \epsilon^2 H_2\left(\frac{1}{3}H_2 + \frac{1}{2}h_1\sigma\right)\phi_{2,i-1}^{k+1} + \left(\sigma\Delta x^2 - \frac{1}{3}\epsilon^2\sigma h_1^2\right)\phi_{1,i}^{k+1}$$

$$+ \left[-\Delta x^2 - \epsilon^2 H_2\left(\frac{2}{3}H_2 + h_1\sigma\right)\right]\phi_{2,i}^{k+1} + \frac{1}{6}\epsilon^2\sigma h_1^2\,\phi_{1,i+1}^{k+1}$$

$$+ \epsilon^2 H_2\left(\frac{1}{3}H_2 + \frac{1}{2}h_1\sigma\right)\phi_{2,i+1}^{k+1} =$$

$$(\sigma\phi_{1,i}^{k} - \phi_{2,i}^{k})\Delta x^2 + \frac{1}{2}(\sigma-1)(-\zeta_{2,i}^{k} - \zeta_{2,i}^{\overline{k+1}})\Delta t\Delta x^2 - \frac{1}{16}\sigma\Delta t$$

$$(\phi_{1,i+1}^{k} - \phi_{1,i-1}^{k})^2 - \frac{1}{16}\sigma\Delta t(\phi_{1,i+1}^{\overline{k+1}} - \phi_{1,i-1}^{\overline{k+1}})^2 + \frac{1}{16}\Delta t$$

$$(\phi_{2,i+1}^{k} - \phi_{2,i-1}^{k}) + \frac{1}{16}\Delta t\,(\phi_{2,i+1}^{\overline{k+1}} - \phi_{2,i-1}^{\overline{k+1}})^2 + \frac{1}{6}\epsilon^2\sigma h_1^2$$

$$(\phi_{1,i+1}^{k} + \phi_{1,i-1}^{k} - 2\phi_{1,i}^{k}) + \epsilon^2 H_2\left(\frac{1}{3}H_2 + \frac{1}{2}h_1\sigma\right)(\phi_{2,i+1}^{k} + \phi_{2,i-1}^{k} - 2\phi_{2,i}^{k})$$

$$-\frac{1}{4}\epsilon^2\Delta t\Delta x^2(h_1\sigma + h_{2,i}^{k})\ddot{h}_{2,i}^{k} - \frac{1}{4}\epsilon^2\Delta t\Delta x^2(h_1\sigma + h_{2,i}^{k+1})\ddot{h}_{2,i}^{k+1} \quad .$$

(3.12)

The procedural execution of this numerical scheme can be described as follows. First, for the predictor stage, equations (3.5) and (3.6) can be used directly to obtain the values of $\zeta_{2,i}^{\overline{k+1}}$ and $\zeta_{1,i}^{\overline{k+1}}$. We note that (3.7) and (3.8) are a set of linear algebraic equations for the potentials $\phi_{1,i}^{\overline{k+1}}$ and $\phi_{2,i}^{\overline{k+1}}$ at the provisional level $\overline{k+1}$.

After the computation for the predictor stage is completed, the next four equations (3.9)-(3.12) can be treated similarly for the corrector stage. That is, $\zeta_{1,i}^{k+1}$ and $\zeta_{2,i}^{k+1}$ can be solved directly from (3.9) and (3.10) and $\phi_{1,i}^{k+1}$ and $\phi_{2,i}^{k+1}$ can be solved from (3.11) and (3.12) by using a method of linear algebra, which will be described in the next section.

3.2 Solution of the Linear Algebraic Equations

For definiteness, let us consider a region of calculation with n inner points and 2 boundary points. Assuming that the boundary values are known or can be obtained, e.g., from the calculation for the preceding time level, before solving these equations (this assumption will be relaxed later in the sequel when the boundary conditions are discussed), then equations (3.7) and (3.8) for the predictor stage can be represented in matrix form:

$$[K]\{x\} = \{b\} , \tag{3.13}$$

where the unknown column vector $\{x\}$ is

$$\{x\} = \{\phi_{1,1}, \phi_{2,1}, \phi_{1,2}, \phi_{2,2}, \cdots, \phi_{1,n}, \phi_{2,n}\}^T , \tag{3.14}$$

for the time-level $\overline{k+1}$ (Superscript T in the above expression means transpose and the boundary values are $\phi_{1,o}, \phi_{2,o}, \phi_{1,n+1}$, and $\phi_{2,n+1}$), $\{b\}$ is obtained from the right hand side of equations (3.7) and (3.8), which is known, and possibly some boundary values may contribute to this vector, and $[K]$ is the constant matrix:

$$[K]=\begin{bmatrix} A & C & 0 & 0 & . & . & & \\ C & A & C & 0 & . & . & & \\ 0 & C & A & C & 0 & . & . & \\ . & 0 & C & A & C & . & . & \\ & & \cdots\cdots & & & & & \\ & & . & . & 0 & C & A & C \\ & & & . & . & 0 & C & A \end{bmatrix} \equiv \begin{bmatrix} k_{11} & k_{12} & k_{13} & k_{14} & & & & \\ k_{21} & k_{22} & k_{23} & k_{24} & & & & \\ k_{31} & k_{32} & k_{33} & k_{34} & k_{35} & k_{36} & & \\ k_{41} & k_{42} & k_{43} & k_{44} & k_{45} & k_{46} & & \\ & & & & & & \cdots\cdots & \\ & & & & & & \cdots & \\ & & & & & & .. & \end{bmatrix} \tag{3.15}$$

where

$$[A] \equiv \begin{bmatrix} \Delta x^2 + \frac{2}{3}\epsilon^2 h_1 & \epsilon^2 h_1 H_2 \\ \sigma\Delta x^2 - \frac{1}{3}\epsilon^2\sigma h_1 & -\Delta x^2 - 2\epsilon^2 H_2\left(\frac{H_2}{3} + \frac{\sigma h_1}{2}\right) \end{bmatrix}$$

$$\equiv \begin{bmatrix} a_{11} & a_{12} \\ a_{21} & a_{22} \end{bmatrix},$$

and

$$[C] \equiv \begin{bmatrix} -\frac{1}{3}\epsilon^2 h_1^2 & -\frac{1}{2}\epsilon^2 h_1 H_2 \\ \frac{1}{6}\epsilon^2\sigma h_1 & \epsilon^2 H_2\left(\frac{H_2}{3} + \frac{\sigma h_1}{2}\right) \end{bmatrix}$$

$$\equiv \begin{bmatrix} c_{11} & c_{12} \\ c_{21} & c_{22} \end{bmatrix}.$$

Similarly, equations (3.11) and (3.12) for the corrector stage can be expressed in the same form as (3.13) except with a different

known $\{b\}$ and with $\{x\}$ in (3.14) representing the unknowns at the time-level k+1. We notice that $[K]$ for both the predictor stage and the corrector stage are the same constant matrix.

In general, $[K]$ is not symmetric, but it is banded with bandwith of 7. Gaussian elimination is used to solve equation (3.13), with partial pivoting to make the solutions reliable. The Gauss elimination procedure with partial pivoting is equivalent to transforming $[K]$ into an upper triangular form through elementary row operations. Thus, it transforms $[K]$ into the multiplication of a series of the elementary matrices, which correspond to the elementary row operations, and an upper triangular matrix. In the problem under consideration, $[K]$ is a constant matrix and the same $[K]$ is used for both the predictor and the corrector stages. Therefore the transformation of $[K]$ needs to be done only once at the beginning of the numerical program and thereafter only some simple calculations are needed at every time step for obtaining the solutions of (3.13). This algorithm thus provides the solution to the system (3.13) very efficiently.

The matrix $[K]$ is decomposed as follows:

$$K = P_1 L_1 P_2 L_2 P_3 L_3 \ldots . P_{n-1} L_{n-1} A$$

where matrix P_i is the elementary matrix which results from row exchange based on the i-th column consideration and is formed as follows. If the maximum of the absolute values of the elements in the i-th column below or at the diagonal occurs at the j-th row (then $j \geq i$), then P_i is obtained by exchanging the i-th row and j-th row of the

unit matrix. If this maximum happens to be at the i-th row, then the row exchange is not needed and the corresponding P_i is the unit matrix itself. The matrix L_i is the product of elementary matrices to represent the Gauss elimination of the elements below the diagonal in the i-th column. It has the following form:

$$L = \begin{bmatrix} 1 & & & & & & & \\ & 1 & & & & & & \\ & & \ddots & & & & & \\ & & & 1 & & & & \\ & & & l_1 & 1 & & & \\ & & & l_2 & & 1 & & \\ & & & & & & \ddots\ddots & \\ & & & & & & & 1 \\ & & & & & & & & 1 \end{bmatrix} .$$

$\uparrow$ i-th column

The upper triangular matrix A would have bandwidth 4 if the procedure is without pivoting. With pivoting, however, the bandwidth of A is 6 in the present case (for the decomposition of general banded matrix [G] with m_1 lines below the diagonal and m_2 lines above the diagonal, the bandwidth of A is m_1+m_2+1, which is the same as that of [G], but in the present case of [K] because of its specific structure, the bandwidth of [A] is 6 instead of 7). So the result of the decomposition contains a banded matrix A, n-1 matrices P, which can be stored as a one-dimensional vector, and n-1 matrices L, which can be stored in a matrix with the size 3x(n-1).

In solving (3.13) at every time step, we first solve for vector {y} from the equation:

$$P_1 L_1 P_2 L_2 \cdots P_{n-1} L_{n-1} \{y\} = \{b\} ,$$

and then solve for the unknown $\{x\}$ using the equation:

$$A\{x\} = \{y\} .$$

These two equations can be solved easily because of the simple structures of the P's, L's and A.

In summary, the procedure from time-level k to time-level k+1 consists of the following steps:

PREDICTOR STAGE:

$\zeta_2^{\overline{k+1}}$ is found directly from (3.5),

$\zeta_1^{\overline{k+1}}$ is found directly from (3.6),

$\phi_1^{\overline{k+1}}$, $\phi_2^{\overline{k+1}}$ is obtained by solving the linear system (3.7) and (3.8).

CORRECTOR STAGE:

ζ_2^{k+1} is found directly from (3.9),

ζ_1^{k+1} is found directly from (3.10),

ϕ_1^{k+1}, ϕ_2^{k+1} is obtained by solving the linear system (3.11) and (3.12).

It remains to deal with the boundary conditions required for handling the values of the unknowns at the boundary nodes of the region of computation so as to allow the computation to proceed with errors less than a specific limit.

3.3 Numerical Boundary Condition and Window Shifting

The region of calculation, termed the "window", is always finite. In order to calculate the solution within a smaller region, to save computer time, and to be able to obtain solutions for very long time behavior, it will be necessary to ascertain a suitable numerical boundary condition that can ensure both convergence and stability of the numerical results by suppressing fictitious reflections from the boundaries.

Three numerical boundary conditions are used in the calculations of the FOUR-equation model and models developed later in this thesis and they are depicted in the following paragraphs:

1. LINEAR BOUNDARY CONDITION.

The method of linear extrapolation is applied to obtain the boundary values of ζ and ϕ from the values at two interior neighboring nodal points. For the FOUR-equation model, they are

$$\zeta_{j,o}^{k+1} = 2\zeta_{j,1}^{k+1} - \zeta_{j,2}^{k+1}, \qquad \zeta_{j,n+1}^{k+1} = 2\zeta_{j,n}^{k+1} - \zeta_{j,n-1}^{k+1},$$

$$\phi_{j,o}^{k+1} = 2\phi_{j,1}^{k+1} - \phi_{j,2}^{k+1}, \qquad \phi_{j,n+1}^{k+1} = 2\phi_{j,n}^{k+1} - \phi_{j,n-1}^{k+1},$$

for both the upper and lower layer ($j = 1, 2$). Similar formulas are obtained for calculating ζ and ϕ at the provisional time-level $\overline{k+1}$. Consequently, the matrix [K] in (3.15) assumes, for the boundary nodes, the form:

$k_{11}= a_{11}+2c_{11}$, $k_{12}= a_{12}+2c_{12}$, $k_{13}= c_{11}-c_{11}= 0$, $k_{14}= c_{12}-c_{12}= 0$,

$k_{21}= a_{21}+2c_{21}$, $k_{22}= a_{22}+2c_{22}$, $k_{23}= c_{21}-c_{21}= 0$, $k_{24}= c_{22}-c_{22}= 0$,

$k_{2n-1,\,2n-3}=c_{11}-c_{11} = 0$, $k_{2n-1,\,2n-2}=c_{12}-c_{12} = 0$,

$$k_{2n-1,\,2n-1}=a_{11}+2c_{11}, \quad k_{2n-1,\,2n}=a_{12}+2c_{12},$$

$k_{2n,\,2n-3}=c_{21}-c_{21} = 0$, $k_{2n,\,2n-2}=c_{22}-c_{22}= 0$,

$$k_{2n,\,2n-1}=a_{21}+2c_{21}, \quad k_{2n,\,2n}= a_{22}+2c_{22} \ .$$

2. OPEN BOUNDARY CONDITION (1).

The unknown boundary values of ζ_i and ϕ_i at time-level $k+1$ are determined by assuming (see Wu & Wu (1982)) that the disturbed motion adjacent to the boundary is regarded as a long wave system propagating outward from the inner region through the boundary with a constant characteristic velocity c. Therefore the open boundary condition is the simple wave equation,

$Q_t \pm c\,Q_x = 0$ at the boundary of the computation region, (3.16)

where Q stands for the wave elevations and the layer-mean potentials in the FOUR-equation model, and the sign is taken such that the wave is propagated from the interior of the computation region to the outside. A signal being propagated with the velocity c from the nodes near a boundary at the time-level k towards the boundary point in general would not necessarily reach a grid point of calculation at the time-level $k+1$. Therefore, the values of these unknowns at this boundary

point are determined by parabolic interpolation from the three consecutive nodal points at the end of the computation region (the window) and are taken as the boundary values of these unknown variables. The required difference equations are

$$
\begin{aligned}
Q_o^{k+1} &= Q_1^k + \frac{1}{2}(Q_2^k - Q_o^k)(c\frac{\Delta t}{\Delta x} - B) \\
&\quad + \frac{1}{2}(Q_o^k + Q_2^k - 2Q_1^k)(c\frac{\Delta t}{\Delta x} - B)^2 \quad , \\
Q_{n+1}^{k+1} &= Q_n^k + \frac{1}{2}(Q_{n-1}^k - Q_{n+1}^k)(c\frac{\Delta t}{\Delta x} - B) \\
&\quad + \frac{1}{2}(Q_{n+1}^k + Q_{n-1}^k - 2Q_n^k)(c\frac{\Delta t}{\Delta x} - B)^2 \quad ,
\end{aligned}
\tag{3.17}
$$

where $B = 1$, Q is the same as before and the subscript 0 denotes the spatial position at the left boundary and the subscript $n+1$ at the right boundary. The two equations in (3.17) can also be obtained from the Taylor series expansion of Q and by making use of (3.16).

3. OPEN BOUNDARY CONDITION (2).

In the two-layer fluid system, there are two characteristic velocities and two corresponding wave systems. The open boundary condition (2) is designed to let both wave systems move outward 'freely'. This condition can be expressed as

$$(Q_t \pm c_s Q_x)\ (Q_t \pm c_f Q_x) = 0 \quad ,$$

where c_s and c_f are the slow and fast characteristic velocities based on the linear theory and the signs are chosen so that the waves always propagated outward from the region of calculation, with the

initial conditions evaluated at the two previous time-levels k and k-1:

$$Q(x, t^k) = R(x) \quad ,$$

$$Q_t(x, t^k) = D(x) \approx \frac{(Q(x, t^k) - Q(x, t^{k-1}))}{\Delta t} \quad .$$

In integral form the solution is

$$Q(x, t) = \frac{1}{(c_f - c_s)}\left[\int_{x \pm c_s(t-t^k)}^{x \pm c_f(t-t^k)} D(s)ds - c_s R(x \pm c_f(t-t^k)) + c_f R(x \pm c_s(t-t^k))\right] \quad ,$$

where the same signs are assigned as before to have the waves always leaving the region of computation.

By using this integral of the boundary condition and assuming a parabolic interpolation near the boundary (3 points), the open boundary condition (2) assumes the expression:

$$Q_o^{k+1} = \frac{\Delta t^2}{(6\Delta x^2)} (c_f^2 + c_f c_s + c_s^2)(-Q_o^{k-1} + 2Q_1^{k-1} - Q_2^{k-1}) +$$

$$\frac{\Delta t^2}{(6\Delta x^2)} (c_f - c_s)^2 (Q_o^k - 2Q_1^k + Q_2^k) +$$

$$\frac{\Delta t}{(4\Delta x)} (c_f + c_s)(-3Q_o^k + 4Q_1^k - Q_2^k + 3Q_o^{k-1} - 4Q_1^{k-1} + Q_2^{k-1})$$

$$+ 2Q_o^k - Q_o^{k-1} \quad ,$$

and

$$Q_{n+1}^{k+1} = \frac{\Delta t^2}{(6\Delta x^2)} (c_f^2 + c_f c_s + c_s^2)(-Q_{n+1}^{k-1} + 2Q_n^{k-1} - Q_{n-1}^{k-1}) +$$

$$\frac{\Delta t^2}{(6\Delta x^2)} (c_f - c_s)^2 (Q_{n+1}^{k} - 2Q_n^{k} + Q_{n-1}^{k}) +$$

$$\frac{\Delta t}{(4\Delta x)} (c_f + c_s)(-3Q_{n+1}^{k} + 4Q_n^{k} - Q_{n-1}^{k} + 3Q_{n+1}^{k-1} - 4Q_n^{k-1}$$

$$+ Q_{n-1}^{k-1}) + 2Q_{n+1}^{k} - Q_{n+1}^{k-1} ,$$

where the notation is the same as that in (3.17). For the open boundary condition (2), the third time-level k-1 is needed to deal with the near-boundary region. Accordingly, additional values of ζ_i and ϕ_i before the initial instant are required for the calculation in a near-boundary region.

For both open boundary conditions (1) and (2)

$$Q_o^{\overline{k+1}} = Q_o^{k+1} , \quad Q_{n+1}^{\overline{k+1}} = Q_{n+1}^{k+1} ,$$

and the matrix [K] in (3.15) for solving the algebraic system is unchanged but with some additional terms admitted to {b} on the right hand side of (3.13).

Finally, we state that the same window shifting technique is used to save computer time and storage as that used by Wu & Wu (1982). In most of our calculations, we will consider a disturbance moving with a uniform velocity. With reference to the absolute frame where the velocity and wave elevation are zero at infinity, we shift the "window" (of calculation) after every N time steps to keep the disturbance suitably located in the window and the prominent

waves well located. The position of the disturbance can be kept stationary relative to the window every N time steps if the following relation is adhered to:

$$\Delta t = \frac{\Delta x}{(U\,N)} \quad , \tag{3.18}$$

where U is the velocity of the disturbance (relative to the absolute frame). This means that the disturbance moves a distance of Δx in time $N\Delta t$.

New boundary points will therefore appear at the upstream boundary every time the window is shifted. The values of the solution at these points are obtained using the open boundary condition (1) and to distinguish this condition from the boundary conditions used for the basic equations the former will be called the window boundary condition and the latter, the equation boundary condition. For the window boundary condition, (3.17) can also be used with B = 2. We notice that for the open boundary condition (2) associated with the basic equations, two new boundary values are required for subsequent calculation of the solution and these two values are furnished by applying the window boundary condition.

The numerical results will be presented in Chapter VIII.

IV. FORCED KDV EQUATION FOR TWO-LAYER SYSTEMS

A forced KdV equation for a two-layer system with a free top surface will be derived by applying the two-timing perturbation method for the case when some external forcings, which can occur as a moving top-surface pressure or a moving bottom disturbance, exist. A numerical scheme for the solution of this equation will also be presented in this chapter.

4.1 Derivation of the Forced KdV Equation

In this section, a two-timing perturbation method will be used and the characteristic velocities will be obtained as the lowest order results and the corresponding forced KdV equation for the wave elevations will be obtained as the next higher order result.

Consider the two-layer system described in Chapter II with ρ_1, η_1, h_1 and ϕ_1 referring to the upper layer and ρ_2, η_2, h_2 and ϕ_2 to the lower layer. The quantities are shown in Figure 2.1 along with the top-surface elevation ζ_1 and the interface elevation ζ_2. Here ϕ is restored to its original meaning, namely, the local velocity potential including dependence on z, instead of the layer-mean potential. In this chapter we shall consider waves propagating only in one horizontal direction x and assume that there is no variation along the y direction (which is the other horizontal direction). The nondimensional variables are defined the same as before:

$$\frac{(x)}{\lambda}, \quad \frac{(z, h, d, \zeta)}{h_o}, \quad (t)\frac{c}{\lambda}, \quad \frac{(\phi)}{c\lambda} \text{ and } \frac{(p)}{\rho_i g h_o}, \tag{4.1}$$

where

$$c = \sqrt{gh_o} \quad . \tag{4.2}$$

Also, with H_2 being a constant and d a small quantity,

$$h_2 = H_2 - d \quad .$$

It is convenient to take

$$h_o = h_1 + H_2 \quad , \tag{4.3}$$

and the small parameter is taken, in accordance with $\alpha = O(\epsilon^2)$ and $\epsilon = \frac{h_o}{\lambda}$, as

$$\alpha = (\frac{h_o}{\lambda})^2 \quad . \tag{4.4}$$

For the remainder of this chapter all the variables are assumed to be dimensionless, except where pointed out otherwise. The Laplace equation becomes

$$\alpha \phi_{xx} + \phi_{zz} = 0 \quad , \tag{4.5}$$

for both layers.

The cumulative nonlinear effects indicate the merit of using two time scales and the slow time τ employed here is

$$\tau = \alpha t \quad . \tag{4.6}$$

Considering any physical quantity as a function of x, z, t and τ instead of $x, z,$ and t, the original partial derivative with respect to t, Q_t, will then be modified to assume the form $Q_t + \alpha Q_\tau$. By using the Bernoulli equation, the boundary conditions become

$$\phi_{1t} + \alpha\phi_{1\tau} + p_o + \frac{1}{2}\phi_{1x}^2 + \frac{1}{2\alpha}\phi_{1z}^2 + \zeta_1 = 0 \quad \text{at } z = \zeta_1 \ , \tag{4.7}$$

$$-\frac{1}{\alpha}\phi_{1z} + \phi_{1x}\zeta_{1x} + \zeta_{1t} + \alpha\zeta_{1\tau} = 0 \quad \text{at } z = \zeta_1 \ , \tag{4.8}$$

$$\sigma(\phi_{1t} + \alpha\phi_{1\tau} + \frac{1}{2}\phi_{1x}^2 + \frac{1}{2\alpha}\phi_{1z}^2 + \zeta_2) = \phi_{2t} + \alpha\phi_{2\tau} + \frac{1}{2}\phi_{2x}^2 + \frac{1}{2\alpha}\phi_{2z}^2 + \zeta_2 \quad \text{at } z = \zeta_2 - h_1 \ , \tag{4.9}$$

$$\alpha\zeta_{2x}(\phi_{1x} - \phi_{2x}) = \phi_{1z} - \phi_{2z} \quad \text{at } z = \zeta_2 - h_1 \ , \tag{4.10}$$

$$\zeta_{2t} + \alpha\zeta_{2\tau} - \frac{1}{\alpha}\phi_{2z} + \phi_{2x}\zeta_{2x} = 0 \quad \text{at } z = \zeta_2 - h_1 \ , \tag{4.11}$$

$$d_t + \alpha d_\tau - \frac{1}{\alpha}\phi_{2z} + \phi_{2x}d_x = 0 \quad \text{at } z = d-1 \ , \tag{4.12}$$

where the subscripts x, z, t, τ denote partial differentiations, $z = \zeta_1$ is the top surface, $z = \zeta_2 - h_1$ is the interface, $z = d-1$ is the bottom and

$$\sigma = \frac{\rho_1}{\rho_2} \ . \tag{4.13}$$

The unknown wave elevations and velocity potentials are expanded as follows:

$$\begin{aligned} \zeta_1 &= \alpha(\zeta_{1(1)}(x, t, \tau) + \alpha\zeta_{1(2)} + \dots) \ , \\ \zeta_2 &= \alpha(\zeta_{2(1)}(x, t, \tau) + \alpha\zeta_{2(2)} + \dots) \ , \\ \phi_1 &= \alpha(\phi_{1(1)}(x, z, t, \tau) + \alpha\phi_{1(2)} + \dots) \ , \\ \phi_2 &= \alpha(\phi_{2(1)}(x, z, t, \tau) + \alpha\phi_{2(2)} + \dots) \ . \end{aligned} \tag{4.14}$$

We recall that the wave elevation ζ is assumed to be of $O(\alpha)$, so that the Ursell number is of $O(1)$. To obtain a self-consistent formulation for the present model, we find that the external forcing functions must be of $O(\alpha^2)$, that is,

$$p_o = \alpha^2 P , \quad P = O(1) , \tag{4.15}$$

and

$$d = \alpha^2 D , \quad D = O(1) . \tag{4.16}$$

After substituting the above expansions for the potentials (4.14) into the Laplace equation (4.5), we find that the potentials must have the following forms,

$$\begin{aligned}
\phi_{1(1)} &= R_{(1)}(x, t, \tau) , \\
\phi_{2(1)} &= L_{(1)}(x, t, \tau) , \\
\phi_{1(2)} &= -\tfrac{1}{2}(z+h_1)^2 R_{(1)xx} + (z+h_1) R_{(2)}(x, t, \tau) + R_{(3)}(x, t, \tau) , \\
\phi_{2(2)} &= -\tfrac{1}{2}(z+1)^2 L_{(1)xx} + L_{(3)}(x, t, \tau) , \\
\phi_{1(3)} &= \tfrac{1}{24}(z+h_1)^4 R_{(1)xxxx} - \tfrac{1}{6}(z+h_1)^3 R_{(2)xx} \\
&\quad - \tfrac{1}{2}(z+h_1)^2 R_{(3)xx} + (z+h_1) R_{(4)}(x, t, \tau) + R_{(5)}(x, t, \tau) , \\
\phi_{2(3)} &= \tfrac{1}{24}(z+1)^4 L_{(1)xxxx} - \tfrac{1}{2}(z+1)^2 L_{(3)xx} + \\
&\quad (z+1) L_{(4)}(x, t, \tau) + L_{(5)}(x, t, \tau) ,
\end{aligned} \tag{4.17}$$

where $R_{(n)}$ and $L_{(n)}$ are arbitrary functions of (x, t, τ) and (4.8), (4.12) and (4.16) have been used to obtain the first, second and fourth of the above equalities. Substituting these expressions into the

boundary conditions (4.7)-(4.12) and equating the corresponding terms of the same orders, we obtain a set of differential equations for R, L and ζ. On the top surface, the dynamical boundary condition (4.7) gives

$$R_{(1)t} + \zeta_{1(1)} = 0 , \tag{4.18}$$

$$-\frac{1}{2} h_1^2 R_{(1)xxt} + h_1 R_{(2)t} + R_{(3)t} + R_{(1)\tau} + P + \frac{1}{2} R_{(1)x}^2 + \zeta_{1(2)} = 0 , \tag{4.19}$$

and the kinematic boundary condition (4.8) gives

$$h_1 R_{(1)xx} + \zeta_{1(1)t} = R_{(2)} , \tag{4.20}$$

$$\zeta_{1(1)} R_{(1)xx} - \frac{1}{6} h_1^3 R_{(1)xxxx} + \frac{1}{2} h_1^2 R_{(2)xx} + h_1 R_{(3)xx} - R_{(4)} + R_{(1)x} \zeta_{1(1)x} + \zeta_{1(2)t} + \zeta_{1(1)\tau} = 0 . \tag{4.21}$$

At the interface between the two fluids the continuity of pressure (4.9) gives

$$\sigma R_{(1)t} - L_{(1)t} + \zeta_{2(1)}(\sigma - 1) = 0 , \tag{4.22}$$

$$\sigma(R_{(3)t} + R_{(1)\tau} + \frac{1}{2} R_{(1)x}^2) + (\sigma - 1)\zeta_{2(2)} + \frac{1}{2} H_2^2 L_{(1)xxt} - L_{(3)t} - L_{(1)\tau} - \frac{1}{2} L_{(1)x}^2 = 0 . \tag{4.23}$$

The kinematic boundary condition in the upper fluid at the interface (4.10) gives

$$-H_2 L_{(1)xx} - R_{(2)} = 0 , \tag{4.24}$$

$$-\zeta_{2(1)}L_{(1)xx}+\zeta_{2(1)}R_{(1)xx}+\zeta_{2(1)x}R_{(1)x}-\zeta_{2(1)x}L_{(1)x}$$

$$+\frac{1}{6}H_2^3\,L_{(1)xxxx}-H_2L_{(3)xx}-R_{(4)}+L_{(4)}=0\ , \qquad (4.25)$$

and in the lower fluid at the interface (4.11) gives

$$H_2L_{(1)xx}+\zeta_{2(1)t}=0\ , \qquad (4.26)$$

$$\zeta_{2(1)}L_{(1)xx}-\frac{1}{6}H_2^3\,L_{(1)xxxx}+H_2L_{(3)xx}+L_{(1)x}\zeta_{2(1)x}$$

$$+\zeta_{2(2)t}+\zeta_{2(1)\tau}-L_{(4)}=0\ . \qquad (4.27)$$

Finally, for the boundary condition on the bottom, (4.12) gives

$$D_t=L_{(4)}\ . \qquad (4.28)$$

The first order equations, (4.18), (4.20), (4.22), (4.24) and (4.26), lead to the following results:

$$\zeta_{1(1)}=-R_{(1)t}\ , \qquad (4.29)$$

$$\zeta_{2(1)}(\sigma-1)=L_{(1)t}-\sigma R_{(1)t}\ , \qquad (4.30)$$

$$\zeta_{2(1)t}=h_1R_{(1)xx}-R_{(1)tt}=-H_2L_{(1)xx}\ , \qquad (4.31)$$

$$\zeta_{2(1)tt}=\zeta_{1(1)tt}-h_1\zeta_{1(1)xx}\ , \qquad (4.32)$$

$$R_{(2)}=\zeta_{2(1)t}\ . \qquad (4.33)$$

Combining and differentiating these relations, we obtain for $R_{(1)}$, $L_{(1)}$, $\zeta_{1(1)}$ and $\zeta_{2(1)}$ the equations:

$$h_1 H_2(1-\sigma)R_{(1)xxxx} + R_{(1)tttt} - R_{(1)ttxx} = 0 \ , \qquad (4.34)$$

$$h_1 H_2(1-\sigma)L_{(1)xxxx} + L_{(1)tttt} - L_{(1)ttxx} = 0 \ , \qquad (4.35)$$

$$h_1 H_2(1-\sigma)\zeta_{1(1)xxxx} + \zeta_{1(1)tttt} - \zeta_{1(1)ttxx} = 0 \ , \qquad (4.36)$$

$$h_1 H_2(1-\sigma)\zeta_{2(1)xxxx} + \zeta_{2(1)tttt} - \zeta_{2(1)ttxx} = 0 \ . \qquad (4.37)$$

The second order equations, namely (4.19), (4.21), (4.23), (4.25), (4.27) and (4.28), are rather involved. To eliminate the unknowns $\zeta_{1(2)}$, $\zeta_{2(2)}$, $L_{(3)}$ and $R_{(4)}$, we combine these equations as follows:

$$H_2(\sigma-1)(4.19)_{xxt} + (4.19)_{ttt} - H_2(\sigma-1)(4.21)_{xx} - (4.21)_{tt}$$

$$- H_2(4.23)_{xxt} + H_2(\sigma-1)(4.25)_{xx} + (4.25)_{tt}$$

$$+ H_2(\sigma-1)(4.27)_{xx}$$

and thus obtain

$$R_{(3)tttt} - R_{(3)xxtt} + h_1 H_2(1-\sigma)R_{(3)xxxx} = B \ . \qquad (4.38)$$

in which

$$B = H_2(1-\sigma)A_{xx} - A_{tt} + H_2(1-\sigma)(\zeta_{2(1)}L_{(1)xx})_{xx}$$

$$+ H_2(1-\sigma)(L_{(1)x}\zeta_{2(1)x})_{xx} + \frac{1}{2}H_2\sigma(R^2_{(1)x})_{xxt}$$

$$- \frac{1}{2}H_2(L^2_{(1)x})_{xxt} + H_2(1-\sigma)\zeta_{2(1)xx\tau} + H_2\sigma L_{(1)xxt\tau}$$

$$+ \frac{1}{6}(\sigma-1)H_2^4 L_{(1)xxxxxx} + \frac{1}{2}H_2^3 L_{(1)xxxxtt} - H_2 L_{(1)xxt\tau}$$

$$+ H_2(\sigma-1)L_{(4)xx} \quad , \tag{4.39}$$

where

$$A = -\zeta_{2(1)}L_{(1)xx} + (\zeta_{2(1)} - \zeta_{1(1)})R_{(1)xx} + \frac{1}{6}H_2^3 L_{(1)xxxx}$$

$$+ \frac{1}{6}h_1^3 R_{(1)xxxx} + \zeta_{2(1)x}R_{(1)x} - \zeta_{2(1)x}L_{(1)x} - \zeta_{1(1)x}R_{(1)x}$$

$$- \frac{1}{2}h_1^2 R_{(2)xx} - \zeta_{1(1)\tau} - \frac{1}{2}h_1^2 R_{(1)xxtt} + h_1 R_{(2)tt}$$

$$+ R_{(1)t\tau} + P_t + \frac{1}{2}(R^2_{(1)x})_t + L_{(4)} \quad .$$

Equation (4.38) can also be expressed as follows:

$$\prod_{i=1}^{4} \left(\frac{\partial}{\partial t} - c_i \frac{\partial}{\partial x}\right) R_{(3)} = B = \text{LTB} + \text{NTB} \quad , \tag{4.40}$$

where LTB represents the linear terms of B and NTB the non-linear terms of B and the c_i's are the characteristic velocities based on linear theory, given by

$$c_i^2 = \frac{1}{2}\left[1 \pm \sqrt{1-4h_1H_2(1-\sigma)}\right] \qquad i = 1, 2, 3, 4 \quad . \tag{4.41}$$

The expression for LTB and NTB are

$$\begin{aligned} LTB = {} & H_2(1-\sigma)[\tfrac{1}{6}h_1^3 R_{(1)xxxxxx} - \tfrac{1}{2}h_1^2 R_{(2)xxxx} - \zeta_{1(1)xx\tau} \\ & - \tfrac{1}{2}h_1^2 R_{(1)xxxxtt} + h_1 R_{(2)xxtt} + P_{xxt}] - L_{(4)tt} \\ & - \tfrac{1}{6}h_1^3 R_{(1)xxxxtt} + \tfrac{1}{2}h_1^2 R_{(2)xxtt} + \zeta_{1(1)tt\tau} + \tfrac{1}{2}h_1^2 R_{(1)xxtttt} \\ & - h_1 R_{(2)tttt} - R_{(1)ttt\tau} - P_{ttt} + H_2(1-\sigma)\zeta_{2(1)xx\tau} \\ & + H_2 R_{(1)xxt\tau} + \tfrac{1}{3}H_2^3 L_{(1)xxxxtt} - H_2 L_{(1)xxt\tau} \end{aligned} \tag{4.42}$$

and

$$\begin{aligned} NTB = {} & H_2(1-\sigma)[(\zeta_{2(1)} - \zeta_{1(1)})R_{(1)xx} + (\zeta_{2(1)x} - \zeta_{1(1)x})R_{(1)x}]_{xx} \\ & + \tfrac{1}{2}H_2(R_{(1)x}^2)_{xxt} - \tfrac{1}{2}H_2(L_{(1)x}^2)_{xxt} \\ & + [L_{(1)xx}\zeta_{2(1)} - (\zeta_{2(1)} - \zeta_{1(1)})R_{(1)xx} - (\zeta_{2(1)x} - \zeta_{1(1)x})R_{(1)x} \\ & + L_{(1)x}\zeta_{2(1)x} - \tfrac{1}{2}(R_{(1)x}^2)_t]_{tt} \quad . \end{aligned} \tag{4.43}$$

The homogeneous form of (4.38) and the first order result (4.34)-(4.37) are simple fourth order wave equations. The general solution of say (4.34) is

$$R_{(1)} = \sum_{i=1}^{4} f_i(x + c_i t) \quad , \tag{4.44}$$

where the f_i's are arbitrary functions. Because $0 < \sigma < 1$, $h_1 + H_2 = 1$, $h_1 > 0$ and $H_2 > 0$ in the present problem, the four c_i's are all

distinct, none vanishing. Notice that τ is inside the functions as a parameter ($f_i(x + c_i t, \tau)$, if written more completely in the component of (4.44)) and the same is implied in the formulas below.

Because the sign of c only changes the directions of wave propagation, we consider $\pm c$ together, and there exist only two possible wave modes in the two-layer systems. These are called the slow mode and the fast mode and have the characteristic velocities

$$c_s = \sqrt{\frac{1 - \sqrt{1-4h_1H_2(1-\sigma)}}{2}}, \tag{4.45}$$

and

$$c_f = \sqrt{\frac{1 + \sqrt{1-4h_1H_2(1-\sigma)}}{2}}. \tag{4.46}$$

The first order term of lower layer potential $L_{(1)}$ can be determined from (4.44) and (4.31) as

$$L_{(1)} = \sum_{i=1}^{4} \frac{1}{H_2} (c_i^2 - h_1) f_i(x + c_i t), \tag{4.47}$$

where the assumption that the velocity vanishing at infinity has been used. Then from (4.30)

$$\zeta_{2(1)} = \sum_{i=1}^{4} (\frac{h_1}{c_i} - c_i) f_i'(x + c_i t), \tag{4.48}$$

where the superscript prime $'$ means the differentiation with respect to the argument $x + c_i t$. From (4.29)

$$\zeta_{1(1)} = - \sum_{i=1}^{4} c_i f_i'(x + c_i t), \tag{4.49}$$

and from (4.33) we find $R_{(2)}$

$$R_{(2)} = \sum_{i=1}^{4} (h_1 - c_i^2) f_i''(x + c_i t) \quad . \tag{4.50}$$

We now assume that the surface pressure and bottom variation can be written as

$$P = \sum_{i=1}^{4} P_i(x + x_i t) \quad , \tag{4.51}$$

$$D = \sum_{i=1}^{4} D_i(x + c_i t) \quad . \tag{4.52}$$

Since τ is implicit in P and D, the disturbance velocities are not necessarily equal to $-c_i$.

Substituting the above expressions for $R_{(1)}$, $L_{(1)}$, $R_{(2)}$, $\zeta_{1(1)}$, $\zeta_{2(1)}$, P and D into the right hand side of equation (4.41) and (4.42) and using equation (4.28) for $L_{(4)}$, we obtain

$$LTB = \sum_{i=1}^{4} L_i(x + c_i t) \quad , \tag{4.53}$$

where

$$\begin{aligned} L_i = {} & f_i^{(6)} \{H_2(1-\sigma)[\tfrac{1}{6} h_1^2 (3c_i^2 - 2h_1) + h_1 c_i^2 (\tfrac{1}{2} h_1 - c_i^2)] \\ & + c_i^2 (c_i^2 - h_1)(\tfrac{1}{3} H_2^2 - \tfrac{1}{2} h_1^2) + h_1 (c_i^2 - h_1) c_i^4 + \tfrac{1}{2} h_1^2 c_i^4 - \tfrac{1}{6} h_1^3 c_i^2\} \\ & + f_{i\tau}'''[H_2(1-\sigma)(\tfrac{1}{c_i} h_1 + c_i) + H_2 \sigma c_i + c_i(h_1 - 3c_i^2)] \\ & + P_i''' c_i[H_2(1-\sigma) - c_i^2] - D_i''' c_i^3 \quad , \end{aligned} \tag{4.54}$$

where $f_i^{(6)}$ means the 6th order derivative of f_i with respect to its argument $x + c_i t$, and

$$\begin{aligned} NTB = \sum_{i=1}^{4}\sum_{j=1}^{4} f_i''' f_j'' [H_2(2c_i + c_j) \\ - \frac{1}{H_2}(c_i^2 - h_1)(c_j^2 - h_1)(5c_i + 3c_j + \frac{1}{c_j} c_i^2) + 3h_1 H_2(1-\sigma)(\frac{1}{c_i} + \frac{1}{c_j}) \\ - h_1(c_i^2 + 2c_i c_j)(\frac{1}{c_i} + \frac{1}{c_j}) - 3c_i^2 c_j] \\ + \sum_{i=1}^{4}\sum_{j=1}^{4} f_i' f_j'''' [H_2 c_j - \frac{1}{H_2}(c_i^2 - h_1)(c_j^2 - h_1)(2c_j + \frac{1}{c_i} c_j^2) \\ + h_1 H_2(1-\sigma)(\frac{1}{c_i} - \frac{1}{c_j}) - h_1 c_j^2 (\frac{1}{c_i} + \frac{1}{c_j}) - c_j^3] . \end{aligned} \tag{4.55}$$

Now let us restrict our formulation to the case of only one mode moving in only one direction. Then the summations in equations (4.53) and (4.55) contain only one term, for a specific i. Since there is a factor $(\frac{\partial}{\partial t} - c_i \frac{\partial}{\partial x})$ in the differential operator on the left hand side of equation (4.40), the inhomogeneous terms with single argument $x + c_i$ on the right hand side of (4.40) would have to give rise to secular terms to the solution unless they are required to vanish. With this requirement we obtain the following equation:

$$\begin{aligned} \frac{3}{H_2} c_i^2 [(h_1 - 2H_2)c_i^2 + h_1 H_2(1-\sigma) - h_1 + H_2](f'f'')'' + [(\frac{1}{3}h_1^3 + \frac{1}{3}H_2^3 + h_1 H_2 \sigma) \\ c_i^2 - h_1 H_2(1-\sigma)(\frac{1}{3}h_1^2 + \frac{1}{3}H_2^2 + h_1 H_2 \sigma)] c_i f^{(6)} + c_i^2 (2 - 4c_i^2) f_\tau''' \\ + [h_1 H_2(1-\sigma) - (h_1 + H_2\sigma)c_i^2] P''' - c_i^4 D''' = 0 , \end{aligned} \tag{4.56}$$

where the subscript i (except c_i) has been omitted and the relation

$$c_i^4 - c_i^2 + h_1 H_2 (1-\sigma) = 0 \ , \tag{4.57}$$

which readily follows from (4.38) or (4.41), has been used.

Integrating (4.56) twice under the condition that the disturbances vanish at infinity, we obtain

$$\begin{aligned} &\frac{3}{H_2} c_i^2 [(h_1 - 2H_2)c_i^2 + h_1 H_2 (1-\sigma) - h_1 + H_2](f' f'') \\ &+[(\tfrac{1}{3}h_1^3 + \tfrac{1}{3}H_2^3 + h_1 H_2 \sigma)c_i^2 - h_1 H_2 (1-\sigma)(\tfrac{1}{3}h_1^2 + \tfrac{1}{3}H_2^2 + h_1 H_2 \sigma]c_i f'''' \\ &+ c_i^2 (2 - 4c_i^2) f_\tau' + [h_1 H_2 (1-\sigma) - (h_1 + H_2 \sigma)c_i^2]P' - c_i^4 D' = 0 \ . \end{aligned} \tag{4.58}$$

In the present case (4.49) is

$$\zeta_{1(1)} = -c_i f_i' \ (x + c_i t) \ , \tag{4.59}$$

and equation (4.58) becomes,

$$\begin{aligned} &\frac{3}{H_2} [(h_1 - 2H_2)c_i^2 + h_1 H_2 (1-\sigma) - h_1 + H_2]\zeta_{1(1)} \zeta_{1(1)}' \\ &-[(\tfrac{1}{3} h_1^3 + \tfrac{1}{3} H_2^3 + h_1 H_2 \sigma)c_i^2 - h_1 H_2 (1-\sigma)(\tfrac{1}{3}h_1^2 + \tfrac{1}{3} H_2^2 + h_1 H_2 \sigma]\zeta_{1(1)}''' \\ &- c_i (2 - 4c_i^2)\zeta_{1(1)\tau} + [h_1 H_2 (1-\sigma) - (h_1 + H_2 \sigma)c_i^2]P' - c_i^4 D' = 0 \ . \end{aligned} \tag{4.60}$$

If we further express $\zeta_{1(1)}$, P and D in terms of ζ_1, p_o and d by the following relations, the first of which is the approximation of the expansion (4.14),

$$\zeta_1 \approx \alpha \zeta_{1(1)} \quad , \tag{4.61}$$

$$p_o = \alpha^2 P \quad , \tag{4.15}$$

$$d = \alpha^2 D \quad , \tag{4.16}$$

and change the arguments τ and $x + c_i t$ back to the arguments x and t by using (4.6), the following equation is obtained

$$a_1(Q_t - c_i Q_x) + a_2 Q Q_x + \alpha a_3 Q_{xxx} + a_4 p_{ox} + a_5 d_x = 0 \quad , \tag{4.62}$$

where

$$\begin{aligned}
Q &= \zeta_1 \quad , \\
a_1 &= c_i(4c_i^2 - 2) \quad , \\
a_2 &= \frac{3}{H_2}\left[c_i^2(h_1 - 2H_2) + h_1 H_2(1-\sigma) + H_2 - h_1\right] \quad , \\
a_3 &= -\left(\tfrac{1}{3}h_1^3 + \tfrac{1}{3}H_2^3 + h_1 H_2 \sigma\right)c_i^2 + h_1 H_2(1-\sigma)\left(\tfrac{1}{3}h_1^2 + \tfrac{1}{3}H_2^2 + h_1 H_2 \sigma\right), \\
a_4 &= h_1 H_2(1-\sigma) - (h_1 + H_2\sigma)c_i^2 \quad , \\
a_5 &= -c_i^4 \, .
\end{aligned} \tag{4.63}$$

If the inhomogeneous forcing terms p_{ox} and d_x are absent, this equation reduces to the well-known Korteweg-de Vries equation, or simply the KdV equation. It contains both nonlinear effects and dispersive effects. In the formulation presented above, one can see

that equation (4. 62) is the evolution equation for the two layer system when the disturbance is moving with a transcritical velocity about a characteristic velocity of the linear system. Equation (4. 62) holds for left-going disturbance when the c_i is positive and x increasing to the right. For right-going waves (4. 62) is also applicable with c_i taken negative in (4. 62) and (4. 63). For the interface elevation ζ_2, a similar KdV equation can be obtained by using the first order relation

$$\zeta_2 \sim (1 - \frac{h_1}{c_i^2})\zeta_1 \ , \tag{4.64}$$

in (4. 62) and (4. 63). The resulting KdV equation has the same form as (4. 62), however, the coefficients are now,

$$Q = \zeta_2 \ ,$$

$$a_1 = 4c_i^2 - 2 \ ,$$

$$a_2 = -\frac{3}{\sigma c_i}\{c_i^2[\frac{h_1}{H_2} + 2\sigma - 1] + (\sigma - 1)[(\sigma + 1)h_1 - H_2]\} \ ,$$

$$a_3 = -\frac{1}{c_i}[c_i^2(\frac{1}{3}h_1^3 + \sigma h_1 H_2 + \frac{1}{3}H_2^3) + (\sigma - 1)h_1 H_2(\frac{1}{3}h_1^2 + \sigma h_1 H_2 + \frac{1}{3}H_2^2)],$$

$$a_4 = -c_i H_2 \sigma \ ,$$

$$a_5 = (h_1 - c_i^2)c_i \ , \tag{4.65}$$

where the characteristic velocity relation (4. 57) has been used.

Some useful first order results can be deduced from equations (4. 44), (4. 47), (4. 48) and (4. 49) for the one-component case using the expansions (4. 14) as follows

$$\zeta_2 \sim (\frac{h_1}{c_i} - c_i)\phi_{1x} \quad ,$$

$$\zeta_2 \sim -\frac{H_2}{c_i}\phi_{2x} \quad ,$$

and

$$\phi_{2x} \sim \frac{1}{H_2}(c_i^2 - h_1)\phi_{1x} \quad . \tag{4.66}$$

When the densities of the two layers are nearly equal, which is a case of practical importance, the forced KdV equation can be further simplified. In this case, σ is approximately equal to 1 and the slow mode wave speed becomes, by (4.45),

$$c_s \sim \sqrt{h_1 H_2(1-\sigma)} \tag{4.67}$$

Consequently, (4.65) can be written as

$$\frac{1}{c_s}\zeta_{2t} - \zeta_{2x} + \frac{3}{2}(\frac{1}{h_1} - \frac{1}{H_2})\zeta_2\zeta_{2x} - \frac{1}{6}\alpha h_1 H_2 \zeta_{2xxx} + \frac{1}{2}H_2 p_{ox} - \frac{1}{2}h_1 d_x = 0 \quad . \tag{4.68}$$

In addition, the following relations can be obtained from (4.64), (4.66) and (4.67):

$$\begin{aligned} \zeta_1 &\sim -H_2(1-\sigma)\zeta_2 \quad , \\ \phi_{1x} &\sim \sqrt{\frac{1}{h_1}H_2(1-\sigma)}\zeta_2 \quad , \\ \phi_{2x} &\sim -\sqrt{\frac{1}{H_2}h_1(1-\sigma)}\zeta_2 \quad , \\ \varphi_{2x} &\sim -\frac{1}{H_2}h_1\phi_{1x} \quad . \end{aligned} \tag{4.69}$$

For the fast mode (with $\sigma \approx 1$), $c_f = 1$ (see equation (4.46)) and we have for ζ_1 the equation

$$\zeta_{1t} - \zeta_{1x} - \frac{3}{2}\zeta_1\zeta_{1x} - \frac{\alpha}{6}\zeta_{1xxx} - \frac{1}{2}p_{ox} - \frac{1}{2}d_x = 0 \ , \qquad (4.70)$$

and for the other flow quantities the relations

$$\begin{aligned} \zeta_2 &\sim H_2\zeta_1 \ , \\ \phi_{1x} &\sim -\zeta_1 \ , \\ \phi_{2x} &\sim -\zeta_1 \ , \end{aligned} \qquad (4.71)$$

and

$$\phi_{1x} \sim \phi_{2x} \ ,$$

which can be obtained similarly as for the slow mode. For the fast mode, equation (4.75) is expected on physical grounds to agree with the case when $\rho_1 = \rho_2$ (i.e., the case of a single homogeneous fluid layer). This is confirmed by comparison with the forced KdV equation given by Lee (1985, equation 2.58) for the homogeneous one layer case.

Sometimes the dimensional equation is desired. The one corresponding to (4.62) and (4.65) is

$$a_1(Q_t - c_iQ_x) + a_2QQ_x + a_3Qxxx + a_4p_{ox} + a_5d_x = 0 \ , \qquad (4.72)$$

with

$$Q = \zeta_2 \ ,$$

$$a_1 = 4c_i^2 - 2gh_o \ ,$$

$$a_2 = -\frac{3g}{H_2\sigma c_i}\{c_i^2[h_1 + (2\sigma-1)H_2] + g(\sigma-1)H_2[(\sigma+1)h_1 - H_2]\} \ ,$$

$$a_3 = -gc_i\left(\frac{1}{3}h_1^3 + \sigma h_1 H_2 h_o + \frac{1}{3}H_2^3\right) - \frac{1}{c_i}g^2(\sigma-1)h_1H_2\left(\frac{1}{3}h_1^2 + \sigma h_1 H_2 + \frac{1}{3}H_2^2\right),$$

$$a_4 = -\frac{1}{\rho_2}c_i H_2 ,$$

$$a_5 = c_i g h_1 - c_i^3 , \qquad (4.73)$$

and

$$c_i^4 - gh_o c_i^2 + g^2 h_1 H_2(1-\sigma) = 0 . \qquad (4.74)$$

All the variables except σ are dimensional in (4.72)-(4.74). The corresponding dimensional forms of (4.67) and (4.68) are,

$$c_s = \sqrt{\frac{gh_1H_2(1-\sigma)}{h_o}} \qquad (4.75)$$

$$\frac{1}{c_s}\zeta_{2t} - \zeta_{2x} + \frac{3}{2}\left(\frac{1}{h_1} - \frac{1}{H_2}\right)\zeta_2\zeta_{2x} - \frac{1}{6}h_1H_2\zeta_{2xxx} + \frac{H_2}{2gh_o\rho_2}p_{ox} - \frac{h_1}{2h_o}d_x = 0 . \qquad (4.76)$$

These forced KdV equations for two layer systems will be analyzed and the results discussed in Chapter VIII. Now the numerical scheme for solving the KdV equation is presented next.

4.2 A Numerical Scheme for the Forced KdV Equation

In the previous section, a forced KdV equation has been derived. Without losing generality, it can be represented in the following form

$$Q_t - c_i Q_x + a_2 QQ_x + a_3 Q_{xxx} + a_4 d_x = 0 , \qquad (4.77)$$

where Q represents the surface elevation of the upper or lower layer or the velocity of the upper or lower layer, d represents the external forcing, which may include both a surface pressure and a variation in the bottom topography, and the a_i's $(i = 2, 3, 4)$ are constant. This equation immediately follows from (4. 72) by a simple division because the first coefficient a_1 in (4. 72) is never zero, which is the case being considered here, that is, with $0 < \sigma < 1$.

Two finite-difference schemes for solving the forced KdV equation are presented below, one of which is explicit and the other, implicit.

A Taylor series expansion of Q with respect to time and the KdV equation (4. 77) are used in the explicit scheme, which is similar to that of Vliegenthart (1971). The series expansion for Q is

$$Q_i^{k+1} = Q_i^k + \Delta t\, Q_{it}^k + \frac{1}{2}(\Delta t)^2 Q_{itt}^k + O(\Delta t^3) \tag{4. 78}$$

with

$$Q_t = c_i Q_x - a_2 Q Q_x - a_3 Q_{xxx} - a_4 d_x \ , \tag{4. 79}$$

$$\begin{aligned} Q_{tt} = {} & -2c_i a_2 Q_x^2 - 2c_i a_2 Q Q_{xx} - 2c_i a_3 Q_{xxxx} + c_i^2 Q_{xx} - c_i a_4 d_{xx} \\ & + 2a_2^2 Q Q_x^2 + a_2^2 Q^2 Q_{xx} + 3a_2 a_3 Q_{xx}^2 + 5a_2 a_3 Q_x Q_{xxx} + 2a_2 a_3 Q_{xxxx} \\ & + a_3^2 Q_{xxxxxx} + a_2 a_4 Q_x d_x + a_2 a_4 Q d_{xx} + a_3 a_4 d_{xxxx} - a_4 d_{xt} \ , \end{aligned} \tag{4. 80}$$

which are obtained by invoking the forced KdV equation several times. The following central differencing approximations are used for the x derivatives in (4. 80) and (4. 81):

$$Q_{ix} = \frac{1}{2\Delta x}(Q_{i+1} - Q_{i-1}) + O(\Delta x^2) ,$$

$$Q_{ixx} = \frac{1}{\Delta x^2}(Q_{i+1} + Q_{i-1} - 2Q_i) + O(\Delta x^2) ,$$

$$Q_{ixxx} = \frac{1}{2\Delta x^3}(Q_{i+2} - 2Q_{i+1} + 2Q_{i-1} - Q_{i-2}) + O(\Delta x^2) ,$$

$$Q_{ixxxx} = \frac{1}{\Delta x^4}(Q_{i+2} - 4Q_{i+1} + 6Q_i - 4Q_{i-1} + Q_{i-2}) + O(\Delta x^2) ,$$

$$Q_{ixxxxxx} = \frac{1}{\Delta x^6}(Q_{i+3} - 6Q_{i+2} + 15Q_{i+1} - 20Q_i + 15Q_{i-1} - 6Q_{i-2} + Q_{i-3}) + O(\Delta x^2) .$$

To use these expressions, six boundary points are needed in every time step forward and boundary contamination of the results (such as by fictitious reflections of waves from the boundary) will occur relatively earlier than the two boundary points schemes, such as the one outlined in Chapter III and the following implicit scheme. In order to diminish such boundary contamination, we will adopt the following implicit scheme to solve the forced KdV equation numerically.

To apply the implicit scheme, we first change the KdV equation to the so-called regularized equation (Benjamin et al. (1972)),

$$Q_t - c_i Q_x + a_2 Q Q_x + \frac{1}{c_i} a_3 Q_{xxt} + a_4 d_x = 0 . \qquad (4.81)$$

which is obtained by making use of the leading order terms in (4.77), namely $Q_t = c_i Q_x$, in approximating the term Q_{xxx} by $c_i^{-1} Q_{xxt}$.

As elucidated by Whitham (1974, p. 463), (4.81) agrees with (4.77) for the dispersive relation on linear approximation for small wave-number k, yet (4.81) is superior to (4.77) for numerical calculations because it can effectively curtain numerical errors of grid sizes (large values of k).

A finite difference method with a predictor-corrector procedure is adopted. The spatial derivatives are approximated by central differencing and temporal derivatives by forward differences. The same window shifting procedure and open-boundary condition are used as described in Chapter III of this thesis. Only the main steps are presented here, and more details of the method can be found in the thesis of Lee (1985), p. 22-26. The resulting formulas are:

PREDICTOR

$$-Q_{i-1}^{\overline{k+1}} + (2 - \frac{1}{a_3} c_i \Delta x^2) Q_i^{\overline{k+1}} - Q_{i+1}^{\overline{k+1}} = 2Q_i^k - Q_{i+1}^k - Q_{i-1}^k$$

$$+ \frac{1}{a_3} c_i [\frac{1}{2}(a_2 Q_i^k - c_i)(Q_{i+1}^k - Q_{i-1}^k)\Delta t \Delta x - Q_i^k \Delta x^2 + a_4 \Delta t \Delta x^2 (d_x)_i^k] ,$$

(4.82)

CORRECTOR

$$-Q_{i-1}^{k+1} + (2 - \frac{1}{a_3} c_i \Delta x^2) Q_i^{k+1} - Q_{i+1}^{k+1} = 2Q_i^k - Q_{i+1}^k - Q_{i-1}^k - \frac{1}{a_3} c_i Q_i^k \Delta x^2$$

$$+ \frac{1}{2a_3} c_i [\frac{1}{2}(a_2 Q_i^k - c_i)(Q_{i+1}^k - Q_{i-1}^k)\Delta t \Delta x + a_4 \Delta t \Delta x (d_x)_i^k]$$

$$+ \frac{1}{2a_3} c_i [\frac{1}{2}(a_2 Q_i^{\overline{k+1}} - c_i)(Q_{i+1}^{\overline{k+1}} - Q_{i-1}^{\overline{k+1}})\Delta t \Delta x + a_4 \Delta t \Delta x^2 (d_x)_i^{k+1}] ,$$

(4.83)

where the same notations are used as in Chapter III and c_i is the characteristic velocity. Both (4.82) and (4.83) are linear algebraic equations and can be represented in the following matrix form

$$[K]\ (x) = (b)\ , \tag{4.84}$$

with $$(x) = \{Q_1, Q_2, \ldots, Q_n\}^T\ , \tag{4.85}$$

$$[K] = \begin{bmatrix} s & -1 & & & & \\ -1 & s & -1 & & & \\ & \ldots\ldots & & & & \\ & & & -1 & s & -1 \\ & & & & -1 & s \end{bmatrix}\ , \tag{4.86}$$

where the subscripts are such that Q_o is for the left boundary value and Q_{n+1} the right one and

$$s = 2 - \frac{1}{a_3} c_i \Delta x^2\ . \tag{4.87}$$

The matrix [K] is tridiagonal. The values of a_3 have been calculated for the two-layer system with h_1 ranging from 0.05 to 0.95 (by 0.05 increment) and for density ratios between 0.05 and 0.95 (with 0.05 increment). Within this range of the parameters all the calculated values of a_3 are negative for both the fast mode and the slow mode. Thus the matrix [K] seems strictly diagonally dominant for the two-layer system

The numerical results will be discussed in Chapter VIII.

V. INTERNAL WAVES WITH A RIGID TOP SURFACE

In this chapter, we consider a two-layer fluid system with a rigid horizontal top surface. The two layers of immiscible, inviscid, and incompressible fluids are unbounded in the horizontal directions and the same notations are used as before, except with the subscript for the interface elevation which is deleted, as shown in Figure 5.1. For predicting the behavior of this system two theoretical models are developed. One is given by a set of three equations of motion for three unknowns: namely, the interface elevation, and the layer-mean velocity potentials for the upper and lower layers. These equations are derived by applying the mass conservation principle and using the Bernoulli equations, similar to the approach described in Chapter II. Because there are three basic equations involved, this model will be called the THREE-equation model. The numerical scheme for computing solutions to the THREE-equation model will also be developed.

Another theoretical model gives a single equation, the forced KdV equation, which is obtained by applying the perturbation method after that introduced by Gardner & Morikawa (1960) for the single layer case.

5.1 The THREE-equation Model

5.1.1 Derivation of the THREE-equation model

The two small parameters are

$$\alpha = \frac{a}{h_o} \ll 1 , \tag{5.1}$$

and

$$\epsilon = \frac{h_o}{\lambda} \ll 1 , \tag{5.2}$$

which are assumed to be related, as before, by

$$\alpha = O(\epsilon^2) .$$

In terms of the dimensionless variables defined in (2.17) and (2.18), the equations and boundary conditions can be expressed as

Laplace equation

$$\phi_{zz} = -\epsilon^2 \nabla^2 \phi , \tag{5.3}$$

Bernoulli equation

$$p + \dot{\phi} + \frac{1}{2} \underline{U}^2 + z = 0 , \tag{5.4}$$

Mass conservation

$$-\dot{\zeta} + \nabla \cdot [(h_1 - \zeta) \underline{\bar{u}}_1] = 0 , \tag{5.5}$$

$$\dot{h}_2 + \dot{\zeta} + \nabla \cdot [(h_2 + \zeta) \underline{\bar{u}}_2] = 0 . \tag{5.6}$$

At the top surface the boundary condition requires that

$$w = 0 \qquad \text{at } z = h_1 . \tag{5.7}$$

At the interface three boundary conditions are imposed,

$$w_1 = \epsilon \left(\frac{\partial \zeta}{\partial t} + \underline{u}_1 \cdot \nabla \zeta\right) \qquad \text{at } z = \zeta , \tag{5.8}$$

$$w_2 = \epsilon \left(\frac{\partial \zeta}{\partial t} + \underline{u}_2 \cdot \nabla \zeta\right) \qquad \text{at } z = \zeta , \tag{5.9}$$

$$p_2 = \sigma p_1 \qquad \text{at } z = \zeta . \tag{5.10}$$

And at the bottom boundary, we have the condition

$$w = -\epsilon \frac{dh_2}{dt} \qquad \text{at } z = -h_2 , \tag{5.11}$$

with $$\sigma = \frac{\rho_1}{\rho_2} . \tag{5.12}$$

In addition, we have, as before,

$$\underline{u} = \nabla\phi \ , \tag{5.13}$$

$$w = \frac{1}{\epsilon}\frac{\partial\phi}{\partial z} \ . \tag{5.14}$$

We further reiterate that

$$\begin{aligned} \zeta &= O(\alpha) \ , \\ \underline{u} &= O(\alpha) \ , \\ w &= O(\alpha\epsilon) \ , \\ h_2 &= H_2 - d \ , \end{aligned} \tag{5.15}$$

with H_2 = constant and $d = O(\alpha)$. The position $z = 0$ is now set at the undisturbed interface position. The Laplace equation is satisfied by the expansion of ϕ, for each layer, as

$$\phi = \alpha \sum_{n=o}^{\infty} \epsilon^{2n} \Phi_{(2n)}(\underline{r}, z, t) \tag{5.16}$$

with

$$\Phi_{(o)} = \varphi_{(o)}(\underline{r}, t) \ , \tag{5.17}$$

$$\Phi_{(2)} = \varphi_{(2)}(\underline{r}, t) + z\varphi_{(3)}(\underline{r}, t) - \frac{1}{2} z^2 \nabla^2 \varphi_{(o)} \ , \tag{5.18}$$

where the linear term of z in $\Phi_{(o)}$ is deleted as required by the top surface and interface boundary conditions (5.7), (5.8) and (5.9) and the assumptions (5.15).

The following relations can be readily obtained

$$\underline{u} = \nabla\phi = \alpha[\underline{u}_{(o)} + \epsilon^2 \underline{u}_{(1)} + \epsilon^4 \underline{u}_{(2)} + \ldots] \ , \tag{5.19}$$

$$w = \frac{1}{\epsilon}\frac{\partial\phi}{\partial z} = \alpha\epsilon[w_{(1)} + \epsilon^2 w_{(2)} + \ldots] \ , \tag{5.20}$$

$$\underline{u}_{(o)} = \nabla\varphi_{(o)}(\underline{r}, t) = \alpha^{-1}\nabla\overline{\phi} + O(\epsilon^2) \ , \tag{5.21}$$

$$\underline{u}_{(1)} = \nabla\Phi_{(2)} \ , \tag{5.22}$$

$$w_{(1)} = \frac{\partial\Phi_{(2)}}{\partial z} = \varphi_{(3)} - z\nabla^2\varphi_{(o)} \ . \tag{5.23}$$

The $\varphi_{(3)}$ terms are determined from the bottom boundary condition and the interface boundary conditions

$$\varphi_{2(3)} = -\dot{h}_2\alpha^{-1} - H_2\nabla^2\varphi_{2(o)} \ , \tag{5.24}$$

$$\varphi_{1(3)} = -\dot{h}_2\alpha^{-1} - H_2\nabla^2\varphi_{2(o)} \ . \tag{5.25}$$

By applying the Bernoulli equations (5.4) to the two sides of the interface, we have for the upper and lower layers

$$\widetilde{p}_1 + \dot{\widetilde{\phi}}_1 + \frac{1}{2}(\widetilde{\underline{u}}\cdot\widetilde{\underline{u}} + \widetilde{w}^2)_1 + \zeta = 0 \ , \tag{5.26}$$

$$\widetilde{p}_2 + \dot{\widetilde{\phi}}_2 + \frac{1}{2}(\widetilde{\underline{u}}\cdot\widetilde{\underline{u}} + \widetilde{w}^2)_2 + \zeta = 0 \ , \tag{5.27}$$

where the quantities with "$\sim$" denote their values at the interface and the subscripts 1 and 2 represent the upper and lower layers, respectively. Equivalently, (5.26) and (5.27) can be expressed as

$$\dot{\overline{\phi}}_1 + \frac{1}{2}(\nabla\overline{\phi}_1)^2 + \zeta + \widetilde{p}_1 = \dot{\overline{\phi}}_1 + \frac{1}{2}(\nabla\overline{\phi}_1)^2 - \dot{\widetilde{\phi}}_1 - \frac{1}{2}(\widetilde{\underline{u}}\cdot\widetilde{\underline{u}} + \widetilde{w}^2)_1 \ , \tag{5.28}$$

$$\dot{\overline{\phi}}_2 + \frac{1}{2}(\nabla\overline{\phi}_2)^2 + \zeta + \widetilde{p}_2 = \dot{\overline{\phi}}_2 + \frac{1}{2}(\nabla\overline{\phi}_2)^2 - \dot{\widetilde{\phi}}_2 - \frac{1}{2}(\widetilde{\underline{u}}\cdot\widetilde{\underline{u}} + \widetilde{w}^2)_2 \ . \tag{5.29}$$

Substituting the series expansions (5.19)-(5.23) into (5.28) and (5.29), we obtain

$$\dot{\bar{\phi}}_1 + \frac{1}{2}(\nabla\bar{\phi}_1)^2 + \zeta + \tilde{p}_1 = (\frac{h_1}{2}\dot{\varphi}_{1(3)} - \frac{1}{6}h_1^2\nabla^2\dot{\varphi}_{1(o)})\alpha\epsilon^2 + O(\alpha^2\epsilon^2, \alpha\epsilon^4),$$

$$\dot{\bar{\phi}}_2 + \frac{1}{2}(\nabla\bar{\phi}_2)^2 + \zeta + \tilde{p}_2 = (-\frac{H_2}{2}\dot{\varphi}_{2(3)} - \frac{1}{6}H_2^2\nabla^2\varphi_{2(o)})\alpha\epsilon^2 + O(\alpha^2\epsilon^2, \alpha\epsilon^4), \tag{5.30}$$

where the following relations have been used

$$\overline{z_1} = \frac{h_1}{2} + O(\alpha) ,$$

$$\overline{z_2} = -\frac{H_2}{2} + O(\alpha) ,$$

$$\overline{z_1^2} = \frac{1}{3}h_1^2 + O(\alpha) ,$$

and

$$\overline{z_2^2} = \frac{1}{3}H_2^2 + O(\alpha) ,$$

By eliminating the $\varphi_{(3)}$'s, p_1 and p_2 from equations (5.24), (5.25), (5.30), and (5.10), the following equation is obtained

$$\dot{\bar{\phi}}_2 - \sigma\dot{\bar{\phi}}_1 + \frac{1}{2}(\nabla\bar{\phi}_2)^2 - \frac{1}{2}\sigma(\nabla\bar{\phi}_1)^2 + \zeta(1-\sigma) = \epsilon^2[\frac{1}{2}H_2\ddot{h}_2 + \frac{\alpha}{3}H_2^2\nabla^2\dot{\varphi}_{2(o)}] +$$

$$+ \sigma\epsilon^2[\frac{1}{2}h_1\ddot{h}_2 + \frac{\alpha}{2}h_1H_2\nabla^2\dot{\varphi}_{2(o)} + \frac{\alpha}{6}h_1^2\nabla^2\dot{\varphi}_{1(o)}] + O(\alpha\epsilon^4, \alpha^2\epsilon^2) . \tag{5.31}$$

Furthermore, from the expansions of the potentials (5.16) and (5.17) we note that $\alpha\varphi_{(o)}$ in (5.31) can be replaced by $\bar{\varphi}$ without affecting the order of the remainder term $O(\alpha\epsilon^4, \alpha^2\epsilon^2)$ and the following

relation between $\overline{\phi}_1$, $\overline{\phi}_2$ and ζ is obtained,

$$\dot{\overline{\phi}}_2 - \sigma\dot{\overline{\phi}}_1 + \frac{1}{2}(\nabla\overline{\phi}_2)^2 - \frac{1}{2}\sigma(\nabla\overline{\phi}_1)^2 + \zeta(1-\sigma) = \frac{\epsilon^2}{2}\ddot{h}_2(H_2 + \sigma h_1) +$$

$$\frac{1}{6}\sigma\epsilon^2 h_1^2 \nabla^2\dot{\overline{\phi}}_1 + \epsilon^2(\frac{1}{3}H_2^2 + \frac{1}{2}\sigma h_1 H_2)\nabla^2\dot{\overline{\phi}}_2 + O(\alpha\epsilon^4, \alpha^2\epsilon^2) \quad . \tag{5.32}$$

To complete the system, two more equations are required and they can be obtained from the continuity equations (5.5) and (5.6), by noting that for long waves,

$$\overline{\nabla\phi}_1 - \nabla\overline{\phi}_1 = O(\alpha\epsilon^4, \alpha^2\epsilon^2) \quad ,$$

and

$$\overline{\nabla\phi}_2 - \nabla\overline{\phi}_2 = O(\alpha\epsilon^4, \alpha^2\epsilon^2) \quad .$$

The two continuity equations then become

$$-\dot{\zeta} + \nabla\cdot[(h_1 - \zeta)\nabla\overline{\phi}_1] = O(\alpha\epsilon^4, \alpha^2\epsilon^2) \quad , \tag{5.33}$$

$$\nabla\cdot[(h_1 - \zeta)\nabla\overline{\phi}_1 + (h_2 + \zeta)\nabla\overline{\phi}_2] = -\dot{h}_2 + O(\alpha\epsilon^4, \alpha^2\epsilon^2) \quad . \tag{5.34}$$

The system of three equations (5.32), (5.33) and (5.34) can be solved numerically using the method similar to that presented in Chapter III, in which case the method involves a scheme for solving a set of linear algebraic equations with a coefficient matrix of bandwidth 7. In the present case of a rigid horizontal top surface it is possible to change the equations into a new form that only has a tridiagonal coefficient matrix instead of a matrix of bandwidth 7.

Another useful relation between the potentials can be obtained from enforcing the top-surface boundary condition, which yields

$$\varphi_{1(3)} = h_1 \nabla^2 \varphi_{1(o)} \quad . \tag{5.35}$$

A simple combination of (5.35) with (5.25) then gives

$$h_1 \nabla^2 \varphi_{1(o)} + H_2 \nabla^2 \varphi_{2(o)} = -\dot{h}_2 \alpha^{-1} \quad , \tag{5.36}$$

which can also be obtained from the continuity equations (5.5) and (5.6). Therefore,

$$h_1 \nabla^2 \overline{\phi}_1 + H_2 \nabla^2 \overline{\phi}_2 = -\dot{h}_2 + O(\alpha \epsilon^2) \quad . \tag{5.37}$$

If (5.37) is multiplied by $\frac{\epsilon^2}{h_1 + \sigma H_2} (\frac{1}{6} \sigma h_1^2 + \frac{1}{3} \sigma H_2^2 + \frac{1}{2} \sigma^2 h_1 H_2)$ and added to (5.31), there results the equation

$$\dot{R} - \epsilon^2 \frac{h_1 H_2 (\sigma h_1 + H_2)}{[3(h_1 + \sigma H_2)]} \nabla^2 \dot{R} + \frac{1}{2} (\nabla R)^2 + \sigma (\nabla R) \cdot (\nabla \overline{\phi}_1) + \frac{1}{2} (\sigma^2 - \sigma) (\nabla \overline{\phi}_1)^2$$

$$+ \zeta (1 - \sigma) = \epsilon^2 \{ \frac{H_2}{2} + \frac{1}{3} \sigma h_1 - \frac{\sigma H_2 (\sigma h_1 + H_2)}{[3(h_1 + \sigma H_2)]} \} \ddot{h}_2 + O(\alpha \epsilon^4, \alpha^2 \epsilon^2) \quad , \tag{5.38}$$

where $$R = \overline{\phi}_2 - \sigma \overline{\phi}_1 \quad , \tag{5.39}$$

which will be called the combined layer-mean potential, or simply the "combined mean potential". Finally, the equation (5.34) with unknowns $\overline{\phi}_1$ and $\overline{\phi}_2$ can be changed to one for R and $\overline{\phi}_1$ as

$$\nabla \cdot \{ [h_1 + \sigma h_2 + \zeta(\sigma - 1)] \nabla \overline{\phi}_1 \} + \nabla \cdot [(h_2 + \zeta) \nabla R] = -\dot{h}_2 + O(\alpha \epsilon^4, \alpha^2 \epsilon^2). \tag{5.40}$$

The required THREE-equation model now is comprised of the three equations (5.33), (5.38) and (5.40) for the unknowns ζ, R and $\overline{\phi}_1$.

5.1.2 A numerical scheme for the THREE-equation model

A finite-difference numerical method using the predictor-corrector two-step procedure has been developed for solving the above three basic equations. The time derivatives are approximated by the forward difference and the spatial derivatives by the central difference.

In the following calculations, only the two-dimensional case will be considered.

In the numerical scheme there are two stages for each time increment Δt. For the first stage, or the predictor stage, the provisional values at the provisional time-level $\overline{k+1}$ are calculated by using the known values at the time-level k. In the second stage, or the corrector stage, the unknown values at the time-level k+1 are obtained from the known values at time-levels k and $\overline{k+1}$. There are three steps in every stage: the first is to calculate ζ explicitly from (5.33), the second is to obtain R implicitly from (5.38), and third is to obtain $\overline{\phi}_1$ implicitly from (5.40). The upper bar over the ϕ_1 and the error terms $O(\alpha\epsilon^4, \alpha^2\epsilon^2)$ will be omitted in the sequel for brevity. Using the same notation as in Chapter III, the detailed formulas for the numerical calculations for the THREE-equation model can be written as follows:

PREDICTOR STAGE:

(5.33):

$$\zeta_i^{\overline{k+1}} = \zeta_i^k + \frac{\Delta t}{(\Delta x^2)}[\phi_{1,i-1}^k(h_1 - \frac{1}{2}\zeta_i^k - \frac{1}{2}\zeta_{i-1}^k) + \phi_{1,i}^k(\frac{1}{2}\zeta_{i-1}^k + \frac{1}{2}\zeta_{i+1}^k + \zeta_i^k - 2h_1) + \phi_{1,i+1}^k(h_1 - \frac{1}{2}\zeta_i^k - \frac{1}{2}\zeta_{i+1}^k)] \quad , \qquad (5.41)$$

(5.38):

$$-R_{i-1}^{\overline{k+1}} + (2+r)R_i^{\overline{k+1}} - R_{i+1}^{\overline{k+1}} = -R_{i-1}^{k} - R_{i+1}^{k} + (2+r)R_i^{k} +$$

$$+ \frac{r\Delta t}{\Delta x^2}\Big[-\frac{1}{8}(R_{i+1}^{k} - R_{i-1}^{k})^2 - \frac{\sigma}{4}(R_{i+1}^{k} - R_{i-1}^{k})(\phi_{1,i+1}^{k} - \phi_{1,i-1}^{k})$$

$$- \frac{(\sigma^2-\sigma)}{8}(\phi_{1,i+1}^{k} - \phi_{1,i-1}^{k})^2 - (1-\sigma)\Delta x^2 \zeta_i^{k} + \Delta x^2 sh_{2,i}^{k}\Big] , \tag{5.42}$$

where r and s are the constants defined by

$$r = \frac{3(h_1 + \sigma H_2)\Delta x^2}{\epsilon^2 h_1 H_2(\sigma h_1 + H_2)} , \tag{5.43}$$

$$s = \frac{\epsilon^2(2\sigma h_1^2 + \sigma H_2^2 + 3h_1 H_2)}{6(h_1 + \sigma H_2)} , \tag{5.44}$$

(5.40):

$$a_i \phi_{1,i-1}^{\overline{k+1}} - (a_i + b_i)\phi_{1,i}^{\overline{k+1}} + b_i \phi_{1,i+1}^{\overline{k+1}} = \frac{1}{2}\Big[(h_{2,i}^{k+1} + h_{2,i+1}^{k+1} + \zeta_i^{\overline{k+1}} + \zeta_{i+1}^{\overline{k+1}})$$

$$(R_{i+1}^{\overline{k+1}} - R_i^{\overline{k+1}}) - (h_{2,i}^{k+1} + h_{2,i}^{k+1} + \zeta_i^{\overline{k+1}} + \zeta_{i-1}^{\overline{k+1}})(R_i^{\overline{k+1}} - R_{i-1}^{\overline{k+1}})\Big] - \Delta x^2 h_{2,i}^{k+1} , \tag{5.45}$$

where

$$a_i = h_1 + \frac{1}{2}\sigma(h_{2,i-1}^{k+1} + h_{2,i}^{k+1}) + \frac{1}{2}(\sigma-1)(\zeta_i^{\overline{k+1}} + \zeta_{i-1}^{\overline{k+1}}) , \tag{5.46}$$

$$b_i = a_{i+1} . \tag{5.47}$$

CORRECTOR STAGE:

(5.33):

$$\zeta_i^{k+1} = \zeta_i^k + \frac{\Delta t}{2\Delta x^2}[\phi^k_{1,i-1}(h_1 - \tfrac{1}{2}\zeta_i^k - \tfrac{1}{2}\zeta_{i-1}^k)$$

$$+ \phi^k_{1,i}(\tfrac{1}{2}\zeta_{i-1}^k + \tfrac{1}{2}\zeta_{i+1}^k + \zeta_i^k - 2h_1) + \phi^k_{1,i+1}(h_1 - \tfrac{1}{2}\zeta_i^k - \tfrac{1}{2}\zeta_{i+1}^k)]$$

$$+ \frac{\Delta t}{2\Delta x^2}[\phi^{\overline{k+1}}_{1,i-1}(h_1 - \tfrac{1}{2}\zeta_i^{\overline{k+1}} - \tfrac{1}{2}\zeta_{i-1}^{\overline{k+1}})$$

$$+ \phi^{\overline{k+1}}_{1,i}(\tfrac{1}{2}\zeta_{i-1}^{\overline{k+1}} + \tfrac{1}{2}\zeta_{i+1}^{\overline{k+1}} + \zeta_i^{\overline{k+1}} - 2h_1) + \phi^{\overline{k+1}}_{1,i+1}(h_1 - \tfrac{1}{2}\zeta_i^{\overline{k+1}} - \tfrac{1}{2}\zeta_{i+1}^{\overline{k+1}})],$$

(5.48)

(5.38):

$$-R_{i-1}^{k+1} + (2+r)R_i^{k+1} - R_{i+1}^{k+1} = -R_{i-1}^k - R_{i+1}^k$$

$$+ (2+r)R_i^k + \frac{r\Delta t}{2\Delta x^2}[-\tfrac{1}{8}(R_{i+1}^k - R_{i-1}^k)^2 - \tfrac{\sigma}{4}(R_{i+1}^k - R_{i-1}^k)(\phi^k_{1,i+1} - \phi^k_{1,i-1})$$

$$- \frac{(\sigma^2-\sigma)}{8}(\phi^k_{1,i+1} - \phi^k_{1,i-1})^2 - (1-\sigma)\Delta x^2\zeta_i^k + \Delta x^2 \ddot{sh}^k_{2,i}$$

$$- \tfrac{1}{8}(R_{i+1}^{\overline{k+1}} - R_{i-1}^{\overline{k+1}})^2 - \tfrac{\sigma}{4}(R_{i+1}^{\overline{k+1}} - R_{i-1}^{\overline{k+1}})(\phi^{\overline{k+1}}_{1,i+1} - \phi^{\overline{k+1}}_{1,i-1})$$

$$- \frac{(\sigma^2-\sigma)}{8}(\phi^{\overline{k+1}}_{1,i+1} - \phi^{\overline{k+1}}_{1,i-1})^2 - (1-\sigma)\Delta x^2\zeta_i^{\overline{k+1}} + \Delta x^2 \ddot{sh}^{k+1}_{2,i}],$$

(5.49)

and (5.40):

$$a_i \phi_{1,i-1}^{k+1} - (a_i+b_i)\phi_{1,i}^{k+1} + b_i \phi_{1,i+1}^{k+1} = -\frac{1}{2}[(h_{2,i}^{k+1} + h_{2,i+1}^{k+1} + \zeta_i^{k+1} + \zeta_{i+1}^{k+1})$$

$$(R_{i+1}^{k+1} - R_i^{k+1}) - (h_{2,i}^{k+1} + h_{2,i-1}^{k+1} + \zeta_i^{k+1} + \zeta_{i-1}^{k+1})(R_i^{k+1} - R_{i-1}^{k+1})]$$

$$- \Delta x^2 \dot{h}_{2,i}^{k+1} \quad , \tag{5.50}$$

where

$$a_i = h_1 + \frac{\sigma}{2}(h_{2,i-1}^{k+1} + h_{2,i}^{k+1}) + \frac{(\sigma-1)}{2}(\zeta_i^{k+1} + \zeta_{i-1}^{k+1}) \quad , \tag{5.51}$$

$$b_i = a_{i+1} \quad . \tag{5.52}$$

The equations (5.42) and (5.49) can easily be solved because the coefficient matrix

$$K_1 = \begin{bmatrix} 2+r & -1 & & & \\ -1 & 2+r & -1 & & \\ & \cdots\cdots & & & \\ & & -1 & 2+r & -1 \\ & & & -1 & 2+r \end{bmatrix} \tag{5.53}$$

is symmetric and strictly diagonally dominant due to the property of $r > 0$, as is obvious from (5.43).

The equations (5.45) and (5.50) have the coefficient matrix

$$K = \begin{bmatrix} -a_1-b_1 & b_1 & & & \\ a_2 & -a_2-b_2 & b_2 & & \\ & \cdots\cdots & & & \\ & a_{n-1} & -a_{n-1}-b_{n-1} & b_{n-1} & \\ & & a_n & -a_n-b_n & \end{bmatrix}, \tag{5.54}$$

which is symmetric from (5.47) and (5.52). From these equations all the a_i and b_i are generally positive if small ζ is considered. This is especially true when the densities of the two layers are close. Under this positive assumption, these algebraic equation systems are well behaved in the sense that their inversion by Gaussian elimination can be performed safely without partial pivoting. (A proof is given in Appendix 1.)

To complete our description of the numerical scheme for the THREE-equation model, we state that the same open boundary condition (1) and the same window shifting scheme as those given in Chapter III can be used. Examples of the numerical results will be presented for this model in Chapter VIII.

5.2 Forced KdV Equation

Another plausible theoretical model for investigating the two-layer fluid system with a rigid horizontal top surface (see Figure 5.1) is the forced KdV equation, which will be derived in this section. Only the case of two-dimensional motions will be considered and all

the quantities will retain their dimensional form. In Chapter IV, it was shown that the waves are slowly varying functions with reference to a frame moving with a velocity close to a characteristic speed. On physical grounds, we expect this to remain valid for the general case of weakly nonlinear and weakly dispersive long waves moving with the disturbance within a transcritical speed range striding across a specific characteristic velocity. Following this reasoning, the required equation can be readily derived by invoking Gardner-Morikawa's transformation (Gardner & Morikawa (1960), equations (29) and (31))

$$\xi = \sqrt{\alpha}(x + ct) \quad , \tag{5.55}$$

$$\tau = \alpha^{3/2} t \quad , \tag{5.56}$$

where α is a small parameter.

With the physical quantities considered as functions of ξ and τ instead of functions of x and t (in addition to z), the above transformation signifies that they have only slow variations in the frame moving with the characteristic velocity c, where c is a constant, unknown quantity which must be determined as a part of the solution.

Corresponding to the new variables ξ and τ, the velocity potentials and the interface displacement ζ assume the following expansions

$$\begin{aligned}
\phi_1 &= \sqrt{\alpha}\,[\phi_{1(1)}(\xi, \tau, z) + \alpha \phi_{1(2)}(\xi, \tau, z) + \dots] \quad , \\
\phi_2 &= \sqrt{\alpha}\,[\phi_{2(1)}(\xi, \tau, z) + \alpha \phi_{2(2)}(\xi, \tau, z) + \dots] \quad , \\
\zeta &= \alpha \zeta_{(1)} + \alpha^2 \zeta_{(2)} + \dots \quad .
\end{aligned} \tag{5.57}$$

From the last formula, the small parameter α infers the order of magnitude of the interfacial wave elevation.

The Laplace equation holds for both layers,

$$\nabla^2\phi = 0 \ . \tag{5.58}$$

The boundary conditions are as follows: with $z = 0$ set at the top surface,

$$\phi_{1z} = 0 \qquad \text{at } z = 0 \ , \tag{5.59}$$

$$[\rho\{\phi_t + \frac{1}{2}(\nabla\phi)^2 + g\zeta\}]_1 = [\rho\{\phi_t + \frac{1}{2}(\nabla\phi)^2 + g\zeta\}]_2 \quad \text{at } z = \zeta - h_1 \ , \tag{5.60}$$

$$\zeta_x(\phi_{1x} - \phi_{2x}) = \phi_{1z} - \phi_{2z} \qquad \text{at } z = \zeta - h_1 \ , \tag{5.61}$$

$$\phi_{1z} = \zeta_t + \phi_{1x}\zeta_x \qquad \text{at } z = \zeta - h_1 \ , \tag{5.62}$$

$$\phi_{2z} = d_t + \phi_{2x}d_x \qquad \text{at } z = d - h_o \ , \tag{5.63}$$

in the same notations as before. With all the flow quantities regarded as functions of ξ, τ and z, the Laplace equation (5.58) becomes

$$(\alpha \frac{\partial^2}{\partial\xi^2} + \frac{\partial^2}{\partial z^2})\phi = 0 \ . \tag{5.64}$$

By further substituting the expansions (5.57) into (5.64), we obtain

1. $$\phi_{1(1)} = R_{(1)}(\xi, \tau) \ , \tag{5.65}$$

$$\phi_{2(1)} = L_{(1)}(\xi, \tau) \ , \tag{5.66}$$

2. $$\phi_{1(2)} = -\frac{1}{2}(z+h_1)^2 R_{(1)\xi\xi}(\xi,\tau)+R_{(2)}(\xi,\tau)(z+h_1)+R_{(3)}(\xi,\tau) \ , \tag{5.67}$$

$$\phi_{2(2)} = -\frac{1}{2}(z+h_o)^2 L_{(1)\xi\xi}(\xi,\tau)+L_{(2)}(\xi,\tau)(z+h_o)+L_{(3)}(\xi,\tau) \ , \tag{5.68}$$

3. $$\phi_{1(3)} = \frac{1}{24}(z+h_1)^4 R_{(1)\xi\xi\xi\xi}(\xi,\tau) - \frac{1}{6}(z+h_1)^3 R_{(2)\xi\xi}(\xi,\tau)$$
$$- \frac{1}{2}(z+h_1)^2 R_{(3)\xi\xi}(\xi,\tau)+R_{(4)}(\xi,\tau)(z+h_1)+R_{(5)}(\xi,\tau) \ , \tag{5.69}$$

$$\phi_{2(3)} = \frac{1}{24}(z+h_o)^4 L_{(1)\xi\xi\xi\xi}(\xi,\tau) - \frac{1}{6}(z+h_o)^3 L_{(2)\xi\xi}(\xi,\tau)$$
$$- \frac{1}{2}(z+h_o)^2 L_{(3)\xi\xi}(\xi,\tau)+L_{(4)}(\xi,\tau)(z+h_o)+L_{(5)}(\xi,\tau) \ , \tag{5.70}$$

where the terms linear in z for (5.65) and (5.66) have been deleted because of the boundary conditions (5.59) and (5.61) by virtue of the expansions (5.57).

As already shown in Chapter IV, the forcing function is assumed to be of order $O(\alpha^2)$.

$$d = \alpha^2 D \ . \tag{5.71}$$

The corresponding expansions of the boundary conditions (5.59)-(5.63) yield the following equations. From (5.59):

$$R_{(2)} - h_1 R_{(1)} = 0 \ , \tag{5.72}$$

$$R_{(4)} = -\frac{1}{6} h_1^3 R_{(1)\xi\xi\xi\xi} + \frac{1}{2} h_1^2 R_{(2)\xi\xi} + h_1 R_{(3)\xi\xi} \ . \tag{5.73}$$

From (5.60):

$$-c\sigma R_{(1)\xi} = -cL_{(1)\xi} + g\zeta_{(1)}(\sigma-1) \ , \tag{5.74}$$

$$\sigma R_{(1)\tau} - L_{(1)\tau} + \sigma c R_{(2)\xi} + \frac{1}{2} c H_2^2 L_{(1)\xi\xi\xi} - c H_2 L_{(2)\xi} - c L_{(3)\xi}$$

$$+ \frac{1}{2} \sigma R_{(1)\xi}^2 - \frac{1}{2} L_{(1)\xi}^2 + g\zeta_{(2)}(\sigma-1) = 0 \ . \tag{5.75}$$

From (5.61):

$$R_{(2)} = L_{(2)} - H_2 L_{(1)\xi\xi} \ , \tag{5.76}$$

$$\zeta_{(1)\xi}(R_{(1)\xi} - L_{(1)\xi}) = R_{(4)} - \frac{1}{6} H_2^3 L_{(1)\xi\xi\xi\xi} + \frac{1}{2} H_2^2 L_{(2)\xi\xi}$$

$$+ H_2 L_{(3)\xi\xi} - L_{(4)} - \zeta_{(1)} R_{(1)\xi\xi} + \zeta_{(1)} L_{(1)\xi\xi} \ . \tag{5.77}$$

From (5.62):

$$H_2 L_{(1)\xi\xi} - L_{(2)} + c\zeta_{(1)\xi} = 0 \ , \tag{5.78}$$

$$\zeta_{(1)} L_{(1)\xi\xi} - \frac{1}{6} H_2^3 L_{(1)\xi\xi\xi\xi} + \frac{1}{2} H_2^2 L_{(2)\xi\xi} + H_2 L_{(3)\xi\xi}$$

$$- L_{(4)} + L_{(1)\xi} \zeta_{(1)\xi} + c\zeta_{(2)\xi} + \zeta_{(1)\tau} = 0 \ . \tag{5.79}$$

From (5.63):

$$L_{(2)} = 0 \ , \tag{5.80}$$

$$L_{(4)} = cD_\xi \ . \tag{5.81}$$

The first order equations can be combined to yield, under the vanishing boundary conditions at infinity, the following relations:

$$-c\zeta_{(1)} = H_2 L_{(1)\xi} = -h_1 R_{(1)\xi} \ , \tag{5.82}$$

$$R_{(2)} = c\zeta_{(1)\xi} \ , \tag{5.83}$$

and

$$c^2 = \frac{gh_1H_2(1-\sigma)}{\sigma H_2+h_1} \tag{5.84}$$

For the next order results, we perform the following operation

$$(5.73)\sigma cH_2 + (5.75)_\xi h_1 H_2 + (5.77)\sigma cH_2 + (5.79)(cH_2\sigma + ch_1)$$

to cancel the unknowns $R_{(3)}$, $R_{(4)}$, $L_{(3)}$ and $\zeta_{(2)}$ with the help of (5.81) and (5.84). The result is the forced KdV equation

$$a_1 Q_\tau + a_2 QQ_\xi + a_3 Q_{\xi\xi\xi} + \frac{1}{2} D_\xi = 0 \ , \tag{5.85}$$

where

$$Q = \zeta_{(1)} \ , \tag{5.86}$$

$$\begin{aligned} a_1 &= -\frac{1}{c}\left(1 + \frac{1}{h_1}\sigma H_2\right) \ , \\ a_2 &= \frac{3}{2}\left(\frac{1}{H_2} - \frac{1}{h_1^2}\sigma H_2\right) , \\ a_3 &= \frac{1}{6} H_2(h_1\sigma + H_2) \ , \end{aligned} \tag{5.87}$$

or expressed in terms of the original variables

$$a_1(Q_t - cQ_x) + a_2 QQ_x + a_3 Q_{xxx} + \frac{1}{2} d_x = 0 \ , \tag{5.88}$$

with

$$Q = \zeta \ , \tag{5.89}$$

and a_1, a_2, and a_3 given by (5.87). We note that the above forced KdV equation, (5.85) or (5.88), represents a theoretical model for left-going long waves with c positive and for right-going waves with c negative. By making use of the first-order relations (5.82), the forced KdV equations for the velocities of the upper and the lower layers are found to have the same form as (5.88) but with different coefficients. The formulas (5.82) may take the more convenient form according to (5.57), (5.65) and (5.66),

$$-c\zeta \approx H_2 u_2 \approx -h_1 u_1 \ , \tag{5.90}$$

where u_1 and u_2 are the velocities in the x-direction for the upper and the lower layers. The previous results in dimensionless form with the notations and normalizations given in Section 5.1 are as follows:

NONDIMENSIONAL

$$a_1(Q_t - cQ_x) + a_2 QQ_x + \epsilon^2 a_3 Q_{xxx} + \frac{1}{2} d_x = 0 \ , \tag{5.91}$$

with the coefficients given by (5.87) and c given by (5.84) with $g = 1$ and (5.90) is also true for the present dimensionless variables. The numerical scheme for solving the forced KdV equation has been presented in Chapter IV and the results will be discussed in Chapter VIII.

VI. FORCED KDV EQUATION FOR CONTINUOUSLY STRATIFIED FLUID SYSTEM

The problem under consideration is concerned with weakly nonlinear long waves in a continuously stratified fluid system, which is assumed to be inviscid and incompressible. The primary density distribution (which prevails in steady state without disturbance) is $\overline{\rho}(z)$ and $\hat{\zeta}(x, y, z_o, t)$ is the vertical displacement of a material surface from its undisturbed position at the $z = z_o$ plane at time $t = 0$,

$$z = z_o + \hat{\zeta}(x, y, z_o, t) \quad . \tag{6.1a}$$

The vertical component of the fluid velocity is then

$$w = \frac{d\hat{\zeta}}{dt} = \hat{\zeta}_t + u\hat{\zeta}_x + v\hat{\zeta}_y \quad . \tag{6.1b}$$

By assuming the fluid to be incompressible we imply that

$$\frac{d\rho}{dt} = \rho_t + u\rho_x + v\rho_y + w\rho_z = 0 \quad . \tag{6.1c}$$

When at rest, the stably stratified density profile,

$$\rho = \overline{\rho}(z) \quad , \tag{6.1d}$$

is assumed given. From the above four equations it follows that

$$\rho(x, y, z, t) = \overline{\rho}\ (z - \hat{\zeta}(x, y, z_o, t)) \quad . \tag{6.1e}$$

Notice that the function ρ on the right-hand side of (6.1e) is simply $\overline{\rho}\ (z_o)$.

As external forcings, we consider surface pressures or bottom variations, and the system is shown in Figure 6.1. Because

of the density variation, the motion in general will be rotational and velocity potentials do not exist. In this chapter the principle of mass conservation and the momentum equations will be used to derive the forced KdV equation for this case. Finally a numerical scheme for determining its coefficients will be presented.

6.1 Mass Conservation and Momentum Equations

Only two-dimensional problems will be considered in this chapter (horizontal **x** and vertical z) and the physical quantities will be given in dimensional form.

The continuity equation,

$$u_x + w_z = 0 \ , \tag{6.2}$$

is a consequence to the assumption (6.1c), where the subscripts stand for partial differentiations as before. Here u is the horizontal velocity and w the vertical component.

The x- and z- components of the momentum equations are

$$\rho(u_t + uu_x + wu_z) = -p_x \ , \tag{6.3}$$

$$\rho(w_t + uw_x + ww_z) = -p_z + g(\bar{\rho} - \rho) \ , \tag{6.4}$$

where p is the disturbed "excess pressure", i.e., the pressure above the local hydrostatic pressure in the state of rest. The boundary conditions at the top surface and at the bottom are:

$$p + \int_{h+\bar{\zeta}}^{h} g\bar{\rho}\,(z)dz = p_o \qquad \text{at } z = h + \bar{\zeta} \ , \tag{6.5}$$

$$\zeta = d \qquad \text{at } z = d \ , \tag{6.6}$$

where $\bar{\zeta}$ is the wave elevation at the top surface ($z = h + \bar{\zeta}$), $z = 0$ is set as datum at the bottom level, d is the bottom depth variation from the level $z = 0$, h is the undisturbed constant water depth, aside from d, and p_o is the external surface pressure acting on the top surface (cf. Figure 6.1).

We again adopt, after Gardner-Morikawa, the transformation

$$\xi = \sqrt{\alpha}(x + ct) \quad , \tag{6.7}$$

$$\tau = \alpha^{3/2} t \quad , \tag{6.8}$$

where α is a small parameter (e.g., a measure of the wave amplitude with reference to depth h), and all the physical quantities are considered as functions of ξ, τ and z. The basic equations and the boundary conditions then become

$$u_\xi \sqrt{\alpha} + w_z = 0 \quad , \tag{6.9}$$

$$\rho(u_\tau \alpha^{3/2} + c\sqrt{\alpha} u_\xi + \sqrt{\alpha} u u_\xi + w u_z) = -\sqrt{\alpha} p_\xi \quad , \tag{6.10}$$

$$\rho(w_\tau \alpha^{3/2} + c\sqrt{\alpha} w_\xi + \sqrt{\alpha} u w_\xi + w w_z) = -p_z + g(\bar{\rho} - \rho) \quad , \tag{6.11}$$

and

$$p = p_o - \int_{h+\bar{\zeta}}^{h} g\bar{\rho}(z)dz \qquad \text{at } z = h+\bar{\zeta} \quad , \tag{6.12}$$

$$\zeta = d \qquad \text{at } z = d \quad . \tag{6.13}$$

6.2 Expansions

For u, ζ, and p, we introduce the following expansions

$$u = \alpha u_1(\xi, \tau, z) + \alpha^2 u_2(\xi, \tau, z) + \ldots ,$$

$$\zeta = \alpha \zeta_1(\xi, \tau, z) + \alpha^2 \zeta_2(\xi, \tau, z) + \ldots , \qquad (6.14)$$

$$p = \alpha p_1(\xi, \tau, z) + \alpha^2 p_2(\xi, \tau, z) + \ldots .$$

In the above expansion for $\zeta(x, z, t)$, ζ_n is regarded as a function of (x, z, t) by inversion of (6.1a) applying the implicit function theorem. The expansion for w can then be deduced as follows:

$$\begin{aligned} w &= \zeta_t + u\zeta_x + w\zeta_z \\ &= \alpha^{3/2}\zeta_\tau + c\sqrt{\alpha}\zeta_\xi + u\sqrt{\alpha}\zeta_\xi + w\zeta_z \\ &= c\zeta_{1\xi}\alpha^{3/2} + (\zeta_{1\tau} + u_1\zeta_{1\xi} + c\zeta_{1\xi}\zeta_{1z} + c\zeta_{2\xi})\alpha^{5/2} \\ &\quad + O(\alpha^{7/2}) . \end{aligned} \qquad (6.15)$$

By substituting these expansions into (6.9)-(6.13), using the small external forcing hypotheses,

$$p_o = \alpha^2 P , \qquad (6.16)$$

$$d = \alpha^2 D , \qquad (6.17)$$

and incorporating the Taylor's series expansion of the density relation (6.1e), the following relations are obtained: for the continuity equation,

$$\begin{aligned} &u_{1\xi} + \alpha u_{2\xi} + c\zeta_{1\xi z} + \alpha[\zeta_{1\tau z} + c\zeta_{2\xi z} + (u_1\zeta_{1\xi})_z \\ &\quad + c(\zeta_{1\xi}\zeta_{1z})_z] = O(\alpha^2) , \end{aligned} \qquad (6.18)$$

for the horizontal momentum equation

$$[\bar{\rho} - \alpha\zeta_1 \bar{\rho}'][cu_{1\xi} + \alpha(cu_{2\xi} + u_{1\tau} + u_1 u_{1\xi} + c\zeta_{1\xi} u_{1z})] + p_{1\xi} + \alpha p_{2\xi}$$

$$= O(\alpha^2) \ , \tag{6.19}$$

where $\bar{\rho}'$ means $\frac{d\bar{\rho}(z)}{dz}$, and for the vertical momentum equation,

$$c^2\zeta_{1\xi\xi}\bar{\rho}\alpha + p_{1z} + \alpha p_{2z} = g[\zeta_1 \bar{\rho}' + \alpha\zeta_2 \bar{\rho}' - \tfrac{1}{2}\alpha\bar{\rho}'' \zeta_1^2] + O(\alpha^2) \ . \tag{6.20}$$

The boundary condition for the top surface becomes

$$p_1 + \alpha p_2 + \alpha\zeta_1 p_{1z} + O(\alpha^2) = \alpha P + g\bar{\rho}(\zeta_1 + \alpha\zeta_2 + \alpha\zeta_{1z}\zeta_1)$$

$$+ \tfrac{1}{2} g\bar{\rho}' \alpha\zeta_1^2 \quad \text{at} \quad z = h \ , \tag{6.21}$$

where $\bar{\zeta}$ has been expanded about $z = h$ by

$$\bar{\zeta} = \zeta(h) + \zeta_z(h)\zeta(h) + O(\alpha^3) \ , \tag{6.22}$$

for x and t fixed. The bottom boundary condition is,

$$\zeta_1 + \alpha\zeta_2 + O(\alpha^2) = \alpha D \quad \text{at} \quad z = 0 \ . \tag{6.23}$$

6.3 The First-Order Equations

Using the boundary conditions that u_j, ζ_j and p_j vanish at infinity, we obtain the first-order equations as

$$p_1 = c^2\bar{\rho}\zeta_{1z} \tag{6.24}$$

$$u_1 = -c\zeta_{1z} \tag{6.25}$$

$$p_1 = g\bar{\rho}\,\zeta_1 \qquad \text{at } z = h \quad , \tag{6.26}$$

and

$$(\bar{\rho}\,\zeta_{1z})_z = \frac{g}{c^2}\,\bar{\rho}'\,\zeta_1 \quad , \tag{6.27a}$$

$$\zeta_1 = 0 \qquad \text{at } z = 0 \quad , \tag{6.27b}$$

$$\zeta_{1z} = \frac{g}{c^2}\,\zeta_1 \qquad \text{at } z = h \quad , \tag{6.27c}$$

The system of equations (6.27) defines an eigenvalue problem whose solution will determine the eigenvalue c and the eigenfunction ζ_1. This problem has, in general, infinitely many eigenvalues and corresponding eigenfunctions and each pair represents one (normal) mode of free oscillations that the system can perform.

Since ξ and τ only appear as parameters in system (6.27), we may assume the solution form by separation of variables as

$$\zeta_1 = E(z)N(\xi, \tau) \quad , \tag{6.28}$$

where $E(z)$ is an eigen-solution of the following Sturm-Liouville problem corresponding to eigenvalue c:

$$(\bar{\rho}\,E')' = \frac{1}{c^2}\,g\bar{\rho}'\,E \quad , \tag{6.29}$$

with the boundary conditions

$$E = 0 \qquad \text{at } z = 0 \quad , \tag{6.30}$$

$$E' = \frac{1}{c^2}\,gE \qquad \text{at } z = h \quad , \tag{6.31}$$

where the prime means differentiation with respect to z. To each normal mode of ζ_1, the corresponding pressure and velocity are given by (6.24) and (6.25).

6.4 Second Order Equations

From equations (6.18)-(6.20) and boundary conditions (6.21) and (6.23), we obtain the second order equations as

$$u_{2\xi} + \zeta_{1\tau z} + c\zeta_{2\xi z} + (u_1 \zeta_{1\xi} + c\zeta_{1\xi}\zeta_{1z})_z = 0 \ , \tag{6.32}$$

$$-\zeta_1 \bar{\rho}' cu_{1\xi} + \bar{\rho}(cu_{2\xi} + u_{1\tau} + u_1 u_{1\xi} + c\zeta_{1\xi}u_{1z}) + p_{2\xi} = 0 \ , \tag{6.33}$$

$$c^2 \zeta_{1\xi\xi}\bar{\rho} + p_{2z} = g(\zeta_2 \bar{\rho}' - \frac{1}{2}\bar{\rho}''\zeta_1^2) \ , \tag{6.34}$$

$$\zeta_2 = D \qquad \text{at } z = 0 \ , \tag{6.35}$$

$$p_2 + \zeta_1 p_{1z} = P + g\bar{\rho}\,\zeta_2 + g\bar{\rho}\,\zeta_1\zeta_{1z} + \frac{1}{2} g\bar{\rho}'\zeta_1^2 \qquad \text{at } z = h \ . \tag{6.36}$$

By eliminating u_2 and p_2 from (6.32)-(6.34) and using (6.28) and (6.25), we find

$$u_1 = -cNE' \ , \tag{6.37}$$

$$c^2(\bar{\rho}\,\zeta_{2\xi z})_z - g\bar{\rho}'\,\zeta_{2\xi} = -g\bar{\rho}''NN_\xi E^2 - c^2\bar{\rho}\,N_{\xi\xi\xi}E - 2cN_\tau(\bar{\rho}E')'$$

$$+c^2 NN_\xi[\bar{\rho}(E'^2 - EE'') + \bar{\rho}'EE']' \ , \tag{6.38}$$

The boundary conditions to this order are found as follows

$$\zeta_2 = D \qquad \text{at } z = 0 \ , \tag{6.39}$$

$$c^2\zeta_{2\xi z} - g\zeta_{2\xi} = \frac{1}{\rho} P_\xi - \frac{2g}{c} N_\tau E + NN_\xi\left(\frac{3g^2}{c^2}E^2 - c^2 EE''\right)$$

$$\text{at } z = h \ . \tag{6.40}$$

Equation (6.38) and boundary conditions (6.39) and (6.40) constitute an inhomogeneous Sturm-Liouville problem for $\zeta_{2\xi}$. Since c has

been determined with ζ_1 and is also an eigenvalue of the system (6.38)-(6.40), it follows from Fredholm's Alternative Theorem that in order to have a solution for ζ_2, (6.38) must satisfy the required compatibility condition. According to the fourth formula of (G) in Ince (1926), p. 268 (there is a mistake, the K inside the integral should be deleted), the inhomogeneous terms of (6.38) must satisfy the following equation, after some simplification,

$$a_1 N_\tau + a_2 N N_\xi + a_3 N_{\xi\xi\xi} + c^2 \bar{\rho}(0) E'(0) D_\xi + E(h) P_\xi = 0 \quad , \tag{6.41}$$

where

$$a_1 = -2c \int_o^h \bar{\rho} E'^2 dz \quad , \tag{6.42}$$

$$a_2 = 3c^2 \int_o^h \bar{\rho} E'^3 dz \quad , \tag{6.43}$$

$$a_3 = c^2 \int_o^h \bar{\rho} E^2 dz \quad , \tag{6.44}$$

This equation is the forced KdV equation we sought. By the relation (see equation (6.14))

$$\zeta \sim \alpha\zeta_1 = \alpha N E \quad , \tag{6.45}$$

the forced KdV equation (6.41) can be restored to the form of original variables as

$$a_1(Q_t - cQ_x) + \frac{a_2}{E(z)} QQ_x + a_3 Q_{xxx} + c^2 \bar{\rho}(0) E'(0) E(z) d_x + E(h) E(z) p_{ox} = 0 \quad , \tag{6.46a}$$

with

$$Q = \zeta \ . \tag{6.46b}$$

Equation (6.46) is for the left- or right-going forced wave motions accordingly as c is positive or negative. If the surface pressure term is absent, (6.46) agrees with equation 3.6 obtained by Grimshaw & Smyth (1985).

For the case of continuously stratified systems with a rigid top surface, the resulting equations are also the forced KdV equation (6.46a,b) with the coefficients (6.42)-(6.44) but with the eigenvalue c and the eigenfunction E now satisfying (6.29) and the boundary conditions

$$E = 0 \qquad \text{at } z = 0 \text{ and } z = h \ . \tag{6.47}$$

For two-layer systems, the density profile is a step function in z, for which case the c and E can be easily derived from the general equations (6.29)-(6.31). There are two values for c^2 and the corresponding E's are linear functions of z in each layer. The resulting KdV equation agrees with that obtained in Chapters IV and Chapter V.

6.5 Eigenvalues and Eigenfunctions

In both cases, whether the top surface is free or a fixed rigid plate, the two eigenvalue problems for ζ_1 given above are self-adjoint Sturm-Liouville systems (Ince (1926), p. 217). However, we note that the eigenvalue c appears not only in the differential equation but also in the top-surface second boundary condition in the system (6.29)-(6.31). For simplicity, $\overline{\rho'}$ is assumed always negative. Under this

assumption it can be proved that the two eigenvalue systems each has infinitely many real eigenvalues and they can be arranged in decreasing order of magnitude as

$$c_o,\ c_1,\ c_2,\ldots,c_j\ldots\ , \tag{6.48}$$

with the limit point zero if positive c_j's are considered. The corresponding eigenfunctions are

$$E_o,\ E_1,\ E_2,\ldots,E_j\ldots\ , \tag{6.49}$$

and E_j has exactly j zeros in the interval $(0, h)$ for $j = 0, 1, 2, \ldots$ On the contrary, every two-layer system has only two eigenvalues and eigenfunctions. As far as known to the author, the only analytical solution (in closed form) of the eigenvalue problems (6.29)-(6.31) or (6.29) and (6.47) with a primary density distribution varying with the depth is that for the exponential distribution $\rho = \exp(-\delta z)$, where $\delta > 0$ (Benney (1966), p. 60). For the density profile $\rho(z)$ in our experiment, the method of Taylor's series expansion will be used to solve the eigenvalue problem.

Nondimensional variable representations will be used in the sequel: z is normalized by h, ρ by a reference density, c^2 by gh and E can be taken as dimensionless. Then the system (6.29) becomes

$$(\bar{\rho}E')' = \frac{1}{c^2}\bar{\rho}'E\ , \tag{6.50a}$$

with the boundary conditions

$$E = 0 \qquad \text{at } z = 0\ , \tag{6.50b}$$

$$E' = \frac{1}{c^2}E \qquad \text{at } z = 1\ . \tag{6.50c}$$

The basic density distribution is assigned the following form, which can be very well fitted for comparison with experiments,

$$\bar{\rho} = \frac{1}{2}(\rho_2 - \rho_1)\tanh[k(H-z)] + \frac{1}{2}(\rho_2 + \rho_1) \quad , \tag{6.51}$$

where ρ_1, ρ_2, k and H are constants with $\rho_2 > \rho_1$, $k > 0$ and $0 < H < 1$. With this density distribution, equation (6.50a) becomes

$$\frac{1}{ak}\{a\tanh[k(H-z)] + b\}\cosh^2[k(H-z)]\,E'' - E' + \frac{1}{c^2}E = 0 \quad , \tag{6.52}$$

where

$$a = \frac{1}{2}(\rho_2 - \rho_1) \quad , \qquad b = \frac{1}{2}(\rho_2 + \rho_1) \quad , \tag{6.53}$$

and

$$b > a > 0 \quad . \tag{6.54}$$

Since equation (6.52) has no singularities on the real z-axis, $0 < z < 1$, its solution may be expanded in Taylor's series at any point in this region. For convergence of the series, the points in the complex z plane where the coefficient of the second order derivative term vanishes are considered and the nearest ones (to the real region $(0, 1)$) are

$$z_1 = H - \frac{\pi}{2k}\,i \quad , \tag{6.55}$$

$$z_2 = H - \frac{1}{2k}\left[\ln\left(\frac{\rho_1}{\rho_2}\right) + \pi i\right] \quad , \tag{6.56}$$

where i is the imaginary unit, $i = \sqrt{-1}$, and $\ln$ denotes natural logarithm. Two Taylor series expansions are employed, one about

$z = 0$ and the other about $z = 1$, with the radius of convergence $R_o = |z_1|$ and $R_1 = |z_2 - 1|$, respectively, where

$$R_o^2 = H^2 + \frac{\pi^2}{4k^2} \quad , \tag{6.57}$$

and

$$R_1^2 = [1 - H - \frac{1}{2k} \ln(\frac{\rho_2}{\rho_1})]^2 + \frac{\pi^2}{4k^2} \quad , \tag{6.58}$$

which readily follow from (6.55) and (6.56). For the case when $(1 - \frac{\rho_1}{\rho_2})$ is small, the two regions of convergence generally have an overlapped region, though when the overlapped region is narrow, a large number of terms of the series will be required.

By using one Taylor series about $z = 0$,

$$E^{(o)} = e_1 + e_2 z + e_3 z^2 + \ldots \quad , \tag{6.59}$$

and the other about $z = 1$,

$$E^{(1)} = E_1 + E_2 Z + E_3 Z^2 + \ldots \quad (Z = z-1) \quad , \tag{6.60}$$

and equation (6.52), the coefficients of these series can be determined if the first two coefficients are known. The relations are

$$\begin{aligned} \frac{(i+2)!}{i!}(b + A)e_{i+3} &= aK(i+1)e_{i+2} - \frac{aK}{c^2} e_{i+1} \\ &- \frac{(i+1)!}{(i-1)!} BK\, e_{i+2} - \frac{i!}{(i-2)!\,2!} AK^2 e_{i+1} \\ &- \frac{(i-1)!}{(i-3)!3!} BK^3 e_i - \ldots - \frac{2!}{i!}(A \text{ or } B)K^i e_3 \quad , \\ & \qquad (i = 0, 1, 2, \ldots) \end{aligned} \tag{6.61}$$

where

$$A = a \sinh(KH) + b \cosh(KH) \qquad (K = 2k) ,$$

and

$$B = -a \cosh(KH) - b \sinh(KH) .$$

For the coefficients E_i, formula (6.61) also holds except now with

$$A = -a \sinh(K-KH) + b \cosh(K-KH) , \quad (K = 2k) ,$$

and

$$B = -a \cosh(K-KH) + b \sinh(K-KH) .$$

By (6.54), $b + A$ is not zero, therefore e_{i+3} can be readily obtained from (6.61).

The first coefficient is required to vanish by the boundary condition at $z = 0$ and e_2 can be arbitrary and normalized to be 1. That is,

$$e_1 = 0, \quad e_2 = 1 . \tag{6.62}$$

The coefficients E_1 and E_2 are specified as follows

$$E_1 = c^2 , \qquad E_2 = 1 . \tag{6.63}$$

Thus, all the coefficients of the expansions, e_i's and E_i's are determined, and so are $E^{(o)}$ and $E^{(1)}$. Finally, $E^{(o)}$ and $E^{(1)}$ can be employed to construct the solution of the eigenvalue system (6.52) considered

$$\begin{aligned} E &= E^{(o)} \qquad (\text{for } 0 < z < z_o) , \\ E &= pE^{(1)} \qquad (\text{for } z_o < z < 1) , \end{aligned} \tag{6.64}$$

where ρ is a constant to be determined by the matching $E^{(o)}$ and $E^{(1)}$ at some desirable matching point z_o located in the overlapped region of convergence. This new E satisfies the boundary conditions and the differential equation in the two separate regions. For this E to be the desired solution, continuities of E and E' at the matching point z_o are required and they are

$$E^{(o)}(z = z_o) = pE^{(1)}(Z = z_o - 1)$$

and

$$E^{(o)\prime}(z = z_o) = pE^{(1)\prime}(Z = z_o - 1) \quad . \tag{6.65}$$

A necessary and sufficient condition for satisfying both conditions in (6.65) is

$$S = E^{(o)}(z = z_o)E^{(1)\prime}(Z = z_o - 1) - E^{(o)\prime}(z = z_o)E^{(1)}(Z = z_o - 1) = 0 \tag{6.66}$$

When this equation is satisfied, p can be found from (6.65) and the eigenfunction E is then determined. Finally, equation (6.66) is used to determine the eigenvalue c. Thus, the eigenvalue and the eigenfunction are solved.

In summary, the procedure of solving the eigenvalue problem (6.52) with boundary conditions (6.50b) and (6.50c) is as follows. First try some value for c; with this c, $E^{(o)}$ and $E^{(1)}$ can be determined and S of (6.66) is calculated. Repeated trials can provide a satisfactory value for the eigenvalue c. Then from either one of (6.65) p is determined, and $E^{(o)}$, $E^{(1)}$ and therefore the eigenfunction E are determined.

For the flat-top surface case, the eigenvalue problem (6.47) can be solved using the preceding formulas with only one revision: the first equation of (6.63) is changed to

$$E_1 = 0 \ . \tag{6.67}$$

After the eigenvalue problem is solved, the coefficients of the forced KdV equation for the continuously stratified system can be obtained numerically by applying formulas (6.42-6.44) and then the forced KdV equation is solved by the method shown in section 4.2. The results will be presented in Chapter VIII.

VII. EXPERIMENTAL STUDY ON THE GENERATION OF INTERNAL SOLITONS

By employing a bottom bump, which moves with a transcritical velocity about a characteristic velocity, along the floor of a two-layer fluid system as a moving disturbance, internal solitons were found, in our laboratory experiments, to be generated, surging ahead of the disturbance (bump) one after another periodically. The present experimental studies are primarily interested in the lower transcritical range of a two-layer fluid system, or in the first internal transcritical range of a continuously stratified fluid system. The equipment and measurements of the experiments will be presented in this chapter.

7.1 Experimental Equipment

The experiments were performed in the wave tank in 004 Thomas Laboratory of the California Institute of Technology. The wave tank, constructed with 0.5 inch glass on all the containing sides, is approximately 7.5 meters long and has a 0.76m (wide) by 0.6m (high) cross section. The unevenness of the tank bottom from the horizontal plane is less than $\pm$ 0.1cm.

The experiments employed a moving bottom bump as an external forcing agency, which is easier to manage than dealing with moving surface pressure disturbances (cf. Figure 7.1). A two-dimensional aluminum bump, with a length of 72cm, which spanned the width of the tank, had a circular-arc top surface and a flat bottom which was adjusted in height so there was a clearance of about

0.05cm from the bottom of the tank at the highest location of the tank bottom. To avoid any undesired electric interference between the bump and the wave gauges, the bump was electrically insulated with a coating of Varsity spray enamel No. 1140. With the coating, the bump had the cross section of 0.66cm high and 4.9cm wide. It was rigidly connected to a towing carriage which can move along the two parallel tracks mounted on the flanged top of the side walls of the tank under tow by a one-fourth HP dc motor (Bodine NSH-55) through a cable and pulley system. The speed of the carriage was controlled remotely using a Minaric variable speed control (Model W63). The carriage could be brought to its working speed (about 6cm/s) from rest very quickly (less than 0.5 second) and then maintained constant for the experiment. The departure of the parallel tracks from the horizontal level was $\pm$ 0.03cm.

The fluids used for the experiments were fresh water in the upper layer and brine in the lower layer, with a specific density of about 1.03. Our experience showed that brine with higher densities would cause some electric behavior not suitable or controllable for taking measurements in the experiments conducted. The brine was dyed red with Schilling food coloring to make the profile of the internal waves stand out pellucidly for easy visualization. Shortly after preparation for the experiment, the fluid system consisted of an upper layer of fresh water, a lower layer of brine, and a narrow mixed layer, called pycnocline, between them, across which the density increases monotonically from the fresh water to the original brine. It is desirable to make this mixing layer as thin as possible for various

reasons, one for making direct comparisons with the two-layer fluid model and another for making the internal wave profile very sharp. To achieve this objective, the following tank-filled procedure was adopted. First, the tank was filled to a desired height with fresh water, say h_1. Then the brine, prepared beforehand to have the desired density and quantity in a separate tank, was fed into the tank to form the lower layer through eight feeding tubes (Resinite vinyl insulation sleeving No. 9 with 0.118 I.D. and 0.20 wall) located evenly apart along the length of a sidewall of the tank. The best results for stratification of the fluid system were obtained with a suitable siphon-feeding rate and with the ends of the feeding tubes directed perpendicular towards and nearly touching the tank bottom so that the brine would spread evenly over the bottom of the tank with least possible disturbance to the formation of the fluid system. An optimum filling rate ranged between about 0.6 to 0.8cm increase in height of the brine layer per hour. Follwing this procedure we found the resulting system to be quite stable, the pycnocline to be relatively thin, and the demarcation surface between the colorless fresh-water layer and the underneath layer of colored brine quite sharp. This sharp layer separation could be maintained, apparently with negligible cross-layer mass diffusion for several hours. This demarcation surface will be called the color interface. The pycnocline was generally found to be about 1.5cm thick at the beginning of a series of experiments (of commonly 10 runs) and about 2cm at the end of the series. Its thickness is defined by the ratio of the maximum density difference $\rho_2 - \rho_1$ (i.e., between ρ_2 at the bottom and ρ_1 at the

top surface) to the maximum density gradient, that is,

$$\delta = \frac{\rho_2 - \rho_1}{\max_{z \in [o, h]} (-\frac{dg}{dz})} \quad . \tag{7.1}$$

We note that the color interface was usually not the surface where the maximum density gradient was found. Let the total depth of the fluid system inside the tank be h after each filling of the brine layer (under the fresh water layer of depth h_1), which would typically take three to four hours to finish, then $H_2 = h-h_1$ would be the height of the brine layer according to the supply from the brine storage. Disregarding the mass diffusion that must have occurred, we call h_1 and H_2 the nominal depths of the upper and the lower layers and their interface, the nominal interface. The color interface was usually found not to coincide with the nominal interface, probably due to some inevitable turbulent mixing during the filling operation and the diffusion effects of the dye and the salt. In general the color interface was found to lie 1 to 2cm higher than the nominal interface for general experimental situations.

The carriage speed was measured by a tacometer (Servo-tek D-C generator ST-721-7B 7v/1000RPM) in contact with one of the tracks. To cross check the carriage speed, two electric switches, 4.2 meters apart and connected to a clock, were used to measure the average speed of the carriage over the middle range of each run.

7.2 Measurements of Wave Elevations and Density Distribution

A set of wave gauges, of resistance type, were used to

measure the elevations of both the top surface waves and the internal waves primarily centered about the pycnocline. These wave gauges were made of parallel stainless wires of various length, 1/16 inch (0.16cm) in diameter, and typically separated by 0.5cm. For measuring the top surface waves, the wave gauge works by the principle that the electric resistance across the two parallel wires varies with an "effective amount" of water between them, and hence the wave elevation can be determined by calibration. For the interfacial wave gauge, the upper part of the parallel wires of the gauge was coated with the GC red GLPT insulating varnish so that only the lower uncoated parts of the wires would provide a measure of the conductivity of the fluid surrounding the wires (cf. Figure 7.2). During experimental measurements, these conductive parts were always kept below the top surface so that the top surface variation would not affect the interfacial wave gauge signal. The vertical location of the interfacial wave gauges were set such that their conducting parts would pierce through the interface and the vertical location of the top surface wave gauges would never reach the interface. Four gauges were used. One of them was for the top surface wave and the others for the internal waves; their locations are shown in Figure 7.1. Three of these gauges, including the one for the top surface waves and two for the internal waves, were fixed with respect to the tank, being mounted on a support beam which spanned the entire length of the tank. The fixed gauge for measuring the top surface waves, FTG (standing for Fixed Top surface wave Gauge), and one of the fixed gauges for the interfacial wave, FIGI (standing

for Fixed Interfacial wave Gauge 1), were both located at 100L from the left starting position of the leading edge of the bump, where L denotes the chord length of the bump. The other fixed gauge for the interfacial wave, FIG2, was located at 40L from the left starting position. A moving gauge for measuring interfacial waves, MIG (for Moving Interfacial Wave Gauge), was fastened on the carriage, to move with the bump during the experiment, at 1.8L to the right of the right edge of the bump (cf. Figure 7.1). The distance between the left and right starting positions was 120L.

The waves were recorded in three ways. The simplest one was by use of a video camera, which was mounted to the carriage and moved with it to record wave profiles near the bump. The second and third were the signals from the wave gauges recorded by means of a chart recorder (Sanborn 8 channel thermal chart recorder (Model 358-100A) and a PDP 11/23 computer throughout each run. The signals from the gauges were taken as input to one arm of the Wheatstone bridge (cf. Figure 7.3) connected to Hewlett-Packard carrier preamplifiers (Model 8805A) which also provided 4.5 volts 2400 Hz excitation signals to each bridge to make the signal-taking from the gauges possible. Because the signals from the preamplifiers still contained some noise of 2400 Hz components, a R-C low-pass filter (with approximately $R = 6k$ ohm and $c = 1\mu$ farad, with a cut-off frequency of about 30 Hz and a stopband of amplification factor less than 0.1 for frequencies larger than 260 Hz) was used to filter out the noise components for every channel. These cleaned and amplified signals were then taken as input to the chart recorder, with a set of

Sanborn low-gain amplifiers (Model 958-2900), and to the computer, using an Analog-to-Digital (A/D) data acquisition system. The computer data acquisition was made at 20 Hz.

Preliminary experiments showed some troublesome interactions between the wave gauges and the brine, giving rise to false signals which seemed to depend on the carriage position along the tank. This problem was later resolved by grounding the tank and the carriage to the power outlet ground point and by placing a grounded tinned copper wire (20 AWG 0.8mm diameter) along a corner of the tank cross section along the entire tank length. In addition, the fixed interfacial wave gauges FIG1 and FIG2 were specially made by using one wire placed at the center as one end to the bridge, surrounded by four grounded wires connected to the grounded end of the bridge (cf. Figure 7.2), and further using three tinned copper wires to weld together the conducting parts of the surrounding wires and thus forming a sparse grounded net. With these improvements, the errors in wave elevation measurements caused by such electric interferences were reduced to less than about 1mm of wave height for each gauge.

The density profiles in the rest state were measured by a density probe, which consisted of a centered stainless wire of 1/32 inch (0.08cm) diameter as one electrode, surrounded by a grounded aluminum ring of 0.4cm inner diameter, 0.1cm thick, and 0.6cm in height as the grounded electrode (cf. Figure 7.4), both ends being fixed on a Plexiglass plate. The immersed part of the central stainless wire above the ring was electrically insulated by a coating of Varsity spray enamel No. 1140. The entire probe was further

platinized according to the standard chemical method (Water (1965), p. 282) before its use in the experiment.

Four 'standard' saline solutions with specific densities accurately set at 1.01, 1.02, 1.03 and 1.04 were prepared and placed in four beakers for calibration in addition to the pure water. The density profiles were recorded around the middle of the tank. To obtain the density profile of the tank water at rest, the probe was moved upward step by step from near the bottom to just below the top surface. More data points were taken near the pycnocline where rapid density variations existed. The locations for calibrating the fixed wave gauges were at their individual working positions (possibly with some small transverse displacements). The location for calibrating the moving gauge MIG was at the starting position.

Results of the calibrations of the gauges and probe were plotted and interpolated for use in each series of experiment; for this purpose their best representation was obtained with cubic curve fittings by the least square method. Typically the error due to the cubic curve fitting was less than 0.3mm displacement for the gauge calibrations.

The experiments were performed first with the nominal depths h_1 = 6cm and H_2 = 2cm. After several experiments, a selective withdrawal was performed to siphon out the fluid in the pycnocline, thereby making the pycnocline effectively thinner. Accordingly, the total depth of the stratified water was slightly reduced. After several more experiments, the selective withdrawal was again performed, further reducing the total depth of the water layer. When the carriage

was moving with the bump in one direction along the tank, the moving wave gauge was in front of the bump, 1.8L ahead of the leading edge of the bump, so it recorded the disturbances in front of the bump and the wave gauges FIG1 and FTG recorded the disturbances at the position initially located at 100L ahead of the bump and for FIG2, the waves at 40L ahead of the bump. When the bump was moving in the other direction, the moving wave gauge was behind the bump, 2.8L behind the leading edge (left edge) of the bump, so it recorded the disturbance behind the bump and the wave gauges FIG1 and FTG recorded the disturbance at the position initially located at 20L ahead of the bump and for FIG2, the waves at 80L ahead of the bump. (cf. Figure 7.1). The density profile measurements and the gauge calibrations were conducted at the beginning and at the end of a set of experiments and also before and after each selective-withdrawal. The measured density profile and the nearest calibration result were used for signal processing and the corresponding numerical calculation. The experimental results, their corresponding numerical calculations and their comparisons will be presented in the next chapter.

VIII. ANALYSES OF THE RESULTS

The results of numerical calculations based on the several theoretical models presented in the foregoing, and the corresponding experimental studies are the topics of this chapter. Only two-dimensional cases will be considered. Of interest are the wave motions generated by such disturbances as a top-surface pressure distribution or a bottom bump, which keeps moving, after an impulsive start from rest, with a uniform velocity U, in a stratified fluid system. The resulting wave generation and evolution from these forcings will be examined in this chapter. Before doing that, let us first consider the wave resistance experienced by the forcing disturbance, which will be used in later discussion.

8.1 The Wave Resistance

External forcings, such as a top surface pressure or a bottom bump, will generally experience a certain resistance and hence must do work on the fluid system, which may vary with time and may be positive or negative. For the case of a top-surface pressure forcing, the resistance a left-going forcing pressure p must sustain is given by

$$R = -\int p\zeta_x dx \ , \tag{8.1}$$

which represents component of the surface pressure $p(x, t)$ acting in the negative x-direction and on the water surface of elevation $\zeta(x, t)$ integrated over the entire forcing region. For forcing pressures of compact support or falling to zero sufficiently fast at infinity, an

integration by parts of (8.1) gives

$$R = \int \zeta p_x dx \ .$$

A positive R signifies a resistance that must be overcome by the forcing disturbance, whereas a negative R means that the external forcing is (temporally) being pushed forward by the fluid system. For symmetric forcing distributions on a finite region, called the forcing region, one can easily see from (8.1) that for a left-going positive pressure, i.e., the external pressure is everywhere greater than the ambient pressure in the forcing region, the free surface elevation should have a negative slope on the average under the forcing pressure to make R postive, or vice versa for the forcing pressure to change it's sign or direction of motion. The wave resistance coefficient, defined as

$$C_R = \frac{R}{\rho_1 g h_o^2} \ , \tag{8.2}$$

where ρ_1 is the density at the top surface, is given by

$$C_R = -\int p\zeta_x dx = \int \zeta p_x dx \ , \tag{8.3}$$

if p and ζ assume the following dimensionless form

$$\frac{p}{\rho_1 g h_o} \ , \quad \frac{\zeta}{h_o} \ .$$

For the bottom forcing case, the wave resistance is

$$R = -\int p h_{2x} dx \ , \tag{8.4}$$

where p is the pressure on the bottom, or in coefficient form

$$C_R = \frac{R}{\rho_2 g h_o^2} \quad , \tag{8.5}$$

where ρ_2 is the density at the bottom. By using the Bernoulli equation, (8.5) can be recast as

$$C_R = -\int \dot{\phi}_2 d_x dx \quad , \tag{8.6}$$

where the higher order terms have been neglected and the variables are nondimensionalized with (2.17). Because the first-order value of the potential is depth-independent, the depth-average potential can be used in (8.6) to the same order terms retained. For the KdV model, the potential ϕ_2 can be converted to a known quantity as follows.

For the two-layer system with a free top surface, the first-order relations (4.47) and (4.48) yield, with consideration of only one component, in dimensionless form,

$$L_{(1)\xi} = -\frac{c_i}{H_2} \zeta_{2(1)} \quad , \tag{8.7}$$

where $\xi = x + c_i t$. Referring to Chapter IV, we have (see equation (4.17))

$$\dot{\phi}_2 + O(\alpha^2) = \alpha \dot{L}_{(1)} = \alpha c_i L_{(1)\xi} \quad .$$

Hence by (8.7),

$$\dot{\phi}_2 + O(\alpha^2) = -\frac{c_i^2}{H_2} \zeta_2 \quad .$$

Therefore, (8.6) for the wave resistance coefficient becomes, for the KdV model,

$$C_R = \frac{1}{H_2} c_i^2 \int \zeta_2 d_x dx + O(\alpha^4) \quad . \tag{8.8}$$

For the two-layer system with a fixed horizontal top surface, the wave resistance coefficient can similarly be calculated. Referring to 5.2, we have, by the Bernoulli equation,

$$R = \int p d_x dx = -\int \rho_2 \dot{\phi}_2 d_x dx + O(\alpha^4) \quad .$$

And from (5.82),

$$L_{(1)\xi} = - \frac{c}{H_2} \zeta_{(1)} \quad ,$$

therefore

$$\dot{\phi}_2 = \frac{c^2}{H_2} \zeta + O(\alpha^2) \quad ,$$

and finally, in dimensionless form,

$$C_R = \frac{c^2}{H_2} \int \zeta d_x dx + O(\alpha^4) \quad . \tag{8.9}$$

For continuously stratified fluid systems, (6.28) and (6.24), which are valid for the top surface either free or fixed, can be used, up to the first order, to give

$$p \approx \alpha c^2 \bar{\rho} N E' \quad ,$$

$$\zeta \approx \alpha E N \quad .$$

The wave resistance coefficient, defined as,

$$C_R = \frac{R}{\bar{\rho}(o)gh^2} \quad , \tag{8.10}$$

can be expressed, on using the above results for p and ζ, in the following dimensionless form

$$C_R \approx c^2 \frac{E'(o)}{E(z)} \int \zeta(z) d_x dx \quad , \tag{8.11}$$

where z is any vertical position such that $E(z)$ is not zero (such selection of z does not affect C_R since $\zeta(z)$ is proportional to $E(z)$).

8.2 Analyses of Results for the Two-layer Forced KdV Equation

Compared with the FOUR-equation or THREE-equation models of the Boussinesq class, the forced KdV equation is simpler and is more promising for further fruitful investigations. Moreover, the well-posedness in regard to the existence, uniqueness and continuous dependence on initial data, etc. of the solution of the forced KdV equation has been proved for some general well-behaved forcing functions and initial data (cf. Bona & Smith (1975), proposition 15). The well-posedness of the solution of the forced regularized KdV equation, also called the PBBM equation (Miura (1976), following Peregrine (1966) and Benjamin, Bona & Mahony (1972)), which has been used in numerical calculations, has been proved in a more straightforward way for some general well-behaved forcing functions and initial data (cf. Benjamin et al. (1972) Theorems 2, 4 and 5).

8.2.1 Theoretical Analyses

First, some simple and useful results can be obtained from the first-order relationships.

For the free top-surface case considered in Chapter IV, (4.64) and (4.69) are the first-order results and they may be converted by using (4.57) to the following more convenient expressions, which are accurate up to the leading-order,

$$\zeta_1 \approx \frac{1}{H_2\sigma}[c_i^2 - H_2(1-\sigma)]\zeta_2 \quad , \tag{8.12}$$

$$u_1 \approx \frac{1}{h_1 H_2 \sigma} \; c_i(H_2 - c_i^2)\zeta_2 \quad , \tag{8.13}$$

$$u_2 \approx -\frac{c_i}{H_2}\,\zeta_2 \quad , \tag{8.14}$$

and $$u_2 \approx \frac{1}{H_2}\,(c_i^2 - h_1)u_1 \quad , \tag{8.15}$$

where u is horizontal velocity, $u = \phi_x$, and the subscript 1 (or 2) represents the upper (or the lower) layer quantities; these expressions are in the dimensionless form defined by (4.1) and the u is normalized by $c = \sqrt{gh_o}$. We can readily verify using (4.57) that for the two-layer system (with $\sigma h_1 H_2 \neq 0$),

$$c_i^2 - H_2\,(1-\sigma) \neq 0 \quad ,$$

and

$$c_i^2 - h_1 \neq 0 \quad . \tag{8.16}$$

For the slow mode, which is of main interests here, one can further show that

$$c_s^2 - H_2(1-\sigma) < 0 \ ,$$

and

$$c_s^2 - h_1 < 0 \ , \tag{8.17}$$

by considering the continuous dependence of the quantities on the left-hand side of the above expressions on the depth and density ratio and by examining the relationship between the roots and coefficients of equations (4.57), including (8.16). On the other hand, for the fast mode ($c_i = c_f$), the left hand side of (8.17) must be all positive with c_s replaced by c_f.

Likewise, for the case of the fixed horizontal top surface considered in Chapter V, one can obtain from (5.82), (5.57) and (5.55) the following first-order relations

$$u_1 \approx \frac{c}{h_1}\zeta \ , \tag{8.18}$$

$$u_2 \approx -\frac{c}{H_2}\zeta \ , \tag{8.19}$$

and

$$u_2 \approx -\frac{h_1}{H_2}u_1 \ . \tag{8.20}$$

Physically, these results mean that to the leading order, the velocities in the upper and the lower layers, and the wave elevations of the top surface, if free, and the interface are all proportional to each other. Furthermore, for the fixed horizontal top-surface case and the slow mode of the free top-surface case, the velocities in the upper and the lower layers are always opposite in direction, signifying that the interface is always a vortex sheet across which the tangential

velocity may have a jump. In addition, the elevation of the top surface, if it is free, is always opposite in sign to that of the interface. For the fast mode, the velocities in the two layers are always in the same direction and both wave elevations are positive.

Secondly, we note that the forced KdV equations for the two-layer case (see equation (4.62)) and the continuous stratification case (see equation (6.46)),

$$Q_t - cQ_x + a_2 QQ_x + a_3 Q_{xxx} + a_4 d_x = 0 \ , \tag{8.21}$$

is analogous to the one-layer (homogeneous fluid system) forced KdV equation (see Lee (1985) (2.58)) which reads for the left going forcings as

$$q_T - (1 + \frac{3}{2} q)q_X - \frac{\alpha}{6} q_{XXX} - \frac{1}{2} D_X = 0 \ , \tag{8.22}$$

where d denotes a bottom bump and/or a top-surface pressure, $\alpha = (\frac{h_o}{\lambda})^2$, and q is the surface wave elevation for the one-layer system. The analogy becomes one-to-one (i.e., equivalent) if the quantities satisfy the scaling law:

$$Q = -\frac{3c}{2a_2} q \ ,$$

$$x = \sqrt{-\frac{6a_3}{\alpha c}} X \ ,$$

$$t = \frac{1}{c} \sqrt{-\frac{6a_3}{\alpha c}} T \ ,$$

and

$$d = \frac{3c^2}{4a_2 a_4} D \ . \tag{8.23}$$

So, to each two-layer case there corresponds a one-layer system given by (8.23) for scaling the variables. It is of interest to note that the Froude number remains invariant under the scaling (8.23) (the characteristic velocity for the one-layer case is normalized to unity in (8.22)). The numerical results for one-layer systems (see Lee (1985), chapter 4) can therefore be used to predict the behavior of wave motions in stratified fluid systems. However, since $\frac{q}{Q}$ and $\frac{d}{D}$ are seen from (8.23) to have different scaling factors in general, the analogous cases are not dynamically similar even with the proper scaling of x and t. Nevertheless, we can conclude on the invariance of Froude number that in stratified fluid systems, disturbances moving with transcritical velocities will generate a series of solitons surging ahead of the disturbance very much similar to the phenomenon known for the one-layer case.

Small Density Difference Case

In this case, the above analyses may be further simplified to enable us to draw some quantitative conclusions.

The slow mode will be considered first. For $(1-\sigma) \ll 1$, the dimensionless form of (4.69), for the case of free top-surface, becomes,

$$\zeta_1 \simeq -H_2(1-\sigma)\zeta_2 \ ,$$

$$u_1 \simeq \sqrt{\frac{1}{h_1} H_2(1-\sigma)\zeta_2} \ ,$$

and

$$u_2 \simeq -\frac{h_1}{H_2} u_1 \ . \qquad (8.24)$$

Clearly, the first equation above shows that the displacements of the two surfaces are always opposite in sign, but the top surface wave elevation is very small compared to the interfacial wave on account of $1-\sigma$ being small. The horizontal velocities in the two layers are always opposite in direction, and the velocity ratio is inversely proportional to the depth ratio for the two layers. So the shallower layer has a larger horizontal velocity in inverse proportion.

The forced KdV equations for the free top-surface case and the rigid horizontal top-surface case become identical as the density differences for the two layers decrease to small values, i. e., they both asymptotically become (4. 68) for the interfacial waves, in dimensionless form. Substituting the coefficients of (4. 68) into the scaling relations (8. 23) yields

$$Q = \frac{h_1 H_2}{h_1 - H_2} q \quad , \tag{8.25}$$

$$x = \sqrt{h_1 H_2}\, X \quad , \tag{8.26}$$

$$t = \frac{1}{\sqrt{1-\sigma}}\, T \quad , \tag{8.27}$$

$$d = \frac{H_2}{h_1 - H_2}\, D \quad , \tag{8.28}$$

and

$$p = \frac{h_1}{H_2 - h_1}\, P, \tag{8.29}$$

where p and P denote the analogous top surface pressures, which are to replace the forcing terms d and D, respectively, in the above KdV equations when a top surface pressure is present. From these

scaling relations, we may draw the following conclusions.

(1) In the one-layer case, the solitons generated to surge ahead of the moving disturbance (called runaway solitons), as predicted by (8.22), are always positive in elevation (without depressions below the undisturbed free surface), no matter whether forcing is positive or negative, as has been reported and communicated by Lee (1985). In other words, the runaway soliton solution q of (8.22) is always positive whatever the forcing function D is. However, by the scaling relation (8.25), the interfacial elevation Q for solitons in a two-layer system is positive or negative accordingly as h_1 is greater or smaller than H_2. This is of course expected on physical grounds that free solitons in two-layer fluid systems always displace away from the thinner layer of fluid into the thicker one. Examples of such negative solitary waves will be shown later.

(2) The density ratio of a two-layer system, σ, takes part only in the time scaling. Therefore the entire wave behavior will remain unchanged with respect to the scaled time (hence with the velocity also scaled) and to the same Froude number.

(3) With regard to the scaling of forcing functions, p and d, we see by comparing (8.28) and (8.29) that the pressure forcing, p, and the bump forcing, d, of the same distribution have different effects on waves, noting that for one-layer systems the surface pressure P and the bottom bump forcing D are exactly equivalent (see Lee (1985)) for the KdV model. For the same system configuration (i.e., the same h_1, hence the same H_2 since $h_1 + H_2 = 1$, aside from the effects due to density ratio as already considered in (2)), effective forcing strengths

(which are best measured by the equivalent D and P of the analogous one-layer system) of the forcings, bottom bump or top-surface pressure, are found to be inversely proportional to distance between the forcing and the interface. In fact, with $p = d$ in (8.28) and (8.29), we have

$$\frac{P(\text{due to } p)}{D(\text{due to } d=p)} = -\frac{H_2}{h_1} \quad .$$

Physically, this means that the closer the forcing to the interface, the larger the interfacial waves will result, for the same strength of the two kinds of disturbances. When h_1 and H_2 are nearly equal, the effective forcing strengths become very small as indicated by the scaling relations (8.28) and (8.29). An interesting case arises when $h_1 = H_2$, which will be discussed later.

Two kinds of effective forcings can be classified, positive and negative, based on the above scaling relations (8.25), (8.26), (8.28) and (8.29). The two categories are:

Positive effective forcing,

$$h_1 \gtrless H_2, \quad \text{with } p \lesssim 0, \text{ or } d \gtrless 0 \quad . \tag{8.30}$$

Negative effective forcing,

$$h_1 \lesssim H_2, \quad \text{with } p \gtrless 0, \text{ or } d \lesssim 0 \quad . \tag{8.31}$$

For the same amplitude of the forcing (same p or d), the same waves will be observed if we exchange h_1 and H_2 and at the same time change the top surface disturbance to the bottom bump disturbance.

More conclusions can be drawn from the above scaling relations, but we will not go further here.

The case of equal depths for the two layers needs a separate consideration. The nonlinear term in the KdV equation (4.68) vanishes as the density ratio $\sigma \to 1$, implying that the existence of free solitons and the runaway solitons would be impossible according to this model (cf. Keulegan (1953), p. 140, also Long (1956), p. 469 (24) and p. 470, Fig. 5). However, this result is a particular consequence to the previous procedure of taking $1-\sigma \to 0$ first and $\frac{h_1}{H_2} \to 1$ afterwards. If we reverse the procedure by first letting $h_1 = H_2$ and then making the density ratio approach unity, we find the resulting nonlinear term small, but not zero.

For the free top-surface case, we obtain

$$c^{-1}Q_t - Q_x + \frac{3}{2}(1-\sqrt{\sigma})QQ_x - \frac{1}{24}\alpha Q_{xxx} - \frac{1}{4}d_x + \frac{1}{4}p_x = 0 \ , \tag{8.32}$$

and for the fixed horizontal top-surface case,

$$c^{-1}Q_t - Q_x - \frac{3}{2}(1-\sigma)QQ_x - \frac{1}{24}\alpha Q_{xxx} - \frac{1}{4}d_x = 0 \ , \tag{8.33}$$

both in dimensionless form. The Q's in the above formulas denote the interface wave elevation. Whether the runaway solitons are positive or negative depends on the sign of the ratio of the coefficients of the nonlinear term and the first time derivative term, as can be seen from the first scaling relation of (8.23). Thus, when $h_1 = H_2$ the runaway (and also free) internal solitons are negative for the free top-surface case and positive for the fixed top-surface case provided the density difference is small. Actually it is also true for arbitrary

densities ((1-σ) not necessarily small), which can be seen from the first scaling formula of (8.23), with a_1 and a_2 given by (4.65) for the free top-surface case and with a_1 and a_2 given by (5.87) for the fixed horizontal top-surface case. A numerical result will be shown for this case later (cf. Figure 8.12).

We conclude this section with a brief account of the fast mode. By a similar procedure as that for the slow mode, the following result is obtained. For a two-layer system with small density differences, the fast mode is almost the same as the only mode in the one-layer case. The wave-elevation-ratio for the top surface and the interface is approximately equal to the corresponding depth-ratio, i.e., 1:H_2, and the fluid velocities in the upper and the lower layers are equal.

8.2.2 Results from Numerical Calculations

The forced KdV equations for stratified fluid systems can be transformed to the one-layer KdV equation by suitable scalings as shown in the preceding section, with the Froude number unaffected by the scaling. Therefore, much advantage can be taken of behaviors already known for various kinds of forcing distributions over a range of transcritical speeds for the one-layer system, as given in an extensive study by Lee (1985). In spite of having this advantage, more calculations will be performed in the present study for various stratified fluid systems in order to investigate more thoroughly the relationships between the characteristics of waves generated, the system configurations and the forcing distributions, to examine the validity of these theoretical models, and to further understand the basic mechanism underlying the phenomenon.

In the present subsection, only the slow mode of two-layer systems with bottom-bump forcing and with a free top surface will be considered. To diminish as much as possible any fictitious reflections from the boundary of the region of computation, the open boundary condition (1) given by (3.16) and the window-shifting scheme described in Chapter III will be adopted in our computation, with the value of c_s assigned to c in (3.16) and in the window-shifting formula for all the cases undertaken. Note that c_s in the present context corresponds to $c = 1$ in one-layer systems according to the present scaling rule. All cases but one will be devoted to the case with small density differences.

The equation adopted here for numerical computations for two-layer systems is the regularized KdV equation (8.21) with an external forcing $d = d(x+Ut)$,

$$Q_t - cQ_x + a_2 QQ_x + \frac{1}{c} a_3 Q_{xxt} + a_4 d_x = 0 \ . \tag{8.34}$$

In the absence of forcing ($d = 0$), the homogeneous equation of (8.34) has as an exact solution, the solitary wave:

$$Q = a \operatorname{sech}^2[k(x + Ut)] \ , \tag{8.35}$$

where

$$U = c - \frac{1}{3} a_2 a \ , \tag{8.36}$$

$$k^2 = \frac{a_2 ac}{4a_3(3c - a_2 a)} \ . \tag{8.37}$$

This free soliton solution was used to test the stability and accuracy of the numerical scheme for solving the two-layer KdV equation and to ascertain an optimum choice of the space-grid and time-grid size, Δx and Δt.

The forced KdV equation (4.62) with the coefficients (4.65) was used for calculating the interfacial wave elevations. The corresponding top-surface wave elevations were deduced by using (4.64).

In all the numerical calculations covered in this chapter, λ was taken to equal h_o in all dimensionless expressions. So the same values of the horizontal coordinate x and of the wave elevation ζ represent the same physical sizes in these two dimensions. All the numerical results are presented in the nondimensional form with normalization (2.17) in this chapter, and for the two-layer system (2.18) is also used.

The result of testing the numerical code developed here versus the exact solution of free soliton (8.35) is shown in Figure 8.1 for a specific case with $H_2 = 0.25$, $\sigma = 0.97$ and the wave amplitude $a = 0.15$ (which is not small as compared with H_2) and with grid size $\Delta x = 0.1$ and $\Delta t = \frac{\Delta x}{2c_s} = 0.665$. The window-shifting velocity was $c_s = 0.0752$ towards the left. The free soliton solution (8.35) was taken as the initial condition and the forcing term in (8.34) was set to zero prior to executing the numerical scheme. The curves in the Figure from top to bottom represent the wave profiles at several times instants: from $t = 0$ to $t = 1330$ with equal time intervals. The left-end (flat) level of each curve represents the undisturbed water surface if not yet reached by the leading wave. The peak values were shown for each curve in Figure 8.1. The values of K in the figure represents the number of calculation cycles and the time for that curve is $K\Delta t$; this notation will be used throughout this chapter. This result shows that the present numerical scheme for this case

(and several others tested) is sufficiently accurate: with only one per cent variation in wave amplitude after traveling a distance more than 120 times the total water depth while the wave phase velocity only has a discrepancy of less than 0.1 per cent between the numerical result and the exact solution (8.36). With this error estimate, we proceed to use $\Delta x = 0.1$ and Δt is determined from (3.18) by a suitable choice of N. N was taken to be 2 for the Froude number $Fr \geq 0.8$ and 4 for $0.4 \leq Fr < 0.8$ in all the calculations carried out. For instance, in the above test case we took $FrN = 2$. In view of the scaling rule for the forced KdV equation, which contains the leading term $Q_t - c_s Q_x$, the relevant quantity for considering proper choice of Δt is $c_s \Delta t/\Delta x$, which is equal to $1/(FrN)$ by (3.18).

The forcing distributions assigned for the numerical calculations are all of the form

$$p_o \text{ or } d = \begin{cases} \frac{1}{2} d_m \{1 - \cos[\frac{2\pi}{L}(x - x_o + Ut)]\} & \text{for } 0 < x - x_o + Ut < L \\ 0 & \text{for other domain of } x \end{cases} \tag{8.38}$$

where x_o is the initial position of the leading edge of the forcing function except those used for making comparisons with the experiments (the above x is the original coordinate without being affected by window shifting). All the initial conditions were set zero for the two-layer-system calculations presented in this subsection. Note the simple relation:

$$U = c_s Fr \ .$$

The numerical results obtained for $Fr = 0.5, 0.7, 0.9, 1, 1.1, 1.22$ and 1.25 are shown in Figures 8.2 to 8.8 with the

parameters $H_2 = 0.2$ and $\sigma = 0.97$ and for the forcing, $L = 1$ and $d_m = 0.05$. These curves except the last one represent the wave profiles at different instants, separated by equal time intervals. The region of forcing lies between the two vertical dashed lines which retains the same horizontal position because of the window shifting. The last curve in each figure shows the variation of the wave resistance coefficient with time and was calculated from (8.8). These results show that within a transcritical speed range, runaway solitons are generated periodically to surge ahead of the forcing disturbance. They also show that when C_R reaches a maximum, a new soliton peak appears just ahead of the bump, and the time interval between successive maxima of C_R provides a convenient measure of the generation period of runaway solitons. The effects of Fr on the runaway solitons will be discussed in the next section in more detail.

Figures 8.9 to 8.11 present the results for different H_2 ($H_2 = 0.3$, 0.7, and 0.9) with $Fr = 1$, $L = 1$, $d_m = 0.05$ and $\sigma = 0.97$. (The result for $H_2 = 0.2$ is already given in Figure 8.5.) The solitons generated are positive for $H_2 = 0.2$ and 0.3 and negative for $H_2 = 0.7$ and 0.9. For $H_2 > 0.5$, it is expected, on scaling considerations in 8.2.1, that negative solitons would be generated if the computing calculation time was long enough for that to occur. For the negative effective forcing, like that with $H_2 = 0.9$, the numerical results indicate that the instant when C_R reaches a minimum is near the instant for a new peak of generated runaway soliton to appear just ahead of the bump and the time interval between successive minima of C_R gives a convenient measure of the generation

period of runaway solitons. To see the soliton generation phenomena for the case of $h_1 = H_2$, a long time of calculation is needed, especially when $(1-\sigma)$ is small. The result for $\sigma = 0.2$ and $h_1 = H_2$ is shown in Figure 8.12 for $Fr = 1$, $L = 1$, $d_m = 0.05$. As expected, a negative soliton is generated for this free top-surface case.

The numerical results showing the effects of varying bump width are presented in Figures 8.13 to 8.15 for $L = 0.5$, 2 and 4 with $H_2 = 0.2$, $\sigma = 0.97$, $d_m = 0.05$. The case of $L = 1$ was shown in Figure 8.5 already. From these results, we see that the generated runaway solitons become stronger, their amplitudes larger and their generation periods shorter, when L is increased from 0.5 to $L = 2$. The effects of the bump-width variation on wave generation is most noticeable for $L \simeq 2$ to 4; for L greater than 4, this trend appears to gradually subside. This is an interesting result and it may be due to the decrease of the gradient of the bump shape when L is increased for d_m fixed because the forcing strength is proportional to d_x in the KdV equation.

The effects due to varying bump height are shown in Figures 8.16 to 8.18 for $d_m = -0.1$, -0.05 and 0.1 with $Fr = 1$, $H_2 = 0.2$, $L = 1$ and $\sigma = 0.97$. The result for $d_m = 0.05$ has been given in Figure 8.5. The amplitudes of the runaway solitons become considerably larger and the generation periods, considerably shorter for bumps of larger height, other parameters being equal. Therefore the effects of bump height are strong. A positive (or negative) d_m corresponds to a positive (or negative) effective forcing in the present case. The negative effective forcing has some features quite different

from positive ones. Compared with the positive effective forcing function of the same size and shape, the runaway solitons generated by the negative forcing have longer generation period, the distance between successively generated solitons is larger and often a region of nearly undisturbed level exists between them. In other words, the generated solitons are more isolated. Further, their wave resistance coefficient curves are not so symmetric about the point of maximum or minimum of C_R as those in positive effective forcing cases.

The effect of varying density-ratios is shown in Figure 8.19 with $\sigma = 0.94$ and with $Fr = 1$, $L = 1$, $d_m = 0.05$ and $H_2 = 0.2$. The cases of small density differences have been discussed in section 8.2.1.1, where it was shown that the effect of σ variation is basically equivalent to a change of time scale. With relation (8.27) for the time scaling and (4.73) for c_s, one can conclude that wave forms should be nearly the same for the same K, the number of computing cycles, for the present case (of small density differences) because the scaling relation (8.27) has a factor $\sqrt{(1-\sigma)}$ and the slow characteristic velocity has the same factor, which is used to determine the size of Δt, and at last σ does not affect the principal results in time $K\Delta t$. This feature is exemplified in Figures 8.19 and 8.5, where we can see almost the same curves for the same K's (but for different times). The distance traversed by the forcing is $K\Delta tU = \frac{1}{N} K\Delta x$ by (3.18). Because Δx and N are not affected by the variation of σ in the case being considered, the same K means equal distance traversed by the forcing disturbance. This property has a practical utility in performing experiments; it means that for the present cases (of

small density differences) a run of one experiment with a given density-ratio in a tank of finite length can be made to exhibit nearly the same wave phenomenon as the result from another run with a different density-ratio but in the same tank (fixed H_2), using the same forcing disturbance and Froude number provided the moving velocity of forcing is properly scaled.

All the numerical computations carried out in this section were performed by the Cray X-MP/12 computer of NRL with single precision. The processing rate is of the order of 100 million floating point operations per second during the effective usage of the computer. For most cases (calculation region of $x = 80$, $K = 1600$ and $\Delta x = 0.1$), the CPU time was about 7 seconds.

8.3 Analyses for the THREE-equation and FOUR-equation Models

The THREE-equation model for the fixed flat top-surface case and the FOUR-equation model for the free top-surface case were derived in Chapters V and II and the numerical schemes for applying these models were presented in Chapters V and III. They can model motions of long waves propagating in arbitrary directions, including three-dimensional wave motions. In sharp contrast, the forced KdV model admits motions in one direction only. So the THREE-equation and FOUR-equation models have applicability of broader scope than the KdV model.

We will first consider the THREE-equation model developed for the two-layer fluid systems covered with a fixed horizontal top surface. The stability and accuracy of the numerical scheme for

solving the three basic equations of this model (see equations (5.33), (5.38) and (5.40)) will be investigated by applying it to computing a free soliton solution (d = 0), employing the KdV equation (5.91) and the first order relations (5.90) to provide the initial data required for computations by the established numerical scheme. More precisely, the three required initial conditions used to test the present scheme are, in dimensionless form, the initial wave elevation,

$$\zeta = a \operatorname{sech}^2 [k(x - x_o)] , \tag{8.39}$$

where x_o is the initial position of the soliton peak and

$$k = \sqrt{\frac{aa_2}{12a_3\epsilon^2}} , \tag{8.40}$$

a_2 and a_3 being given by (5.87)(ϵ was taken to be 1) and the initial layer-mean potential of the upper layer,

$$\phi_1 = \frac{ca}{h_1 k} \tanh [k(x - x_o)] ,$$

where c is given by (5.84), and the initial combined potential

$$R = - \frac{ac}{h_1 H_2 k} (h_1 + \sigma H_2) \tanh [k(x - x_o)] .$$

The solitary wave in (8.39) is an exact solution of the KdV equation (5.91) without the forcing term. The numerical result of this test computation is presented in Figure 8.20 for the case with $H_2 = 0.25$, $\sigma = 0.97$, wave amplitude $a = 0.15$ and the grid size $\Delta x = 0.1$ and $\Delta t = \frac{\Delta x}{(2c_s)} = 0.664$ (corresponding to FrN = 2 in (3.18)). The window-shifting velocity is $c_s = 0.0753$. The peak value of each

wave profile is shown on the curve. Because the initial condition is not the exact solution of the THREE-equation model, there was some slight decrease of the amplitude at early times, but the wave amplitude becomes nearly constant from the fourth curve on. Beyond this initial stage of "adjustment", the relative variation of wave amplitude is less than 0.2 per cent over the traversed distance of 153 times the water depth. Based on this numerical study, the grid size of $\Delta x = 0.1$ will be adopted while taking, for selection of Δt, $N = 2$ for $Fr \geqslant 0.9$; $N = 4$ for $0.4 \leqslant Fr < 0.9$; $N = 8$ for $Fr = 0.2$ and 0.3.

The numerical results for the Froude number $Fr = 0.2$, 0.5, 0.7, 0.8, 0.9, 1, 1.1 and 1.2 and for zero initial conditions are shown in Figures 8.21 to 8.28 for $H_2 = 0.2$, $\sigma = 0.97$, $L = 1$ and $d_m = 0.05$. As before, the last curve in these figures represents the wave resistance coefficient, which is calculated from (8.6). Almost the same qualitative behaviors are observed of the resulting wave motions shown in these figures for the present two-layer case as those for the one-layer case obtained by Lee (1985). They are also similar to the solutions of the KdV equation shown in Figures 8.2 to 8.8. Therefore the solutions of the KdV equation are also used in the following discussion.

The basic behaviors are as follows. As Fr is increased from 0.2 to 0.7, new solitary waves appear in front of the bump, increasing in amplitude with increasing Fr, though still very small. The parts of the trailing waves near the trailing edge of the bump are nearly stationary relative to the bump, increasingly becoming greater as Fr is increased. For $Fr = 0.8$ and 0.9, solitary waves of considerable

amplitude are generated to run upstream, followed by a region of very uniform depression behind the bump, prolonging in extent with time. In this high subcritical regime, the fluctuations in wave elevation of the successively generated solitons seem to gradually fall off with advancing time, accompanied by a similar curve for the wave resistance coefficient.

For the critical case, $Fr = 1$, the wave resistance coefficient curve becomes very regularly periodic, such as shown in Figure 8.5. The successive maxima of $10^4 C_R$ are 1.082, 1.051, 1.047, 1.048 and 1.049 and the successive minima are 0.6674, 0.6794, 0.6806, 0.6795 and 0.6778. The time intervals beteeen consecutive maxima of C_R are 204.4 for the first interval and then 205.9, 207.3 and 203.1. The region of depression is very uniform in depth (the minimum level reached there being at -0.0725, -0.0725, -0.0724, -0.724 and -0.0724 from the first (top) curve to the fifth one) and is extending in length. This region of depression is followed by a trailing train of cnoidal-like waves. For $Fr = 1.1$ and 1.22 (Figures 8.6 to 8.7), the trailing waves become weaker and the depression regions are no longer so flat as when $Fr = 1$. In all the cases when upstream running solitons exist, their amplitudes and the period of their generation increase with increasing Fr until Fr reaches a value, which is about 1.2, beyond which the phenomenon of upstream running soliton generation by moving disturbances ceases to occur. In view of the result that the free solitary wave of greatest height has $Fr = \frac{4}{3}$ for the one-layer system (Whitham (1974), p. 480), no runaway solitons would be generated for $Fr > \frac{4}{3}$. It is believed to be also true for

stratified fluid systems because of the correspondence between the stratified fluid systems and the one-layer system for the same Froude number by suitable scaling conversions of other flow quantities (see section 8.2.1).

The FOUR-equation scheme was also tested using the solution for free solitons of the slow mode for a two-layer system with a free top-surface, given by Peters & Stoker (1960) (called type No. 2 for a two-layer system). The initial conditions are, in nondimensional form, (h_2 = const = H_2 because it is forcing-free, and in the following, s is their l_1, and k is their d)

$$\zeta_2 = a\,\mathrm{sech}^2 A \quad ,$$

$$\zeta_1 = \frac{aH_2}{sh_1 - H_2}\,\mathrm{sech}^2 A \quad ,$$

$$\phi_1 = -\frac{\sqrt{a}sc}{(sh_1 - H_2)k}\tanh A \quad ,$$

and

$$\phi_2 = \frac{\sqrt{a}c}{H_2 k}\tanh A \quad , \qquad (8.41)$$

with $A = \sqrt{a}k(x - x_o)$,

$$k = \frac{1}{2\epsilon H_2}\sqrt{\frac{3[s^2(h_1 - H_2) + sH_2(H_2 - 2h_1) + H_2^2]}{(sh_1 - H_2)(h_1 s - h_1^2 - H_2^2 - 3\sigma h_1 H_2)}} \quad ,$$

$$s = \frac{2H_2}{1 - \sqrt{1 + 4(\sigma - 1)h_1 H_2}} \quad ,$$

and

$$c^2 = \frac{H_2}{s + \dfrac{a[s^2(h_1-H_2)+sH_2(H_2-2h_1)+H_2^2]}{H_2(sh_1-H_2)[2sh_1(\sigma-1)+1]}} \quad ,$$

where x_o is a constant representing the initial position of the soliton peak, and a is positive for a positive free soliton. The test cases are for $H_2 = 0.2$ and $\sigma = 0.95$. The numerical scheme for solving the FOUR-equation presented in Chapter III is found to be less satisfactory than the schemes for the KdV equation and the THREE-equation model. The size of Δt required for yielding reliable results is considerably smaller than that used for the KdV equation and the THREE-equation model. For the present test case, which is shown in Figures 8.29 and 8.32, Δt is taken to be half of Δx. In the Figures 8.29 to 8.32. $\Delta x = 0.1$, $\Delta t = 0.05$, $a = 0.05$, $H = 0.2$, and $\sigma = 0.95$. The technique of window shifting was not used in these calculations. There are 14 curves in each figure, in which solid lines represent interface waves and dashed lines represent the top surface waves. The undisturbed levels of the interfacial waves and the top-surface waves are put in the same position. The top curves represent the initial waves and the second set of curves, the waves at time $t = 20$. They proceed with an equal time interval of 20 reaching the bottom curves where $t = 120$.

The boundary condition used to obtain the results shown in Figures 8.29 and 8.30 was the open boundary condition (1), (see section 3.2.2)). In Figure 8.29, the wave amplitude changes from

0.05 at the top (initial) to the following: 0.05263, 0.05343, 0.05393, 0.05393, 0.05396, 0.05394 and it keeps nearly constant at later stages. To test the validity of the open boundary condition, the same case was calculated with only half the size of the previous computation region (the right half of the original region being deleted) and so the soliton would have passed the boundary before the computation ends. The result of this second computation was subtracted from the full region result for the same reduced region, and this difference is shown in Figure 8.30, with the wave scale magnified 25 times to exhibit small errors. From Figure 8.30, we see that fictitious reflections from the boundary totaled less than 4 per cent of the incident wave amplitude and the main differences in the first two groups are the relative error in predicting very small top surface waves.

The open boundary condition (2) (see section 3.2.3) was used to obtain the results in Figures 8.31 and 8.32. Like Figures 8.26 and 8.27, Figure 8.31 shows the propagation of the free soliton through a full computation region and Figure 8.32 presents the difference between the computations in the half x range (12) and in the full x range (24). The only difference between Figures 8.30 and Figures 8.32 is the boundary condition; the former used open boundary condition (1) and the latter open boundary condition (2). The result shown in Figure 8.32 is better than that in Figure 8.30. The difference is small for the interface wave but is substantial for the top-surface wave. In Figure 8.32, where open boundary condition (2) was used, reflection of the top-surface wave from the boundary is nearly zero as compared with the interface waves in Figure 8.32 and with the

corresponding results given in Figure 8.30. This comparative study shows that the open boundary condition (2) is a significant improvement over condition (1) in letting both fast-mode components and slow-mode components go freely out of the boundary.

Further tests with different a, Δx and Δt were performed on the numerical scheme for the FOUR-equation model. The results showed that for the stability of the numerical scheme, Δt must be taken considerably smaller than that used in the scheme for the THREE-equation model and Δx should be large enough and it is required to be larger for higher waves. Good results were obtained with $\Delta x = 0.05$ for a wave amplitude of $a = 0.05$, as in the above test case. But Δx should be about 0.2 for $a = 0.075$ to maintain the desired numerical stability, and we should take $\Delta x = 0.4$ for $a = 0.1$ with $\Delta t < \Delta x/2$ for that two-layer test system. The above grid size estimates are concerned primarily with the slow mode motions generalized by the forcing. So computations with the FOUR-equation scheme are only suitable for small waves and large horizontal scales. Only four numerical results of the FOUR-equation scheme will be presented in the following.

The first case is for the bottom bump forcing. The numerical scheme for the FOUR-equation model was executed to obtain results for $H_2 = 0.2$, $\sigma = 0.96$, $d_m = 0.06$, $U = 0.07$ ($c_s = 0.080$ therefore $Fr = 0.87$), $L = 2$, $\Delta x = 0.4$ and $N = 40$ (then $\Delta t = 0.143$). The open boundary condition (2) was used and the initial conditions are zero. The results in Figure 8.33 show that the top-surface wave is very small indeed and by virtue of this result the

THREE-equation model is expected to be also applicable for this case. The solution of the THREE-equation for the fixed horizontal top-surface case was obtained for the same parameters (same Δx but different N, N = 4 here), as shown with dash-dot lines in the same figure for comparison. The two theoretical models are found to be in good agreement. So the THREE-equation model can be used to provide good approximate solutions for the free top surface case when the density differences are small.

The second and third cases are concerned with the top surface pressure forcings. Their initial conditions are those of the stationary equilibrium solution, i. e., both the potentials and the interface waves were zero and the top free surface had a hydrostatic response to the pressure acting on it. The computation was carried out for $\sigma = 0.96$, $Fr = 1.00$ ($U = c_s = 0.0716$), pressure distribution width $L = 2$, $\Delta x = 0.4$ and $N = 40$ in Figures 8.34 and 8.35, with application of the open boundary condition (2). Further, for Figure 8.34 the top surface pressure had amplitude $d_m = -0.15$, acting on water with $H_2 = 0.15$ and $d_m = 0.0254$ and $H_2 = 0.85$ for Figure 8.35. In the former case, the upper layer was thicker than the lower one, so only positive solitons can appear, whereas the situation is opposite for the latter figure. The top surface waves are noted to have a major peak just under the forcing pressure, which maintained its magnitude and position throughout.

Figure 8.36 shows the numerical result for the fast mode, i. e., when the forcing pressure was moving at a speed near the largest characteristic velocity of the two-layer system. The parameters

used were $H_2 = 0.3$, $\sigma = 0.97$, $d_m = 0.12$, $U = 0.9$ ($Fr = 0.9$, $c_f = 0.997$), $L = 2$, $N = 2$ and $\Delta x = 0.4$. The linear boundary condition described in section (3.3, 1.) was used in this case and the initial condition is the stationary solution. The result is very similar to that of the KdV equation for the corresponding case.

To compare the results of the FOUR-equation and the KdV equation, the numerical solution of the KdV equation is calculated for the case of figure 8.34. Both interface wave curves are shown in figure 8.37 with solid lines representing the solution of the FOUR-equation model and dashed lines, the KdV solution (by the implicit scheme). Also included in the figure is the solution of the KdV equation obtained by the explicit scheme, shown with dash-dot lines. In computing solutions to the KdV equation we took, $\Delta x = 0.4$ and $N = 8$. The figure shows a good agreement between the solutions of the FOUR-equation model, the KdV equation with implicit scheme and the KdV equation with explicit scheme for this case.

The computation of the results of the THREE-equation and the FOUR-equation models were conducted on a VAX 11/780 digital computer in the Booth Computing Center of the California Institute of Technology. The CPU time for figure 8.24, solution of THREE-equation model, ($\Delta x = 0.1$, calculation region = 60, number of calculation cycles $K = 1200$) was about 7 minutes and the CPU time for figure 8.35, solution of the FOUR-equation model, ($\Delta x = 0.4$, calculation region = 120, $K = 4400$) was about 26 minutes.

8.4 Analyses of the Forced KdV Equation for Continuously Stratified Systems and Comparisons with Experimental Results

The forced KdV equation for continuously stratified systems and its numerical scheme were presented in chapter VI and its numerical results will be discussed in the present section. The experimental aspects were discussed in chapter VII and the experimental results and comparisons between the numerical results and the experimental results will be investigated in the present section.

Figure 8.38 is a typical density probe calibration result, in which the points are the measured data and the line is obtained by cubic curve-fitting. Figure 8.39 shows a typical density profile of a stratified fluid system, prepared according to the procedure specified earlier. The points represent the data points acquired by using the calibrated density probe and a depth gauge; these points are curve-fitted very well to a hyperbolic tangent distribution by the method of least-squares.

We will consider only the cases in which the speed of the disturbance is near the characteristic velocity of the first internal wave mode, which is c_1 in (6.48). In these cases, the top surface wave is invariably very small and is commonly undiscernible, as can be attested by the experimental data shown in Figure 8.40 (in dimensionless form), a case which is typical. The coefficients of the KdV equation (6.45) and c_1 can be obtained from the results of curve-fitting for ρ_1, ρ_2, k and H (defined in (6.51)) by using the series method described in section 6.5. Typically, 150 terms were taken and the ratio of the next remainder term (the 151th term) over the summation of first 150 terms of the series would be less than 10^{-6}, so c_1 can be determined very

accurately. A typical eigenfunction is shown in Figure 8.41 for the case: $\rho_1 = 1$, $\rho_2 = 1.026$, $k = 7.78$ and $H = 0.278$. As stated in chapter VI, this eigenfunction corresponding to c_1 has one zero inside the depth range (0, 1) of the system. For the general case corresponding to our experiments, this zero is generally very close to the top surface, hence rendering the value of this eigenfunction at the top surface very small. This salient feature of the first eigenmode is consistent with the physical observation because the wave elevation at the top surface is proportional to this eigenfunction according to (6.45). The maximum of the absolute value of this eigenfunction is not at the position H, but at a position about 0.07 above H. From the numerical results, c_1 seems to decrease with decreasing k (when the pycnocline becomes thicker). For our experiments, k is between 6 and 9, and c_1 is about 80% to 90% of the c_s of the two-layer system with the same ρ_1, ρ_2 and H.

In all the numerical calculations performed corresponding to our experimental situations, the forcing shape was taken to be the same as the bump used in the experiment, which is a circular-arc and the d_x term in the forced KdV equation was approximated by the central difference of d. Δx was taken to be $\frac{1}{5}$ L and N was taken to be 2 except for Figure 8.42, where $N = 4$. All the initial conditions are zero. All the numerical results are for the wave elevation at the horizontal level of $z = H$.

Figures 8.42 to 8.48 give the numerical and experimental results in the increasing order of the Froude number (based on c_1). Each figure consists of two parts; the upper part depicts two snapshots of

the numerical results of wave elevation at $z = H$, one at $t = \frac{1}{2}t_e$ and the other at $t = t_e$ where t_e is the dimensionless time instant of motion last computed. The lower part presents the experimental data, received from the gauges MIG, FIG1 and FIG2, and the corresponding numerical results plotted together for comparison (solid lines give numerical results and dashed lines, experimental recordings). For right-going runs of the carriage, waves are propagated first to gauge FIG2 (the second curve in the lower part of figures) and then to gauge FIG1 (the third curve) while the first curve records the wave measured by the moving gauge MIG ahead of the disturbance. For left-going runs, the waves are propagated first to gauge FIG1 (the second curve) and then to gauge FIG2 (the third curve) and the first curve (MIG) records the wave behind the disturbance.

Figure 8.42 presents results for $Fr = 0.659$, $H = 0.278$, $\sigma = 0.975$, velocity of the moving disturbance $U = 0.0403$, the bump width $L = 0.671$ and the bump height $d_m = 0.0904$ acquired during a left-going run. Generation of upstream internal solitary waves are predicted, but the experimental recordings exhibit more waves than in the numerical results. However, the amplitudes of the trailing waves measured experimentally are much less than those of the numerical results. The recording of the trailing wave by gauge MIG shows a considerable departure from the numerical results, this is because according to the numerical results, the near field of the trailing waves soon becomes stationary, with the gauge positioned at a positive wave elevation, whereas in the experiment trailing waves were being developed and a trough happened to recede slowly downward.

The case in Figure 8.43 corresponding to $Fr = 0.972$, $H = 0.278$, $\sigma = 0.975$, $U = 0.0595$, $L = 0.671$ and $d_m = 0.0904$, for a right-going run. For the upstream waves, agreement between theory and experiment seems fairly satisfactory in most of the major qualitative aspects. More specifically, the upstream-running internal solitary waves given by the experimental recordings are somewhat smaller in amplitude and delayed and slower in phase than those of the numerical results, especially in the last curve, where the waves have propagated for some distance after being generated. Further numerical results of the KdV equation are shown in Figure 8.43 for two-layer systems obtained for the same forcing and the same σ and H as those measured in the experiment; they are represented by dash-dot lines. Obviously, the numerical results based on the continuously stratified fluid model seem to be more satisfactory than those given by the two-layered fluid model in light of this comparison with experiments.

Figure 8.44 presents more results for the case of $Fr = 0.985$, $H = 0.244$, $\sigma = 0.970$, $U = 0.0611$, $L = 0.613$ and $d_m = 0.0825$ for a left-going run. Similar behaviors are seen here as in Figure 8.43. The next four figures are for supercritical cases. In Figure 8.45, we have $Fr = 1.09$, $H = 0.271$, $\sigma = 0.973$, $U = 0.0693$, $L = 0.645$ and $d_m = 0.0868$ for a left-going run. The numerical results for the FIG2 station show the generation of a soliton of a considerable amplitude but the internal wave developed more slowly and was unable to run ahead of the bump within the limited time of the experiment. Figure 8.46 is for the case with $Fr = 1.16$, $H = 0.244$,

$\sigma = 0.970$, $U = 0.0722$, $L = 0.613$ and $d_m = 0.0825$ and for a right-going run. The numerical and experimental curves for the FIG2 station and a large part of the early time results for MIG are found in good agreement. Further, the curves associated with MIG show that a runaway soliton was about to be generated experimentally. The next cases are shown in Figure 8.47 for $Fr = 1.18$, $H = 0.269$, $\sigma = 0.970$, $U = 0.0750$, $L = 0.613$ and $d_m = 0.0825$ for a left-going run. The last case of study is shown in Figure 8.48 for $Fr = 1.26$, $H = 0.269$, $\sigma = 0.970$, $U = 0.0798$, $L = 0.613$ and $d_m = 0.0825$, and for a right-going run. In these supercritical cases the resulting waves are small except in a region around the bump, and the numerical results are in rather good agreement with the experimental recordings.

In summary, all these results show a good qualitative agreement between theory and experiment for all the main features of these internal runaway solitons. At small Froude numbers, the upstream-running internal waves are small but the period of their generation is also short. With increasing Froude number, the generated upstream-running internal solitons become larger in amplitude and the period of generation becomes longer, until no upstream internal wave is generated when a certain supercritical Froude number is reached. Quantitatively, most of the cases investigated show that the internal solitons so generated have smaller amplitudes and larger generation periods in the experiments than in numerical calculations. Since our theoretical model is inviscid, the viscous effects can not be readily accounted for without having these models appropriately modified and these effects are thought to be a most likely cause of the discrepancies between theory

and experiment. To give a crude estimate of the viscous effects, the decay formula for free internal solitons in a two-layer system, given by Leone, Segur & Hammack (1982) (7a) and (7b), was used to calculate the decay of the first soliton in Figure 8. 43, with the kinematic viscosity of water taken to be $0.01 cm^2/s$. If the amplitude of the first soliton at FIG2, 0. 1, is taken as the initial amplitude, the calculated amplitude when this soliton reaches the FIG1 position, after traversed 60L distance, is about 0. 038, whereas its recorded amplitude in the experiment at the corresponding position is about 0. 077. So the decay rate for the leading solitary wave obtained from the theoretical formula given by Leone et al. is considerably stronger than that derived from our experimental recording. There are two possible explanations for this difference. First, the decay rate may be higher in two-layer cases than in continuously stratified cases which are equivalent by analogy. The truth of this variance between the two categories of fluid systems remains to be seen. To include the viscous effect into the continuously stratified cases as well as in the process of the generation stage, further research is required. Second, the external forcing may still be reacting on the wave and thus reducing its decay rate. Some fine structures of the flow field were observed about the position of the first trailing wave during the experiment; they are believed to be related to wave breaking, which in turn enhanced the mixing process, and may contribute to the discrepancies between the experimental recordings and the numerical results in the trailing wave region.

IX. SUMMARY

The phenomenon of generation of internal solitons by disturbances moving with a transcritical velocity through a stratified fluid system has been verified by the numerical results of several different forced KdV models and by two theoretical models of generalized Boussinesq class as well as by experiments. Similar to the one-layer (of homogeneous fluid) case, solitons are found to be generated and to surge ahead of a moving disturbance, which moves with a uniform transcritical velocity U where U is close to a characteristic velocity of the stratified fluid system. With increasing U, both the amplitude of the solitons generated and the period of soliton generation increase until this phenomenon ceases to occur at a certain supercritical Froude number about 1.2. For the Froude number very close to 1, solitons seem to be generated almost periodically and indefinitely.

Most of the cases considered here are for the slow mode motion of a two-layer fluid system or for the first internal wave mode of a continuously stratified fluid system, and for small density variations of the system. In these cases, the internal solitary waves so generated exhibit similar features as those of the one-layer case. However, the top surfaces, if free, remain almost undisturbed.

Two categories of theoretical models have been developed here for investigating stratified fluid systems; one is of the generalized Boussinesq class, which is particularly suitable for describing wave motions propagating in all directions, the other is the generalized Korteweg-de Vries class, which can describe wave motions primarily in one direction. These theoretical models have been found satis-

factory for predicting weakly nonlinear and weakly dispersive long internal waves in a stratified fluid system and for evaluating their generation and evolution under the influence of external forcings which may be in motion. External forcing disturbances have been exemplified by top surface pressures and moving bottom unevenness, while the top surface of the system may be either free or covered with a rigid horizontal plate. The basic equations of the Boussinesq class for the free top-surface case of two-layer systems form the FOUR-equation model and that for two-layer systems with a rigid horizontal top-surface gives the THREE-equation model.

From the analyses of the KdV model for two-layer systems, the generated solitons are found to have the following salient features:

The velocities in the upper and the lower layers and the wave elevations are all proportional to each other to the leading order. Furthermore, for the rigid horizontal top-surface case and for the slow mode motion with a free top surface, the velocities in the two layers are always opposite in direction. For every case in a two-layer system, there always exists a unique, corresponding, homogeneous one-layer case with the same Froude number and related by known scaling laws. With this correspondence, the wave behaviors in a stratified two-layer system can be observed in the simpler situation of a homogeneous one-layer system with the same Froude number and with the other variable correlated by scaling.

When the densities of the upper and the lower layers of a two-layer system are nearly equal, the wave behaviors are as follows. For the slow mode motion, unless the depths of the two-layers are

nearly equal, interfacial solitary waves, which are generated in whatever manner and are settled in form, always extend away from the narrower layer. This is apparent from the scaling rules for the correspondence of two-layer system to a unique one-layer system, and the effect of variations in the density-ratio for the two-layer system is only to alter the time scale (and hence also the velocity scale). In comparing the top surface pressure forcing and the bottom disturbance forcing, their effective forcing strengths are found to have a factor inversely proportional to the distance between the forcing position and the interface.

Several numerical schemes have been developed for solving problems with the FOUR-equation model, the THREE-equation model and the various forced KdV equations. They are finite-differencing methods with a modified Euler's predictor-and-corrector technique. The effects of the physical properties of the basic fluid system and the forcing on generations of internal solitons were discussed with numerical results. Comparison between these different theoretical models has demonstrated their consistency for the various cases considered.

The forced KdV equation for continuously stratified fluid systems has been derived by applying the perturbation method. To obtain solutions, it is required to first find the characteristic velocities and the corresponding coefficients of the KdV equation from the primary density profile of the system by solving an associated eigenvalue problem. There are infinitely many modes for this system. The first mode, with the largest characteristic velocity, is similar to the homogeneous one-layer case, in which the largest displacement occurs

at the top surface. The next mode is called the first internal mode, and is the main interest in this study.

Experiments were performed with a bottom bump as a forcing disturbance moving near the characteristic velocity of the first internal mode. The fluids used for the experiments were fresh water in the upper layer and brine in the lower layer. The experimental results have produced valuable data concerning all the basic features of the generations of internal solitons stated previously. The experimental results have been compared with the numerical results of the forced KdV equation for continuously stratified systems and with the other model for two-layer systems. Quantitatively, the numerical results based on the continuously stratified fluid model seem to be more satisfactory than those given by the two-layered fluid models in comparison with experiment. Generally speaking, the experimental recordings give periods of soliton generation appreciably longer than predicted by the various theories and this discrepancy is believed to be related to viscous effects. To include the viscous effects in the calculations for continuously stratified systems under the influence of external forcing excitations, further research is required.

APPENDIX

SOME PROPERTIES OF THE COEFFICIENT MATRIX (5.54)

During the Gauss's elimination procedure for a tridiagonal matrix

$$A = \begin{bmatrix} a_{21} & a_{31} & & & & \\ a_{12} & a_{22} & a_{32} & & & \\ & a_{13} & a_{23} & a_{33} & & \\ & & \cdots\cdots & & & \\ & & & & a_{1n} & a_{2n} \end{bmatrix} , \tag{A.1}$$

without the partial pivoting (i. e., without the row exchange), the ith diagonal element r_i becomes as follows, after the subdiagonal (i. e., below the diagonal) elements in the first (i - 1)th, if $i > 1$, columns vanish by the eliminations,

$$\begin{aligned} r_1 &= a_{21} = D_1 , \\ r_i &= \frac{D_i}{D_{i-1}} \qquad \text{for } i = 2, 3, \ldots, n , \end{aligned} \tag{A.2}$$

where D_i is the determinant that is formed by the first i rows and the first i columns of the matrix A.

PROPERTY 1

For the matrix

$$B = \begin{bmatrix} -a_1-b_1 & b_1 & & & \\ a_2 & -a_2-b_2 & b_2 & & \\ & a_3 & -a_3-b_3 & b_3 & \\ & & \cdots\cdots & & \\ & & & a_n & -a_n-b_n \end{bmatrix} , \qquad (A.3)$$

the following relations

$$D_i (-1)^i > 0 \qquad \text{for } i = 1,2,\ldots,n \ , \qquad (A.4)$$

$$(D_i + b_i D_{i-1})(-1)^i > 0 \qquad \text{for } i = 2,3,\ldots,n \qquad (A.5)$$

where D_i is the determinant formed by the first i rows and the first i columns of the matrix B, are valid if all the a_i's and b_i's are positive.

PROOF

$$D_1 = -a_1 - b_1 < 0 \ ,$$

$$D_2 = a_2a_1 + a_1b_2 + b_1b_2 > 0 \ , \qquad (A.6)$$

$$D_2 + b_2D_1 = a_1a_2 > 0 \ .$$

Therefore (A. 4) are valid for $i = 1,2$ and (A. 5) are valid for $i = 2$. Following the induction method, suppose that

$$D_i(-1)^i > 0 \ ,$$

and

$$(D_i + b_i D_{i-1})(-1)^i > 0$$

for $i = 2,3,\ldots,k$. Then

$$D_{k+1} = (-a_{k+1} - b_{k+1})D_k - a_{k+1}b_kD_{k-1}$$

$$= -a_{k+1}(D_k + b_kD_{k-1}) - b_{k+1}D_k \quad , \qquad \text{(A. 7)}$$

hence

$$D_{k+1}(-1)^{k+1} = a_{k+1}(D_k + b_kD_{k-1})(-1)^k + b_{k+1}D_k(-1)^k > 0 \ ,$$

and

$$(D_{k+1} + b_{k+1}D_k)(-1)^{k+1} = a_{k+1}(D_k + b_kD_{k-1})(-1)^k > 0 \quad .$$

Q. E. D.

This property implies that B is nonsingular. Actually more strong conclusions can be reached:

$$D_i(-1)^i > (i+1)m^i \qquad \text{for } i = 2, \ldots, n \ , \qquad \text{(A. 8)}$$

and $$(D_i + b_iD_{i-1})(-1)^i > m^i \quad \text{for } i = 2, 3, \ldots, n \ , \qquad \text{(A. 9)}$$

where $m = \min_{i=1,2,\ldots,n} (a_i, b_i)$.

PROPERTY 2

Under the conditions in the property 1,

$$|r_i| > b_1 \qquad \text{for } i = 1, 2, \ldots, n-1 \ . \qquad \text{(A. 10)}$$

PROOF

For i = 1, it is obvious.

For i = 2, by virtue of the relations (A. 6) ,

$D_2 + b_2D_1 > 0$,

and using (A. 2)

$$r_2 = \frac{D_2}{D_1} \quad ,$$

it follows that

$$|r_2| > b_2 \quad ,$$

because $D_1 < 0$.

For $i > 2$, from (A.7), we have

$$D_i = -a_i(D_{i-1} + b_{i-1}D_{i-2}) - b_iD_{i-1} \qquad \text{for } i = 3, 4, \ldots, n-1 \quad ,$$

and from (A. 4) and (A. 5), we have

$$(D_{i-1} + b_{i-1}D_{i-2})(-1)^{i-1} > 0 \qquad \text{for } i = 3, 4, \ldots, n-1 \quad ,$$

$$D_{i-1}(-1)^{i-1} > 0 \qquad \text{for } i = 3, 4, \ldots, n-1 \quad ,$$

therefore

$$|D_i| > |b_iD_{i-1}| \quad ,$$

because of the positiveness of a_i's and b_i's.

By (A. 2)

$$r_i = \frac{D_i}{D_{i-1}} \qquad \text{for } i = 3, 4, .., n-1 \quad ,$$

it follows that

$$|r_i| > b_i \qquad \text{for } i = 3, 4, \ldots, n-1 \quad . \qquad \text{Q. E. D.}$$

For the matrix K in (5. 54), it has above properties and because it is also symmetric, so

$$|r_i| > a_{i+1} \qquad \text{for } i = 1, 2, .., n-1 \quad .$$

Due to this property, the procedure of the Gauss's elimination always keeps the absolute value of the diagonal element larger than the absolute values of the subdiagonal elements in its column. In other words, the procedure with partial pivoting does not exchange the rows of the matrix because it will find that the diagonal element is always larger than the subdiagonal elements in the absolute values in the same column. In view of this property, the Gauss's elimination method without the partial pivoting can be used safely for the system with the coefficient matrix K in (5.54).

REFERENCES

Akylas, T. R. 1984 On the excitation of long nonlinear water waves by a moving pressure distribution. J. Fluid Mech., vol. 141, pp. 455-466.

Baines, P. G. 1977 Upstream influence and Long's model in stratified flows. J. Fluid Mech., vol. 82, pp. 147-159.

Baines, P. G. 1979 Observation of stratified flow over two-dimensional obstacles in fluid of finite depth. Tellus, vol. 31, pp. 351-371.

Benjamin, T. B. 1966 Internal waves of finite amplitude and permanent form. J. Fluid Mech., vol. 25, pp. 241-270.

Benjamin, T. B. 1967 Internal waves of permanent form in fluids of great depth. J. Fluid Mech., vol. 29, pp. 559-592.

Benjamin, T. B., F. R. S., Bona, J. L. and Mahony, J. J. 1972 Model equations for long waves in nonlinear dispersive systems. Phil. Trans. Roy. Soc. London, vol. 272, pp. 47-78.

Benney, D. J. 1966 Long non-linear waves in fluid flows. J. Math. & Phys., vol. 45, pp. 52-63.

Bona, J. L. and Smith, R. 1975 The initial value problem for the KdV equation. Phys. Trans. Roy. Soc. London., vol. 278, pp. 555-604.

Chereskin, T. K. 1983 Generation of internal waves in Massachusetts Bay. J. Geoph. Res., vol. 88 (c4), pp. 2649-2661.

Cole, S. L. 1985 Transient waves produced by flow past a bump. Wave Motion, vol. 7, pp. 579-587.

Eriksen, C. C. 1978 Measurements and models of find structure, internal gravity waves, and wave breaking in the deep ocean. J. Geoph. Res., vol. 83, pp. 2989-3009.

Ertekin, R. C. 1984 Soliton generation by moving disturbances in shallow water: Theory, computation and experiments. Ph. D. Dissertation, University of California, Berkeley.

Farmer, D. M. and Smith, J. D. 1980 Tidal interaction of stratified flow with a sill in Knight Inlet. Deep-Sea Res., vol. 27A, pp. 239-254.

Gardner, C. S. and Morikawa, G. K. 1960 Similarity in the asymptotic behavior of collision-free hydromagnetic waves and water waves. NYO-9082. New York Univ.

Gargett, A. E. 1976 Generation of internal waves in the Strait of Georgia, British Columbia. Deep-Sea Res., vol. 23, pp. 17-32.

Gilreath, H. E. and Brandt, A. 1985 Experiments on the generation of internal waves in a stratified fluid. AIAA J., vol. 23, pp. 693-700.

Grimshaw, R. H. J. and Smyth, N. 1985 Resonant flow of a stratified fluid over topography. Res. report, No. 14, Dept. of Math., Univ. of Melbourne, Australia.

Halpern, D. 1971 Observations on short-period internal waves in Massachusetts Bay. J. Marine Res., vol. 29, pp. 116-132.

Hammack, J. L. 1980 Baroclinic tsunami generation. J. Phys. Ocean, vol. 10, pp. 1455-1467.

Haury, L. R. 1979 Tidally generated internal wave packets in Massachusetts Bay. Nature, vol. 278, pp. 312-317.

Huang, D-B, Sibul, O.J., Webster, W.C., Wehausen, J.V., Wu, D-M, & Wu, T.Y. 1982 Ship moving in the transcritical range. Proc. Conf. on Behavior of Ships in Restricted Waters, vol. 2, 26.1-26.12, Varna, Bulgaria.

Hurdis, D.A. and Pao, H.P. 1975 Experimental observation of internal solitary waves in a stratified fluid. Phys. Fluids, vol. 18, pp. 385-386.

Ince, E.L. 1926 Ordinary differential equations. Dover Publ. Inc., New York.

Joseph, R.J. 1977 Solitary waves in a finite depth fluid. J. Phys. A., vol. 10, pp. 225-227.

Kao, T.W., Pan, F-S and Renouard, D. 1985 Internal solitons on the pycnocline: generations, propagation, and shoaling and breaking over a slope. J. Fluid Mech., vol. 159, pp. 19-53.

Keulegan, G.H. 1953 Characteristics of internal solitary waves. J. Res. Natl. Bur. Stand., vol. 51, pp. 133-140.

Koop, C.G. and Butler, G. 1981 Internal solitary waves in a two fluid system. J. Fluid Mech., vol. 112, pp. 225-251.

Kubota, T., Ko, D.R.S. and Dobbs, L.D. 1978 Weakly-nonlinear, long internal gravity waves in stratified fluids of finite depth. J. Hydron., vol. 12, pp. 157-165.

Lansing, F.S. and Maxworthy, T. 1984 On the generation and evolution of internal gravity waves. J. Fluid Mech., vol. 145, pp. 127-149.

Lee, C-Y. and Beardsley, R.C. 1974 The generation of long nonlinear internal waves in a weakly stratified shear flow. J. Geoph. Res., vol. 79, pp. 453-462.

Lee, S-J. 1985 Generation of long water waves by moving disturbances. Ph. D. Thesis, California Institute of Technology, Pasadena, CA.

Leone, C., Segur, H. and Hammack, J. L. 1982 Viscous decay of long internal solitary waves. Phys. Fluids, vol. 25, pp. 942-944.

Lepelletier, T. G. 1981 Tsunamis-harbor osillations induced by nonlinear transient long waves. Ph. D. Thesis, California Institute of Technology, Pasadena, CA.

Liu, A. K., Kubota, T. and Ko, D. R. S. 1980 Resonant transfer of energy between nonlinear waves in neighboring pycnoclines. Studies Appl. Math., vol. 63, pp. 25-45.

Locke, L. 1980 Waves beneath the sea. Lamp. Summer 1980.

Long, R. R. 1956 Solitary waves in the one- and two-fluid systems. Tellus, vol. 8, pp. 460-471.

Long, R. R. 1970 Stratified flow. Film notes.

Maxworthy, T. 1979 A note on the internal solitary waves produced by tidal flow over a three-dimensional ridge. J. Geophys. Research., vol. 84, pp. 338-346.

Mei, C. C. 1986 Radiation of solitons by slender bodies advancing in a shallow channel. J. Fluid Mech., vol. 162, pp. 53-67.

Miura, R. M. 1976 The Korteweg-de Vries equation: a survey of results. SIAM Rev., vol. 18, pp. 412-459.

Ono, H. 1975 Algebraic solitary waves in stratified fluids. J. Phys. Soc. Japan, vol. 39, pp. 1082-1091.

Osborne, A.R., Burch, T.L. and Scarlet, R.I. 1978 Influence of internal waves on deep-water drilling. J. Petro. Tech., vol. 30, pp. 1497-1504.

Osborne, A.R. and Burch, T.L. 1980 Internal solitons in the Andaman Sea. Science, vol. 208, pp. 451-460.

Peregrine, D.H. 1966 Calculations of the development of an undular bore. J. Fluid Mech., vol. 25, pp. 321-330.

Perry, R.B. and Schimke, G.R. 1970 Large-amplitude internal waves observed off the northwest coast of Sumatra. J. Geoph. Res., vol. 70, pp. 2319-2324.

Peters, A.S. and Stoker, J.J. 1960 Solitary waves in liquids having nonconstant density. Comm. Pure Appl. Math., vol. 13, pp. 115-164.

Ursell, F. 1953 The long-wave paradox in the theory of gravity waves. Proc. Camb. Phil. Soc., vol. 49, pp. 685-694.

Vliegenthart, A.C. 1971 On finite difference methods for the KdV equation. J. Engn. Math., vol. 5, pp. 137-155.

Water, I. 1965 Standard methods for the examination of water and wastewater.

Whitham, G.B. 1974 Linear and nonlinear waves. John Wiley & Sons, Inc., New York, N.Y.

Wu, T.Y. 1966 Radiation and dispersion of internal waves. 6th Symp. Naval Hydrod., Washington, D.C.

Wu, T.Y. 1979 On tsunamis propagation-evaluation of existing models. Tsunamis-Proc. of the National Science Foundation Workshop, organized and edited by Hwang, L.S. and Lee, Y.K., Tetra Tech Inc., Pasadena, CA, pp. 110-149.

Wu, T. Y. 1984 New birth to runaway solitons. Symp. on Frontiers in Applied Mechanics and Biomechanics at University of California, San Diego. In Frontiers in Biomechanics, Springer-Verlag, New York.

Wu, T. Y. 1986 On generation of solitary waves by moving disturbances. IUTAM Sym.

Wu, T. Y. and Mei, C. C. 1967 Two-dimensional gravity waves in a stratified ocean. Phys. Fluids, vol. 10, pp. 482-486.

Wu, D-M and Wu, T. Y. 1982 Three-dimensional nonlinear long waves due to moving surface pressure. Proc. 14th Sym. Naval Hydro., National Academic Press, Washington, D. C., pp. 103-125.

Yih, C-S and Guha, C. R. 1955 Hydraulic jump in a fluid system of two layers. Tellus, vol. 7, pp. 358-366.

Ziegenbein, J. 1969 Short internal waves in the Strait of Gibraltar. Deep-Sea Res., vol. 16, pp. 479-487.

Ziegenbein, J. 1970 Spatial observations of short internal waves in the Strait of Gibraltar. Deep-Sea Res., vol. 17, pp. 867-875.

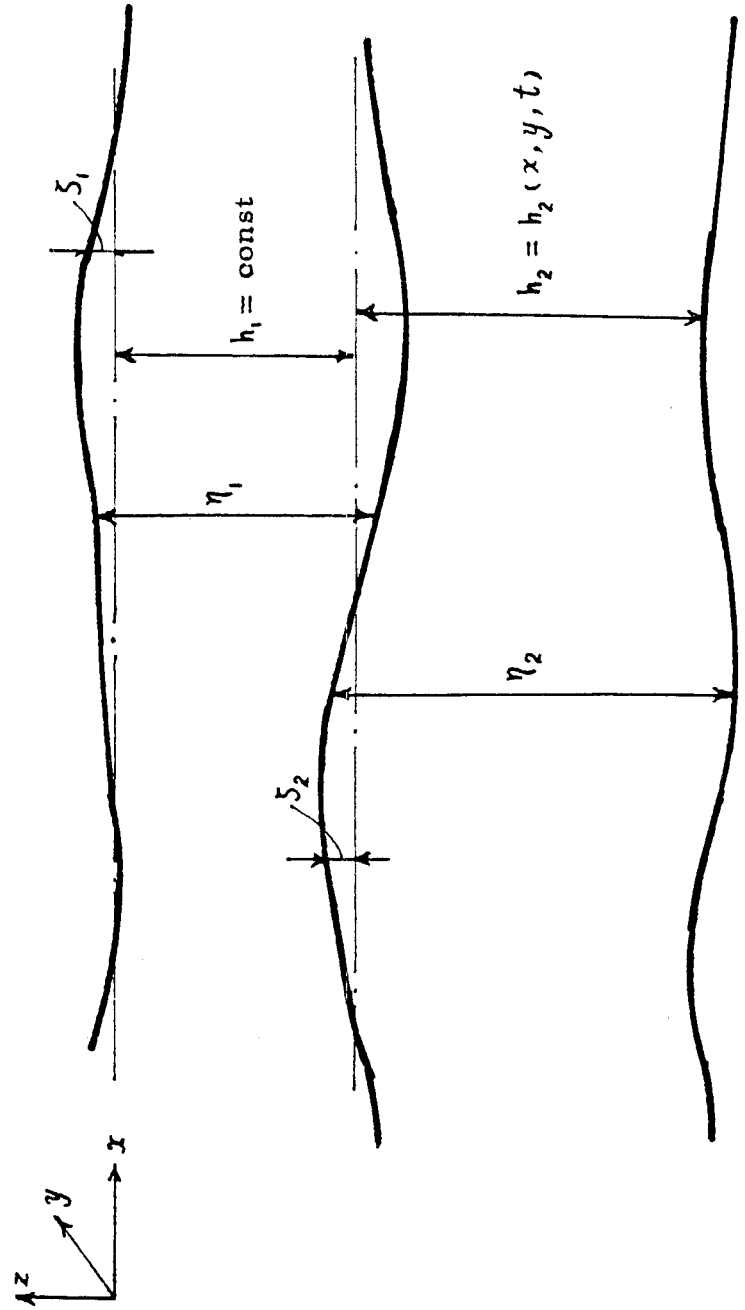

FIGURE 2.1 SKETCH FOR A TWO-LAYER FLUID SYSTEM

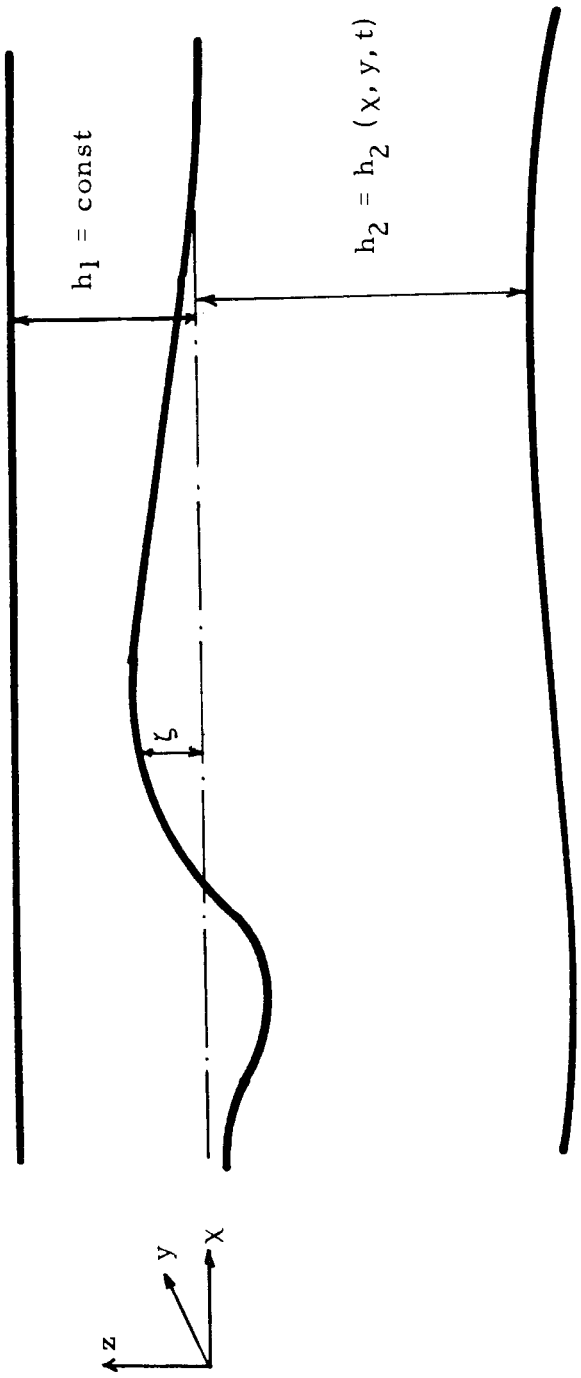

Fig. 5.1 Sketch for a two-layer system with rigid horizontal top surface

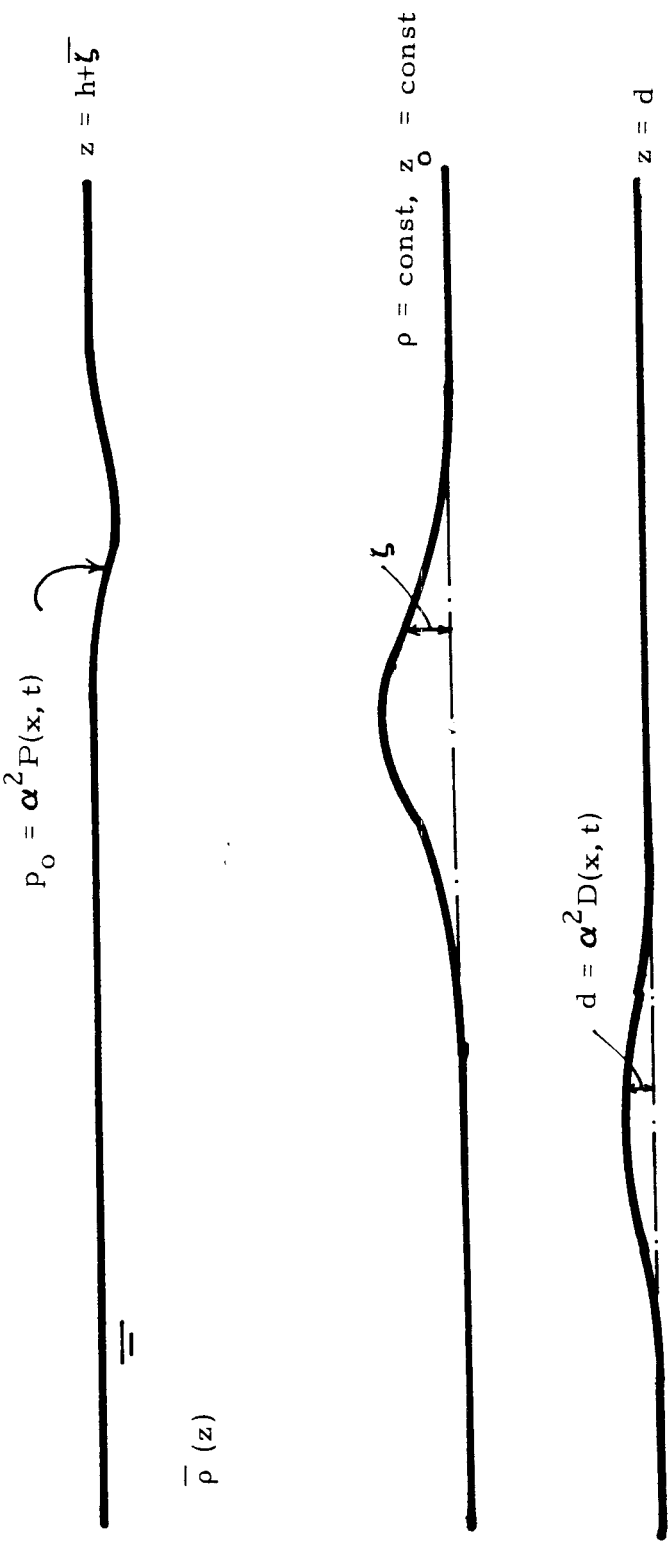

Fig. 6.1 Sketch for a continuously stratified fluid system.

Unit mm

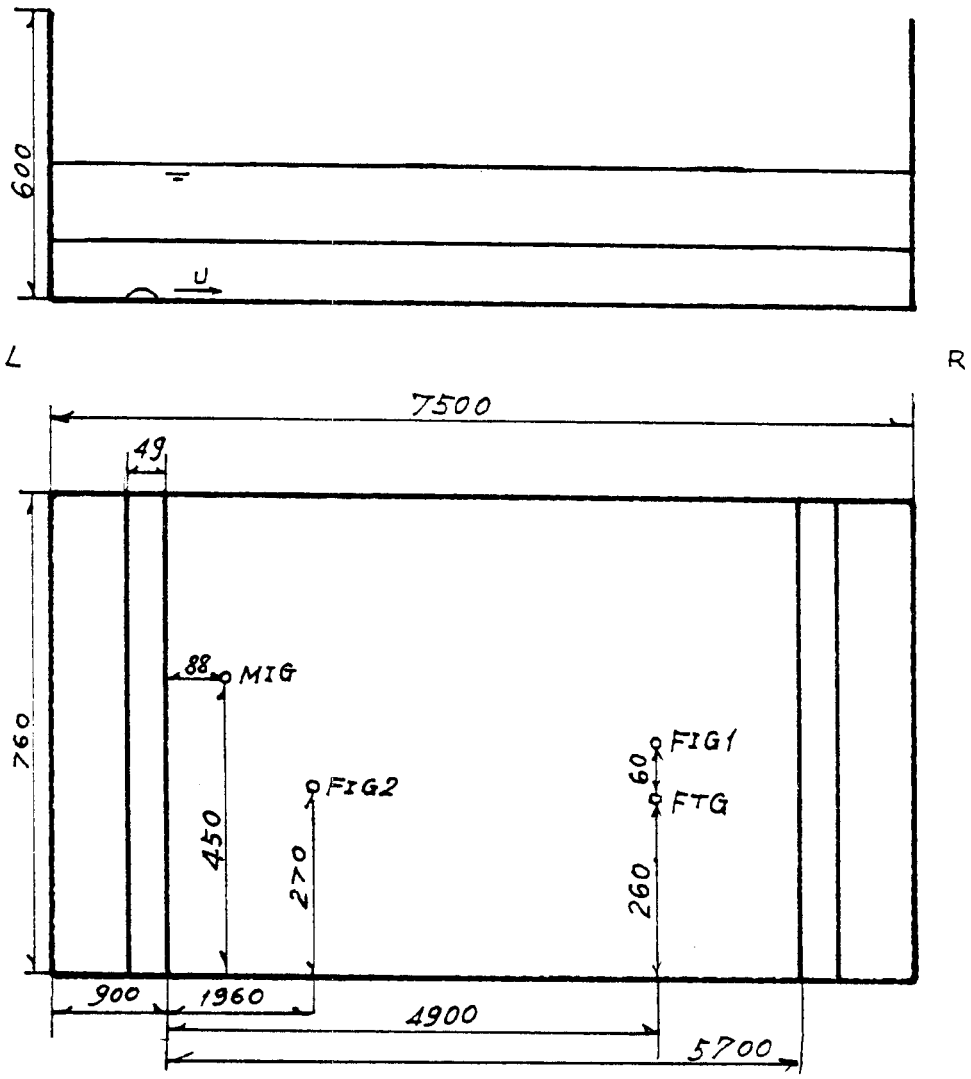

Fig. 7.1 Locations of the wave gauges

Interfacial wave gauge

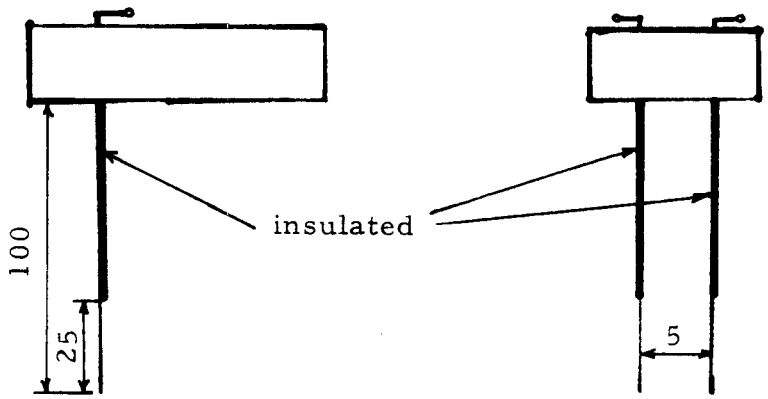

Shielded interfacial wave gauge

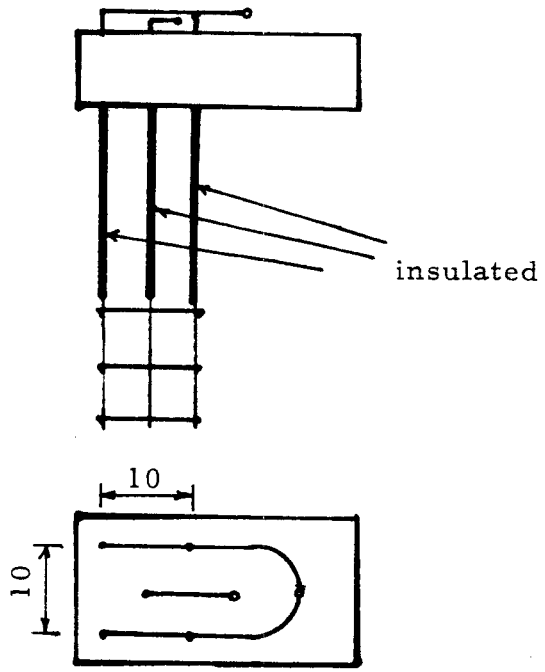

Unit mm

Fig. 7.2 Drawings of typical wave gauges.

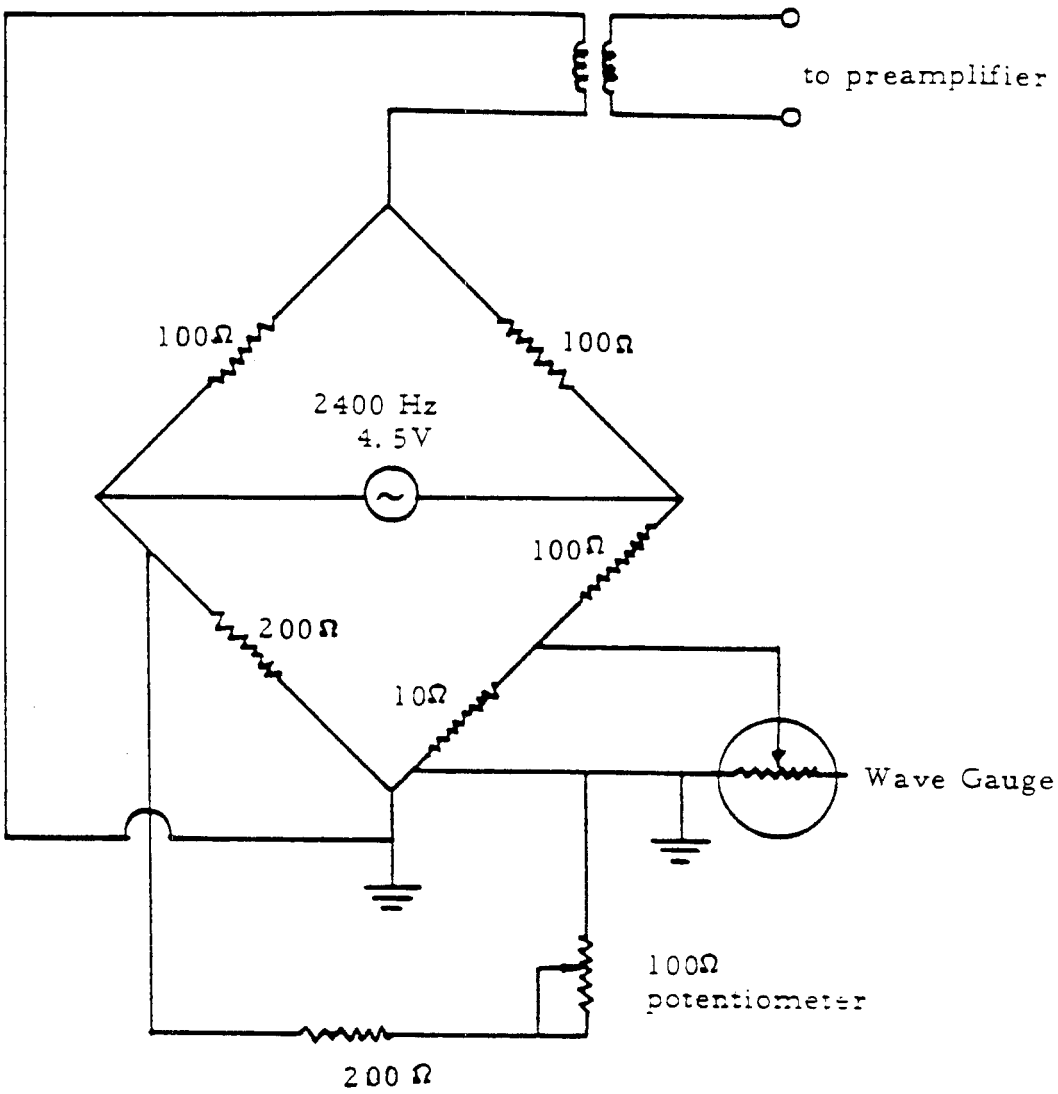

7.3 Circuit diagram for wave gauges.

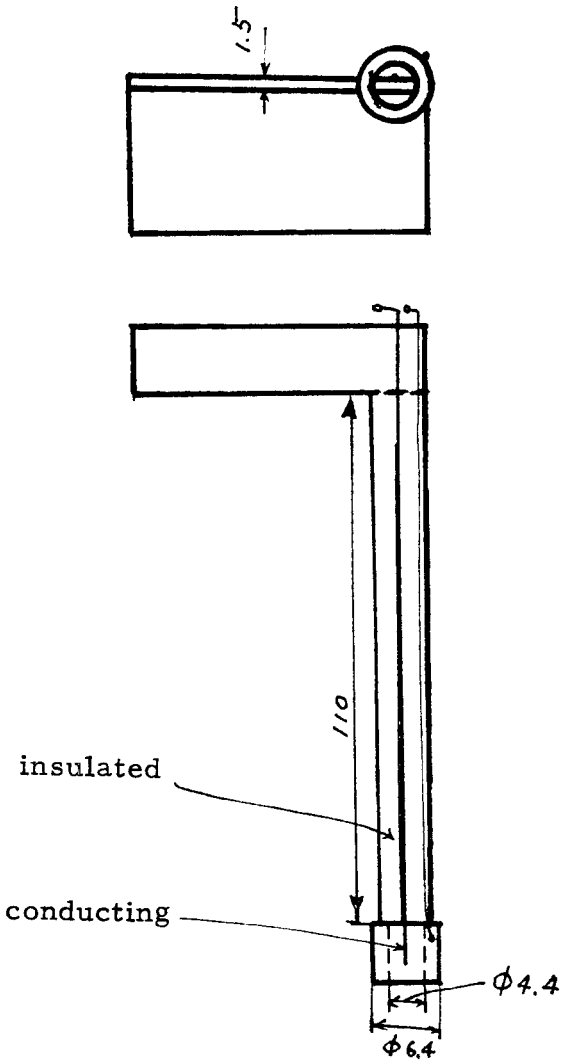

Fig. 7.4 Drawing of a density probe.

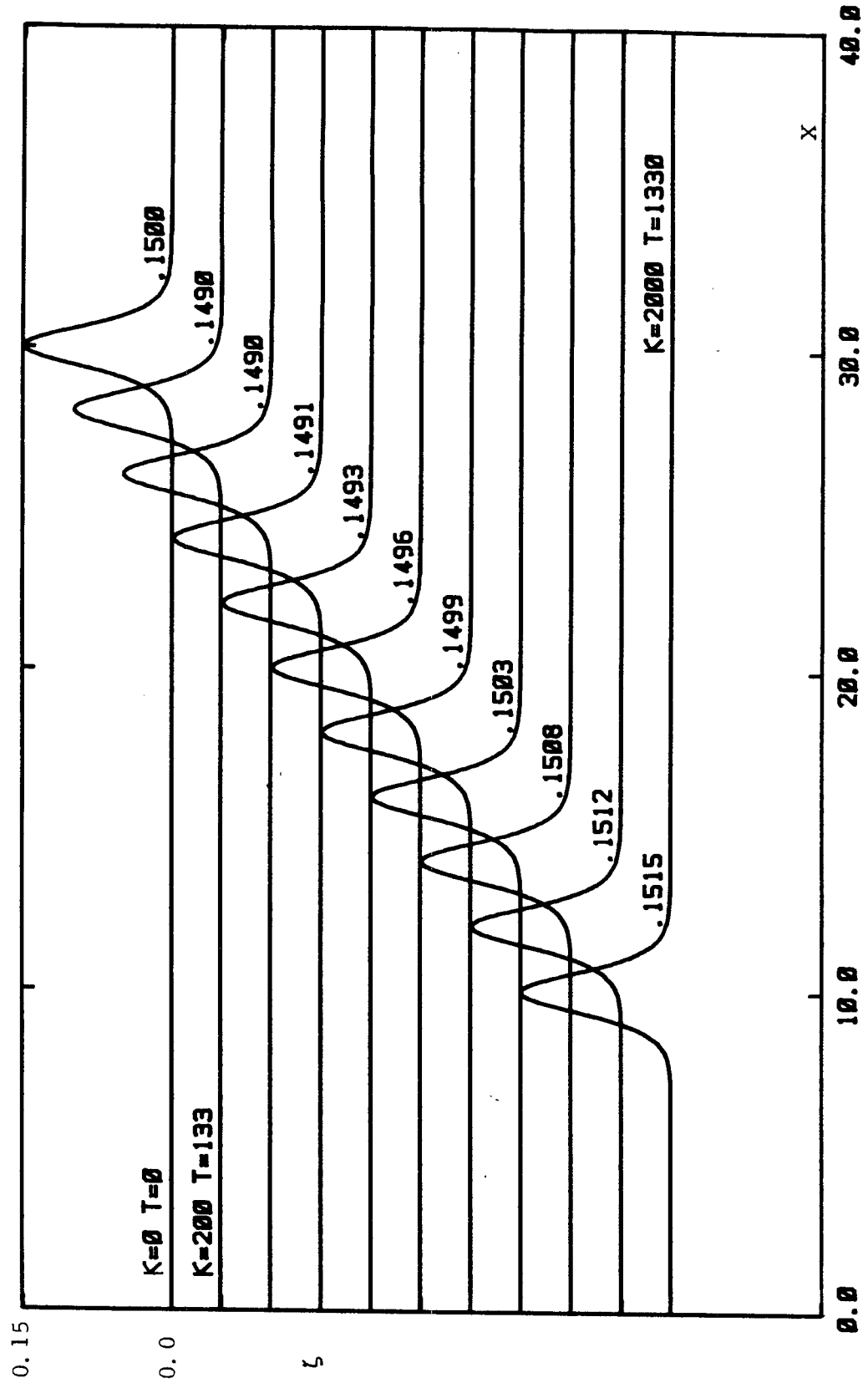

Fig. 8.1 Stability test of the numerical KdV model for two-layer with free top surface using the soliton as initial condition, $H_2 = 0.25$, $\sigma = 0.97$ and initial amplitude of the soliton $a = 0.15$.

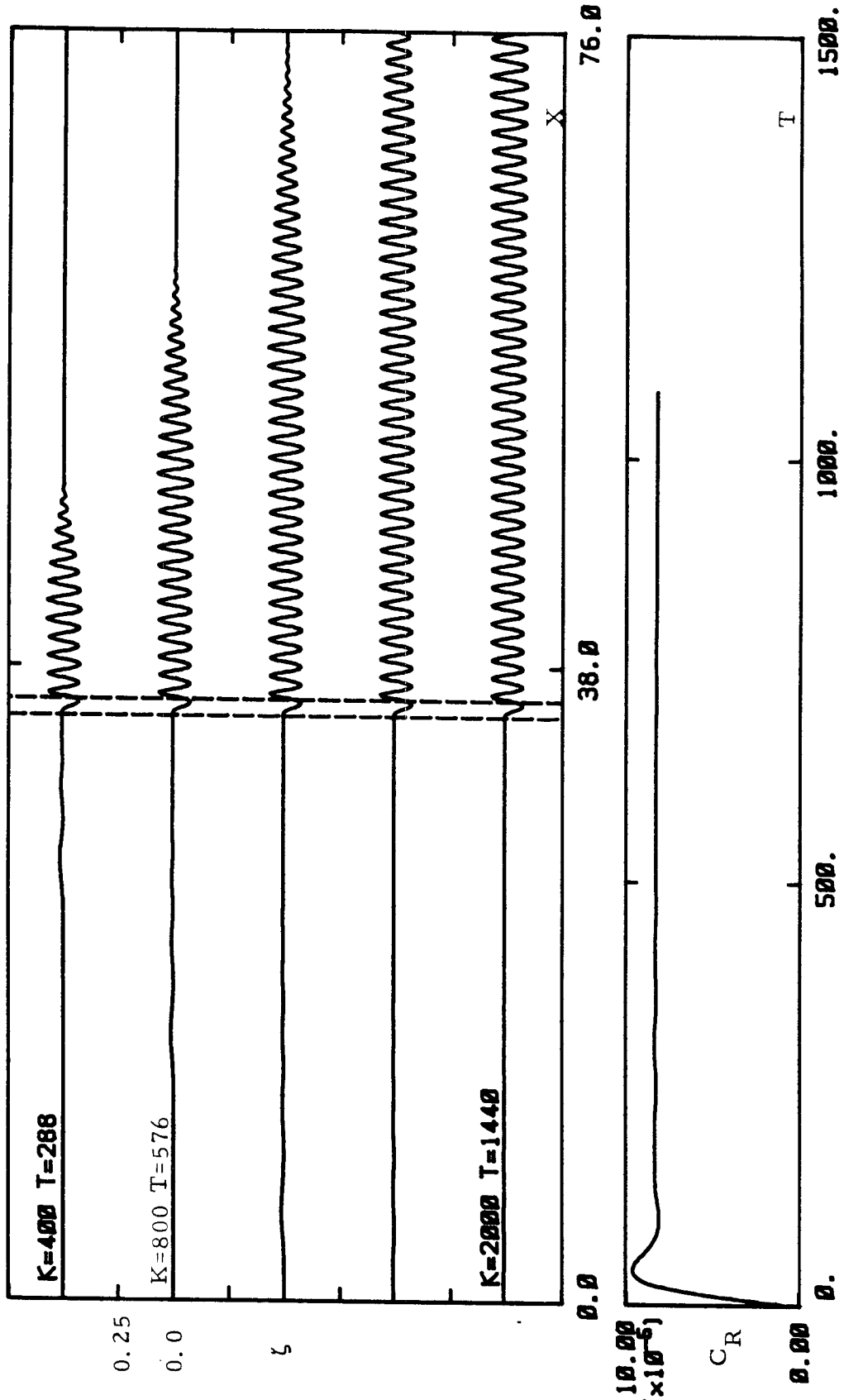

Fig. 8.2 The interface wave elevation and the wave resistance coefficient of the bottom bump given by the numerical KdV model for the two-layer system with free top surface for $H_2 = 0.2$, $\sigma = 0.97$, $L = 1$, $d_m = 0.05$ and $Fr = 0.5$.

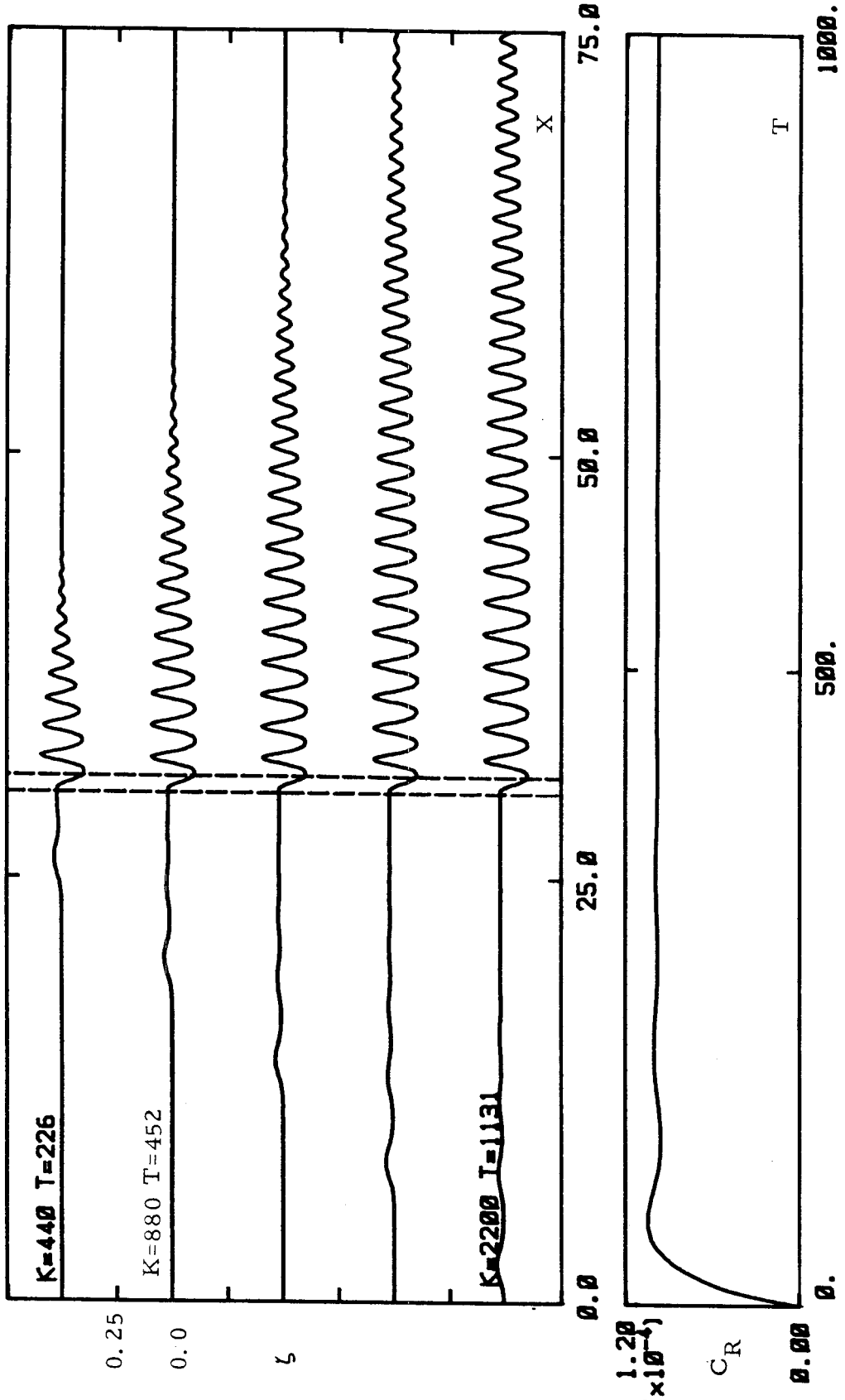

Fig. 8.3 The interface wave elevation and the wave resistance coefficient of the bottom bump given by the numerical KdV model for the two-layer system with free top sufrace for $H_2 = 0.2$, $\sigma = 0.97$, $L = 1$, $d_m = 0.05$ and $Fr = 0.7$.

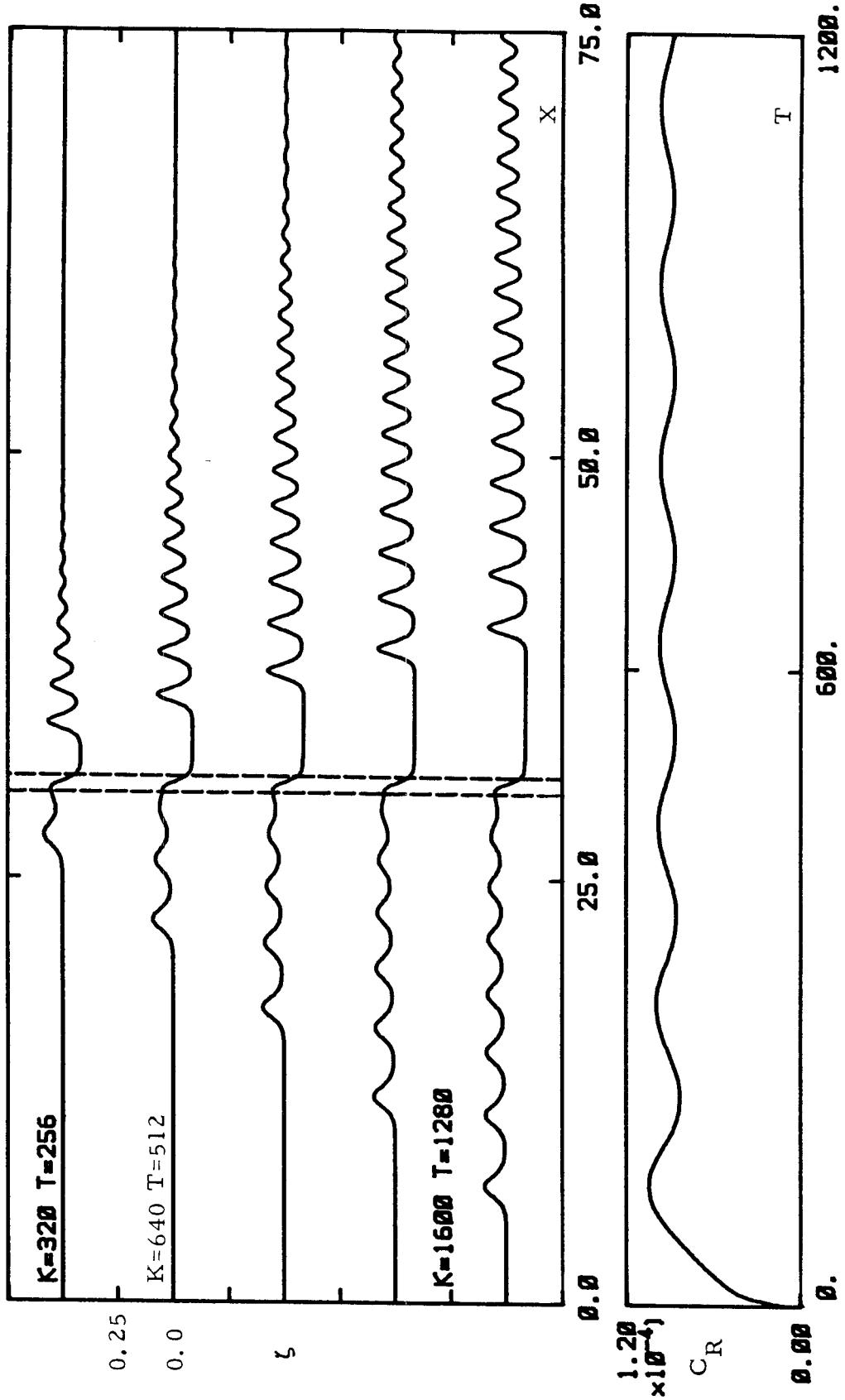

Fig. 8.4 The interface wave elevation and the wave resistance coefficient of the bottom bump given by the numerical KdV model for the two-layer system with free top surface for $H_2 = 0.2$, $\sigma = 0.97$, $L = 1$, $d_m = 0.05$ and $Fr = 0.9$.

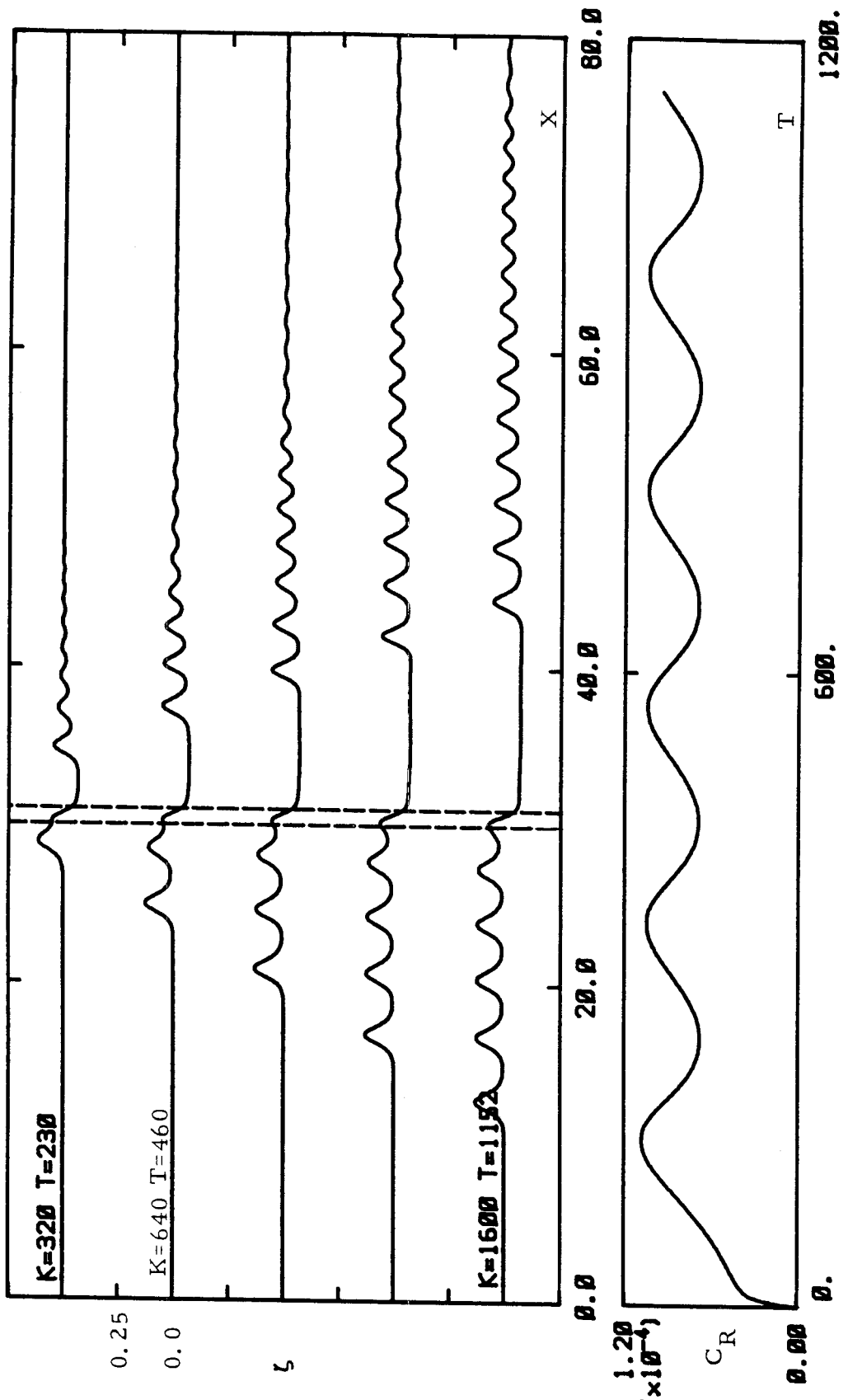

Fig 8.5 The interface wave elevation and the wave resistance coefficient of the bottom bump given by the numerical KdV model for the two-layer system with free top surface for $H_2 = 0.2$, $\sigma = 0.97$, $L = 1$, $d_m = 0.05$ and $Fr = 1$.

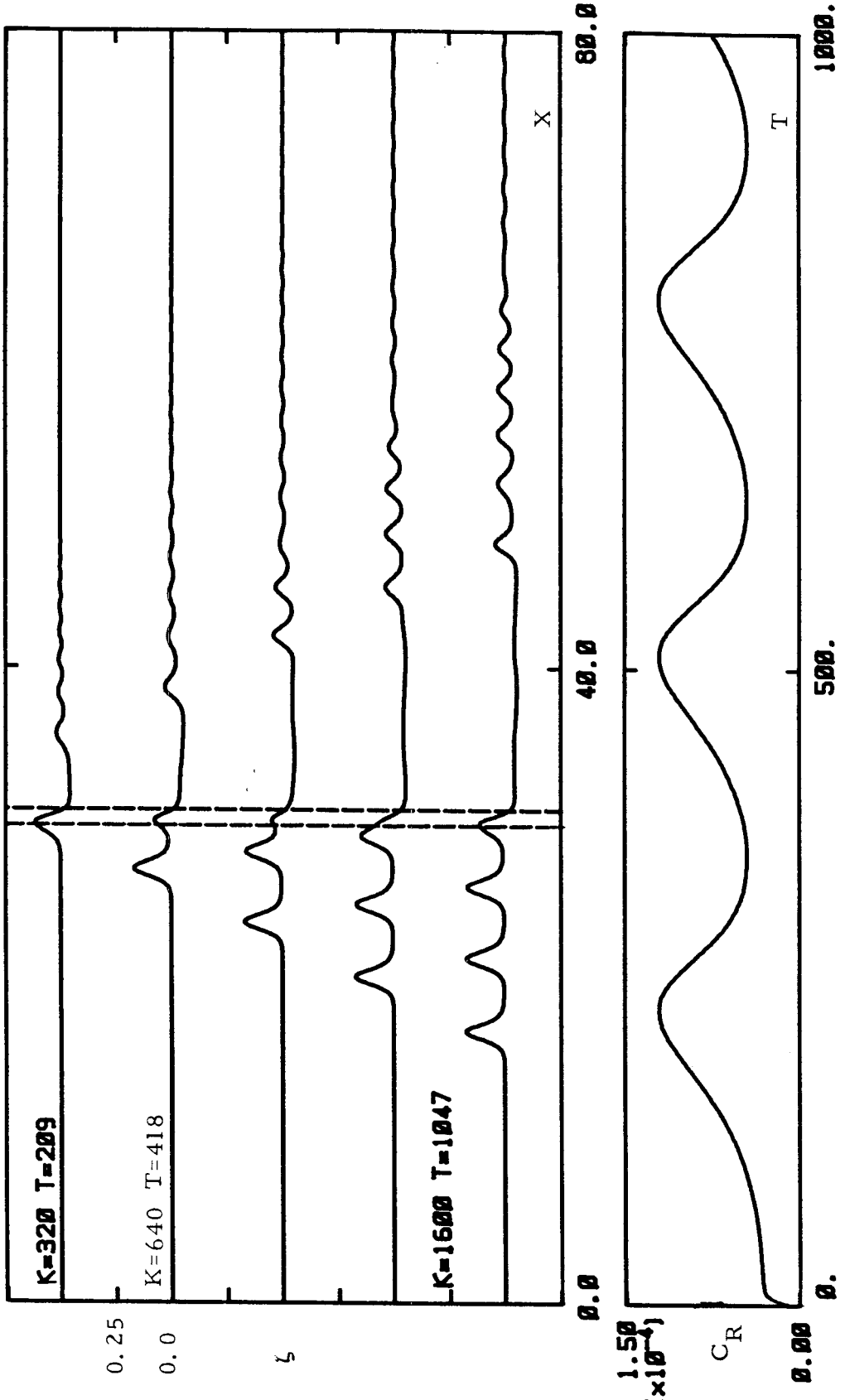

Fig. 8.6 The interface wave elevation and the wave resistance coefficient of the bottom bump given by the numerical KdV model for the two-layer system with free top surface for $H_2 = 0.2$, $\sigma = 0.97$, $L = 1$, $d_m = 0.05$ and $Fr = 1.1$.

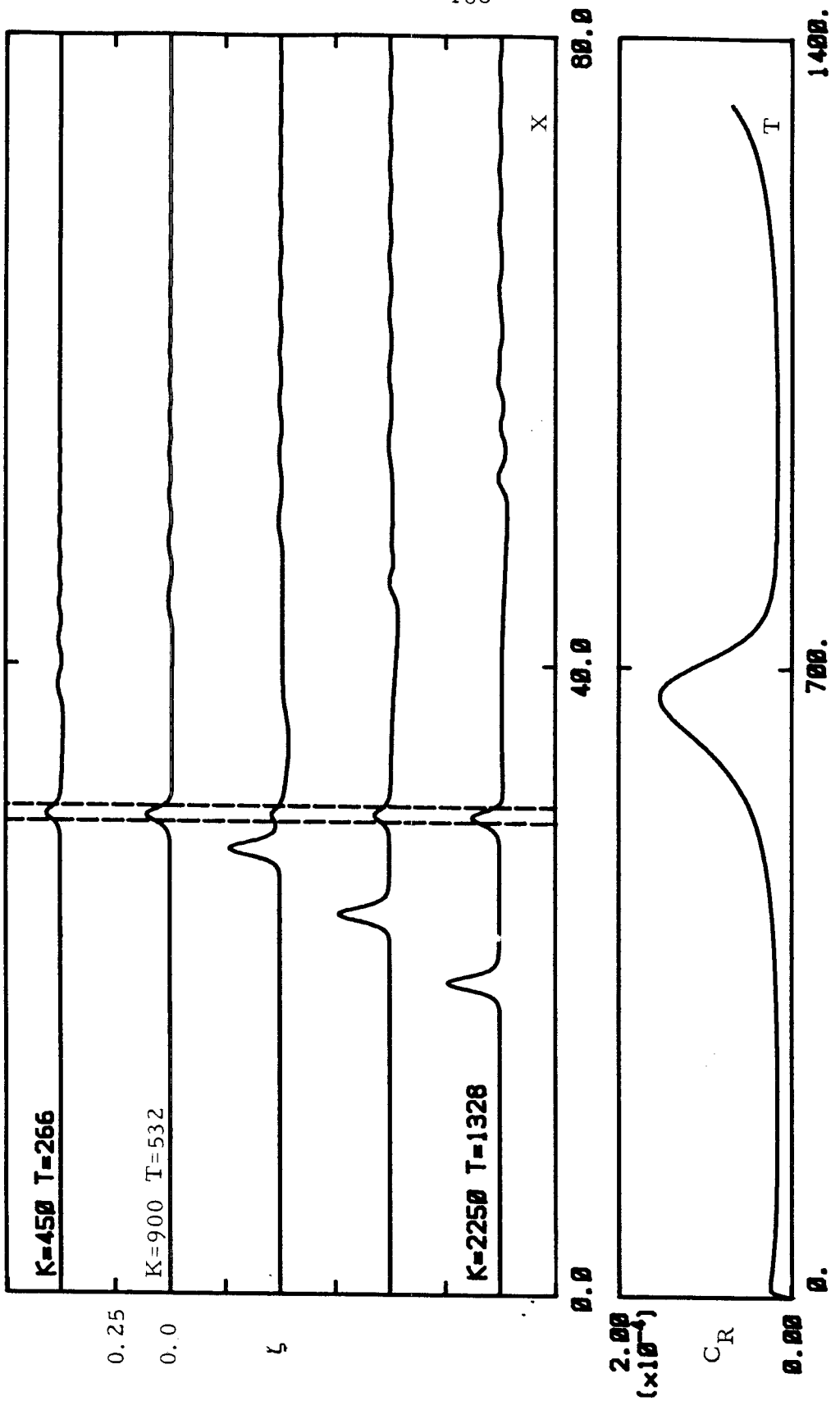

Fig. 8.7 The interface wave elevation and the wave resistance coefficient of the bottom bump given by the numerical KdV model for the two-layer system with free top surface for $H_2 = 0.2$, $\sigma = 0.97$, $L = 1$, $d_m = 0.05$ and $Fr = 1.22$.

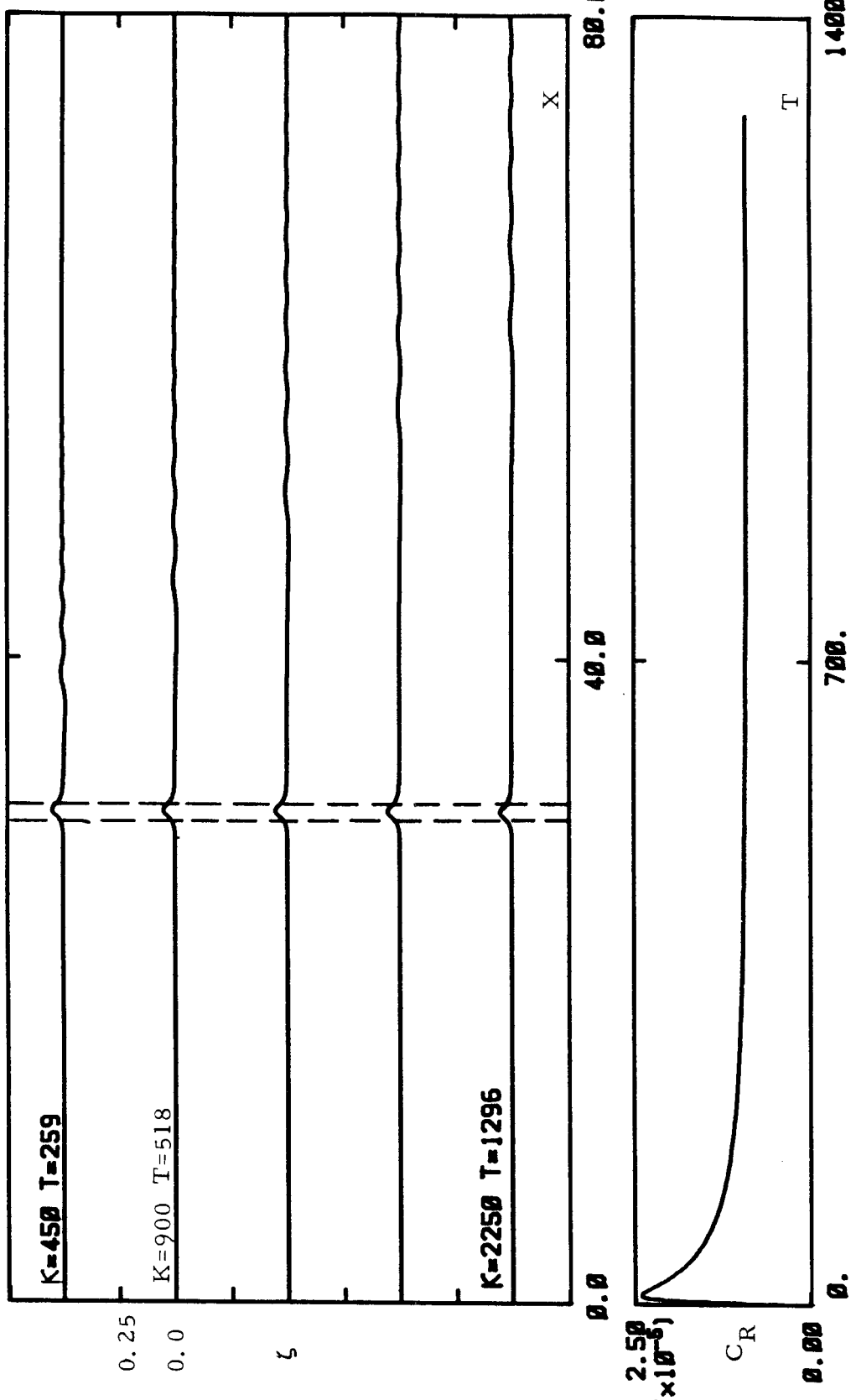

Fig. 8.8 The interface wave elevation and the wave resistance coefficient of the bottom bump given by the numerical KdV model for the two-layer system with free top surface for $H_2 = 0.2$, $\sigma = 0.97$, $L = 1$, $d_m = 0.05$ and $Fr = 1.25$.

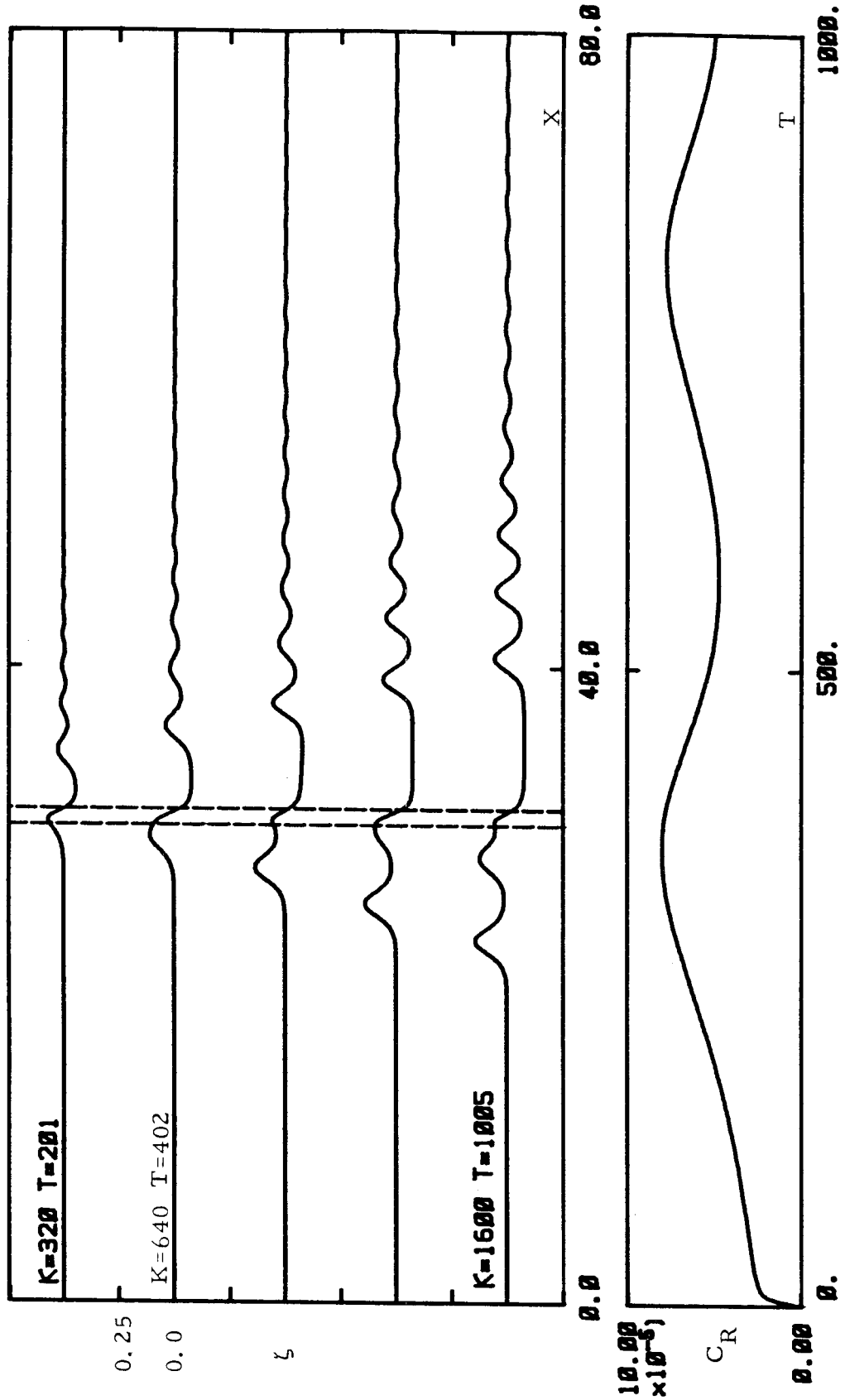

Fig. 8.9 The interface wave elevation and the wave resistance coefficient of the bottom bump given by the numerical KdV model for the two-layer system with free top surface for $H_2 = 0.3$, $\sigma = 0.97$, $L = 1$, $d_m = 0.05$ and $Fr = 1$.

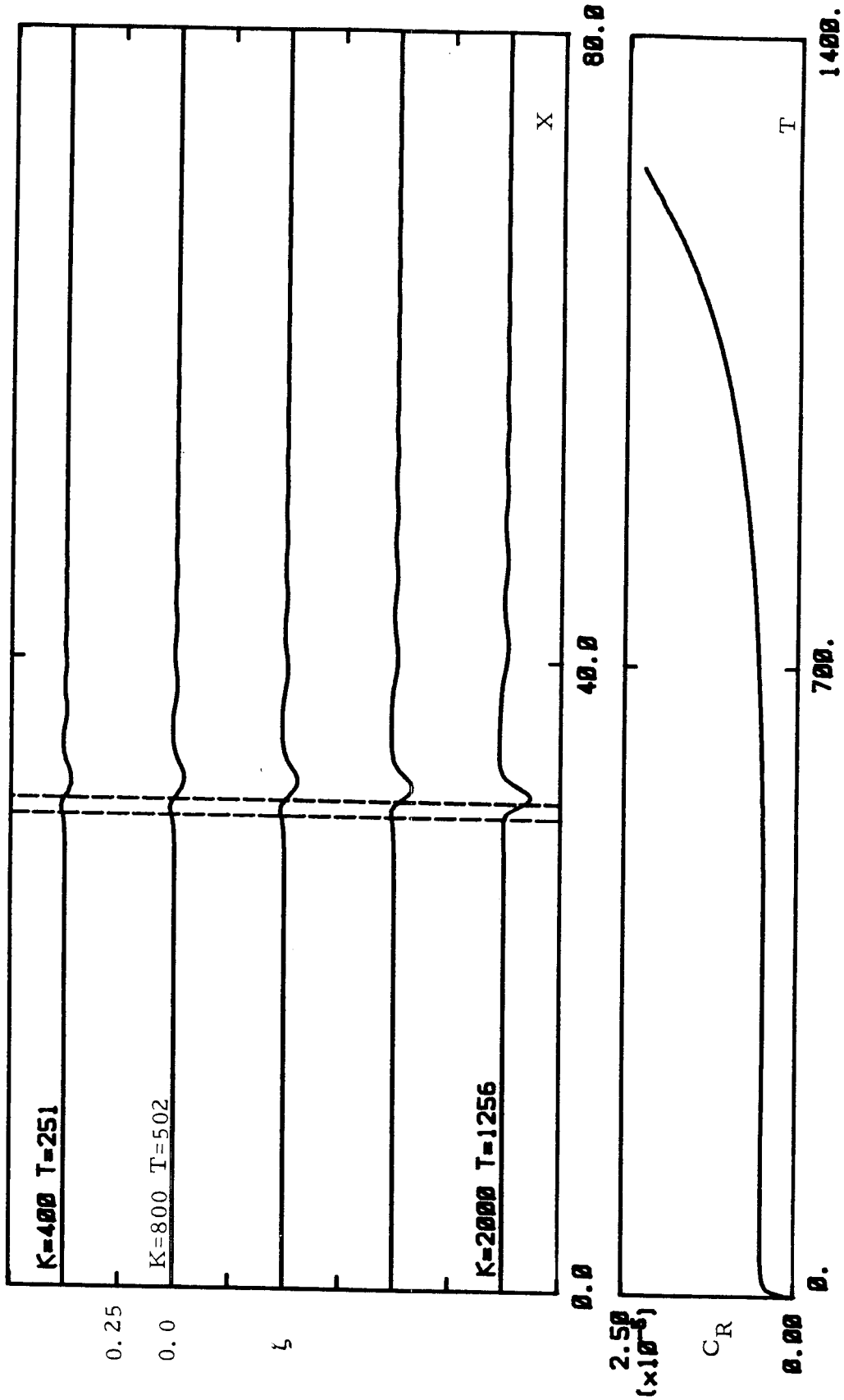

Fig 8.10 The interface wave elevation and the wave resistance coefficient of the bottom bump given by the numerical KdV model for the two-layer system with free top surface for $H_2 = 0.7$, $\sigma = 0.97$, $L = 1$, $d_m = 0.05$ and $Fr = 1$.

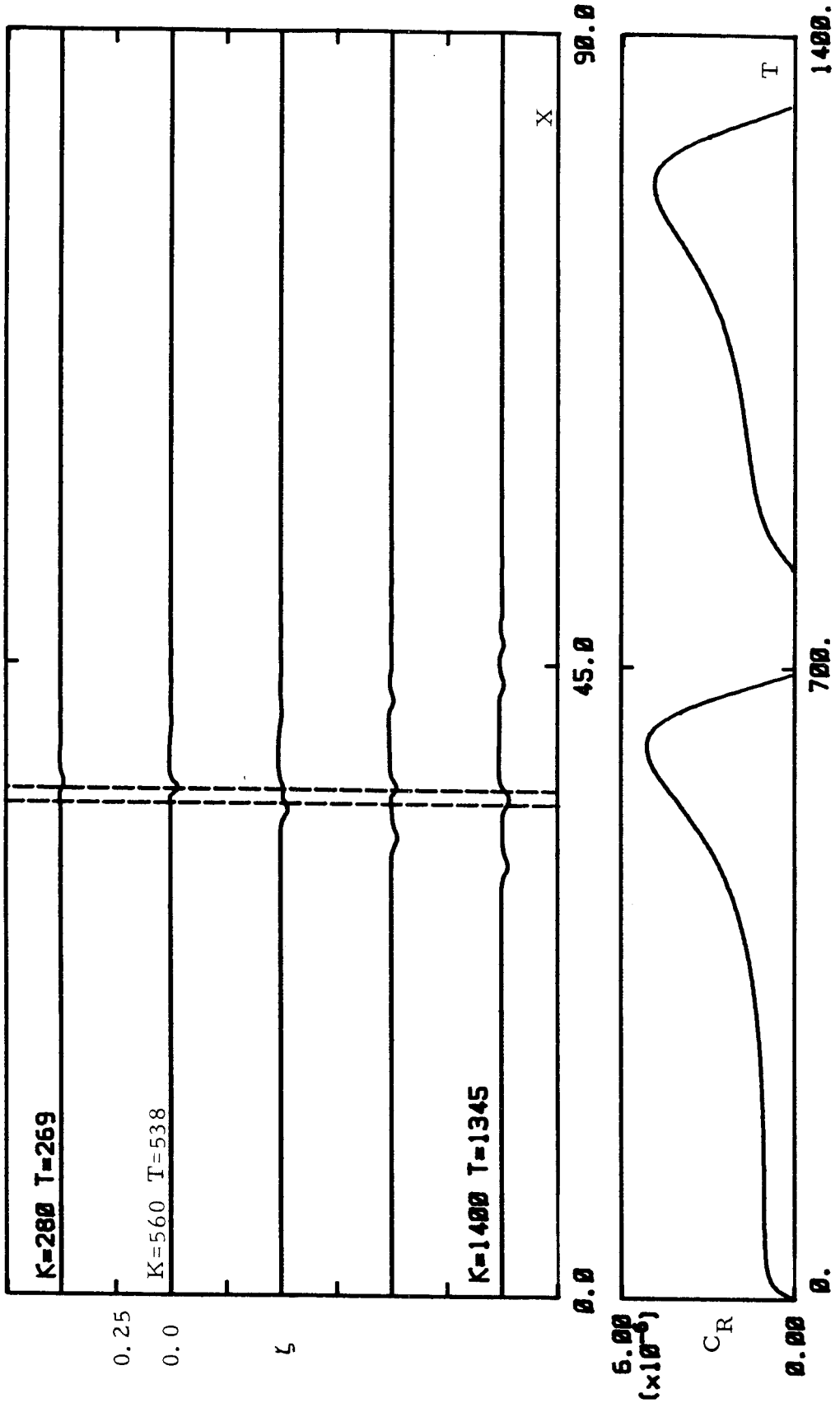

Fig. 8.11 The interface wave elevation and the wave resistance coefficient of the bottom bump given by the numerical KdV model for the two-layer system with free top surface for $H_2 = 0.9$, $\sigma = 0.97$, $L = 1$, $d_m = 0.05$ and $Fr = 1$.

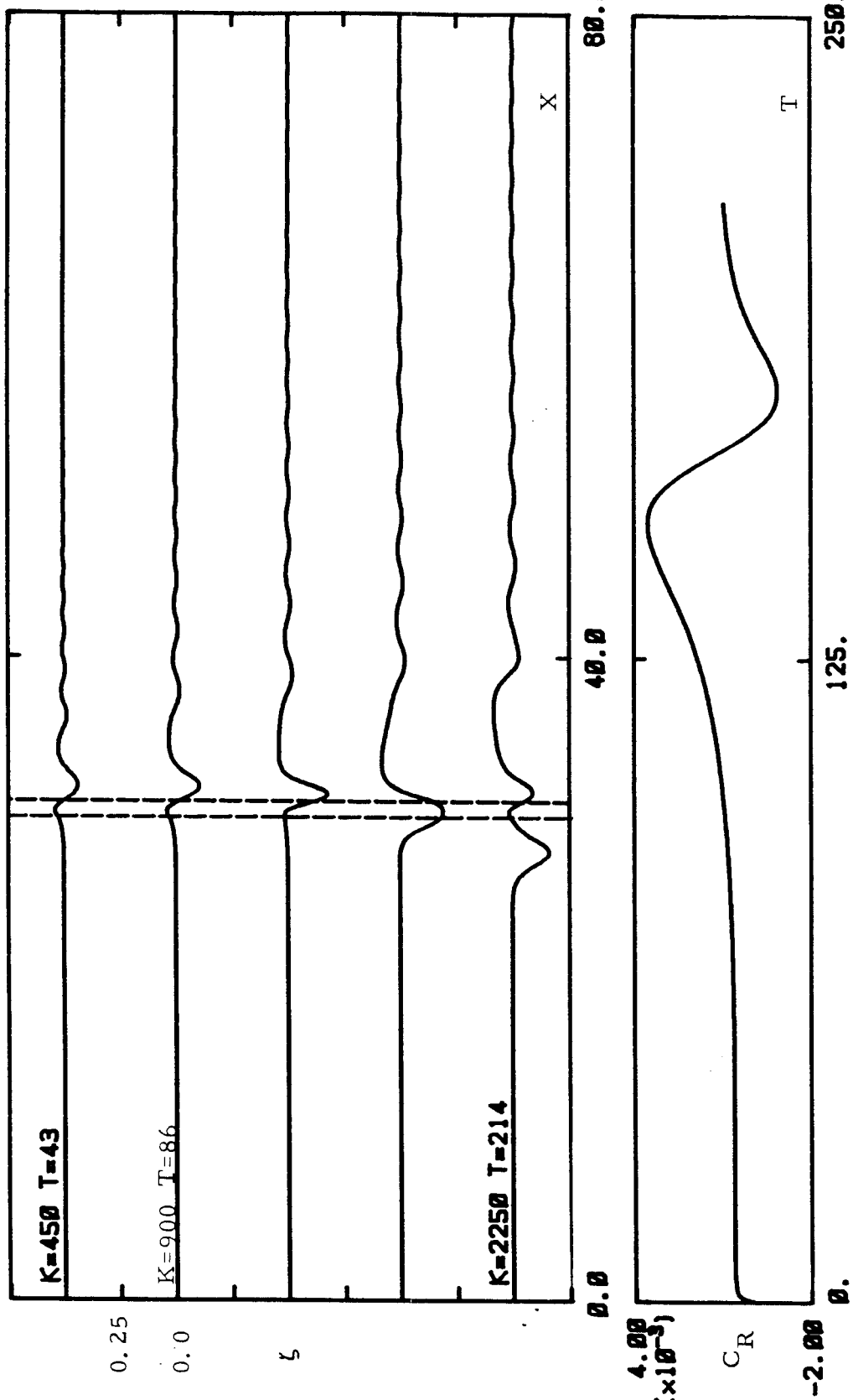

Fig. 8.12 The interface wave elevation and the wave resistance coefficient of the bottom bump given by the numerical KdV model for the two-layer system with free top surface for $H_2 = 0.5$, $\sigma = 0.2$, $L = 1$, $d_m = 0.05$ and $Fr = 1$.

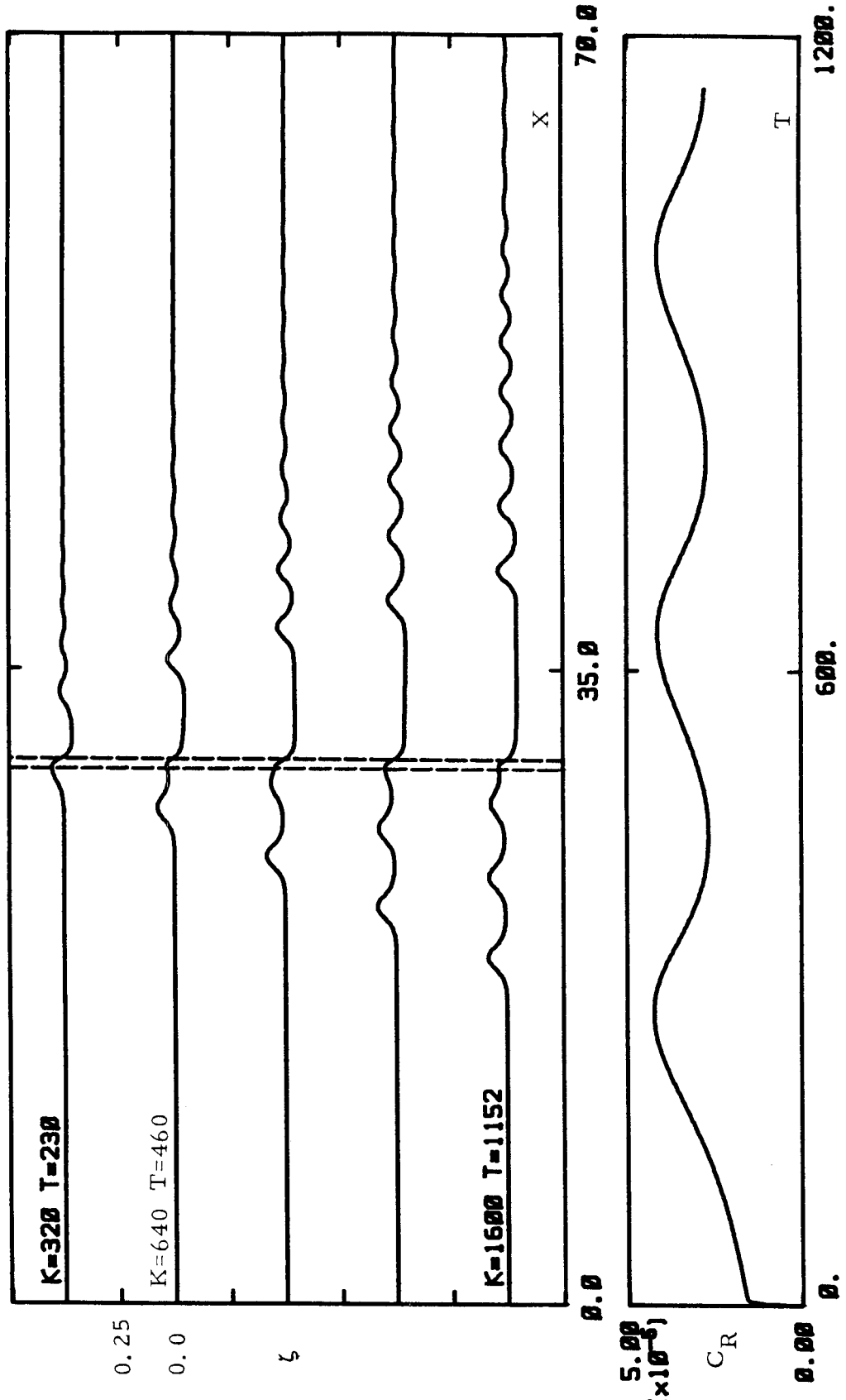

Fig. 8.13 The interface wave elevation and the wave resistance coefficient of the bottom bump given by the numerical KdV model for the two-layer system with free top surface for $H_2 = 0.2$, $\sigma = 0.97$, $L = 0.5$, $d_m = 0.05$ and $Fr = 1$.

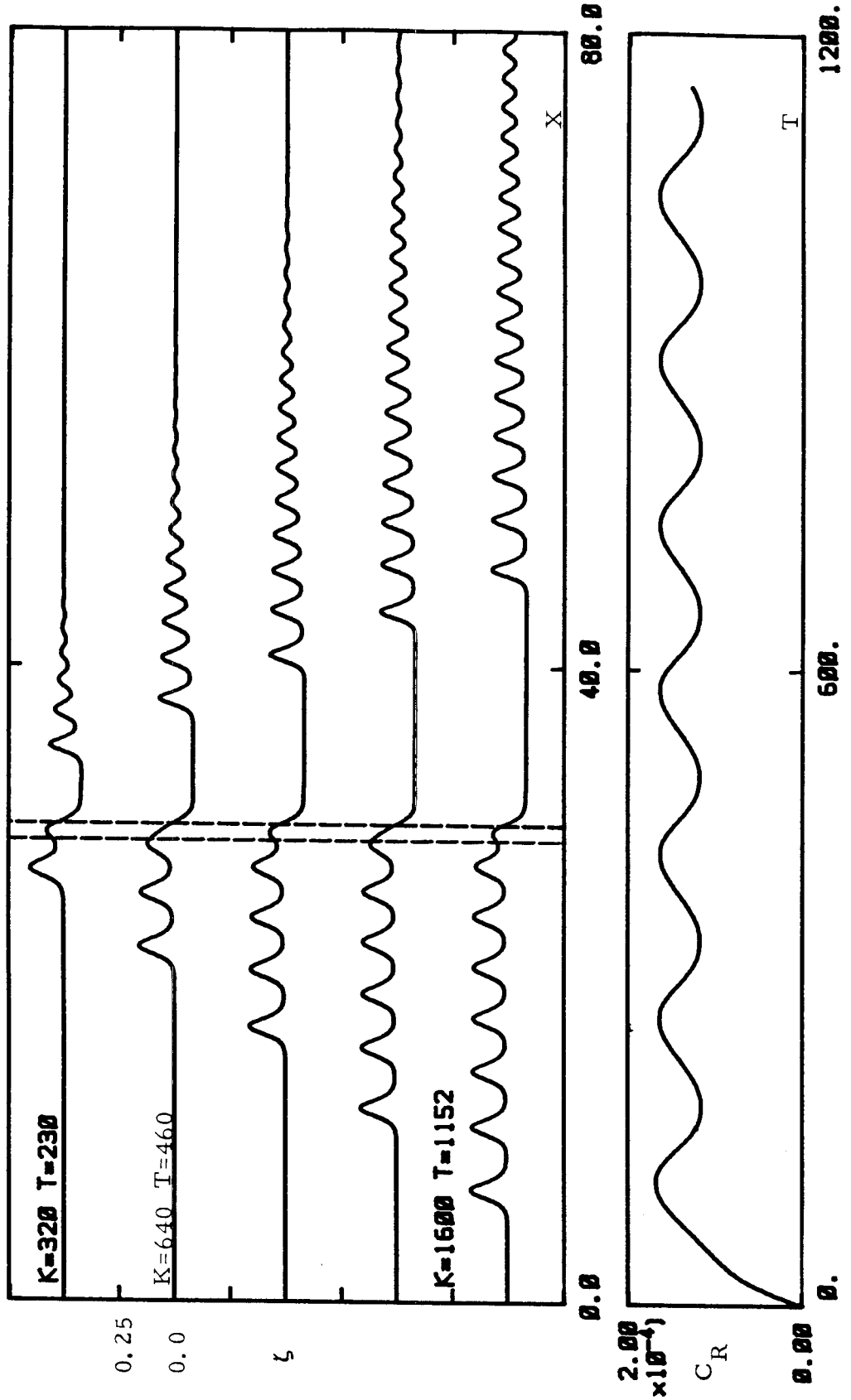

Fig. 8.14 The interface wave elevation and the wave resistance coefficient of the bottom bump given by the numerical KdV model for the two-layer system with free top surface for $H_2 = 0.2$, $\sigma = 0.97$, $L = 2$, $d_m = 0.05$ and $Fr = 1$.

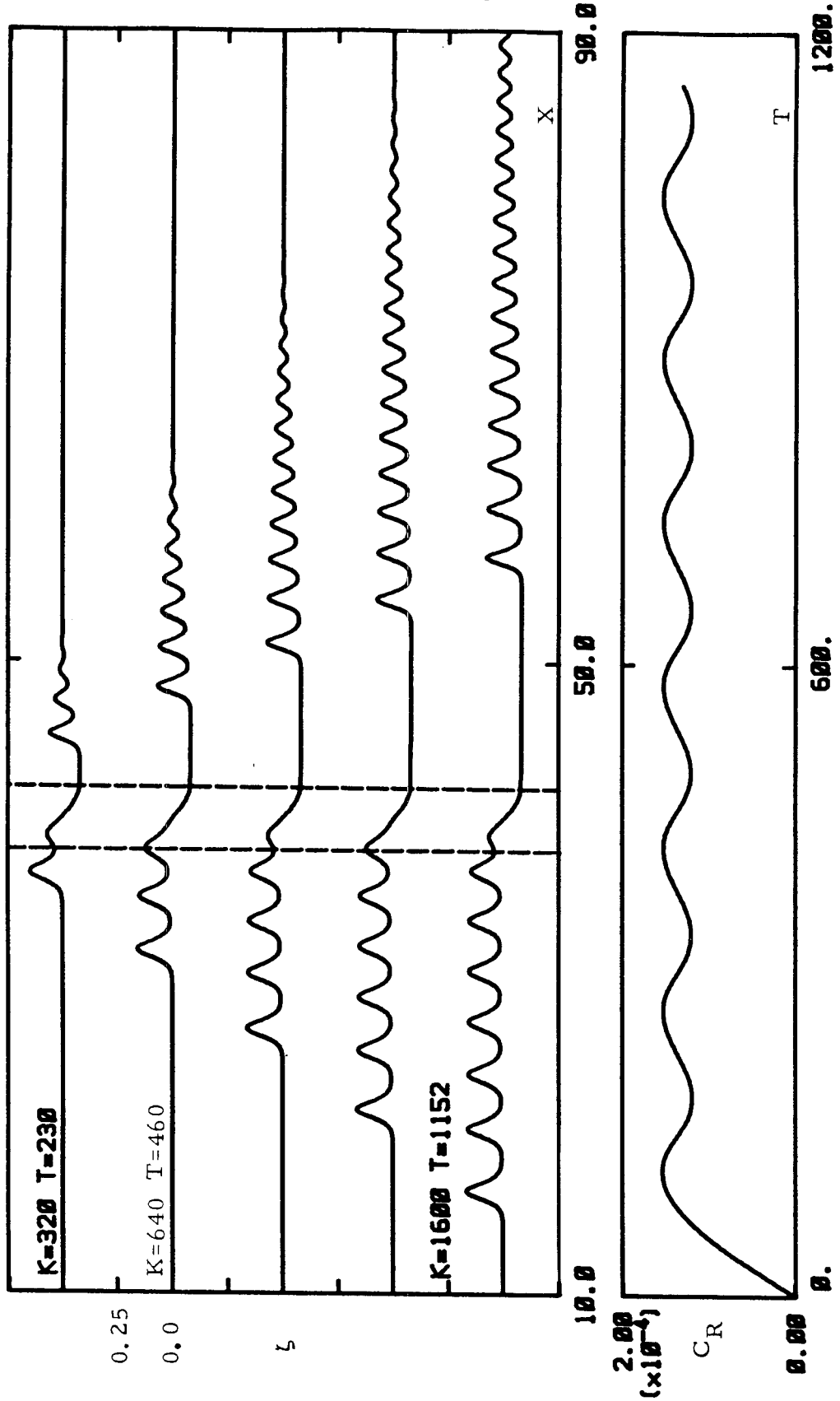

Fig. 8.15 The interface wave elevation and the wave resistance coefficient of the bottom bump given by the numerical KdV model for the two-layer system with free top surface for $H_2 = 0.2$, $\sigma = 0.97$, $L = 4$, $d_m = 0.05$ and $Fr = 1$.

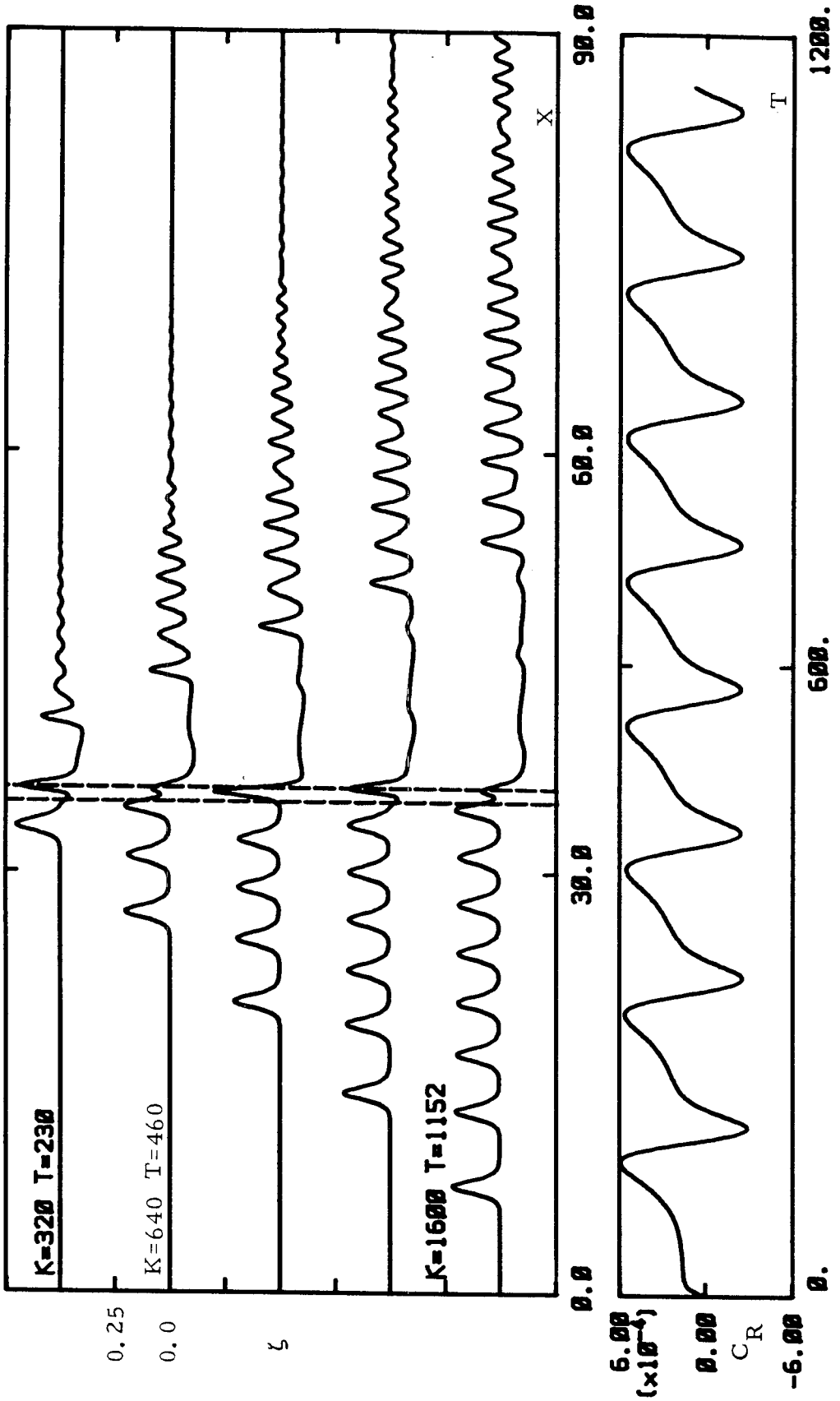

Fig. 8.16 The interface wave elevation and the wave resistance coefficient of the bottom bump given by the numerical KdV model for the two-layer system with free top surface for $H_2 = 0.2$, $\sigma = 0.97$, $L = 1$, $d_m = -0.1$ and $Fr = 1$.

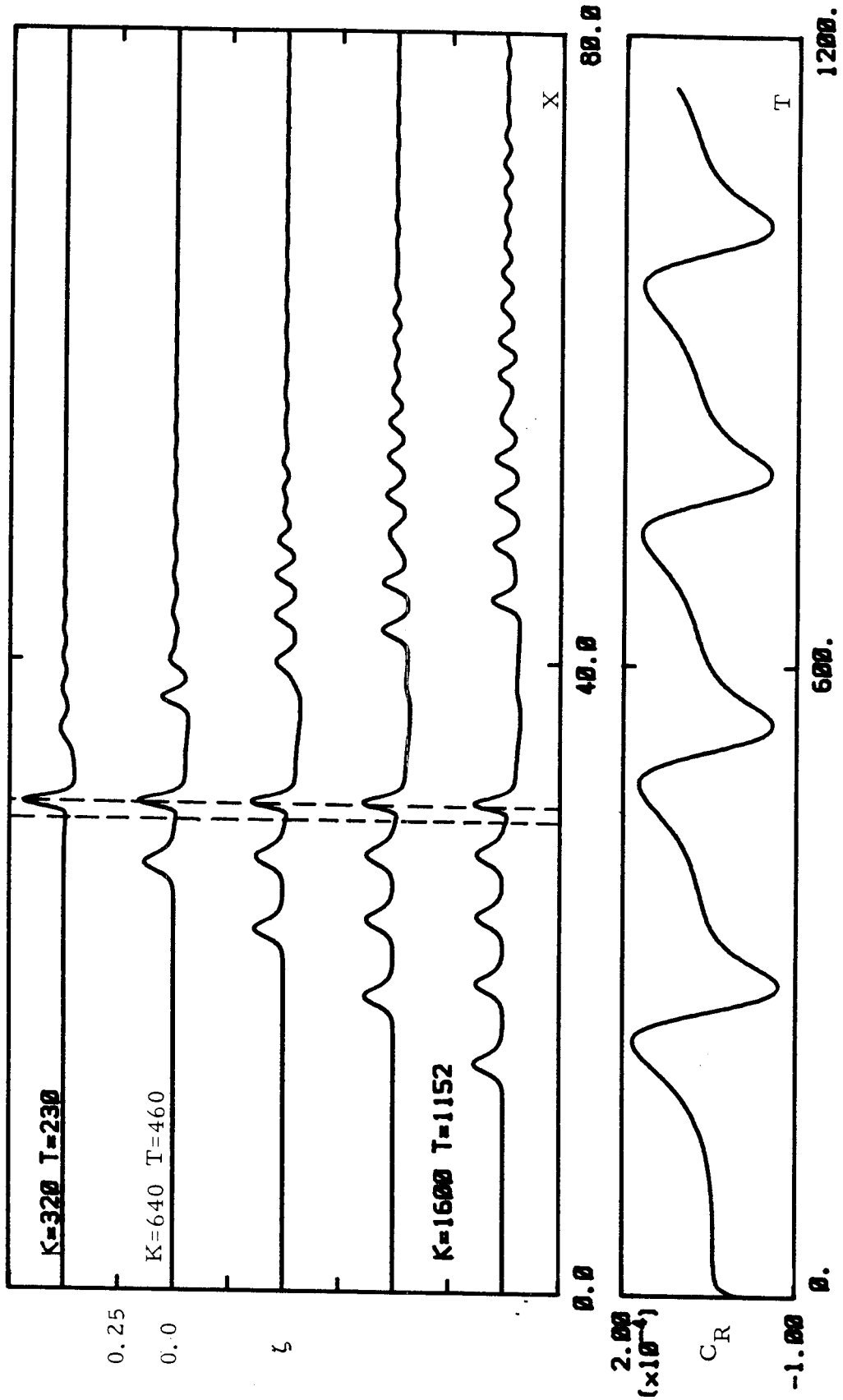

Fig. 8.17 The interface wave elevation and the wave resistance coefficient of the bottom bump given by the numerical KdV model for the two-layer system with free top surface for $H_2 = 0.2$, $\sigma = 0.97$, $L = 1$, $d_m = -0.05$ and $Fr = 1$.

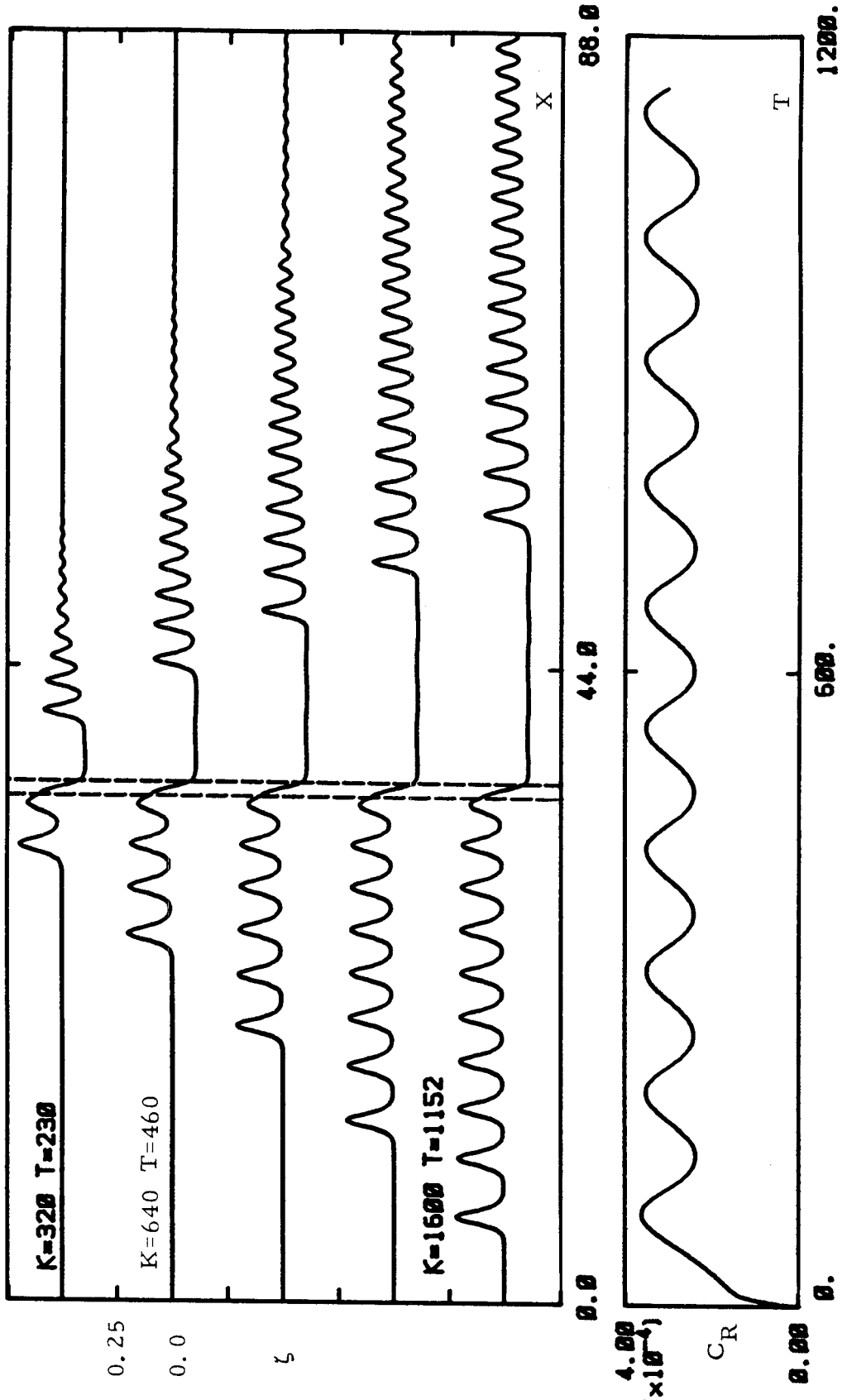

Fig. 8.18 The interface wave elevation and the wave resistance coefficient of the bottom bump given by the numerical KdV model for the two-layer system with free top surface for $H_2 = 0.2$, $\sigma = 0.97$, $L = 1$, $d_m = 0.1$ and $Fr = 1$.

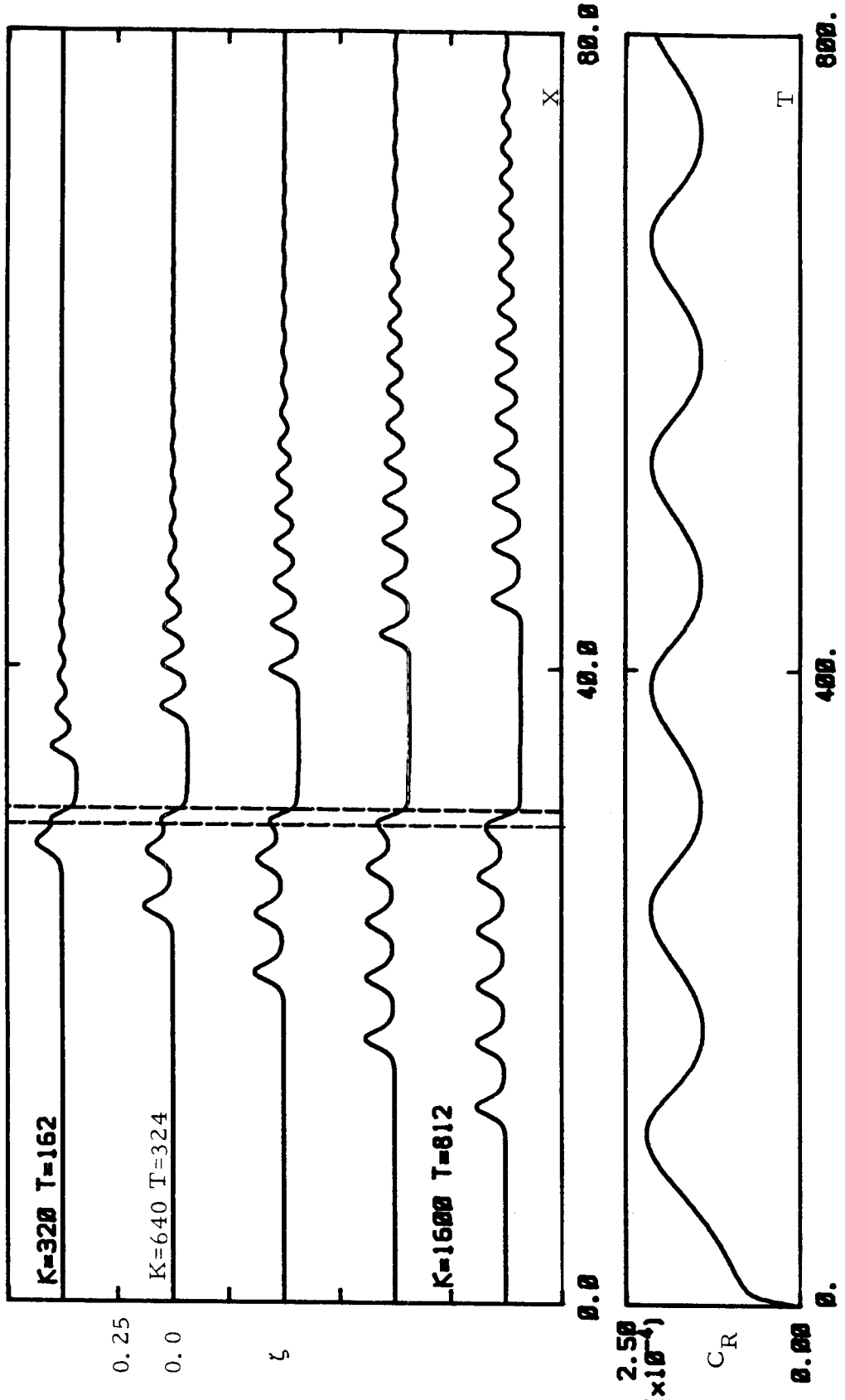

Fig. 8.19 The interface wave elevation and the wave resistance coefficient of the bottom bump given by the numerical KdV model for the two-layer system with free top surface for $H_2 = 0.2$, $\sigma = 0.94$, $L = 1$, $d_m = 0.05$ and $Fr = 1$.

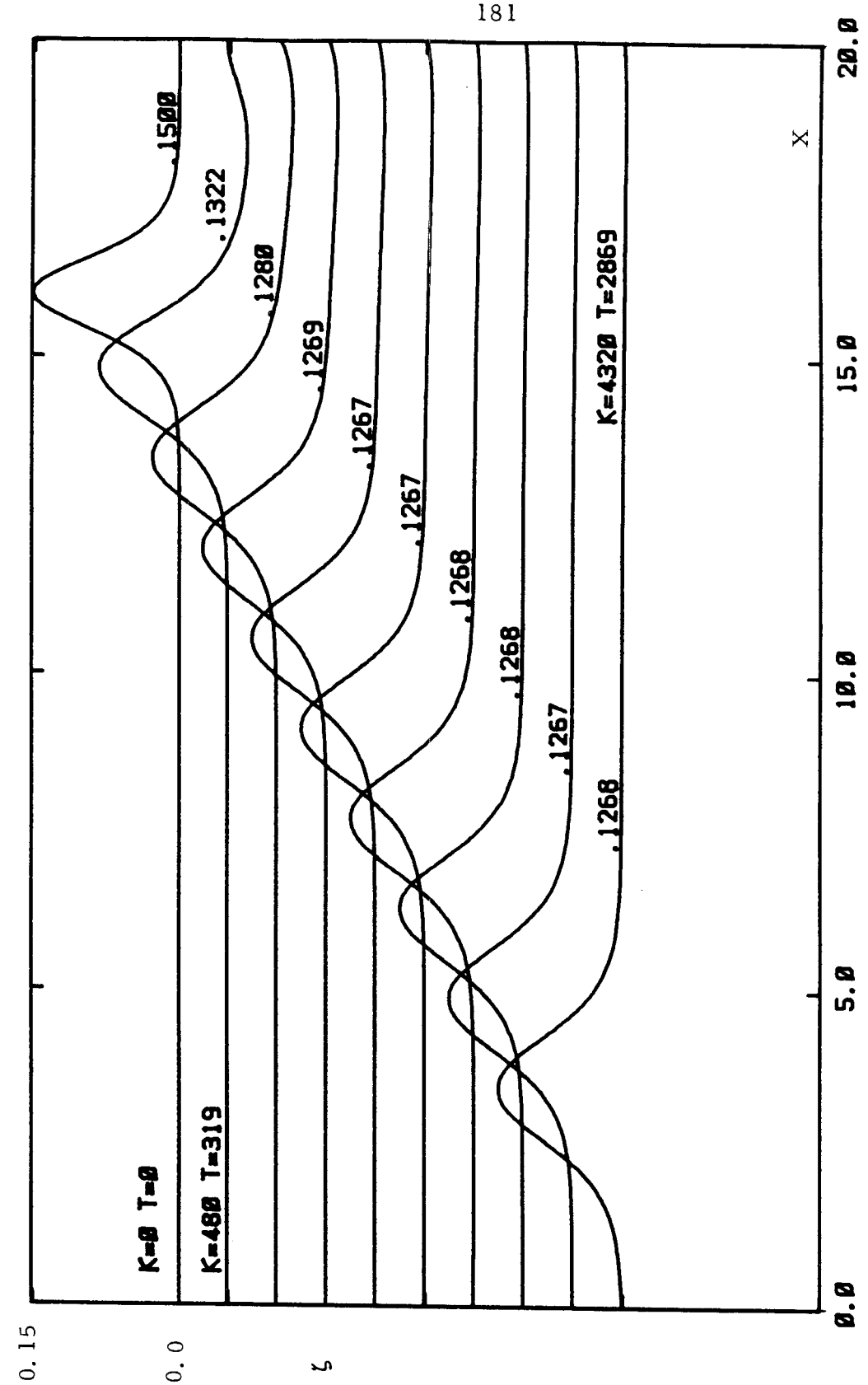

Fig. 8.20 Stability test of the numerical THREE-equation model using the soliton as initial condition, $H_2 = 0.25$, $\sigma = 0.97$, initial amplitude of the soliton a = 0.15.

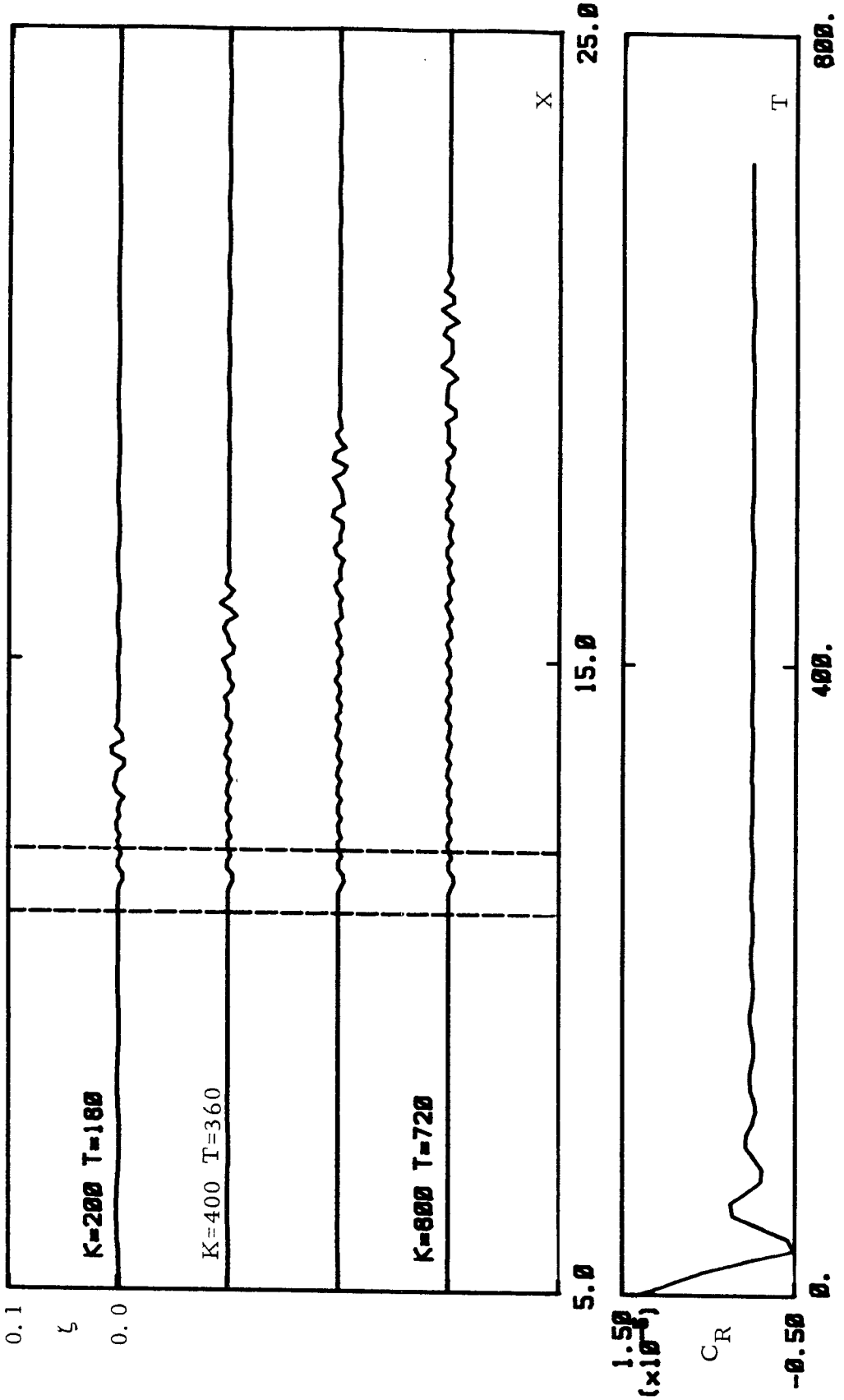

Fig. 8.21 The interface wave elevation and the wave resistance coefficient of the bottom bump given by the numerical THREE-equation model for $H_2 = 0.2$, $\sigma = 0.97$, $L = 1$, $d_m = 0.05$ and $Fr = 0.2$.

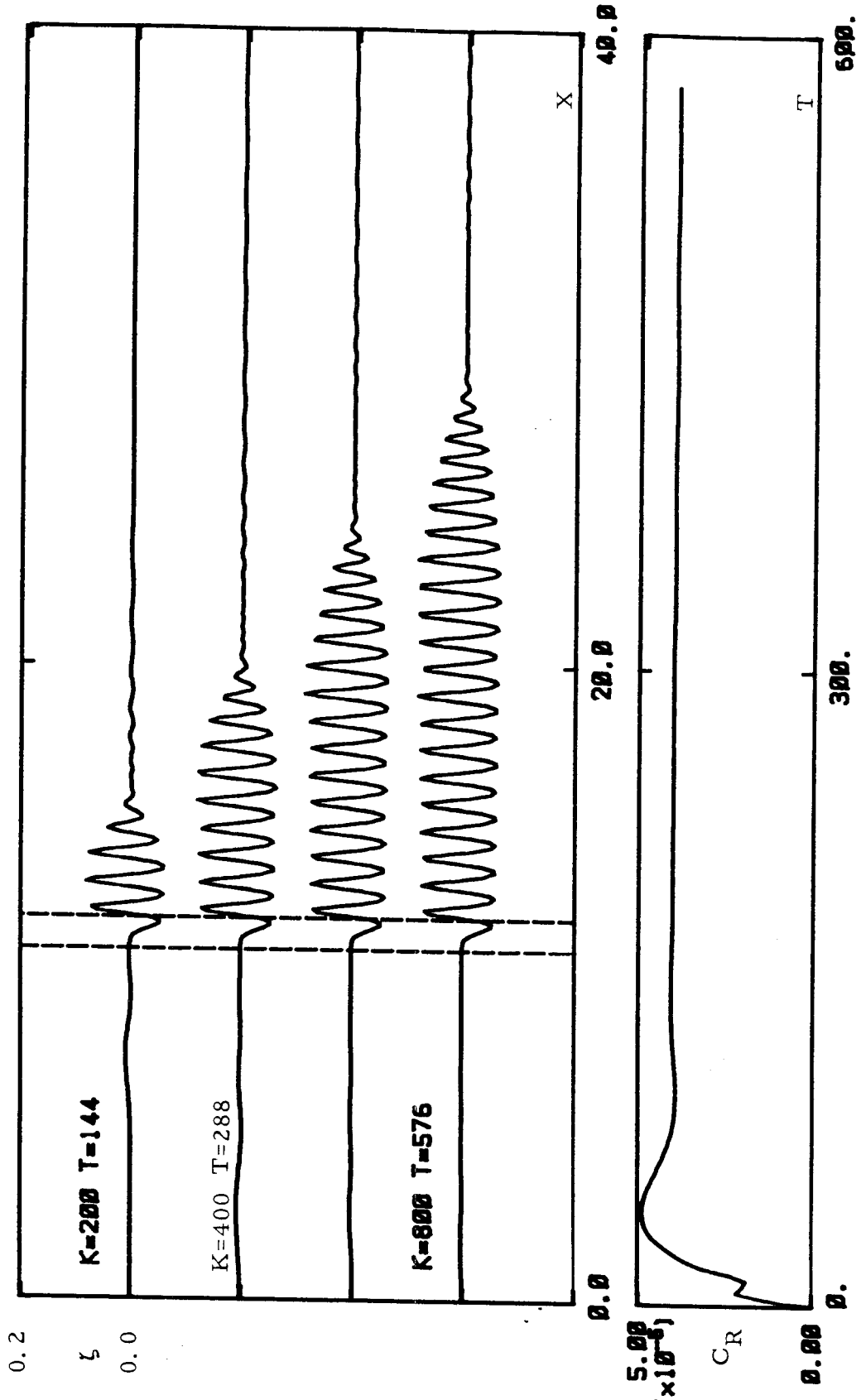

Fig. 8.22 The interface wave elevation and the wave resistance coefficient of the bottom bump given by the numerical THREE-equation model for $H_2 = 0.2$, $\sigma = 0.97$, $L = 1$, $d_m = 0.05$ and $Fr = 0.5$.

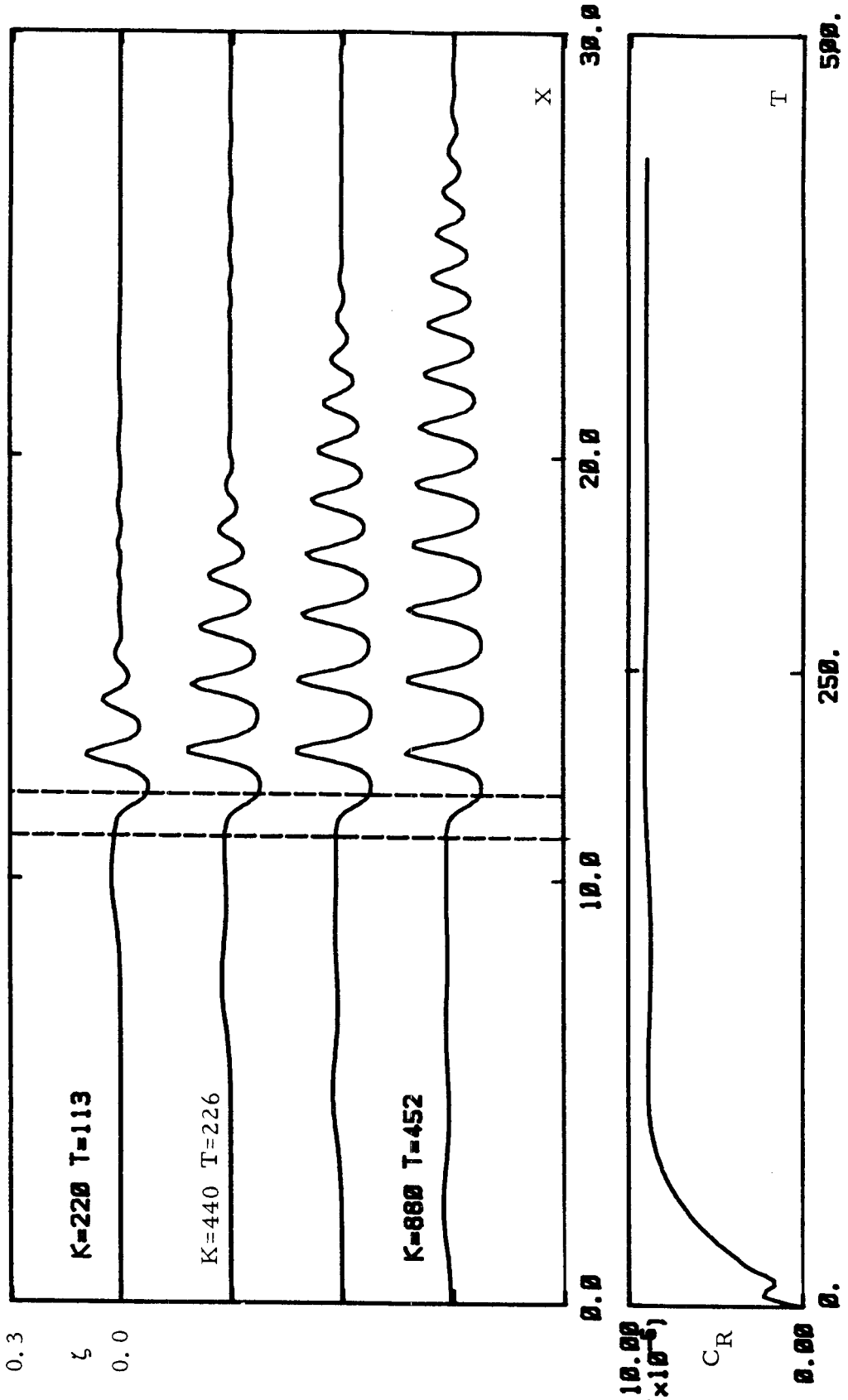

Fig. 8.23 The interface wave elevation and the wave resistance coefficient of the bottom bump given by the numerical THREE-equation model for $H_2 = 0.2$, $\sigma = 0.97$, $L = 1$, $d_m = 0.05$ and $Fr = 0.7$.

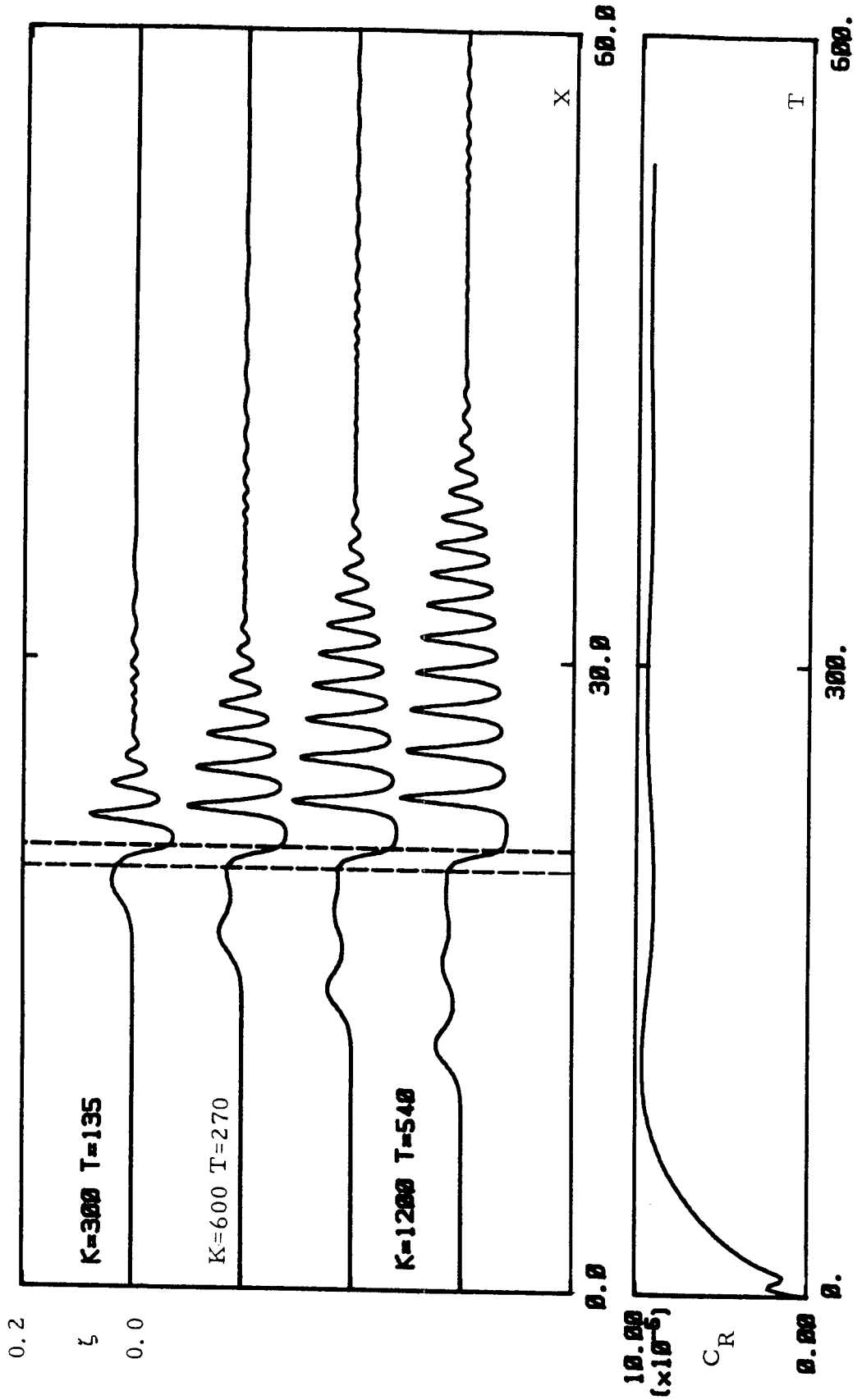

Fig. 8.24 The interface wave elevation and the wave resistance coefficient of the bottom bump given by the numerical THREE-equation model for $H_2 = 0.2$, $\sigma = 0.97$, $L = 1$, $d_m = 0.05$ and $Fr = 0.8$.

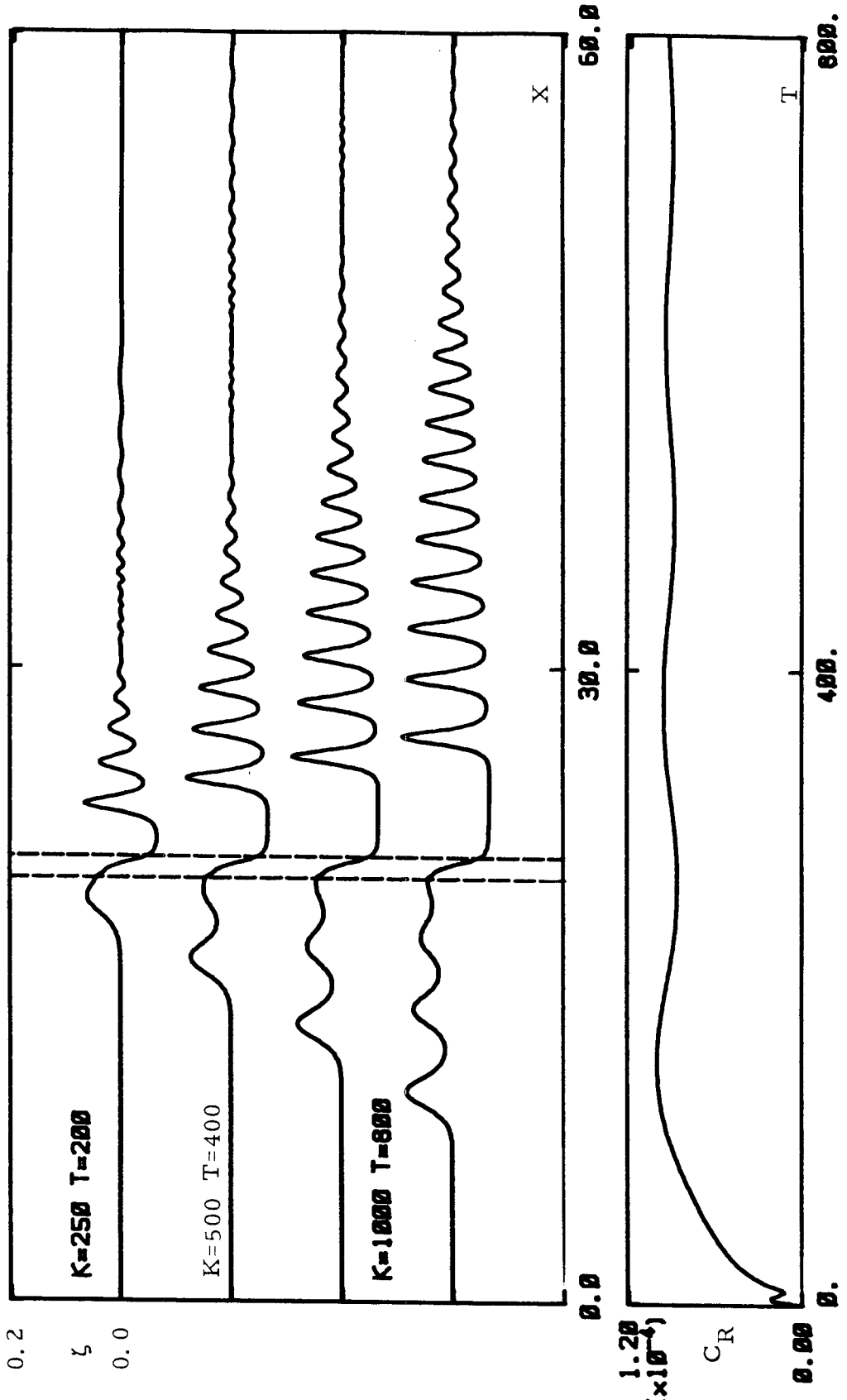

Fig. 8.25 The interface wave elevation and the wave resistance coefficient of the bottom bump given by the numerical THREE-equation model for $H_2 = 0.2$, $\sigma = 0.97$, $L = 1$, $d_m = 0.05$ and $Fr = 0.9$.

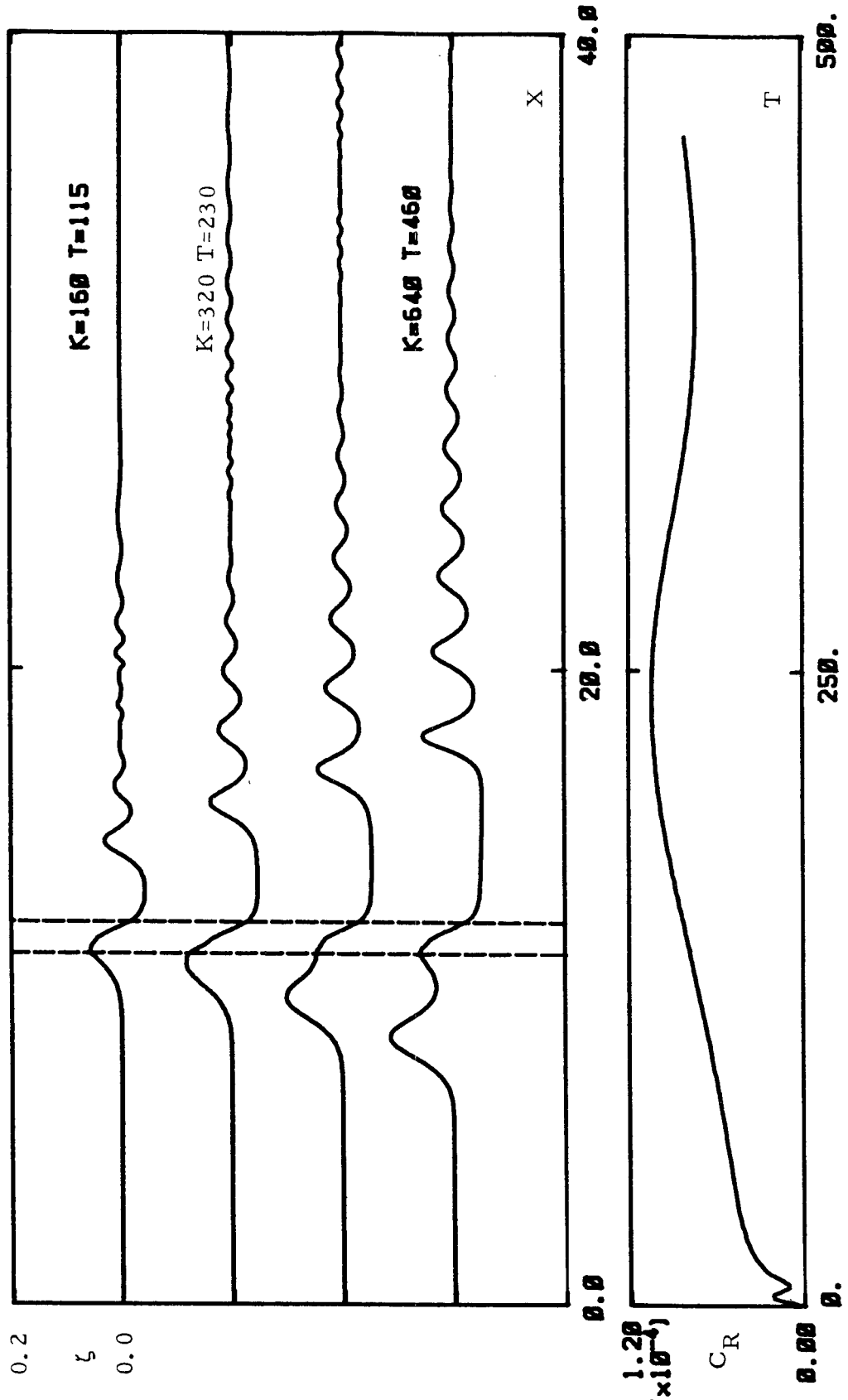

Fig. 8.26 The interface wave elevation and the wave resistance coefficient of the bottom bump given by the numerical THREE-equation model for $H_2 = 0.2$, $\sigma = 0.97$, $L = 1$, $d_m = 0.05$ and $Fr = 1$.

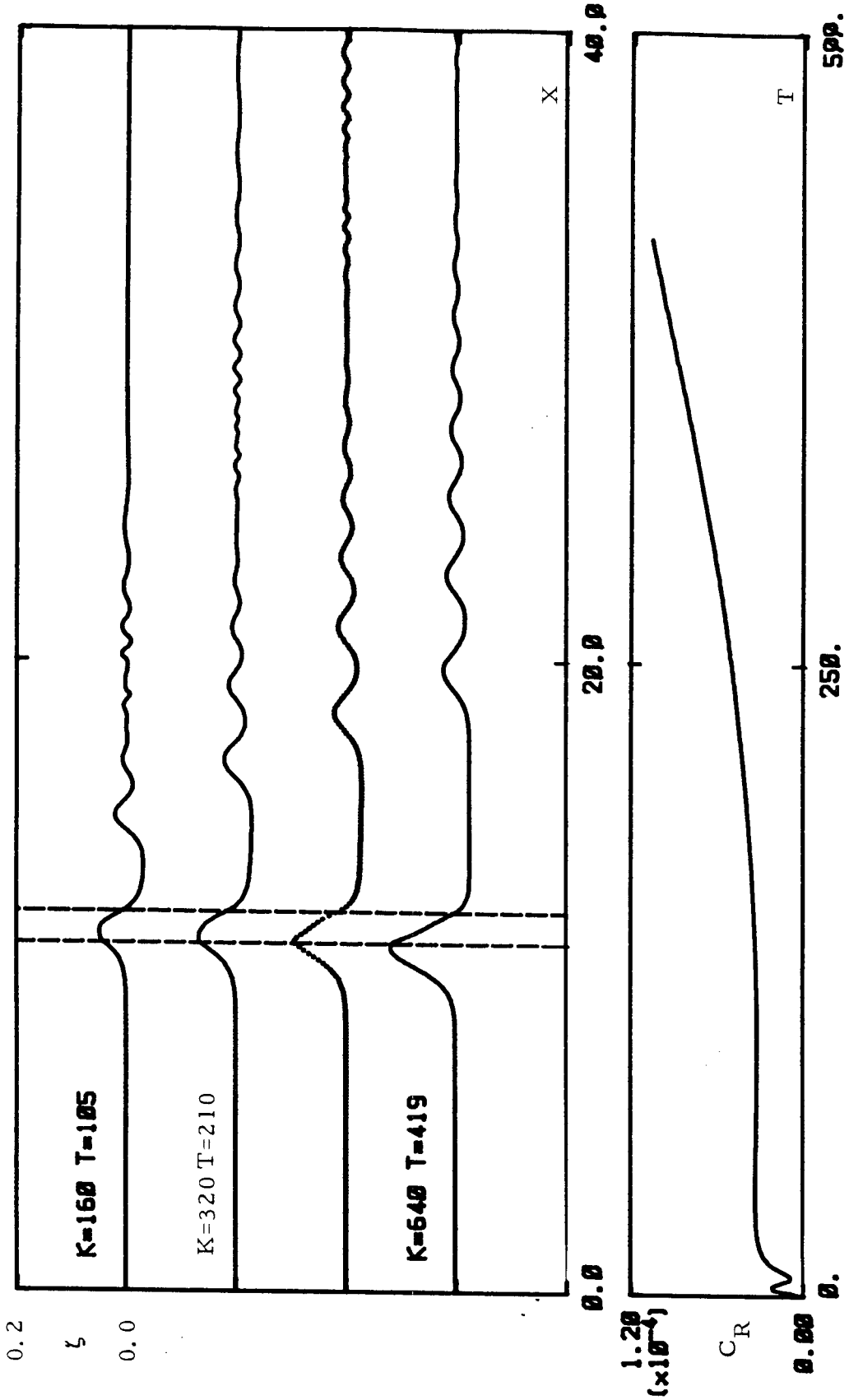

Fig. 8.27 The interface wave elevation and the wave resistance coefficient of the bottom bump given by the numerical THREE-equation model for $H_2 = 0.2$, $\sigma = 0.97$, $L = 1$, $d_m = 0.05$ and $Fr = 1.1$.

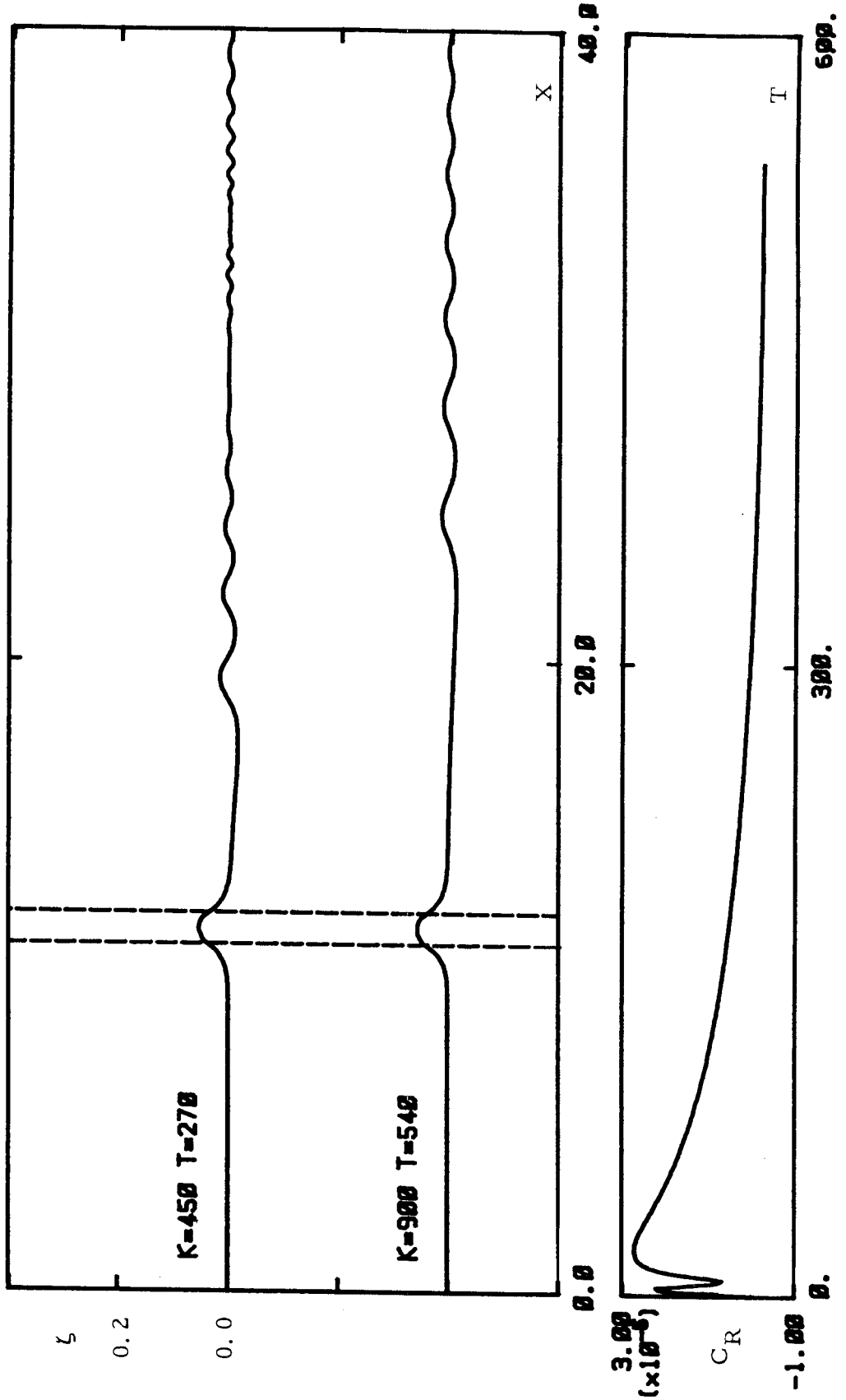

Fig. 8.28 The interface wave elevation and the wave resistance coefficient of the bottom bump given by the numerical THREE-equation model for $H_2 = 0.2$, $\sigma = 0.97$, $L = 1$, $d_m = 0.05$ and $Fr = 1.2$.

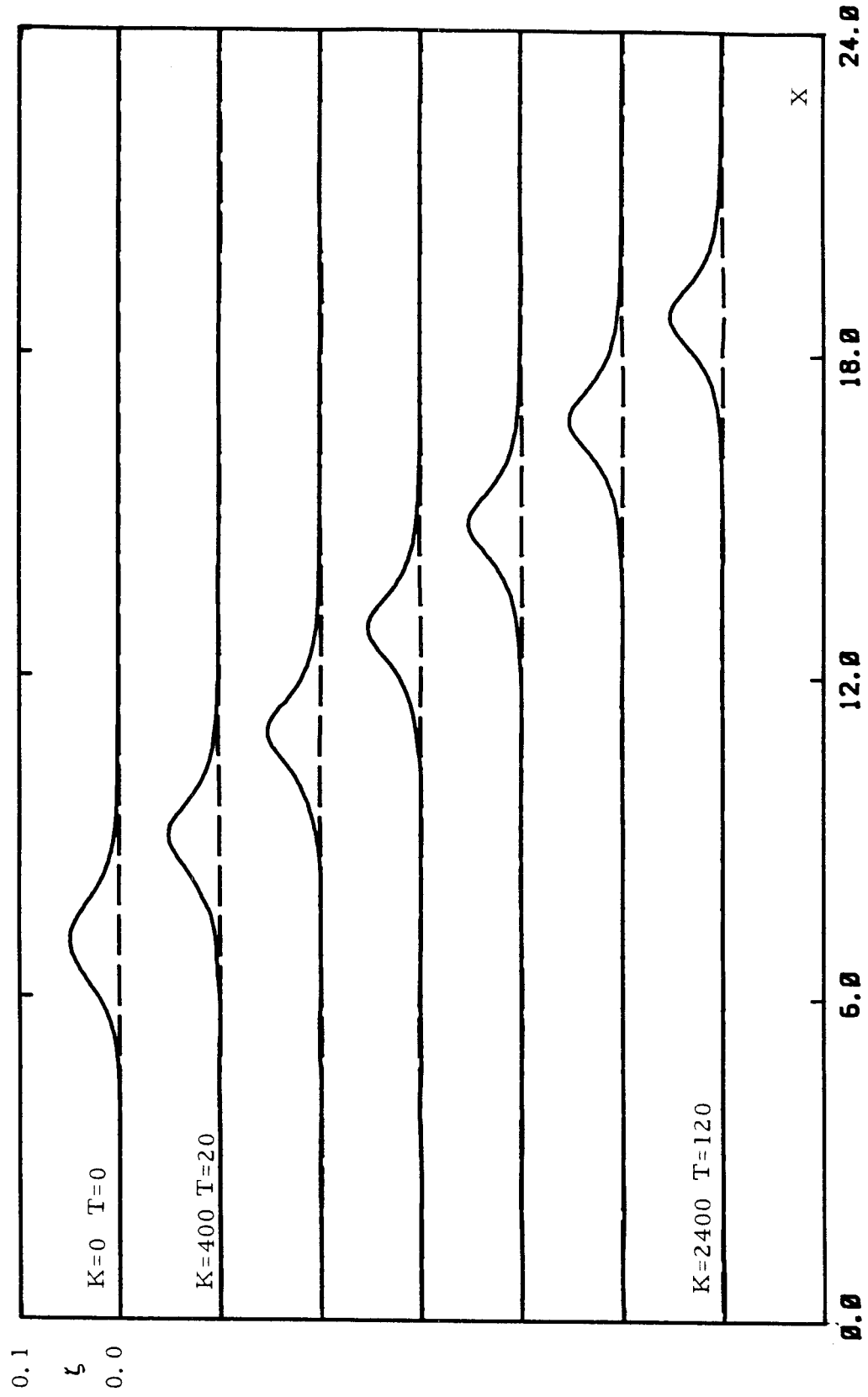

Fig. 8.29 Stability test of the numerical FOUR-equation model using the soliton as initial condition for $H_2 = 0.2$, $\sigma = 0.95$ and intitial amplitude of the soliton a = 0.05 with open boundary condition (1).

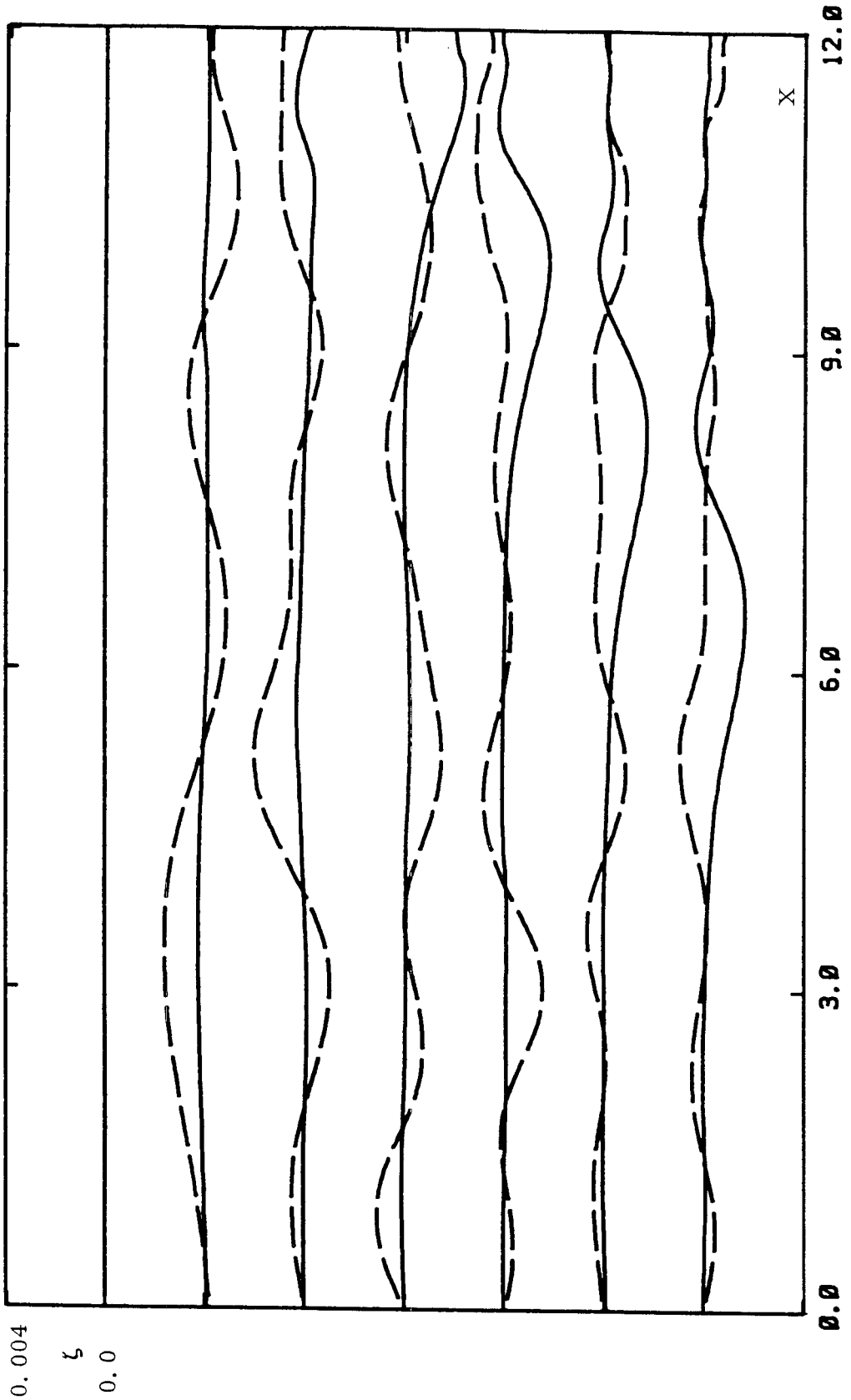

Fig. 8.30 Test of the boundary condition (1) for the numerical FOUR-equation model using the soliton as initial condition, $H_2 = 0.2$, $\sigma = 0.95$ and initial amplitude of soliton $a = 0.05$, with two different window sizes.

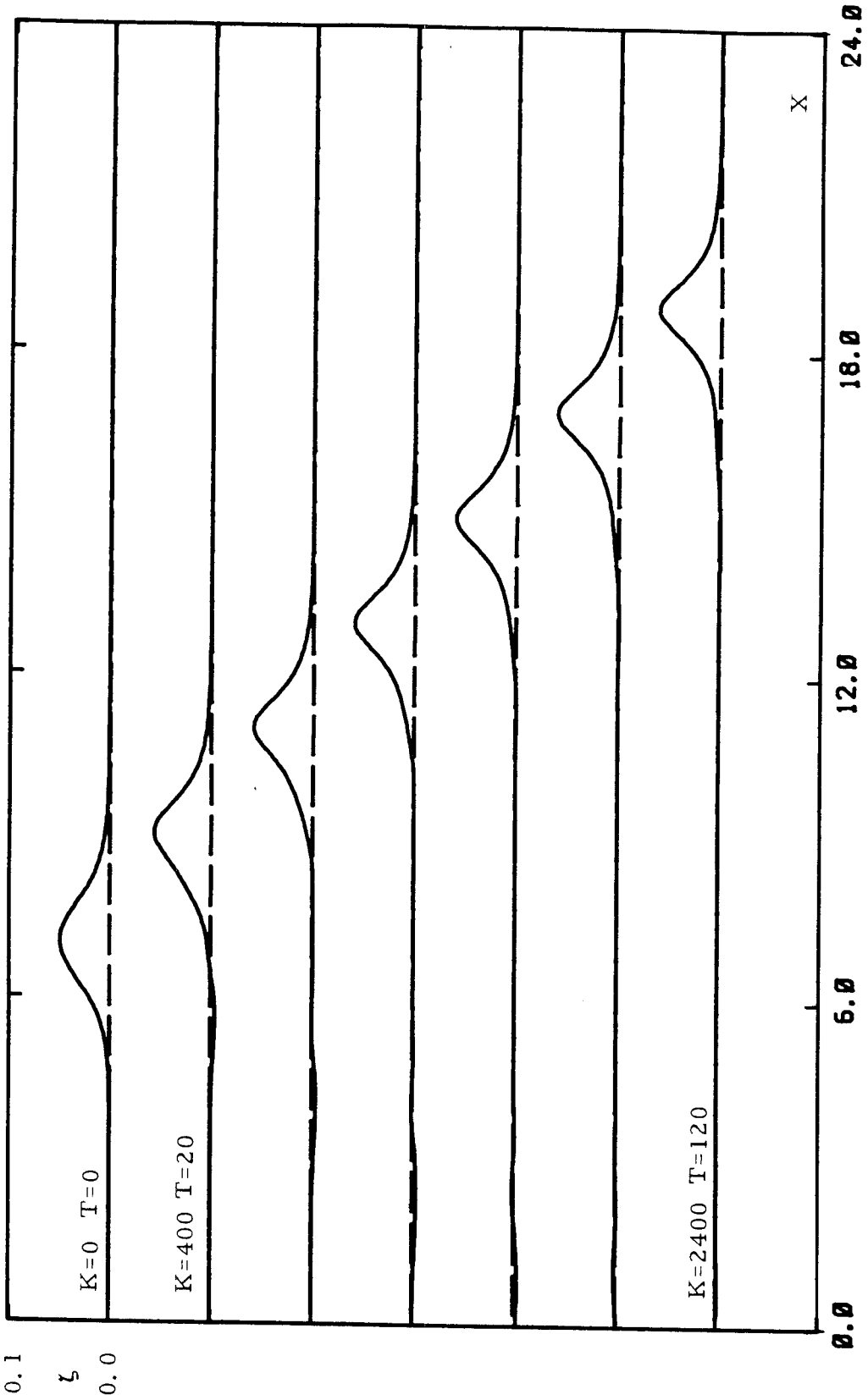

Fig. 8.31 Stability test of the numerical FOUR-equation model using the soliton as initial condition for $H_2 = 0.2$, $\sigma = 0.95$ and initial amplitude of the soliton $a = 0.05$ with open boundary condition (2).

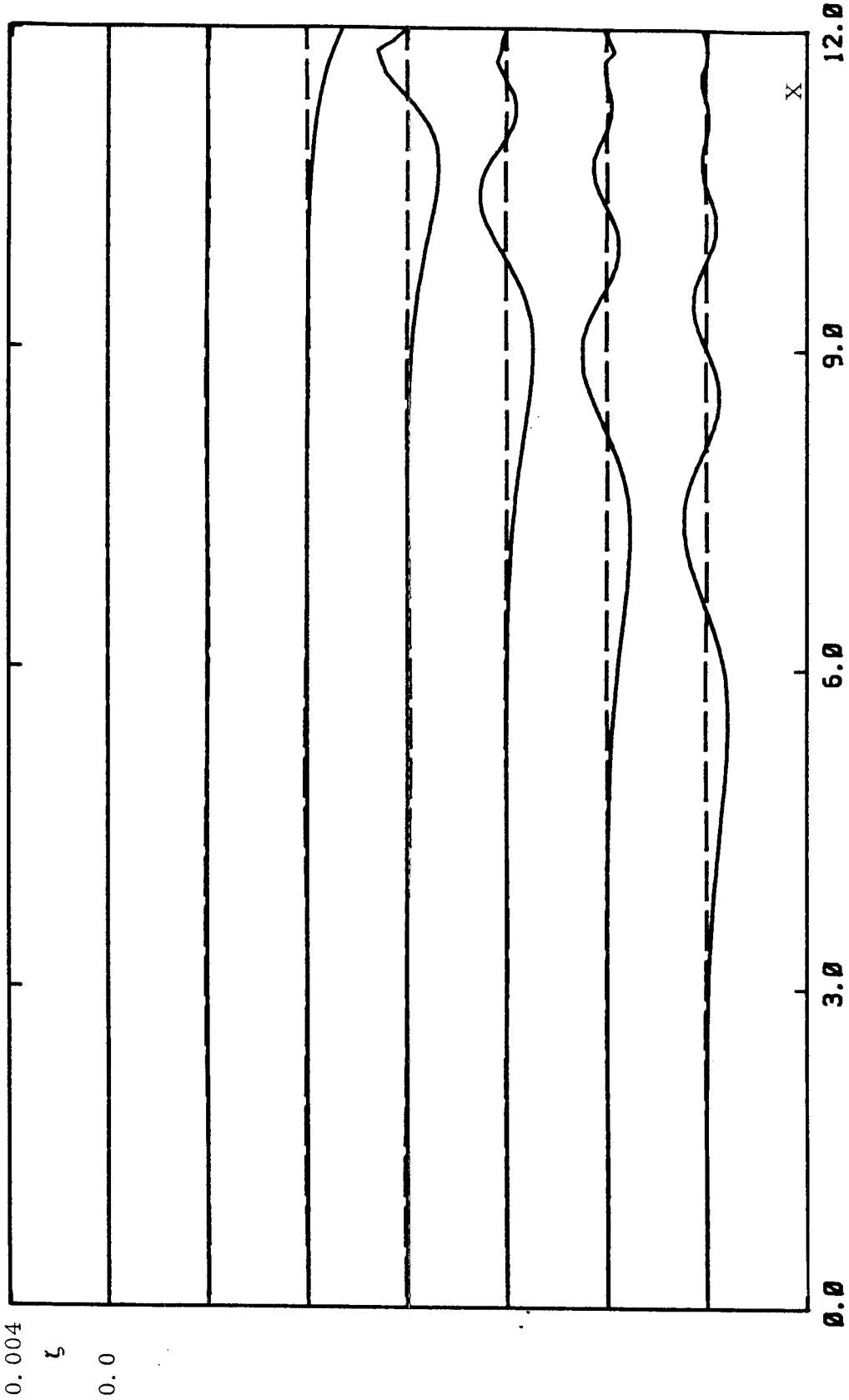

Fig. 8.32 Test of the boundary condition (2) for the numerical FOUR-equation model using the soliton as initial condition, $H_2 = 0.2$, $\sigma = 0.95$ and initial amplitude of soliton $a = 0.05$, with two different window sizes.

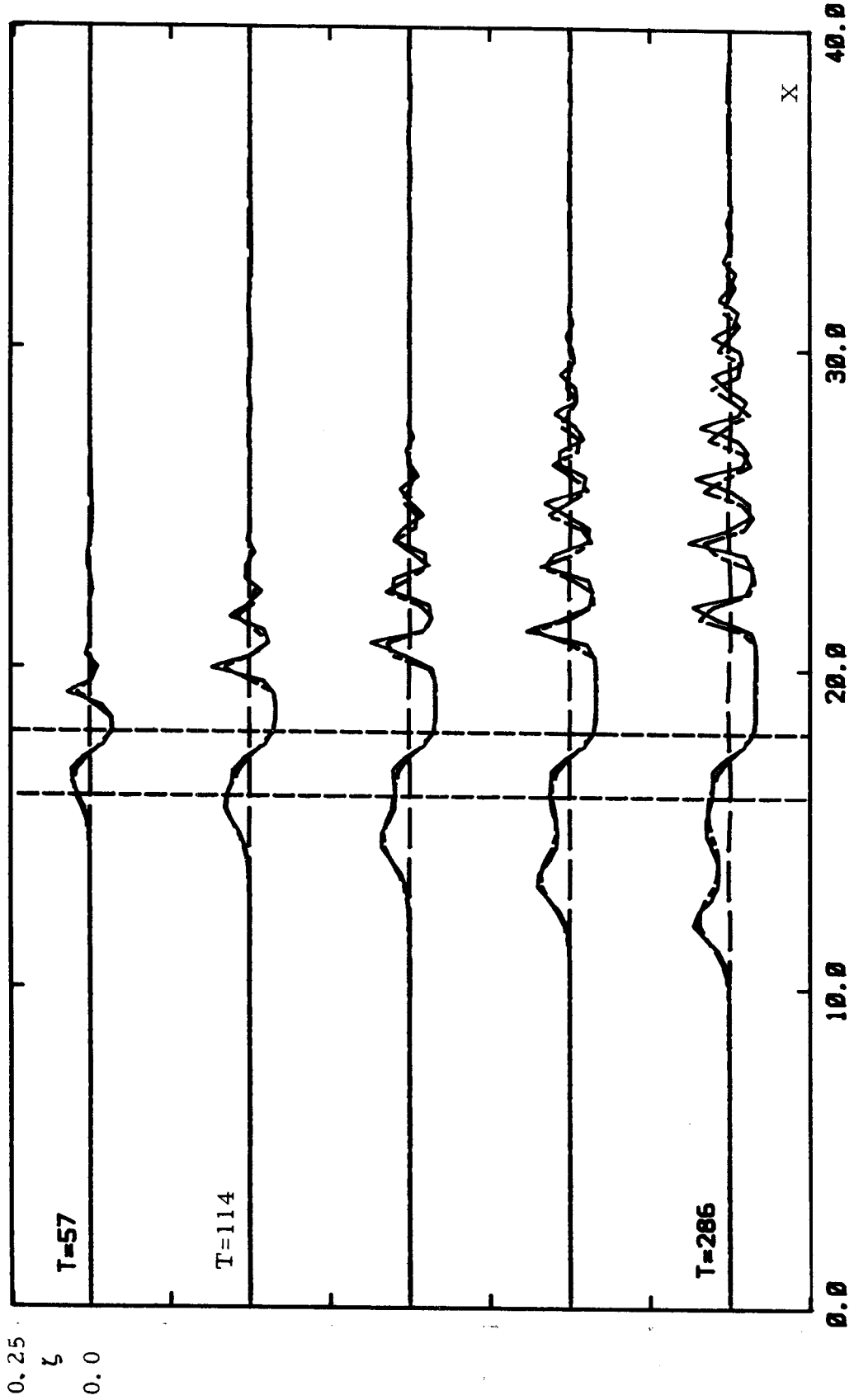

Fig. 8.33 Comparison of the interfacial wave obtained from FOUR-equation (solid lines) and that obtained from THREE-equation (dash-dot lines) for $H_2 = 0.2$, $\sigma = 0.999$, $L = 1$, $d_m = 0.05$.

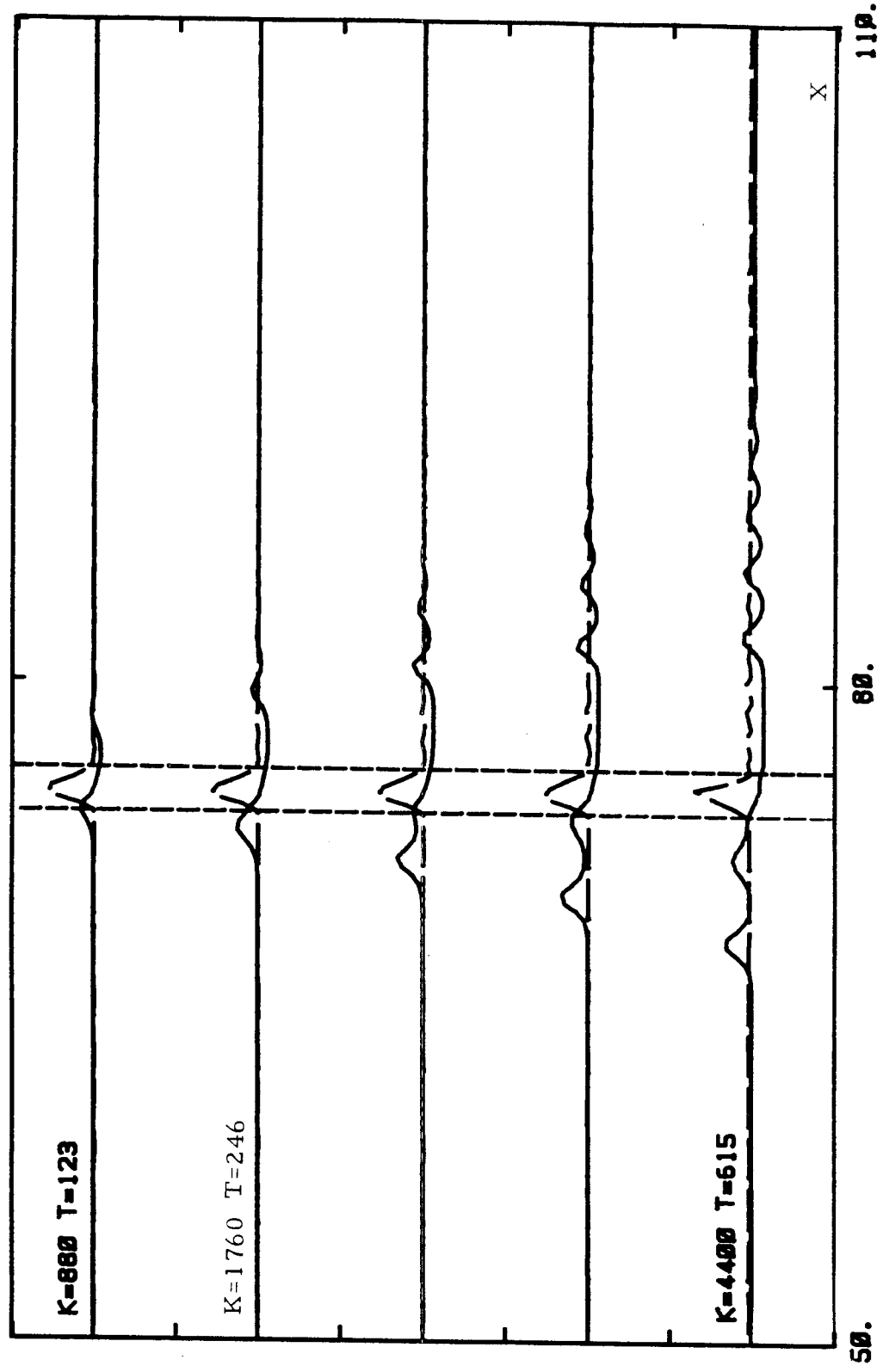

Fig. 8.34 The top surface (dash lines) and interface (solid lines) wave elevation of the top surface pressure forcing given by FOUR-equation for $H_2 = 0.15$, $\sigma = 0.96$, $L = 2$, the amplitude of the pressure forcing $d_m = -0.15^2$ and $Fr = 1$.

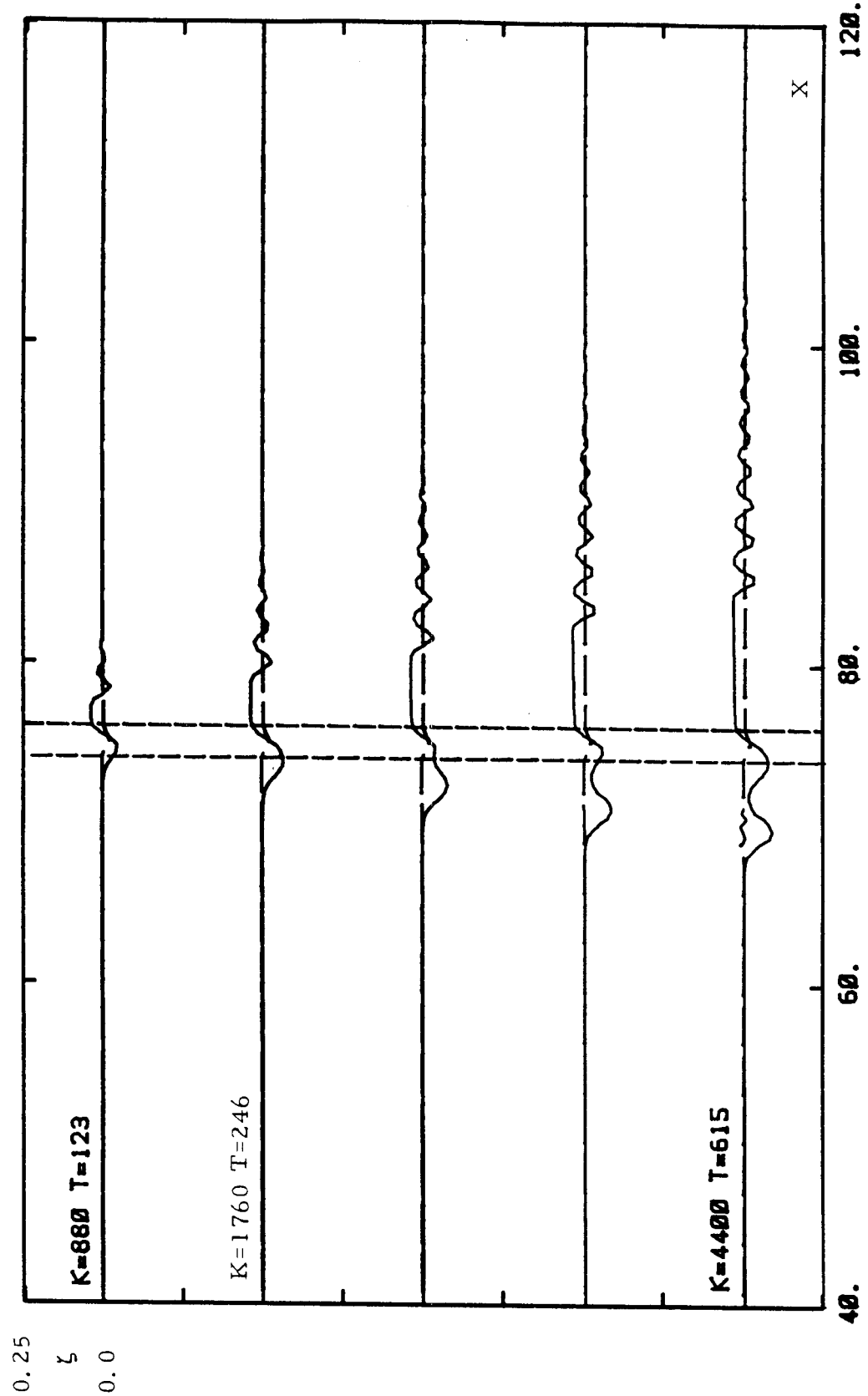

Fig. 8.35 The top surface (dash lines) and interface (solid lines) wave elevation of the top surface pressure forcing given by FOUR-equation for $H_2 = 0.85$, $\sigma = 0.96$, $L = 2$, the amplitude of the pressure forcing $d_m = 0.0254$ and $Fr = 1$.

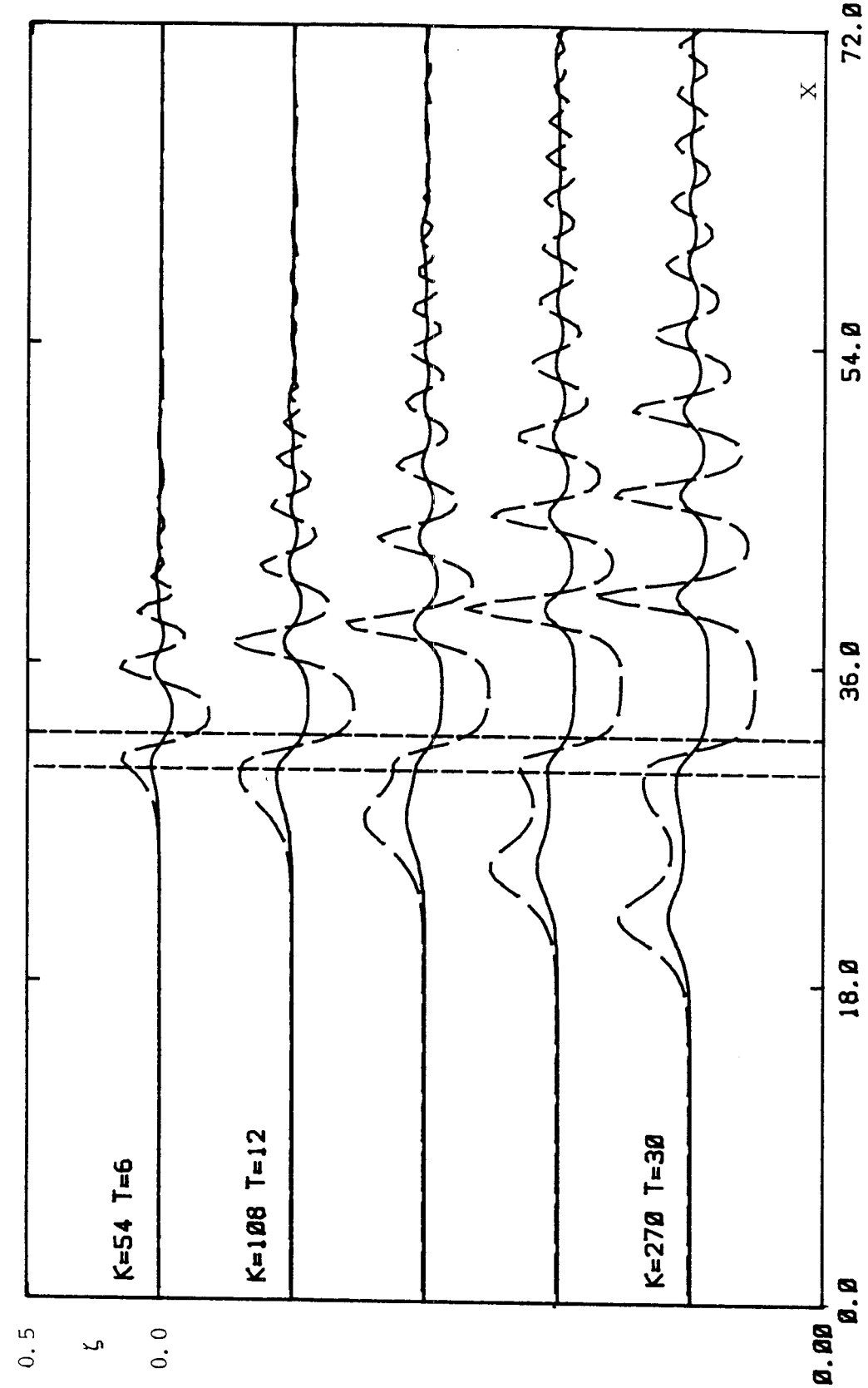

Fig. 8.36 The top surface (dash lines) and interface (solid lines) wave elevation of the top surface pressure forcing given by FOUR-equation for $H_2 = 0.3$, $\sigma = 0.97$, $L = 2$, the amplitude of the pressure forcing $d_m = 0.12$ and $Fr = 0.9$ (only case of fast mode).

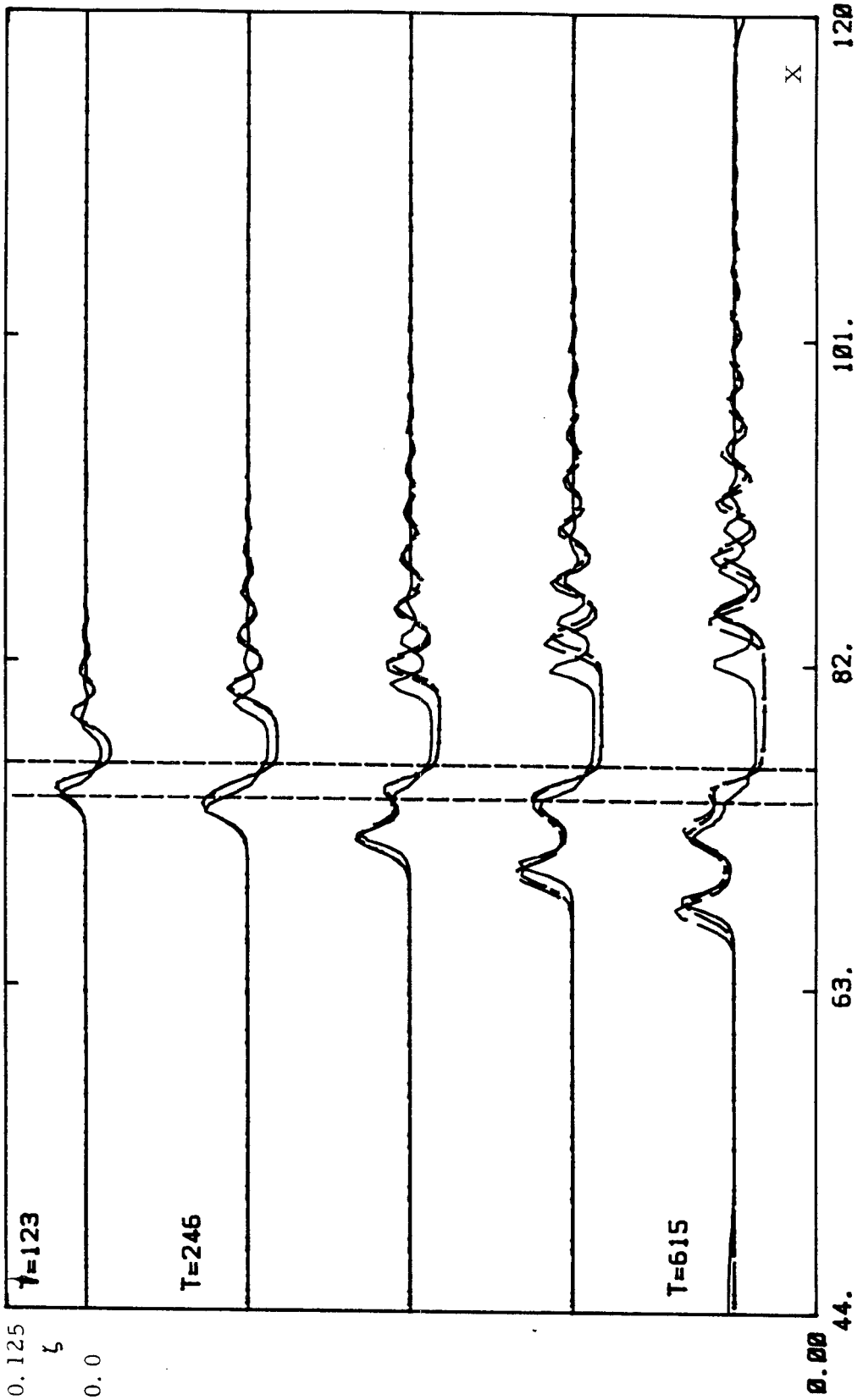

Fig. 8.37 Comparison of the interface elevations between the numerical solutions given by the FOUR-equation model (solid lines), KdV model with implicit scheme (dashed lines) and KdV model with explicit scheme (dash-dot lines) for $H_2 = 0.15$, $\sigma = 0.96$, $L = 2$, the amplitude of the pressure forcing $d_m = -0.15$ and $Fr = 1$.

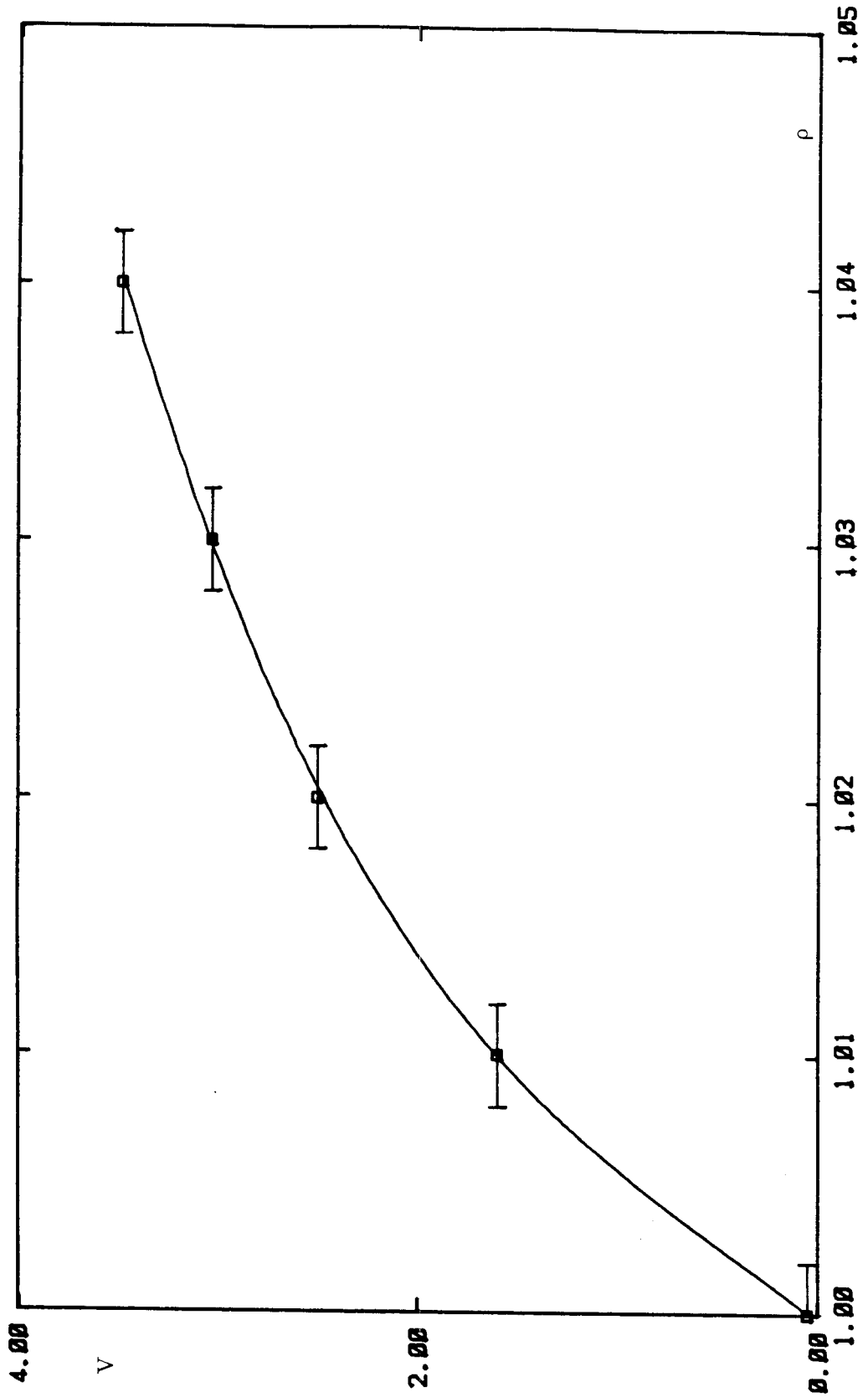

Fig. 8.38. A typical result of density probe calibration.

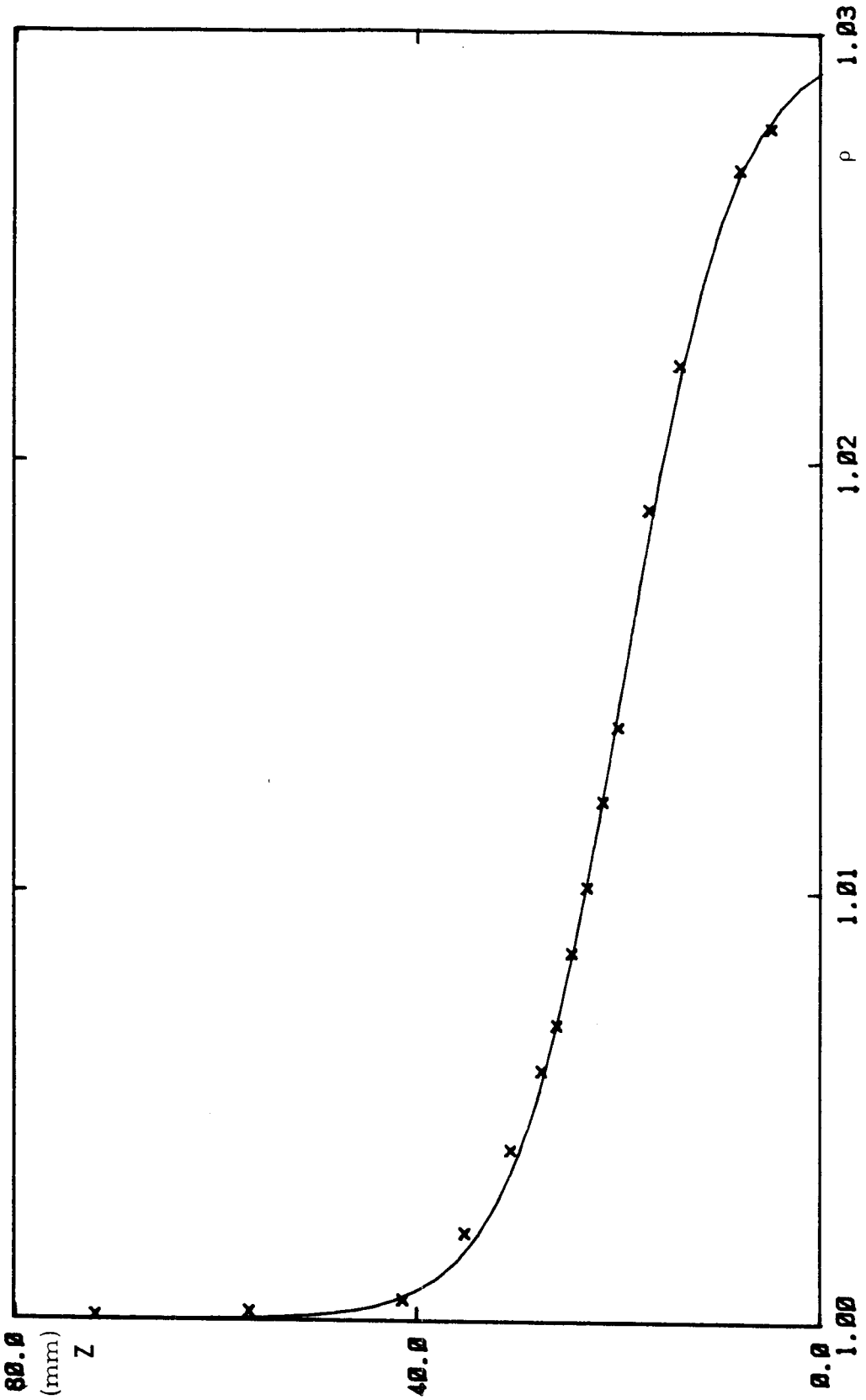

Fig. 8.39 A typical density profile inside the wave tank.

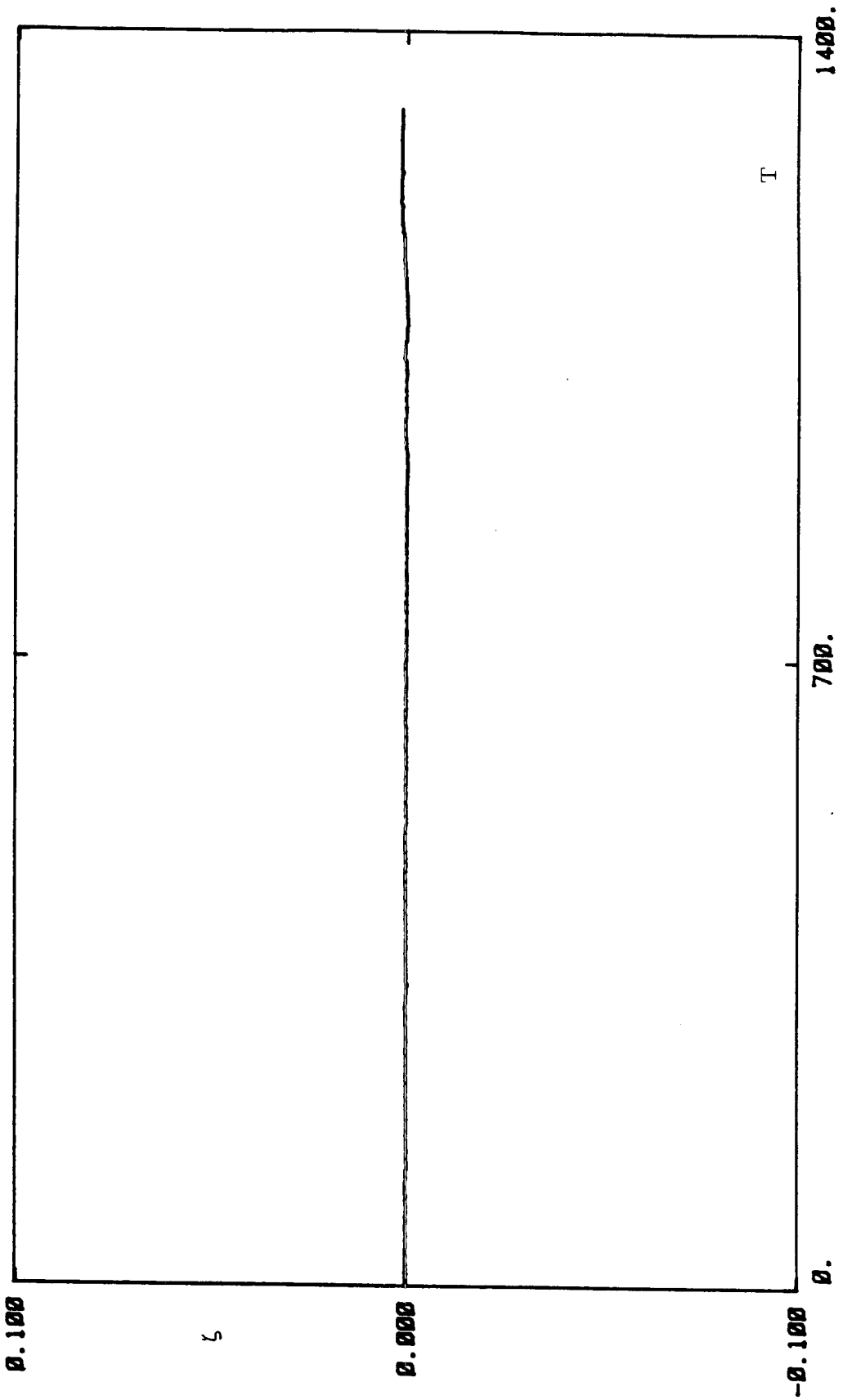

Fig. 8.40 A typical top surface wave recording.

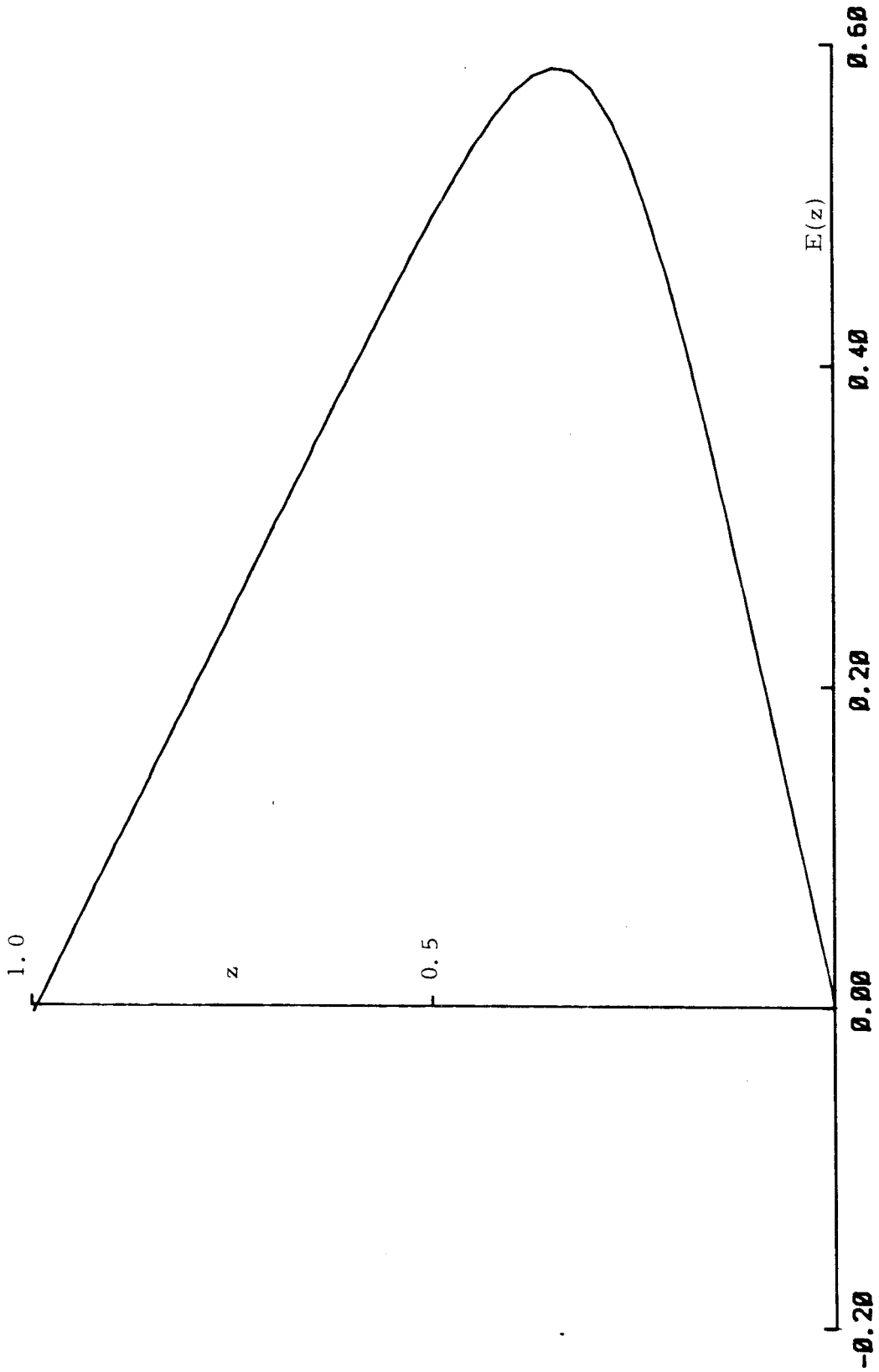

Fig. 8.41 A typical eigenfunction for continuously stratified fluid system with free top surface of first internal mode for $\rho_1 = 1$, $\rho_2 = 1.026$, $k = 7.78$ and $H = 0.278$.

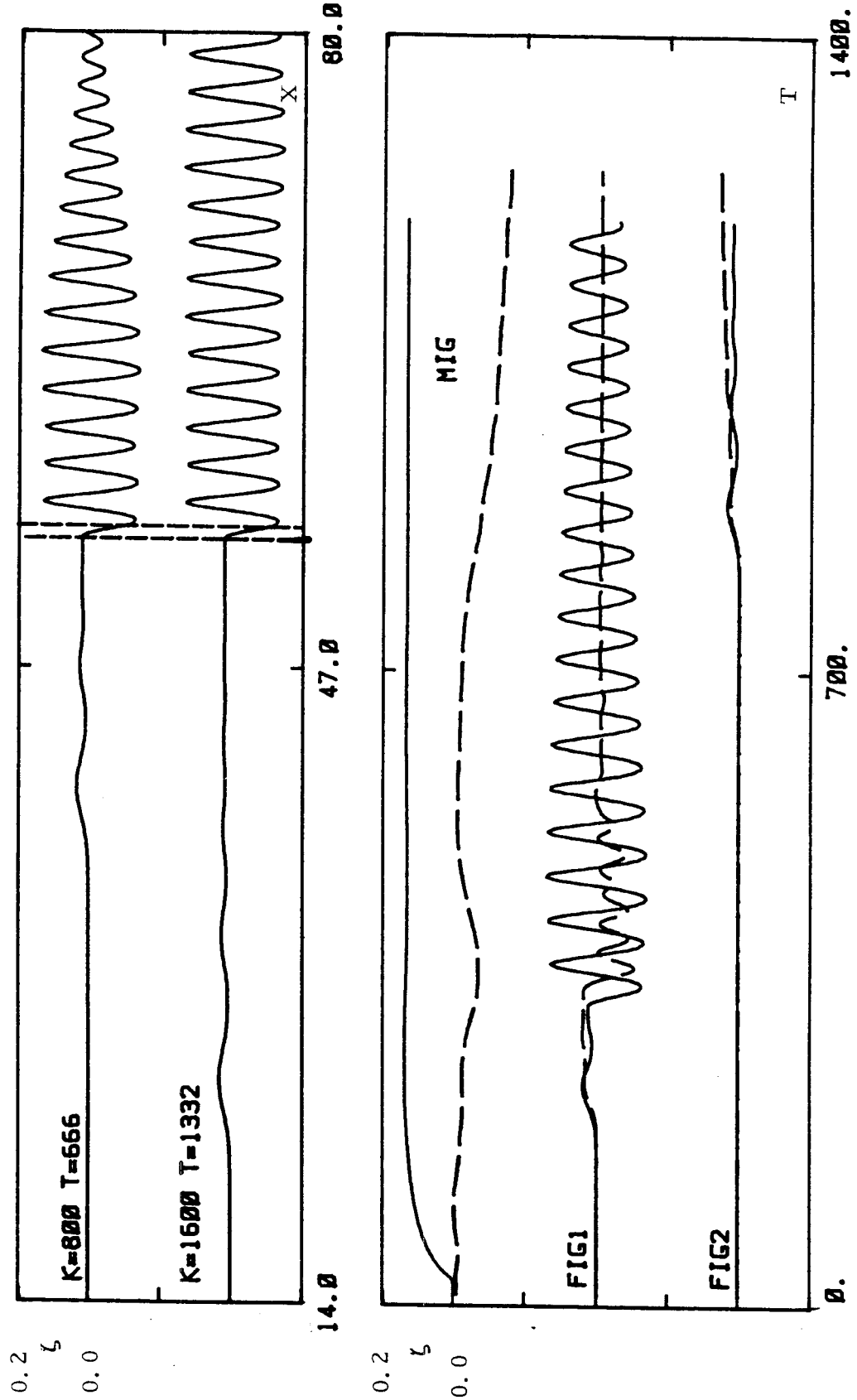

Fig. 8.42 Comparison of the interface (or pycnocline) elevations between the experimental data (dashed lines) and the numerical solution given by the KdV model for continuously stratified fluid system for $Fr = 0.66$.

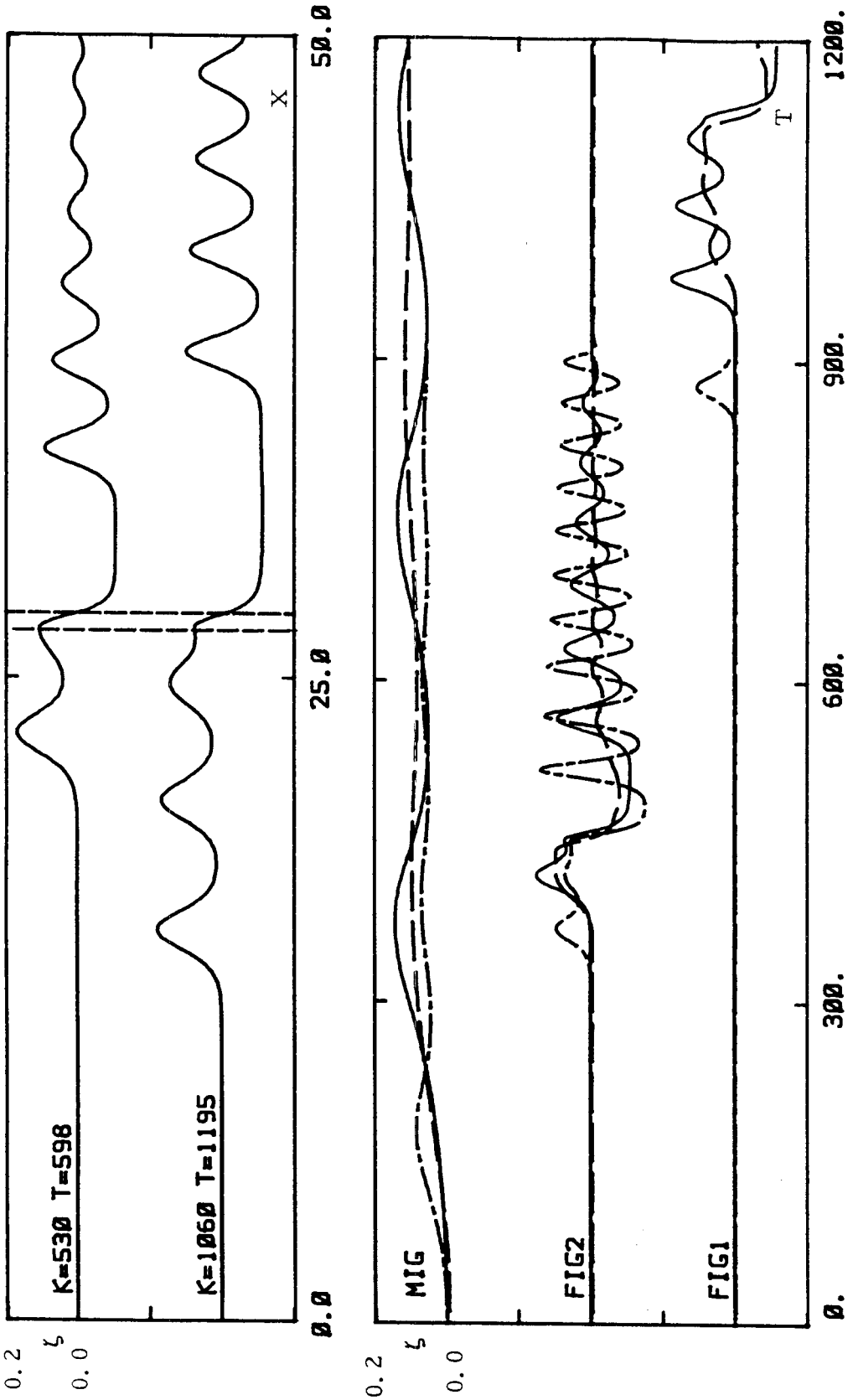

Fig. 8.43 Comparison of the interface (or pycnocline) elevations between the experimental data (dashed lines) and the numerical solution given by the KdV model for continuously stratified fluid system for Fr = 0.97. Dash-dot lines denote the numerical results given by the KdV equation for two-layer fluid system in the corresponding situation.

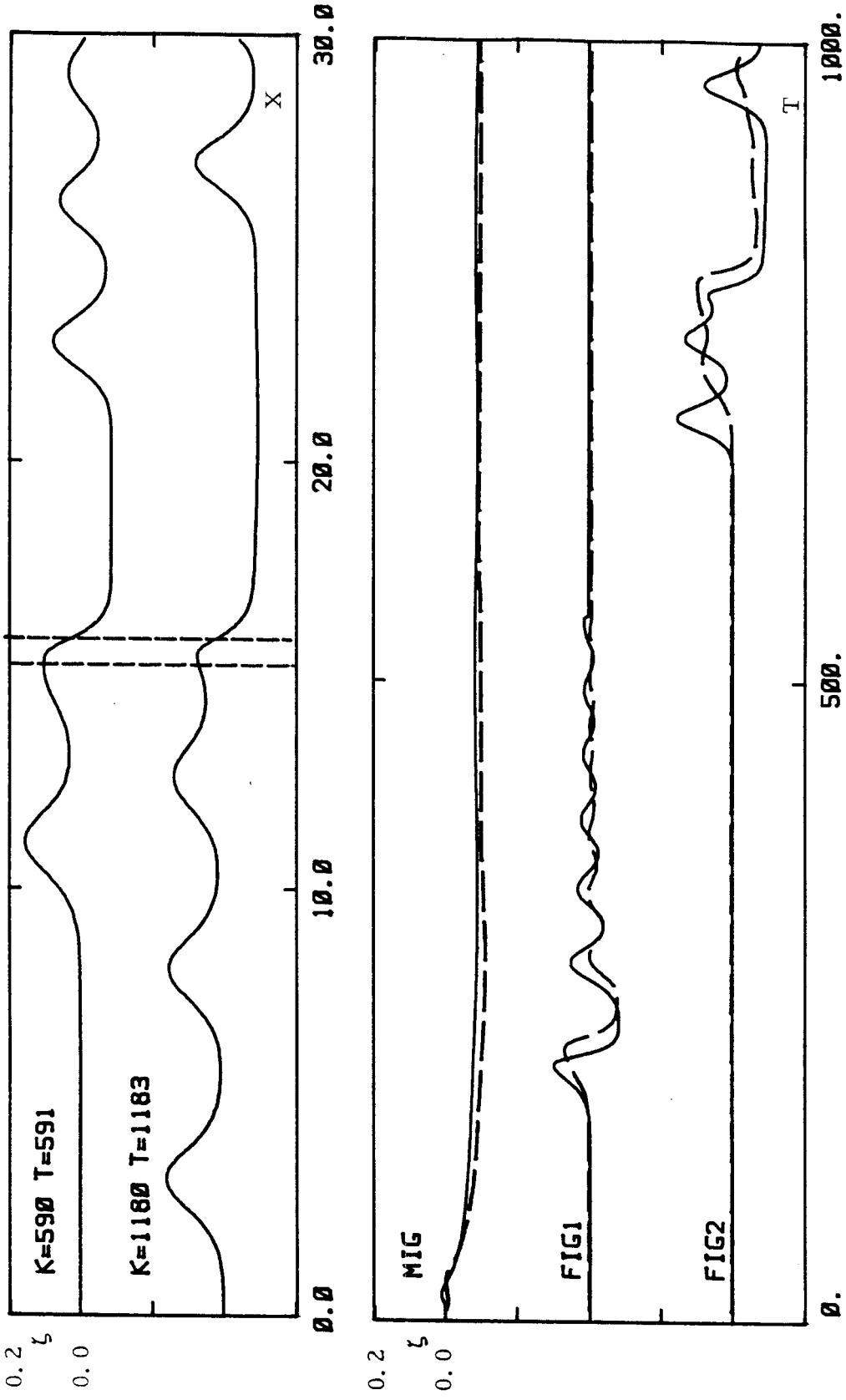

Fig. 8.44 Comparison of the interface (or pycnocline) elevations between the experimental data (dashed lines) and the numerical solution given by the KdV model for continuously stratified fluid system for Fr = 0.99.

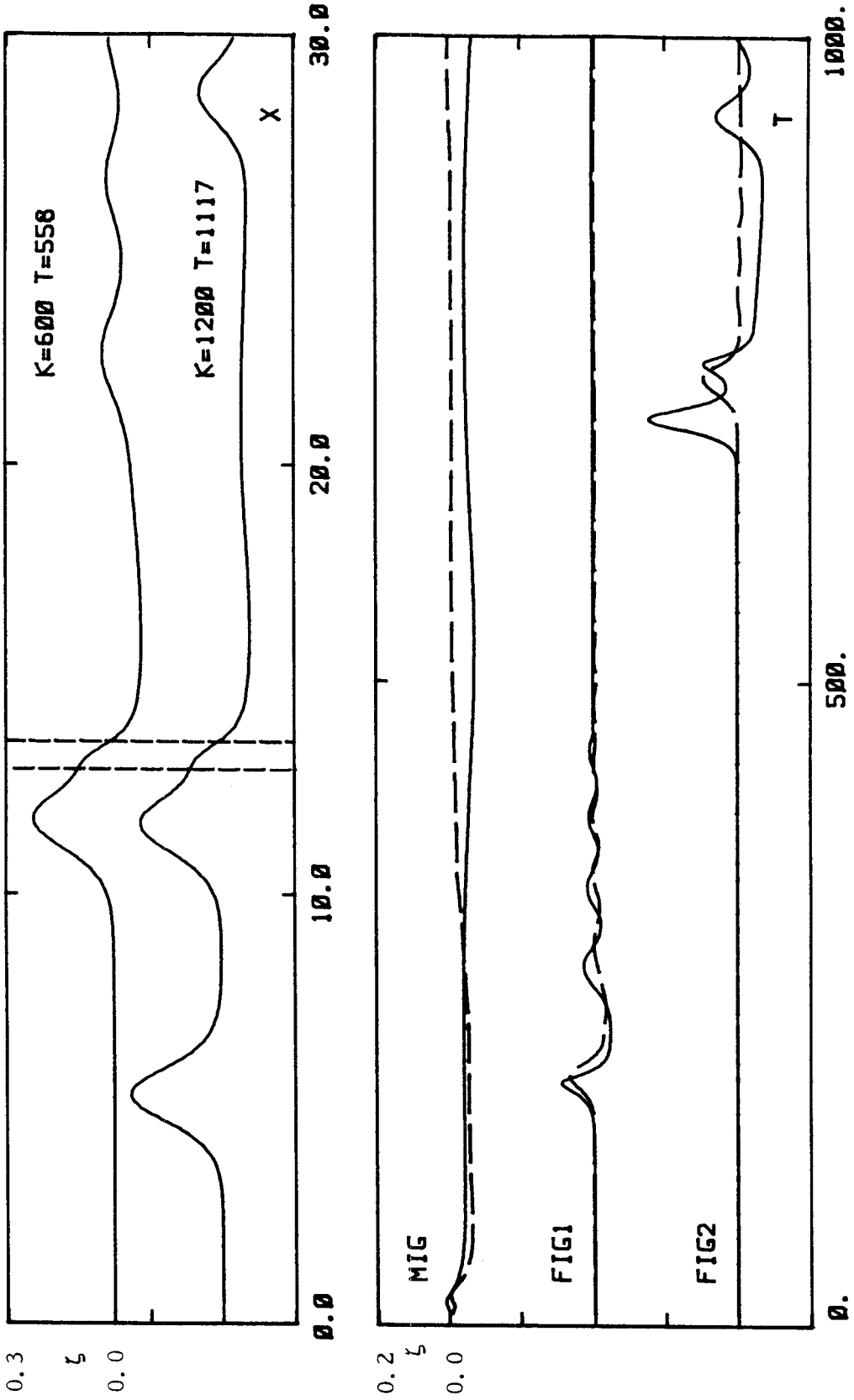

Fig. 8.45 Comparison of the interface (or pycnocline) elevations between the experimental data (dashed lines) and the numerical solution given by the KdV model for continuously stratified fluid system for $Fr = 1.09$.

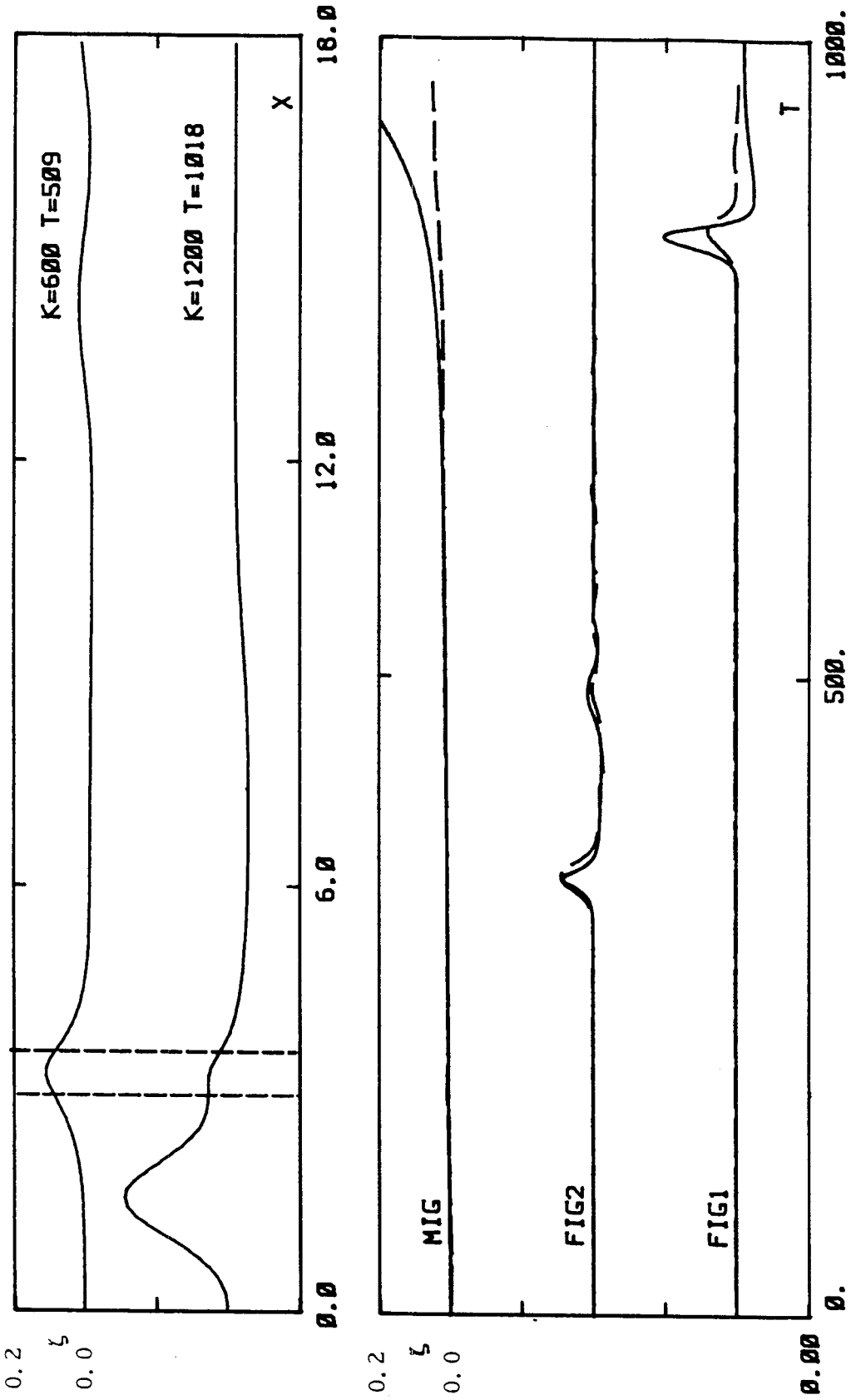

Fig. 8.46 Comparison of the interface (or pycnocline) elevations between the experimental data (dashed lines) and the numerical solution given by the KdV model for continuously stratified fluid system for Fr = 1.16.

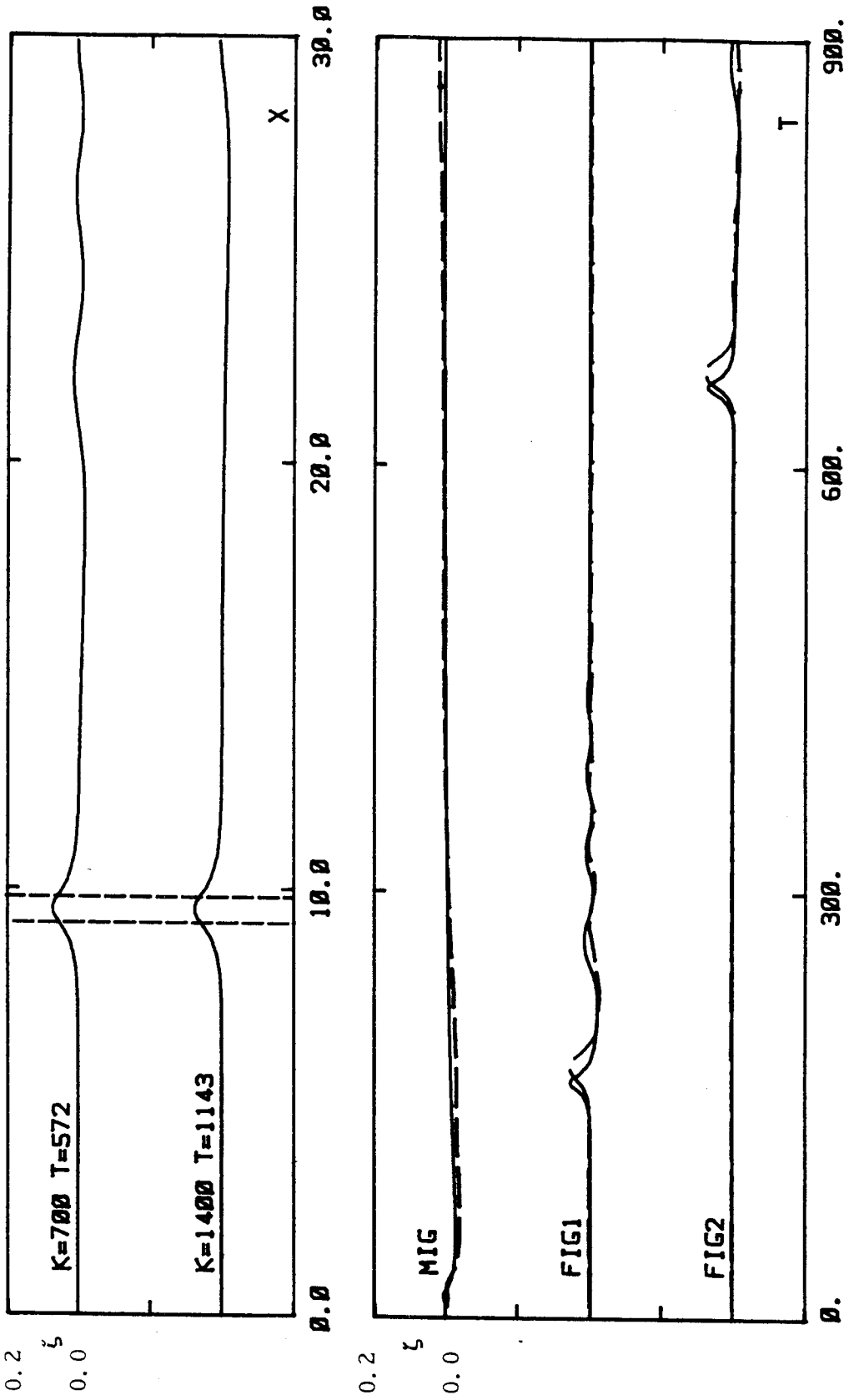

Fig. 8.47 Comparison of the interface (or pycnocline) elevations between the experimental data (dashed lines) and the numerical solution given by the KdV model for continuously stratified fluid system for $Fr = 1.18$.

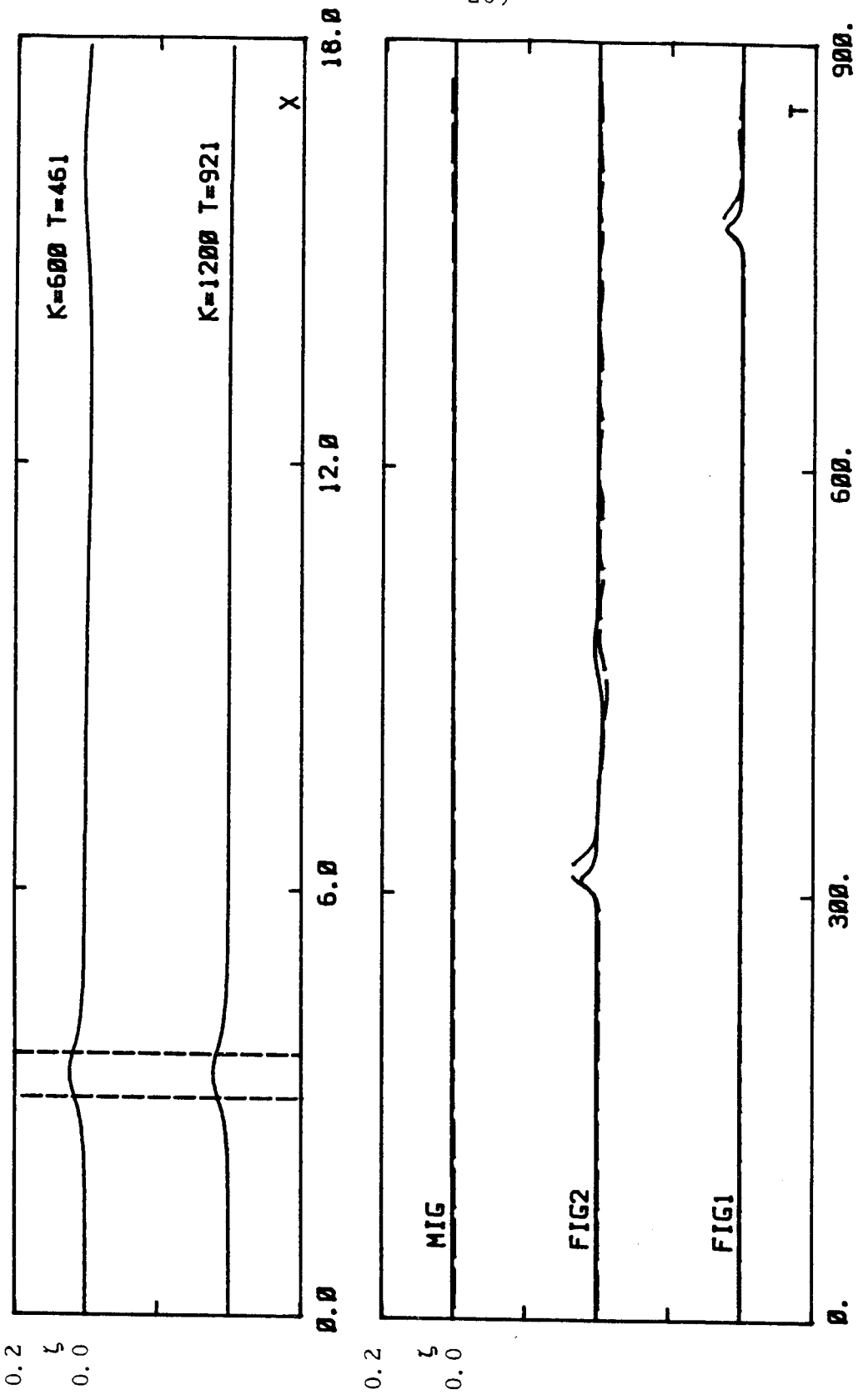

Fig. 8.48 Comparison of the interface (or pycnocline) elevations between the experimental data (dashed lines) and the numerical solution given by the KdV model for continuously stratified fluid system for Fr = 1.26.